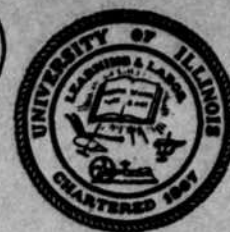MICROCOPY RESOLUTION TEST CHART
NATIONAL BUREAU OF STANDARDS-1963-A

CIVIL ENGINEERING STUDIES

LEVEL

AD A094763

WAVE PROPAGATION PROBLEMS IN CERTAIN ELASTIC ANISOTROPIC HALF SPACES

By
C. G. CARACOSTIS
and
A. R. ROBINSON

DTIC
ELECTE
FEB 9 1981

C

UNIVERSITY OF ILLINOIS
at URBANA-CHAMPAIGN
URBANA, ILLINOIS
DECEMBER 1980

DDC FILE COPY

81 2 09 185

WAVE PROPAGATION PROBLEMS IN CERTAIN

ELASTIC ANISOTROPIC HALF SPACES

by

C. G. Caracostis

A. R. Robinson

A Technical Report of

Research Sponsored by

THE OFFICE OF NAVAL RESEARCH
DEPARTMENT OF THE NAVY

Contract No. N00014-75-C-0614

Project No. NR 064-183

University of Illinois
at Urbana-Champaign
Urbana, Illinois

December 1980

30272-101

REPORT DOCUMENTATION PAGE	1. REPORT NO. UILU-ENG-80-2022 SRS-487		2.	3. Recipient's Accession No.
4. Title and Subtitle Wave Propagation Problems in Certain Elastic Anisotropic Half Spaces.				5. Report Date December 1980
				6.
7. Author(s) Constantine G. Caracostis and Arthur R. Robinson				8. Performing Organization Rept. No. SRS No. 487
9. Performing Organization Name and Address Department of Civil Engineering University of Illinois at Urbana-Champaign Urbana, Illinois 61801				10. Project/Task/Work Unit No. NR 064-183
				11. Contract(C) or Grant(G) No. (C) N00014-75-C-0164 (G)
12. Sponsoring Organization Name and Address Material Science Division Structural Mechanics Program (code 474) Office of Naval Research (800 Quincy Street) Arlington, Virginia 22217				13. Type of Report & Period Covered Technical Report
				14.
15. Supplementary Notes				

Doctoral thesis,

AD A094763

16. Abstract (Limit: 200 words)

The Smirnov-Sobolev method of self-similar potentials is used to solve certain wave propagation problems in anisotropic media. The solutions are expressed in terms of analytic functions which are determined from the boundary conditions in a straightforward manner. Two types of problems are considered. The first type concerns the two-dimensional case of an orthotropic material under plain-strain conditions subjected to a suddenly applied line force on the surface or in the interior of a half space. The second type treats the three-dimensional problem of a point force suddenly applied on the surface of a transversely isotropic half space. This solution is formed, in general, by a rotational superposition of the solutions for a plane strain and for an antiplane problem with appropriately defined boundary conditions. The mapping of the wave fields in the complex domain composed of a four-sheeted Riemann surface is examined in detail. Some of the techniques used in the numerical treatment of certain singularities are briefly discussed. The numerical results are given in the form of time histories for the displacements and stresses in the two-dimensional case and as time histories of only the displacements in the three-dimensional case.

17. Document Analysis a. Descriptors

Elastic Wave Propagation
Anisotropic Materials
Orthotropy
Plane Strain
Transverse Isotropy
Half Space

b. Identifiers/Open-Ended Terms

c. COSATI Field/Group

18. Availability Statement Approved for public release: Distribution unlimited	19. Security Class (This Report) Unclassified	21. No. of Pages 212
	20. Security Class (This Page) Unclassified	22. Price

(See ANSI-Z39.18) See Instructions on Reverse OPTIONAL FORM 272 (4-77)
(Formerly NTIS-35)
Department of Commerce

176010

iii

ACKNOWLEDGMENT

Accession For	
NTIS CRA&I	☑
DTIC TAB	☐
Unannounced	☐
Justification	
By	
Distribution/	
Availability Codes	
Dist	Avail and/or Special
A	

iv

TABLE OF CONTENTS

LIST OF TABLES

viii

LIST OF FIGURES

1. INTRODUCTION

1.1 <u>Object and Scope</u>

Wave propagation problems in linearly elastic, homogeneous, anisotropic media have attracted increased interest in recent years. Aside from the inherent interest in the subject as part of theoretical mechanics, results of investigations in this area have sufficient practical engineering applications to motivate further explorations of the math- ematical and computational difficulties involved. In the past, the effects of anisotropy were often neglected as being of secondary importance in the dynamics of elastic media. However, when detailed computations are carried out for wave propagation in isotropic media using large digital computers and involving massive arithmetic effort, it would seem that more attention should be given to what are possibly significant effects of anisotropy.

Several theoretical investigations have been stimulated by the development of ultrasonic techniques for the measurement of the dynamic elastic constants in pure crystals, where anisotropy plays a fundamental role. These techniques were based on the availability of the necessary electronic equipment to excite and detect mechanical vibrations of high frequency which enabled experimental researchers to observe the characteristics of propagation of disturbances with wave lengths very small in comparison with the dimensions of the source and specimen. In theoretical seismology, increased attention has been given to studies concerning the effects of a possible continental anisotropy in the propagation of seismic waves, in particular the Rayleigh surface waves.

Seismic waves are also of great interest in earthquake engineering. Specifically, the effect of anisotropy on strong ground-motion records requires further exploration. The propagation of waves in piezoelectric crystals, the dynamic behavior of composite materials, and a variety of problems in solid state physics and geophysics fall into the range of applications where an increased knowledge of dynamics of anisotropic materials is desirable.

The object of the present study is to provide analytical and computational techniques to obtain solutions for the transmission of waves from a point force in a linearly elastic, homogeneous, anisotropic medium. Two types of problems have been undertaken. The first concerns the two-dimensional problem of a line force applied to the surface or in the interior of an orthotropic material, i.e. a material which has at each point three orthogonal planes of elastic symmetry. The boundary plane is taken parallel to one of the symmetry planes and the applied load is a step function in time. The stresses are determined directly as functions of a complex variable while the displacements require the evaluation of a simple quadrature. The second type of problems considered in this study concerns a step force applied to the surface of a transversely isotropic material. Transverse isotropy is a special case of anisotropy in which there is at every point of the medium one axis of elastic symmetry while all directions perpendicular to that axis are equivalent. The dynamic response given by the three displacements in a cylindrical coordinate system requires the calculation of a simple quadrature in the complex plane.

1.2 Previous Related Studies

Investigations concerning anisotropic wave propagation can be traced back to the research work on crystal optics at the end of the last century which laid down the foundation for a qualitative understanding of the effects of anisotropy on elastic waves propagating in a solid medium. Rigorous theoretical developments awaited the availability of ultrasonic techniques which occured several decades later and spurred a renewed interest in the subject.

The basic principles of the theory of elastic wave propagation in anisotropic media can be found in the monographs by Hearmon [15]*, Fedorov [13], Musgrave [25], Auld [3], and Chadwick and Smith [8]. Recent advances of elastic waves at crystalline interfaces were discussed by Musgrave [26] who also included a list of original contributions to various specialized problems. Kraut [19] examined the problem of a vertical line force on the surface of a transversely isotropic material, De [10] discussed the Rayleigh wave contribution to the displacements produced by a suddenly applied force at the surface, while Payton [34, 35] gave the solutions for suddenly applied point force and for time dependent line load in an unbounded transversely isotropic medium. In all these solutions the method of analysis is based on the classical multiple transform techniques, with the attendant computational difficulties.

A different approach was followed by Sveklo [44] who examined the two-dimensional problem of an instantaneous pulse in an anisotropic medium by employing the Smirnov-Sobolev method of complex solutions, which

---

*Numbers in brackets refer to entries in the List of References.

was initially applied for isotropic solids [39, 40]. Sveklo used the same approach to solve the problem of a force applied on the surface of a half-space (Lamb's problem) [45]. The anisotropy of the material was defined by three elastic constants. The same type of material was used by the same author to examine dynamic problems with mixed boundary conditions [46]. Reflected and refracted waves at the interface of two anisotropic media with three elastic constants were examined by Osipov [27] who also in a number of other publications covered topics such as the behavior of the wave propagation velocities in materials with four elastic constants [28], the application of the Smirnov-Sobolev method to formulate solutions for anisotropic materials [29,30], the examination of the Rayleigh type waves [31], and some cases of mapping of the wave fields on the complex plane [32]. A number of errors have been noted in Osipov's work; some of them were recognized and corrected by the author himself in later publications. Lamb's problem in anisotropic media was also examined by Budaev [5, 6, 7] in terms of certain dimensionless quantities derived from the elastic constants.

1.3 Method of Solution

Two-dimensional wave propagation problems in homogeneous elastic anisotropic bodies require the solution of a system of two partial differential equations. The Smirnov-Sobolev method of self-similar potentials utilizes some important results of complex analysis to derive the solutions as analytic functions of a complex variable. The complex variable is determined from an equation which describes the general solution of the equations of motion in terms of the characteristic

surfaces.

A given set of boundary conditions which are homogeneous functions of the x, y and t variables provides the necessary equations to determine the analytic functions or potentials mentioned previously. The real part of the complex solutions constitutes the answer to a problem because the real part of the complex stresses and/or displacements represents the prescribed boundary conditions.

The anisotropy of the medium in the two-dimensional problems is defined by four elastic constants. The applied load is given as a line force parallel to the elastic direction so that the conditions of plane strain are satisfied. When the medium is unbounded, two types of waves propagate from the source of disturbance. The first type is called quasi-longitudinal and the second quasi-transverse in analogy with the isotropic case. The existence of a plane boundary introduces reflected, surface and head waves.

The solution of the three-dimensional equations of motion for a transversely isotropic medium is reduced, by the technique of rotational superposition described in Chapter 3, to the solution of equations of motion for a plane strain problem and an antiplane problem. Both of these cases are treated in Chapter 2. Thus, the simplicity of the method of self-similar potentials is preserved in developing three-dimensional solutions.

The study is organized as follows. Chapter 2 briefly explains the Smirnov-Sobolev method as it is applicable to anisotropic materials of a certain kind and gives the solutions to a variety of two-dimensional problems. Chapter 3 explains the technique of rotational superposition

and presents the solution of certain axisymmetric and non-axisymmetric problems in the form of the displacements. The often intricate mapping of the wave fields in the complex domain defined by a four-sheeted Riemann surface is the subject of Chapter 4. In Chapter 5 numerical results are discussed together with some of the techniques required to overcome inherent computational difficulties. A summary of the study, conclusions and recommendations for further research are given as Chapter 6.

1.4 Notation

The symbols used in this study are defined in the text where they first appear. For convenient reference, those most frequently used are listed below.

a, b, c, d, e	elastic parameters of orthotropic and transversely isotropic materials
A, B, C, D, E	the five material cases according to the configuration of the quasi-transverse wave front
$A_\theta, B_\theta, C_\theta, D_\theta$	curves on the complex domain which separate the regions of mapping the quasi-longitudinal and the quasi-transverse wave field
A_{01}, A_{02}	points in the wave fields which map on the branch points Θ_{01} and Θ_{02}
$c_{ij} \ (i, j = 1, 2, \ldots 6)$	elastic constants of a general anisotropic material
$C_\kappa \ (\kappa = 1, 2, 3)$	contours of integration in the three-dimensional problems
E_X	normal strain in the X-direction

$f_1(\omega_0)$, $f_2(\omega_0)$	weighting functions
F_h, F_v	magnitudes of horizontal and vertical forces
FS-H	the plane strain problem of a horizontal step force in the full-space
$G_\kappa(\theta_\kappa)$	function defined in Eq. (3.25)
HS-V	the plane strain problem of a vertical step force on the surface of a half-space
HS-IH	the plane strain problem of a horizontal step force in the interior of a half-space
K_1, K_2, L, M	quantities involving the elastic parameters, defined in Eq. (2.10)
$L_\kappa(\theta)$, $M_\kappa(\theta)$	functions defined in Eq. (2.24)
$\bar{n}_\kappa$	unit vector normal to the tangent at the wave front
N_1, N_2, N_3, N_4, N_5	quantities involving the elastic parameters, defined in Eq. (2.10) and (C.10)
$Q(\theta_\kappa)$	function defined in Eq. (2.20)
r	the radial coordinate in the cylindrical system
$R(\theta)$	Rayleigh function in anisotropic media defined in Eq. (2.28)
$R_\kappa(\theta)$, $\tilde{R}(\theta)$	functions defined in Eqs. (2.47) and (2.48)
S_1, S_2, S_3, S_4	the four sheets of the complete Riemann surface
$S_\kappa(\theta)$	function defined in Eq. (2.24)
t	the time variable

8

t_p, t_s, t_{s1}, t_{s2}	arrival times of the wave fronts
t_{p0}, t_{s0}	the times of the beginning of the mapping of the two wave fields in the complex domain
u_x, u_y, u_z	displacement components of the plane strain and the antiplane problems (an asterisk indicates the complex quantities)
u_{x0}^*, u_{y0}^*	complex displacements at the free surface ($y = 0$)
u_r, u_ω, u_y	displacement components in the three-dimensional problems (an asterisk indicates the complex quantities)
U_X, U_Y, U_Z	displacement components of the plane strain and the antiplane problems as used to develop the three-dimensional solutions
W	angular quantity ($= \omega - \omega_0$)
x, y, z	the cartesian coordinate system
x_R, y_R	coordinates of a point in the (x, y) plane
X, Y, Z	a cartesian coordinate system rotated by ω_0 about the $y \equiv Y$ axis
y_0	the y-coordinate of the point where the force is applied in the interior of the half-space
α_κ, β_κ	the angular quantities shown in Fig. 2
β^*, $\tilde{\beta}^*$, β^{1*}, β^{2*}, $\tilde{\beta}^{1*}$, $\tilde{\beta}^{3*}$	values of the quantity β_κ corresponding to various values of θ_κ (see Table 1)
γ	$= x_R/y_R$
γ_{xy}, γ_{xz}, γ_{yz}, γ_{ry}, $\gamma_{r\omega}$, $\gamma_{y\omega}$	shear strains
Γ_c	a value of γ such that the point (x_R, y_R) is located inside the sector formed from the cusps and the origin

Γ_0 — any value of γ that is not Γ_c

δ_κ ($\kappa = 1, 2, 3$) — function defined by Eqs. (2.16) and (2.31)

δ_κ' ($\kappa = 1, 2, 3$) — $= \partial\delta_\kappa/\partial\theta_\kappa$

$\Delta_\kappa, \Delta_\kappa'$ ($\kappa = 1, 2, 3$) — functions equivalent to δ_κ, δ_κ', as used for the three-dimensional problems

$\epsilon_\kappa, \zeta_\kappa$ — real and imaginary parts of θ_κ

$\epsilon_x, \epsilon_y, \epsilon_z, \epsilon_r, \epsilon_\omega$ — normal strains

E_κ, Z_κ — real and imaginary parts of $\lambda_\kappa(\theta_\kappa)$

η — dimensionless coordinate (= y/t)

$\eta_1, \eta_2, \eta_1', \eta_2'$ — values of η at the crossings of the wave fronts with the η-axis

$\eta^*, \eta^{1*}, \eta^{2*}$ — points on the η-axis which correspond to various values of θ according to conditions given in Chapter 4

θ — complex parameter

$\theta^{1*}, \theta^{2*}, \theta^*, \theta^{**}, \tilde\theta^{1*}, \tilde\theta^{2*}, \tilde\theta^*$ — real values of θ corresponding to cusps and nodes (double points) of the quasi-transverse wave front (see Table 1)

$\Theta_A, \Theta_D, \Theta_{01}, \Theta_{02}$ — the branch points on the Riemann surface

κ — index referring to the quasi-longitudinal wave ($\kappa=1$), the quasi-transverse wave ($\kappa=2$) or the shear wave in the antiplane problem ($\kappa=3$)

$\lambda_\kappa(\theta)$ ($\kappa = 1, 2, 3$) — function defined in Eqs. (2.19) and (2.32)

ξ — dimensionless coordinate (= x/t)

$\xi_1, \xi_2, \xi_1', \xi_2'$ — values of ξ at the crossings of the wave fronts with the ξ-axis

10

ξ_{01}	the ξ-coordinate of a node located on the ξ-axis
$\Pi(\theta)$	function defined in Eq. (2.27)
ρ	mass density of the material
σ_x, σ_y	normal stresses in the two-dimensional problems (an asterisk indicates the complex quantities)
σ_{x0}^*	complex normal stress at the free surface $(y=0)$
σ_r, σ_ω, σ_y	normal stresses in the cylindrical coordinate system
$\sum\limits_{\kappa=1}^{2}$	summation symbol
Σ_X, Σ_Y	normal stresses for plane strain problems as used to develop the three-dimensional solutions
Σ_y^*	complex self-similar fictitious normal stress
τ_{xy}, τ_{xz}, τ_{yz}	shear stresses of the plane strain and the antiplane problem (an asterisk indicates the complex quantities)
$\tau_{r\omega}$, τ_{ry}, $\tau_{y\omega}$	shear stresses in the cylindrical coordinate system
T_{XY}, T_{XZ}, T_{YZ}	shear stresses of the plane strain and antiplane problems as used to develop the three-dimensional solutions
T_{xy}^*	complex self-similar fictitious shear stresses
υ	variable used in Chapter 3 $(= r\cos W)$
$\phi_\kappa(\theta)$ $\phi_\kappa'(\theta)$	functions defined in Eqs. (4.9) and (4.12)
$\psi_\kappa(\theta)$, $\psi_\kappa'(\theta)$	functions defined in Eqs. (4.4) and (4.11)

ω the angular coordinate in the cylindrical system

$\Omega_\kappa(\theta), \Omega_{\kappa j}(\theta)$ self-similar potential functions

2. TWO-DIMENSIONAL WAVE PROPAGATION PROBLEMS
IN ANISOTROPIC MATERIALS

2.1 Generalized Hooke's Law

In continuous media the stresses and strains at a point are completely
expressed by the corresponding tensors. Each component of the stress
tensor can be written as a function of the components of the strain tensor.
Under the assumptions that the deformation takes place at a fixed
temperature, and that the initial unstrained state is also unstressed, the
linear parts of these functional relations between stresses and strains
comprise a system of equations known as the generalized Hooke's law.

In a cartesian coordinate system, where the engineering notation for
the stresses and strains is used, the generalized Hooke's law can be
written in the form [43]

$$\sigma_x = c_{11}\epsilon_x + c_{12}\epsilon_y + c_{13}\epsilon_z + c_{14}\gamma_{yz} + c_{15}\gamma_{zx} + c_{16}\gamma_{xy}$$

$$\sigma_y = c_{21}\epsilon_x + c_{22}\epsilon_y + c_{23}\epsilon_z + c_{24}\gamma_{yz} + c_{25}\gamma_{zx} + c_{26}\gamma_{xy}$$

$$\sigma_z = c_{31}\epsilon_x + c_{32}\epsilon_y + c_{33}\epsilon_z + c_{34}\gamma_{yz} + c_{35}\gamma_{zx} + c_{36}\gamma_{xy}$$

$$\tau_{yz} = c_{41}\epsilon_x + c_{42}\epsilon_y + c_{43}\epsilon_z + c_{44}\gamma_{yz} + c_{45}\gamma_{zx} + c_{46}\gamma_{xy} \qquad (2.1)$$

$$\tau_{zx} = c_{51}\epsilon_x + c_{52}\epsilon_y + c_{53}\epsilon_z + c_{54}\gamma_{yz} + c_{55}\gamma_{zx} + c_{56}\gamma_{xy}$$

$$\tau_{xy} = c_{61}\epsilon_x + c_{62}\epsilon_y + c_{63}\epsilon_z + c_{64}\gamma_{yz} + c_{65}\gamma_{zx} + c_{66}\gamma_{xy}$$

The coefficients c_{ij} (i, j = 1, 2, ...6) are the elastic constants or
moduli of the material. In homogeneous materials they are independent
of the system coordinates. Moreover, the existence of a quadratic strain
energy function imposes the symmetry conditions

$$c_{ij} = c_{ji} \quad (i, j = 1, 2, \ldots 6) \tag{2.2}$$

In the most general case of anisotropic materials, the number of independent coefficients required to determine the elastic behavior is twenty-one.[*] The existence of axes or planes of elastic symmetry together with an appropriate orientation of the coordinate system such that some or all of the coordinate axes are parallel to the symmetry axes or planes causes a reduction of the number of constants required to describe the material. The highest degree of elastic symmetry is exhibited by isotropic media, which require only two elastic constants. A discussion of the method used to obtain the necessary constraint equations among the constants c_{ij}, which must hold whenever various degrees of elastic symmetry are present, can be found in Love [21, §105] and Voigt [49].

2.2 Plane Strain Problems

The solution of dynamic problems in anisotropic materials with triclinic symmetry, i.e. involving all twenty-one elastic constants, presents formidable computational difficulties, mostly as a result of the large number of parameters involved. However, great insight into the effects of anisotropy can be gained by the study of materials which possess higher degrees of symmetry.

2.2.1 Orthotropic Materials

Consider an elastic anisotropic medium which at each point has three mutually perpendicular planes of elastic symmetry. These may be taken

----

[*]This number is based on the energy approach of Green. See Love [21] for a discussion of the controversy between the followers of Green's approach and the "atomic" modelers who advocated the "rari-constant" theory using fewer constants.

parallel to the axes of an orthogonal coordinate system. In this system
it can be shown that the following coefficients vanish

$$c_{14}=c_{15}=c_{16}=c_{24}=c_{25}=c_{26}=c_{34}=c_{35}=c_{36}=c_{45}=c_{46}=c_{56}=0 \qquad (2.3)$$

The remaining nine constants characterize an important class of anisotropic
materials most widely known as orthotropic. When the conditions of plane
strain are fulfilled, i.e.

$$u_z = \gamma_{yz} = \gamma_{zx} = 0 \qquad (2.4)$$

the stress-strain relations (2.1) are written in the simple form

$$\sigma_x = c_{11}\varepsilon_x + c_{12}\varepsilon_y$$
$$\sigma_y = c_{12}\varepsilon_x + c_{22}\varepsilon_y \qquad (2.5)$$
$$\tau_{xy} = c_{66}\gamma_{xy}$$

The other stresses are

$$\tau_{yz} = \tau_{zx} = 0$$
$$\sigma_z = c_{13}\varepsilon_x + c_{23}\varepsilon_y \qquad (2.6)$$

Equations (2.5) involve four independent elastic constants and determine
the plane strain problem of orthotropic materials in the x-y coordinates.[*]
In the dynamic problems of this study, it is convenient to use a new set
of parameters, indicated by the letters a, b, c and d which are defined as

_____

[*]The elastic constants c_{13} and c_{23} are not in any way involved in the
solution of the plane problem and are required only for determining the
stress σ_z normal to the plane of deformation(x, y).

$$a = \frac{c_{11}}{\rho}, \; b = \frac{c_{22}}{\rho}, \; c = \frac{c_{12}+c_{66}}{\rho}, \; d = \frac{c_{66}}{\rho} \qquad (2.7)$$

where ρ is the mass density of the material. These parameters have units of velocity to the second power $[L^2/T^2]$ and are subject to the conditions

$$a > 0, \; b > 0, \; d > 0, \; ab-(c-d)^2 > 0 \qquad (2.8)$$

stemming from the requirement of a positive definite strain energy function.

It has been observed that for all known media the constraints

$$a > d \qquad \text{and} \qquad b > d \qquad (2.9)$$

although not necessary for the positive definite character of the strain energy, seem to be satisfied.[*]

The following quantities involving the elastic parameters will appear frequently throughout this study and require an early definition

$$
\begin{aligned}
L &= ab + d^2 - c^2 \\
K_1 &= ab - (c-d)^2 \\
K_2 &= ab - (c+d)^2 \\
N_1 &= (a-d)(b-d) - c^2 \\
N_2 &= b(a-d) - c^2
\end{aligned} \qquad (2.10a)
$$

---

[*]This is reminiscent of the better known fact that values of Poisson's ratio in the range (0, -1) do not violate the condition for a positive definite strain energy, but are never observed in isotropic materials.

$$N_3 = a(b-d) - c^2$$

$$N_4 = d^2(b-d)^2 - K_1 K_2 \tag{2.10b}$$

$$M = (b+d) N_1 - d(a-b) (b-d) = bN_1 + d [(b-d)^2 - c^2]$$

It will be seen later that the range of values assumed by certain of these quantities greatly influences the procedure for computation of the wave fields, even requiring separation into different cases or sub-classes of orthotropic materials.

2.2.2 The Equations of Motion

The consideration of the equilibrium of an infinitesimal element in the two-dimensional space and the application of the linearized strain-displacement formulas

$$\varepsilon_x = \frac{\partial u_x}{\partial x}$$

$$\varepsilon_y = \frac{\partial u_y}{\partial y} \tag{2.11}$$

$$\gamma_{xy} = \frac{\partial u_x}{\partial y} + \frac{\partial u_y}{\partial x}$$

in the stress-strain relations (2.5), results in the equations of motion expressed in terms of the displacements

$$a \frac{\partial^2 u_x}{\partial x^2} + d \frac{\partial^2 u_x}{\partial y^2} + c \frac{\partial^2 u_y}{\partial x \partial y} = \frac{\partial^2 u_x}{\partial t^2}$$

$$\tag{2.12}$$

$$c \frac{\partial^2 u_x}{\partial x \partial y} + d \frac{\partial^2 u_y}{\partial x^2} + b \frac{\partial^2 u_y}{\partial y^2} = \frac{\partial^2 u_y}{\partial t^2}$$

The displacement vector $\bar{u}$ (u_x, u_y) can be decomposed by Helmholtz's formula [37]

$$\bar{u} = \text{grad } \phi + \text{curl } \bar{\psi} \tag{2.13}$$

into a sum of two vectors. The first vector represents the irrotational or longitudinal part given from a scalar potential function ϕ, while the second is formed from a vector potential function $\bar{\psi}$, satisfying the condition div $\bar{\psi} = 0$, and represents the equivoluminal or tranverse part of $\bar{u}$. Equation (2.13) applied to two-dimensional wave propagation problems is equivalent to the following two relations

$$u_x = \frac{\partial \phi}{\partial x} + \frac{\partial \psi}{\partial y}, \qquad\qquad u_y = \frac{\partial \phi}{\partial y} - \frac{\partial \psi}{\partial x} \tag{2.14}$$

where ψ stands for the z-component of the vector $\bar{\psi}$.

Direct application of these last expressions to the equations of motion (2.12) leads to a system of equations in terms of the potentials ϕ and ψ, i.e.

$$\frac{\partial}{\partial x}\left[a\,\frac{\partial^2 \phi}{\partial x^2} + (c+d)\,\frac{\partial^2 \phi}{\partial y^2} - \frac{\partial^2 \phi}{\partial t^2} \right] + \frac{\partial}{\partial y}\left[(a-c)\,\frac{\partial^2 \psi}{\partial x^2} + d\,\frac{\partial^2 \psi}{\partial y^2} - \frac{\partial^2 \psi}{\partial t^2} \right] = 0$$

$$\tag{2.15}$$

$$\frac{\partial}{\partial y}\left[(c+d)\,\frac{\partial^2 \phi}{\partial x^2} + b\,\frac{\partial^2 \phi}{\partial y^2} - \frac{\partial^2 \phi}{\partial t^2} \right] - \frac{\partial}{\partial y}\left[d\,\frac{\partial^2 \psi}{\partial x^2} + (b-c)\,\frac{\partial^2 \psi}{\partial y^2} - \frac{\partial^2 \psi}{\partial t^2} \right] = 0$$

It should be noted that the equations are coupled, unlike the isotropic case where the same process leads to two equations each involving only one of the potentials. The physical meaning is that, in general, each of the two solutions occurring in anisotropic media includes both irrotational and equivoluminal components in the displacement vector.

2.3 The Method of Self-Similar Potentials

The method of self-similar potentials or functionally invariable
solutions is a powerful technique developed by the Soviet mathematicians
V. I. Smirnov and S. L. Sobolev [39, 40] to solve the equations of motion
in problems of two-dimensional elasticity with initial or boundary
conditions given as homogeneous functions of the spatial and time variables.
An extended description of the method with applications to certain contact
problems is given by Thompson and Robinson [47]. The application of the
same method in solving dynamic problems in a three-dimensional space is
given by Johnson and Robinson [18] and Farewell and Robinson [12], while
Seyyedian and Robinson [38] solved the problem of the buried dislocation
pulse in a layered half space by a combination of self-similar solutions.
In all these cases the medium was considered to be isotropic.

The following sections present a brief exposition of the method of
self-similar potentials as applied to solve dynamic problems in homogeneous,
linearly elastic, anisotropic bodies.

2.3.1 The Solution of the Equations of Motion

The general solution of the partial differential equations of motion
(2.15) for an initial disturbance concentrated at the origin of the $y \geq 0$
half space can be written in the form

$$\delta_\kappa \equiv t - x\theta_\kappa - y\lambda_\kappa(\theta_\kappa) = 0 \qquad (\kappa = 1, 2) \qquad (2.16)$$

which defines the characteristic surfaces through the origin in terms of
a parameter θ_κ. Here $\lambda_\kappa(\theta_\kappa)$ is an analytic function to be determined

later. This form is chosen because it yields a simple expression for θ_K on the y=0 plane where the boundary conditions must be satisfied. On this plane $\theta_K = t/x$, i.e. the parameter is uniquely determined for every point and is the same for each solution of the wave equations. A more detailed discussion of Eq. (2.16) is given in Chapter 4 in conjunction with the mapping of the x, y, t space into the complex plane.

The parametrization of the characteristic surfaces by the quantity θ_K implies that any analytical functions of θ_K must satisfy the equations of motion. Let $\phi_K(\theta_K)$ and $\psi_K(\theta_K)$ be two functions with continuous first, second and third derivatives. Using the expressions provided in Appendix A and substituting $\phi = \phi_K(\theta_K)$ and $\psi = \psi_K(\theta_K)$ in Eq. (2.15), one arrives at the equivalent system

$$
\begin{aligned}
&-\theta_K [a\theta_K^2 + (c+d)\, \lambda_K^2(\theta_K) - 1]\, \phi_K'(\theta_K) - \\
&-\lambda_K(\theta_K)\, [(a-c)\theta_K^2 + d\lambda_K^2(\theta_K) - 1]\, \psi_K'(\theta_K) = 0 \\
&-\lambda_K(\theta_K)\, [(c+d)\theta_K^2 + b\lambda_K^2(\theta_K) - 1]\, \phi_K'(\theta_K) + \\
&+\theta_K\, [d\theta_K^2 + (b-c)\, \lambda_K^2(\theta_K) - 1]\, \psi_K'(\theta_K) = 0
\end{aligned}
\tag{2.17}
$$

where $\phi_K'(\theta_K)$ and $\psi_K'(\theta_K)$ denote first derivatives with respect to θ_K. The condition for the system to possess a non-vanishing solution is

$$
\begin{aligned}
F(\theta_K, \lambda_K) &\equiv bd\lambda_K^4(\theta_K) - (b+d-L\theta_K^2)\lambda_K^2(\theta_K) + \\
&+ (1-a\theta_K^2)(1-d\theta_K^2) = 0
\end{aligned}
\tag{2.18}
$$

The solution of this biquadratic equation defines the function $\lambda_K(\theta_K)$ as

$$\lambda_K(\theta_K) = \pm \left[\frac{b+d - L\theta_K^2 + (-1)^K \sqrt{Q(\theta_K)}}{2bd} \right]^{\frac{1}{2}} \tag{2.19}$$

where

$$Q(\theta_K) = (b+d-L\theta_K^2)^2 - 4bd(1-a\theta_K^2)(1-d\theta_K^2) =$$

$$= (b-d)^2 - 2M\theta_K^2 + K_1 K_2 \theta_K^4 \tag{2.20}$$

The complete representation of $\lambda_K(\theta_K)$ on a four-sheeted Riemann surface can be found in Appendix B. There exist four different types of Riemann surfaces denoted by I, II, III and IV according to the location of the branch points on the complex domain. Once the sign of the outside radical is fixed (see Chapter 4), the two distinct values of $\lambda_K(\theta_K)$ define by Eq. (2.16) the variable θ_K as the parameter of the characteristic surfaces. Under these conditions the real and imaginary parts of any analytic functions $\Phi_K(\theta_K)$ and $\Psi_K(\theta_K)$ give solutions to the equations of motion. If in a given domain the θ_K as function of x, y and t assumes real values, then any arbitrary real functions of θ_K with continuous derivatives up to the third order will also be solutions of Eq. (2.15)

The importance of the method of self-similar potentials lies in the simplicity of the determination of the analytic functions $\Phi_K(\theta_K)$ and $\Psi_K(\theta_K)$. In the class of problems undertaken by this study, four of these functions are required to determine the solution. However, the homogeneous system (2.17) provides a value for the quotient

$$\frac{\Phi'_\kappa(\theta_\kappa)}{\Psi'_\kappa(\theta_\kappa)} \qquad (\kappa = 1, 2)$$

As a result, the four functions $\Phi'_1(\theta_1)$, $\Psi'_1(\theta_1)$, $\Phi'_2(\theta_2)$ and $\Psi'_2(\theta_2)$ are not independent but for each value of the index κ only one of the two functions $\Phi'_\kappa(\theta_\kappa)$, $\Psi'_\kappa(\theta_\kappa)$ needs to be determined; the other can immediately be obtained by use of Eq. (2.17). The complex solutions of the Smirnov-Sobolev method must contain both of these functions for each of the two wave fields since $\Phi'_\kappa(\theta_\kappa)$ is associated with the longitudinal component and $\Psi'_\kappa(\theta_\kappa)$ is associated with the transverse component of the displacement vector. It turns out, however, to be simpler to pursue the solution in terms of new functions $\Omega_\kappa(\theta_\kappa)$ hereafter referred to as "potentials." Either of the two relations in Eq. (2.17) can be used to define these potentials; the first of the two has been chosen. Thus,

$$\frac{\Phi'_\kappa(\theta_\kappa)}{\lambda_\kappa(\theta_\kappa)\ [(a-c)\ \theta_\kappa^2 + d\lambda_\kappa^2(\theta_\kappa) - 1]} =$$

$$= \frac{\Psi'_\kappa(\theta_\kappa)}{\theta_\kappa\ [a\theta_\kappa^2 + (c+d)\ \lambda_\kappa^2(\theta_\kappa) - 1]} = \Omega_\kappa(\theta_\kappa) \quad (\kappa=1, 2) \qquad (2.21)$$

The ratio of the functions $\Phi'_\kappa(\theta_\kappa)$ and $\Psi'_\kappa(\theta_\kappa)$ is a measure of how close the solution comes to a pure longitudinal wave in the anisotropic media. In the case of isotropic materials (Appendix G) the denominator of the second fraction in Eq. (2.21) becomes zero for $\kappa=1$ while the denominator of the first fraction vanishes for $\kappa=2$. The longitudinal wave is, then, described by $\Phi'_1(\theta_1)$ and the transverse wave by $\Psi'_2(\theta_2)$ while $\Psi'_1(\theta_1) = \Phi'_2(\theta_2) = 0$.

2.3.2 The Determination of the Self-Similar Potentials

For given initial or boundary conditions, the determination of the solution of a particular wave propagation problem requires the calculation of the potentials $\Omega_\kappa(\theta_\kappa)$. The methods of complex analysis are extremely useful at this point. The real boundary tractions, given as homogeneous functions of space and time, can be expressed as analytic functions in the half-space $y \geq 0$ by means of the Schwartz integral formula [9]:

$$T^*(\theta) = -\frac{1}{i\pi} \int_{-\infty}^{\infty} \frac{T(\xi,t)}{\xi-x} \, d\xi \tag{2.22}$$

where T indicates the real traction and T^* the complex traction as a function of the complex parameter θ which assumes real values t/x on the boundary $y=0$ plane. The final result is given in terms of complex functions where the real and imaginary parts correspond respectively to the real and imaginary parts of the complex boundary conditions given by T^*.

It can easily be verified that the complex valued displacements and stresses (indicated by an asterisk) can be written as follows

$$u_x^* = \frac{\partial}{\partial t} \left[\sum_{\kappa=1}^{2} \int_0^{\theta_\kappa} c\theta\lambda_\kappa(\theta) \, [\theta^2 + \lambda_\kappa^2(\theta)] \, \Omega_\kappa(\theta) \, d\theta \right]$$

$$u_y^* = -\frac{\partial}{\partial t} \left[\sum_{\kappa=1}^{2} \int_0^{\theta_\kappa} [\theta^2 + \lambda_\kappa^2(\theta)] \, [a\theta^2 + d\lambda_\kappa^2(\theta) - 1] \, \Omega_\kappa(\theta) \, d\theta \right]$$

$$\sigma_x^*/\rho = \frac{\partial^2}{\partial t^2} \left[\sum_{\kappa=1}^{2} \int_0^{\theta_\kappa} \lambda_\kappa(\theta) L_\kappa(\theta) \, \Omega_\kappa(\theta) \, d\theta \right] \tag{2.23}$$

$$\sigma_y^*/\rho = \frac{\partial^2}{\partial t^2} \left[\sum_{\kappa=1}^{2} \int_0^{\theta_\kappa} \lambda_\kappa(\theta) \, S_\kappa(\theta) \, \Omega_\kappa(\theta) \, d\theta \right]$$

$$\tau_{xy}^*/\rho = \frac{\partial^2}{\partial t^2} \left[\sum_{\kappa=1}^{2} \int_0^{\theta_\kappa} \theta M_\kappa(\theta) \, \Omega_\kappa(\theta) \, d\theta \right]$$

23

where

$$L_\kappa(\theta) = - [\theta^2 + \lambda_\kappa^2(\theta)] \left\{ d[a\theta^2 + d\lambda_\kappa^2(\theta) - 1] + c[1 - d\lambda_\kappa^2(\theta)] \right\}$$

$$S_\kappa(\theta) = [\theta^2 + \lambda_\kappa^2(\theta)] \left\{ b[a\theta^2 + d\lambda_\kappa^2(\theta) - 1] - c(c-d)\theta^2 \right\} \qquad (2.24)$$

$$M_\kappa(\theta) = d[\theta^2 + \lambda_\kappa^2(\theta)] [a\theta^2 + (d-c)\lambda_\kappa^2(\theta) - 1]$$

The self-similarity of the potentials implies that the boundary tractions are homogeneous functions of the space and time variables of order n=-2. The generalization of the method to obtain solutions for a problem where the given tractions are homogeneous functions of order n is only a matter of a simple n-fold differentiation (for n positive) or n-fold integration (for n negative) with respect to t (see reference [47], section 2.8). On the y=0 boundary plane only the tractions σ_y and τ_{xy} are applied. The complex self-similar tractions on the same plane are given by a double integration with respect to t of the corresponding expressions in Eq. (2.23), i.e.

$$\Sigma_y^*/\rho = \sum_{\kappa=1}^{2} \int_0^{\theta_\kappa} \lambda_\kappa(\theta) \, S_\kappa(\theta) \, \Omega_\kappa(\theta) \, d\theta$$

$$\qquad (2.25)$$

$$T_{xy}^*/\rho = \sum_{\kappa=1}^{2} \int_0^{\theta_\kappa} \theta M_\kappa(\theta) \, \Omega_\kappa(\theta) \, d\theta$$

This system of equations is solved, after the integral is removed by a differentiation with respect to θ, to give the expressions for the potentials in terms of the self-similar tractions

$$\Omega_1(\theta) = \frac{\theta M_2(\theta) \ (\Sigma_y^{*'}/\rho) - \lambda_2(\theta) \ S_2(\theta) \ (T_{xy}^{*'}/\rho)}{\Pi(\theta)}$$

(2.26)

$$\Omega_2(\theta) = \frac{-\theta M_1(\theta) \ (\Sigma_y^{*'}/\rho) + \lambda_1(\theta) \ S_1(\theta) \ (T_{xy}^{*'}/\rho)}{\Pi(\theta)}$$

where

$$\Pi(\theta) = \theta \ [\lambda_1(\theta) \ S_1(\theta) \ M_2(\theta) - \lambda_2(\theta) \ S_2(\theta) \ M_1(\theta)] =$$

$$= cd\theta \ [\lambda_1(\theta) - \lambda_2(\theta)] \ [\theta^2 + \lambda_1^2(\theta)] \ [\theta^2 + \lambda_2^2(\theta)] \ R(\theta)$$

(2.27)

and

$$R(\theta) = (K_1\theta^2 - b) \ \lambda_1(\theta)\lambda_2(\theta) + a\theta^2 - 1$$

(2.28)

Here $R(\theta)$ is the equivalent of the Rayleigh function for anisotropic media.

2.4 The Antiplane Problem

A general definition and the treatment of a variety of antiplane problems can be found in reference [23]. In this study, a special case of antiplane problems is considered, where all the non-vanishing displacement and stress components are parallel to the normal to the plane (x, y) and are functions of x, y, and t [18]. In such a case, points lying in planes parallel to (x, y) before deformation cease to do so after deformation. The development of solutions for transversely isotropic materials, presented in the next chapter, requires the formal solution to this kind of problem. The equation of motion is written

$$e \ \frac{\partial^2 u_z}{\partial x^2} + d \ \frac{\partial^2 u_z}{\partial y^2} = \frac{\partial^2 u_z}{\partial t^2}$$

(2.29)

where the elastic parameters e and d are defined from the stress-strain relations

$$\tau_{zx} = \rho e \gamma_{zx} = \rho e \frac{\partial u_z}{\partial x}$$

$$\tau_{yz} = \rho d \gamma_{yz} = \rho d \frac{\partial u_z}{\partial y}$$

(2.30)

The displacement u_z is only a function of x, y and t. It is not difficult to show that the characteristic surfaces in this case are defined by the equation

$$\delta_3 \equiv t - x\theta_3 - y\lambda_3(\theta_3) = 0$$

(2.31)

where

$$\lambda_3(\theta_3) = \sqrt{e/d} \ (e^{-1} - \theta_3^2)^{\frac{1}{2}}$$

(2.32)

The solution is given in terms of a displacement function

$$w = Re \ [w^*(\theta_3)]$$

and in the case of self-similar tractions is expressed by the relations

$$u_z^* = \int_0^t \left[\int_0^{\theta_3} w^{*'}(\theta) \ d\theta \right] d\tau$$

$$\tau_{zx}^*/\rho = - e \int_0^{\theta_3} \theta w^{*'}(\theta) \ d\theta$$

(2.33)

$$\tau_{yz}^*/\rho = - d \int_0^{\theta_3} \lambda_3(\theta) \ w^{*'}(\theta) \ d\theta$$

For a given boundary traction the third of Eqs. (2.33) determines the displacement function w (θ) on the boundary. The complete solution is

given by Eq. (2.33).

2.5 Wave Propagation in a Half-Space Resulting from the Sudden Application of a Line Force on the Surface

The determination of the potentials for two-dimensional problems in anisotropic materials follows the same sequence of steps used to determine the potentials in isotropic materials [47, Chapter 2]. Only a brief outline will be given here. The magnitudes of the vertical and horizontal forces are denoted by F_v and F_h.

2.5.1 The Vertical Surface Force

The complex tractions obtained from the boundary conditions can be written in the form

$$\Sigma_y^{*'}(\theta) = -\frac{F_v}{i\pi}$$

$$T_{xy}^{*'}(\theta) = 0 \tag{2.34}$$

which determine, by means of Eq. (2.26) the potentials

$$\Omega_1(\theta) = -\frac{F_v}{i\pi\rho c} \frac{[a\theta^2 + (d-c)\,\lambda_2^2(\theta) - 1]}{[\lambda_1(\theta) - \lambda_2(\theta)]\,[\theta^2 + \lambda_1^2(\theta)]\,R(\theta)}$$

$$\Omega_2(\theta) = \frac{F_v}{i\pi\rho c} \frac{[a\theta^2 + (d-c)\,\lambda_1^2(\theta) - 1]}{[\lambda_1(\theta) - \lambda_2(\theta)]\,[\theta^2 + \lambda_2^2(\theta)]\,R(\theta)} \tag{2.35}$$

The solution for a step vertical line force is then given by the following expressions

$$u_x^* = -\frac{F_v}{i\pi\rho} \sum_{\kappa=1}^{2} \left[\int_0^{\theta_\kappa} \frac{\theta\lambda_\kappa(\theta) [a\theta^2+(d-c)\lambda_{3-\kappa}^2(\theta) - 1]}{[\lambda_\kappa(\theta) - \lambda_{3-\kappa}(\theta)] R(\theta)} d\theta \right]$$

$$u_y^* = \frac{F_v}{i\pi\rho b} \sum_{\kappa=1}^{2} \left[\int_0^{\theta_\kappa} \frac{(1-a\theta^2) [(d-c)\theta^2 + b\lambda_{3-\kappa}^2(\theta) - 1]}{[\lambda_\kappa(\theta) - \lambda_{3-\kappa}(\theta)] R(\theta)} d\theta \right]$$

$$\sigma_x^* = \frac{F_v}{i\pi b} \sum_{\kappa=1}^{2} \left[\frac{\lambda_\kappa(\theta_\kappa) [K_1\theta_\kappa^2(1-a\theta_\kappa^2) + c[a\theta_\kappa^2+b\lambda_{3-\kappa}^2(\theta_\kappa) - 1]]}{\delta_\kappa' [\lambda_\kappa(\theta_\kappa) - \lambda_{3-\kappa}(\theta_\kappa)] R(\theta_\kappa)} + \right.$$
$$\left. + \frac{d\,\lambda_\kappa(\theta_\kappa) [1-b\lambda_{3-\kappa}^2(\theta_\kappa)]}{\delta_\kappa' [\lambda_\kappa(\theta_\kappa) -\lambda_{3-\kappa}(\theta_\kappa)] R(\theta_\kappa)} \right] \qquad (2.36)$$

$$\sigma_y^* = \frac{F_v}{i\pi} \sum_{\kappa=1}^{2} \left[\frac{\lambda_\kappa(\theta_\kappa) (1-a\theta_\kappa^2) [b\lambda_{3-\kappa}^2(\theta_\kappa) - 1]}{\delta_\kappa' [\lambda_\kappa(\theta_\kappa) - \lambda_{3-\kappa}(\theta_\kappa)] R(\theta_\kappa)} + \right.$$
$$\left. + \frac{(c-d)^2 \theta_\kappa^2 \lambda_\kappa(\theta_\kappa) \lambda_{3-\kappa}^2(\theta_\kappa)}{\delta_\kappa'[\lambda_\kappa(\theta_\kappa)-\lambda_{3-\kappa}(\theta_\kappa)] R(\theta_\kappa)} \right]$$

$$\tau_{xy}^* = \frac{F_v}{i\pi b} \sum_{\kappa=1}^{2} \left[\frac{\theta_\kappa(a\theta_\kappa^2-1) (K_1\theta_\kappa^2-b-c+d)}{\delta_\kappa' [\lambda_\kappa(\theta_\kappa) - \lambda_{3-\kappa}(\theta_\kappa)] R(\theta_\kappa)} \right]$$

where

$$\delta_\kappa' = \frac{\partial\delta_\kappa}{\partial\theta_\kappa} = -x-y\lambda_\kappa'(\theta_\kappa) \qquad (2.37)$$

and λ_κ' is the derivative of the function $\lambda_\kappa(\theta_\kappa)$ with respect to θ_κ
(see Eq. (4.3)).

2.5.2 The Horizontal Surface Force

In a similar manner, the complex boundary tractions for the horizontal
surface force are

$$\Sigma_y^{*'}(\theta) = 0$$

$$T_{xy}^{*'}(\theta) = \frac{F_h}{i\pi} \tag{2.38}$$

which determine the potentials

$$\Omega_1(\theta) = \frac{F_h}{i\pi\rho cd} \frac{\lambda_2(\theta)\ [b\{a\theta^2+d\lambda_2^2(\theta) - 1\} - c(c-d)\ \theta^2]}{\theta\ [\lambda_1(\theta) - \lambda_2(\theta)]\ [\theta^2+\lambda_1^2(\theta)]\ R(\theta)}$$

$$\Omega_2(\theta) = -\frac{F_h}{i\pi\rho cd} \frac{\lambda_1(\theta)\ [b\{a\theta^2+d\lambda_1^2(\theta) - 1\} - c(c-d)\ \theta^2]}{\theta\ [\lambda_1(\theta)-\lambda_2(\theta)]\ [\theta^2+\lambda_2^2(\theta)]\ R(\theta)} \tag{2.39}$$

The displacement and stress field for a horizontal line force in the form or a step function in time applied at the origin is given by the following expressions

$$u_x^* = \frac{F_h}{i\pi\rho d} \sum_{\kappa=1}^{2} \left[\int_0^{\theta_\kappa} \frac{\lambda_\kappa(\theta)\ \lambda_{3-\kappa}(\theta)\ [b\{a\theta^2+d\lambda_{3-\kappa}^2(\theta) - 1\} - c(c-d)\theta^2]}{[\lambda_\kappa(\theta) - \lambda_{3-\kappa}(\theta)]\ R(\theta)} d\theta \right]$$

$$u_y^* = -\frac{F_h}{i\pi\rho} \sum_{\kappa=1}^{2} \left[\int_0^{\theta_\kappa} \frac{\theta\lambda_{3-\kappa}(\theta)\ [a\theta^2+(d-c)\ \lambda_\kappa^2(\theta) - 1]}{[\lambda_\kappa(\theta) - \lambda_{3-\kappa}(\theta)]\ R(\theta)} d\theta \right]$$

$$\sigma_x^* = -\frac{F_h}{i\pi} \sum_{\kappa=1}^{2} \left[\frac{\theta_\kappa\ \lambda_\kappa(\theta_\kappa)\ \lambda_{3-\kappa}(\theta_\kappa)\ [K_1\ \lambda_\kappa^2(\theta_\kappa) - a-c+d]}{\delta_\kappa'\ [\lambda_\kappa(\theta_\kappa) - \lambda_{3-\kappa}(\theta_\kappa)]\ R(\theta_\kappa)} \right] \tag{2.40}$$

$$\sigma_y^* = -\frac{F_h}{i\pi} \sum_{\kappa=1}^{2} \left[\frac{\theta_\kappa\ \lambda_\kappa(\theta_\kappa)\ \lambda_{3-\kappa}(\theta_\kappa)\ (K_1\theta_\kappa^2 - b-c+d)}{\delta_\kappa'\ [\lambda_\kappa(\theta_\kappa)-\lambda_{3-\kappa}(\theta_\kappa)]\ R(\theta_\kappa)} \right]$$

$$\tau_{xy}^* = -\frac{F_h}{i\pi} \sum_{\kappa=1}^{2} \left[\frac{\lambda_{3-\kappa}(\theta_\kappa)\ [(c-d)^2\ \theta_\kappa^2\ \lambda_\kappa^2(\theta_\kappa) + (a\theta_\kappa^2-1)\ [1-b\lambda_\kappa^2(\theta_\kappa)]}{\delta_\kappa'\ [\lambda_\kappa(\theta_\kappa) - \lambda_{3-\kappa}(\theta_\kappa)]\ R(\theta_\kappa)} \right]$$

2.6 Reflection of Waves from a Plane Boundary

When a disturbance generated by a source in the interior of a half-space reaches the free surface the conditions imposed by the presence of the boundary must be fulfilled. The result is the creation of reflected and surface waves. Prior to the arrival of the incident waves, the motion of the body is not affected by the presence of the free surface; i.e. the displacements and stresses are identical with the solution in an unbounded medium. Upon arrival of each incident wave at the surface, two reflected waves appear and their effect on the solution is represented by corresponding potentials which must be determined.

Since the characteristic surfaces of the quasi-longitudinal and quasi-transverse incident waves must pass through point $x=0$, $y=y_0$ where the force is applied, they can be expressed by the equations

$$\delta_\kappa \equiv t - x\theta_\kappa - (y-y_0)\,\lambda_\kappa(\theta_\kappa) = 0 \quad (\kappa=1,\,2) \tag{2.41}$$

In the Smirnov-Sobolev procedure it is essential to parametrize the characteristic surfaces of the reflected waves in a way that each incident and its two reflected waves are given by the same value of the parameter on the free surface $y=0$. Thus, if $\kappa=1$ in Eqs. (2.41) denotes the quasi-longitudinal wave, the characteristic surfaces for the reflected quasi-longitudinal wave are

$$\delta_{11} \equiv t - x\theta_{11} + (y+y_0)\,\lambda_1(\theta_{11}) = 0 \tag{2.42}$$

and the surfaces for the reflected quasi-transverse are

$$\delta_{12} \equiv t - x\theta_{12} + y\lambda_2(\theta_{12}) + y_0\lambda_1(\theta_{12}) = 0 \tag{2.43}$$

Similarly, the reflected quasi-longitudinal and quasi-transverse waves produced by an incident quasi-transverse wave are expressed respectively by

$$\delta_{21} \equiv t - x\theta_{21} + y\lambda_1(\theta_{21}) + y_0\lambda_2(\theta_{21}) = 0 \tag{2.44}$$

$$\delta_{22} \equiv t - x\theta_{22} + (y+y_0)\,\lambda_2(\theta_{22}) = 0 \tag{2.45}$$

It can be shown that the conditions of a free-traction boundary (i.e., $\sigma_y = 0$, $\tau_{xy} = 0$ on $y=0$) provide the necessary equations to determine the reflected potentials. Straightforward algebraic work leads to the following expressions

$$\Omega_{11}(\theta) = \frac{\lambda_1(\theta) + \lambda_2(\theta)}{\lambda_1(\theta) - \lambda_2(\theta)}\,\Omega_1(\theta)$$

$$\Omega_{12}(\theta) = \frac{2\,\lambda_1(\theta)}{c\,[\lambda_1(\theta) - \lambda_2(\theta)]}\,\frac{[\theta^2 + \lambda_1^2(\theta)]}{[\theta^2 + \lambda_2^2(\theta)]}\,\frac{R_1(\theta)}{R(\theta)}\,\Omega_1(\theta)$$

$$\tag{2.46}$$

$$\Omega_{21}(\theta) = -\frac{2\lambda_2(\theta)}{c\,[\lambda_1(\theta) - \lambda_2(\theta)]}\,\frac{[\theta^2 + \lambda_2^2(\theta)]}{[\theta^2 + \lambda_1^2(\theta)]}\,\frac{R_2(\theta)}{R(\theta)}\,\Omega_2(\theta)$$

$$\Omega_{22}(\theta) = -\frac{\lambda_1(\theta) + \lambda_2(\theta)}{\lambda_1(\theta) - \lambda_2(\theta)}\,\frac{\tilde{R}(\theta)}{R(\theta)}\,\Omega_2(\theta)$$

where

$$R_\kappa(\theta) = (K_1\,\theta^2 - b - c + d)\,[a\theta^2 + d\lambda_\kappa^2(\theta) - 1] \tag{2.47}$$

and

$$\tilde{R}(\theta) = (K_1\,\theta^2 - b)\,\lambda_1(\theta)\,\lambda_2(\theta) - a\theta^2 + 1 \tag{2.48}$$

The double-indexed reflected potentials are related to the incident potentials having the same first index while the second index indicates the type of wave, i.e. $\kappa=1$ refers to quasi-longitudinal and $\kappa=2$ to quasi-transverse waves. For example, $\Omega_{12}(\theta)$ indicates the potential of the reflected quasi-transverse wave caused from an incident quasi-longitudinal wave. The displacements and stresses for self-similar potential problems can be written

$$
u_x^* = \frac{\partial}{\partial t} \sum_{\kappa=1}^{2} \left[\int_0^{\theta_\kappa} c\theta\lambda_\kappa(\theta)\,[\theta^2 + \lambda_\kappa^2(\theta)]\,\Omega_\kappa(\theta)\,d\theta + \right.
$$
$$
\left. + \sum_{j=1}^{2} \int_0^{\theta_{\kappa j}} c\theta\lambda_j(\theta)\,[\theta^2 + \lambda_j^2(\theta)]\,\Omega_{\kappa j}(\theta)\,d\theta \right]
$$

$$
u_y^* = -\frac{\partial}{\partial t} \sum_{\kappa=1}^{2} \left[\int_0^{\theta_\kappa} [\theta^2 + \lambda_\kappa^2(\theta)]\,[a\theta^2 + d\lambda_\kappa^2(\theta) - 1]\,\Omega_\kappa(\theta)\,d\theta - \right.
$$
$$
\left. - \sum_{j=1}^{2} \int_0^{\theta_{\kappa j}} [\theta^2 + \lambda_j^2(\theta)]\,[a\theta^2 + d\lambda_j^2(\theta) - 1]\,\Omega_{\kappa j}(\theta)\,d\theta \right]
$$

$$
\sigma_x^*/\rho = \frac{\partial^2}{\partial t^2} \sum_{\kappa=1}^{2} \left[\int_0^{\theta_\kappa} \lambda_\kappa(\theta)\,L_\kappa(\theta)\,\Omega_\kappa(\theta)\,d\theta + \right. \qquad (2.49)
$$
$$
\left. + \sum_{j=1}^{2} \int_0^{\theta_{\kappa j}} \lambda_j(\theta)\,L_j(\theta)\,\Omega_{\kappa j}(\theta)\,d\theta \right]
$$

$$
\sigma_y^*/\rho = \frac{\partial^2}{\partial t^2} \sum_{\kappa=1}^{2} \left[\int_0^{\theta_\kappa} \lambda_\kappa(\theta)\,S_\kappa(\theta)\,\Omega_\kappa(\theta)\,d\theta + \right.
$$
$$
\left. + \sum_{j=1}^{2} \int_0^{\theta_{\kappa j}} \lambda_j(\theta)\,S_j(\theta)\,\Omega_{\kappa j}(\theta)\,d\theta \right]
$$

$$\tau_{xy}^*/\rho = \frac{\partial^2}{\partial t^2} \sum_{\kappa=1}^{2} \left[\int_0^{\theta_\kappa} \theta M_\kappa(\theta)\, \Omega_\kappa(\theta)\, d\theta - \right.$$

$$\left. - \sum_{j=1}^{2} \int_0^{\theta_{\kappa j}} \theta M_j(\theta)\, \Omega_{\kappa j}(\theta)\, d\theta \right]$$

The above equations simplify considerably for points on the surface, where

$$\theta_1 = \theta_{11} = \theta_{12} \qquad \text{and} \qquad \theta_2 = \theta_{21} = \theta_{22} \qquad (2.50)$$

It is not difficult to show that for a force parallel to the y-axis the incident potentials are

$$\Omega_1^v(\theta) = - \frac{F_v}{2i\pi\rho bd} \frac{1}{\lambda_1(\theta)\,[\lambda_1^2(\theta) - \lambda_2^2(\theta)]\,[\theta^2+\lambda_1^2(\theta)]}$$

$$\Omega_2^v(\theta) = \frac{F_v}{2i\pi\rho bd} \frac{1}{\lambda_2(\theta)\,[\lambda_1^2(\theta) - \lambda_2^2(\theta)]\,[\theta^2+\lambda_2^2(\theta)]} \qquad (2.51)$$

and for a force parallel to the x-axis

$$\Omega_1^h(\theta) = - \frac{F_h}{2i\pi\rho cd} \frac{a\theta^2+d\lambda_2^2(\theta) - 1}{\theta\,[\lambda_1^2(\theta) - \lambda_2^2(\theta)]\,(1-a\theta^2)\,[\theta^2+\lambda_1^2(\theta)]}$$

$$\Omega_2^h(\theta) = \frac{F_h}{2i\pi\rho cd} \frac{a\theta^2+d\lambda_1^2(\theta) - 1}{\theta[\lambda_1^2(\theta) - \lambda_2^2(\theta)]\,(1-a\theta^2)\,[\theta^2+\lambda_2^2(\theta)]} \qquad (2.52)$$

Therefore, the general solution to a line force applied at x=0, y=0 parallel to the positive x or y axis and varying as a step function in time can be determined from Eqs. (2.49) by integrating once with respect to time. In this way, all the functions involved are determined completely.

2.7 Surface Displacements and Stresses

The examination of the dynamic response of a point located on the free surface y=0, due to a disturbance in the interior of a half space is greatly simplified by the relations in Eq. (2.50). After some algebraic manipulations, the surface displacements and stresses for a step force applied at $y=y_0$ and parallel to the surface can be written as

$$u_{x0}^{*(H)} = \frac{F_h}{i\pi\rho db} \sum_{\kappa=1}^{2} \left[\int_0^{\theta_\kappa} \frac{\lambda_\kappa(\theta)\ \lambda_{3-\kappa}(\theta)\ U_{x\kappa}^{(H)}}{[\lambda_\kappa(\theta)-\lambda_{3-\kappa}(\theta)]\ [\lambda_\kappa^2(\theta)-\lambda_{3-\kappa}^2(\theta)]\ R(\theta)}\ d\theta \right]$$

$$u_{y0}^{*(H)} = \frac{F_h}{i\pi\rho db} \sum_{\kappa=1}^{2} \left[\int_0^{\theta_\kappa} \frac{\theta\lambda_\kappa(\theta)\ U_{y\kappa}^{(H)}(\theta)}{[\lambda_\kappa(\theta)-\lambda_{3-\kappa}(\theta)]\ [\lambda_\kappa^2(\theta)-\lambda_{3-\kappa}^2(\theta)]\ R(\theta)}\ d\theta \right]$$

$$\sigma_{x0}^{*(H)} = \frac{F_h}{i\pi bd} \sum_{\kappa=1}^{2} \left[\frac{\theta_\kappa\ \lambda_\kappa(\theta_\kappa)\ \lambda_{3-\kappa}(\theta_\kappa)\ U_{\sigma\kappa}^{(H)}(\theta_\kappa)}{\delta_\kappa'[\lambda_\kappa(\theta_\kappa)-\lambda_{3-\kappa}(\theta_\kappa)]\ [\lambda_\kappa^2(\theta_\kappa)-\lambda_{3-\kappa}^2(\theta_\kappa)]\ R(\theta_\kappa)} \right]$$

$$(2.53)$$

$$\sigma_{y0}^{*(H)} = \tau_{xy}^{*(H)} = 0$$

where

$$U_{x\kappa}^{(H)}(\theta) = (K_1\theta^2-b)\ [d\theta^2+b\lambda_\kappa^2(\theta)-1]-$$
$$-b[a\theta^2+d\lambda_{3-\kappa}^2(\theta)-1] + c\theta^2(K_1\theta^2-b-c+d) \qquad (2.54)$$

$$U_{y\kappa}^{(H)}(\theta) = (K_1\theta^2-b-c+d)\ [a\theta^2+d\lambda_{3-\kappa}^2(\theta)-1] +$$
$$+c(K_1\theta^2-b)\ \lambda_{3-\kappa}^2(\theta) - c(a\theta^2-1) \qquad (2.55)$$

$$U_{\sigma\kappa}^{(H)}(\theta) = a(K_1\theta^2-b+d)\ [d\theta^2+b\lambda_\kappa^2(\theta)-1] +$$

$$+ d(K_1\theta^2-b-2c+d)\ [a\theta^2+d\lambda_{3-\kappa}^2(\theta) - 1] + c(K_1\theta^2-b-2c+d) -$$

$$- c(c-d)\ (K_1\theta^2-b)\ \lambda_\kappa^2(\theta)-cd(K_1\ \theta^2-b-c)\ \lambda_{3-\kappa}^2(\theta) \tag{2.56}$$

and

$$\delta_\kappa' = -x + y_0\ \lambda_\kappa'(\theta_\kappa) \tag{2.57}$$

When the force is perpendicular to the surface the expressions for the surface displacements are

$$u_{x0}^{*(v)} = -\ \frac{F_v}{i\pi\rho db}\ \sum_{\kappa=1}^{2}\ \left[\ \int_0^{\theta_\kappa} \frac{\theta\lambda_{3-\kappa}(\theta)\ U_{x\kappa}^{(v)}(\theta)}{[\lambda_\kappa(\theta)-\lambda_{3-\kappa}(\theta)]\ [\lambda_\kappa^2(\theta)-\lambda_{3-\kappa}^2(\theta)]\ R(\theta)}\ d\theta\ \right]$$

$$\tag{2.58}$$

$$u_{y0}^{*(v)} = \frac{F_h}{i\pi\rho db^2}\ \sum_{\kappa=1}^{2}\ \left[\ \int_0^{\theta_\kappa} \frac{(1-a\theta^2)\ U_{y\kappa}^{(v)}(\theta)}{[\lambda_\kappa(\theta)-\lambda_{3-\kappa}(\theta)]\ [\lambda_\kappa^2(\theta)-\lambda_{3-\kappa}^2(\theta)]\ R(\theta)}\ d\theta\ \right]$$

where

$$U_{x\kappa}^{(v)}(\theta) = (K_1\theta^2-b-c+d)\ [a\theta^2+d\lambda_\kappa^2(\theta)-1] +$$

$$+ c[(K_1\theta^2-b)\ \lambda_\kappa^2(\theta) + (1-a\theta^2)] = U_{y(3-\kappa)}^{(H)}(\theta) \tag{2.59}$$

$$U_{y\kappa}^{(v)}(\theta) = (K_1\theta^2-b)\ [d\theta^2+b\lambda_{3-\kappa}^2(\theta) - 1] - b\ [a\theta^2+d\lambda_\kappa^2(\theta) - 1] +$$

$$+ c\theta^2(K_1\theta^2-b-c+d) = U_{x(3-\kappa)}^{(H)}(\theta) \tag{2.60}$$

The stresses are

$$\sigma_{x0}^{*(v)} = - \frac{F_v}{i\pi db^2} \sum_{\kappa=1}^{2} \left[\frac{U_{\sigma K}^{(v)}(\theta_\kappa)}{\delta_\kappa' [\lambda_\kappa(\theta_\kappa) - \lambda_{3-\kappa}(\theta_\kappa)]} \times \right.$$

$$\left. \times \frac{\lambda_{3-\kappa}(\theta_\kappa)}{[\lambda_\kappa^2(\theta_\kappa) - \lambda_{3-\kappa}^2(\theta_\kappa)] R(\theta_\kappa)} \right] \qquad (2.61)$$

$$\sigma_{y0}^{*(v)} = \tau_{xy}^{*(v)} = 0$$

where

$$U_{\sigma K}^{*(v)}(\theta_\kappa) = b \left[d \left[a\theta_\kappa^2 + d\lambda_\kappa^2(\theta_\kappa) - 1 \right] + c \left[1 - d\lambda_\kappa^2(\theta_\kappa) \right] \right] \times$$
$$\times \left[(K_1\theta_\kappa^2 - b) \lambda_\kappa^2(\theta_\kappa) - a\theta_\kappa^2 + 1 \right] +$$
$$+ \theta_\kappa^2 (K_1\theta_\kappa^2 - b - c + d) \left[cd(a\theta_\kappa^2 - 1) - ad \left[d\theta_\kappa^2 + b\lambda_{3-\kappa}^2(\theta_\kappa) - \right. \right.$$
$$\left. \left. - 1 \right] + c^2 \right] \qquad (2.62)$$

3. THE POINT FORCE IN A TRANSVERSELY
ISOTROPIC HALF SPACE

3.1 General Remarks

Anisotropic materials possessing an axis of elastic symmetry at each point such that all directions perpendicular to that axis are equivalent are called transversely isotropic. The propagation of transient disturbances in media of this type is a subject of both mathematical and geophysical interest. Highly compressed sedimentary material where the vertical compression induces significantly different properties in that direction can be modeled as transversely isotropic. Of particular importance in seismology and earthquake engineering are composite media having different isotropic layers. When the thickness of individual layers is small compared with wave-length, many of the characteristics of elastic wave propagation are similar to those of transversely isotropic media. Backus [4] has given conditions under which the homogeneous, transversely isotropic medium can indeed be the long-wave equivalent of a layered isotropic medium made of just two homogeneous, isotropic materials.

The high degree of symmetry exhibited by transversely isotropic materials reduces the number of independent elastic constants required to define its behavior to five [21,§105]. The same number of constants is also required by hexagonal crystals which have an axis of elastic symmetry of order six. Hence, "transverse isotropy" and "hexagonal aeolotropy" are used interchangeably.

Very few solutions for any but trivial problems are available in the literature even for isotropic materials in a three-dimensional space. This study utilitizes the method of rotational superposition of plane and anti-

plane problems to obtain solutions for the problem of a suddenly applied point force on the surface of a transversely isotropic half-space. The axis of elastic symmetry is taken perpendicular to the free surface. The case of the subsurface load, although not treated here, can be obtained by utilizing the same technique on the two-dimensional solutions for the point force in the interior of the half-space given at the end of Chapter 2.

3.2 Equations of Motion

Consider a cylindrical coordinate system (r, ω, y) where the y-axis is parallel to the axis of elastic symmetry. The stress-strain relations for a transversely isotropic material can be written as

$$\sigma_r = c_{11} \epsilon_r + c_{13} \epsilon_\omega + c_{12} \epsilon_y$$

$$\sigma_\omega = c_{13} \epsilon_r + c_{11} \epsilon_\omega + c_{12} \epsilon_y$$

$$\sigma_y = c_{12} (\epsilon_r + \epsilon_\omega) + c_{22} \epsilon_y \tag{3.1}$$

$$\tau_{ry} = c_{66} \gamma_{ry}$$

$$\tau_{y\omega} = c_{66} \gamma_{y\omega}$$

$$\tau_{r\omega} = \frac{(c_{11} - c_{13})}{2} \gamma_{r\omega}$$

The equations of equilibrium for the medium are

$$\frac{\partial \sigma_r}{\partial r} + \frac{1}{r} \frac{\partial \tau_{r\omega}}{\partial \omega} + \frac{\partial \tau_{ry}}{\partial y} + \frac{\sigma_r - \sigma_\omega}{r} + Z_r = 0$$

$$\frac{\partial \tau_{r\omega}}{\partial r} + \frac{1}{r} \frac{\partial \sigma_\omega}{\partial \omega} + \frac{\partial \tau_{y\omega}}{\partial y} + \frac{2\tau_{r\omega}}{r} + Z_\omega = 0 \qquad (3.2)$$

$$\frac{\partial \tau_{ry}}{\partial r} + \frac{1}{r} \frac{\partial \tau_{y\omega}}{\partial \omega} + \frac{\partial \sigma_y}{\partial y} + \frac{\tau_{ry}}{r} + Z_y = 0$$

where Z_r, Z_ω and Z_y are the body forces. The application of the usual
small strain, small rotation strain-displacement relations

$$\varepsilon_r = \frac{\partial u_r}{\partial r} \qquad\qquad \gamma_{ry} = \frac{\partial u_r}{\partial y} + \frac{\partial u_y}{\partial r}$$

$$\varepsilon_\omega = \frac{u_r}{r} + \frac{1}{r} \frac{\partial u_\omega}{\partial \omega} \qquad\qquad \gamma_{y\omega} = \frac{\partial u_\omega}{\partial y} + \frac{1}{r} \frac{\partial u_y}{\partial \omega} \qquad (3.3)$$

$$\varepsilon_y = \frac{\partial u_y}{\partial y} \qquad\qquad \gamma_{r\omega} = \frac{1}{r} \frac{\partial u_r}{\partial \omega} + \frac{\partial u_\omega}{\partial r} - \frac{u_\omega}{r}$$

to Eqs. (3.1) and (3.2) results in the following equations of motion in
terms of the displacements

$$c_{11} \frac{\partial^2 u_r}{\partial r^2} + c_{66} \frac{\partial^2 u_r}{\partial y^2} + \frac{c_{11}-c_{13}}{2r^2} \frac{\partial^2 u_r}{\partial \omega^2} + (c_{12}+c_{66}) \frac{\partial^2 u_y}{\partial r \partial y} +$$

$$+ \frac{c_{11}+c_{13}}{2r} \frac{\partial^2 u_\omega}{\partial r \partial \omega} + \frac{c_{11}}{r} \frac{\partial u_r}{\partial r} + \frac{3c_{11}-c_{13}}{2r^2} \frac{\partial u_\omega}{\partial \omega} - \frac{c_{11}}{r^2} u_r = \rho \frac{\partial^2 u_r}{\partial t^2}$$

$$\frac{c_{11}+c_{13}}{2r} \frac{\partial^2 u_r}{\partial r \partial \omega} + \frac{c_{12}+c_{66}}{r} \frac{\partial^2 u_y}{\partial y \partial \omega} + \frac{c_{11}-c_{13}}{2} \frac{\partial^2 u_\omega}{\partial r^2} + c_{66} \frac{\partial^2 u_\omega}{\partial y^2} + \qquad (3.4)$$

$$+ \frac{c_{11}}{r^2} \frac{\partial^2 u_\omega}{\partial \omega^2} + \frac{3c_{11}-c_{13}}{2r^2} \frac{\partial u_r}{\partial \omega} + \frac{c_{11}-c_{13}}{2r} \frac{\partial u_\omega}{\partial r} - \frac{c_{11}-c_{13}}{2r^2} u_\omega = \rho \frac{\partial^2 u_\omega}{\partial t^2}$$

$$(c_{12} + c_{66}) \frac{\partial^2 u_r}{\partial r \partial y} + c_{66} \frac{\partial^2 u_y}{\partial r^2} + c_{22} \frac{\partial^2 u_y}{\partial y^2} + \frac{c_{66}}{r^2} \frac{\partial^2 u_y}{\partial \omega^2} +$$

$$+ \frac{c_{12}+c_{66}}{r} \frac{\partial^2 u_\omega}{\partial y \partial \omega} + \frac{c_{12}+c_{66}}{r} \frac{\partial u_r}{\partial y} + \frac{c_{66}}{r} \frac{\partial u_y}{\partial r} = \rho \frac{\partial^2 u_y}{\partial t^2}$$

In addition to the elastic parameters defined by Eq. (2.7) a further constant "e" is often introduced,

$$e = \frac{c_{11} - c_{13}}{2\rho} \tag{3.5}$$

Solutions will be given in terms of the five elastic parameters a, b, c, d and e which must satisfy the conditions

$$a>0, \ b>0, \ d>0, \ e>0, \ b(a-e) - (c-d)^2 > 0 \tag{3.6}$$

These are equivalent to the requirement that the strain energy be positive.

3.3 The Method of Rotational Superposition

The application of the method of rotational superposition to solve certain three-dimensional wave propagation problems in isotropic materials can be found in references [12, 18, 47]. Some repetition of the basic principles cannot be avoided in applying the method to anisotropic materials.

Consider the half space of Fig. 1, where (X, Y) defines the plane of deformation for the plane strain and antiplane problems, and (x, y) is the reference plane for the coordinate angle ω. If U_X, U_Y denote the displacements of the plane problem and U_Z the displacement of the antiplane problem, their contribution to the three dimensional displacements at point P (r, ω, y) can be expressed by the relations

$$u_r = U_X \ [r\cos (\omega_0 - \omega), \ Y, \ t] \cos (\omega_0 - \omega) -$$

$$- U_Z \ [r\cos (\omega_0 - \omega), \ Y, \ t] \sin (\omega_0 - \omega)$$

$$u_\omega = U_X \ [r\cos (\omega_0 - \omega), \ Y, \ t] \sin (\omega_0 - \omega) +$$

$$+ U_Z \ [r\cos (\omega_0-\omega), \ Y, \ t] \cos (\omega_0-\omega) \qquad (3.7)$$

$$u_y = U_Y \ [r\cos (\omega_0-\omega), \ Y, \ t]$$

The superposition of the effects of all plane and antiplane problems at different angular orientations ω_0 multiplied by weighting functions $f_1(\omega_0)$ and $f_2(\omega_0)$ which are going to be defined later, results in a three-dimensional wave field for isotropic materials [18]. The same principle applied in the present case gives the expressions

$$u_r = \int_0^\pi U_X \ [r\cos (\omega_0-\omega), \ Y, \ t] \cos (\omega_0-\omega) \ f_1 \ (\omega_0) \ d\omega_0 -$$
$$- \int_0^\pi U_Z \ [r\cos (\omega_0-\omega), \ Y, \ t] \sin (\omega_0-\omega) \ f_2 \ (\omega_0) \ d\omega_0$$
$$u_\omega = \int_0^\pi U_X \ [r\cos (\omega_0-\omega), \ Y, \ t] \sin (\omega_0-\omega) \ f_1 \ (\omega_0) \ d\omega_0 + \qquad (3.8)$$
$$+ \int_0^\pi U_Z \ [r\cos (\omega_0-\omega), \ Y, \ t] \cos (\omega_0-\omega) \ f_2 \ (\omega_0) \ d\omega_0$$
$$u_y = \int_0^\pi U_Y \ [r\cos (\omega_0-\omega), \ Y, \ t] \ f_1 \ (\omega_0) \ d\omega_0$$

Straightforward application of these displacements to the equations of motion (3.4) shows that the latter are satisfied if

$$c_{11} \frac{\partial^2 U_X}{\partial X^2} + c_{66} \frac{\partial^2 U_X}{\partial Y^2} + (c_{12}+c_{66}) \frac{\partial^2 U_Y}{\partial X \partial Y} = \rho \ \frac{\partial^2 U_X}{\partial t^2}$$

$$(c_{12}+c_{66}) \frac{\partial^2 U_X}{\partial X \partial Y} + c_{66} \frac{\partial^2 U_Y}{\partial X^2} + c_{22} \frac{\partial^2 U_Y}{\partial Y^2} = \rho \ \frac{\partial^2 U_Y}{\partial t^2} \qquad (3.9a)$$

and

$$\frac{c_{11}-c_{13}}{2} \frac{\partial^2 U_Z}{\partial X^2} + c_{66} \frac{\partial^2 U_Z}{\partial Y^2} = \rho \ \frac{\partial^2 U_Z}{\partial t^2} \qquad (3.9b)$$

These are the equations of motion for the plane strain and antiplane problems. Consequently, the rotational superposition of plane solutions results in a three-dimensional field which satisfies the equations of motion and thus, by uniqueness, is the solution. It is interesting to see what happens to stresses under this operation. By use of Eqs. (3.1), (3.3) and (3.8) it is not difficult to arrive at the expressions

$$
\sigma_r = \int_0^\pi \left\{ [c_{11} \cos^2 (\omega_0 - \omega) + c_{13} \sin^2 (\omega_0 - \omega)] \frac{\partial U_X}{\partial X} + \right.
$$
$$
\left. + c_{12} \frac{\partial U_Y}{\partial Y} \right\} f_1(\omega_0) \; d\omega_0 -
$$
$$
- \frac{(c_{11} - c_{13})}{2} \int_0^\pi \frac{\partial U_Z}{\partial X} \sin 2(\omega_0 - \omega) \; f_2(\omega_0) \; d\omega_0
$$

$$
\sigma_\omega = \int_0^\pi \left\{ [c_{11} \sin^2(\omega_0 - \omega) + c_{13} \cos^2(\omega_0 - \omega)] \frac{\partial U_X}{\partial X} + \right.
$$
$$
\left. + c_{12} \frac{\partial U_Y}{\partial Y} \right\} f_1(\omega_0) \; d\omega_0 +
$$
$$
+ \frac{c_{11} - c_{13}}{2} \int_0^\pi \frac{\partial U_Z}{\partial X} \sin 2(\omega_0 - \omega) \; f_2(\omega_0) \; d\omega_0
$$

$$
\sigma_y = \int_0^\pi [c_{12} \frac{\partial U_X}{\partial X} + c_{22} \frac{\partial U_Y}{\partial Y}] \; f_1(\omega_0) \; d\omega_0
$$

$$
\tau_{ry} = \int_0^\pi c_{66} \left[\frac{\partial U_X}{\partial Y} + \frac{\partial U_Y}{\partial X} \right] \cos (\omega_0 - \omega) \; f_1(\omega_0) \; d\omega_0 - \tag{3.10}
$$
$$
- \int_0^\pi c_{66} \frac{\partial U_Z}{\partial Y} \sin (\omega_0 - \omega) \; f_2(\omega_0) \; d\omega_0
$$

$$
\tau_{y\omega} = \int_0^\pi c_{66} \left[\frac{\partial U_X}{\partial Y} + \frac{\partial U_Y}{\partial X} \right] \sin(\omega_0 - \omega) \; f_1(\omega_0) \; d\omega_0 +
$$
$$
+ \int_0^\pi c_{66} \frac{\partial U_Z}{\partial Y} \cos(\omega_0 - \omega) \; f_2(\omega_0) \; d\omega_0
$$

$$\tau_{r\omega} = \int_0^\pi \frac{c_{11}-c_{13}}{2} \frac{\partial U_X}{\partial X} \sin 2(\omega_0-\omega) \ f_1(\omega_0) \ d\omega_0 +$$

$$+ \int_0^\pi \frac{c_{11}-c_{13}}{2} \frac{\partial U_Z}{\partial X} \cos 2(\omega_0-\omega) \ f_2(\omega_0) \ d\omega_0$$

By virtue of the relations between stresses, strains and displacements in the two-dimensional case, these equations can be rewritten

$$\sigma_r = \int_0^\pi \Sigma_X \ f_1(\omega_0) \ d\omega_0 - (c_{11}-c_{13}) \int_0^\pi E_X \sin^2(\omega_0-\omega) \ f_1(\omega_0) \ d\omega_0 -$$

$$- \int_0^\pi T_{XZ} \sin 2(\omega_0-\omega) \ f_2(\omega_0) \ d\omega_0$$

$$\sigma_\omega = \int_0^\pi \Sigma_X \ f_1(\omega_0) \ d\omega_0 - (c_{11}-c_{13}) \int_0^\pi E_X \cos^2(\omega_0-\omega) \ f_1(\omega_0) \ d\omega_0 +$$

$$+ \int_0^\pi T_{XZ} \sin 2(\omega_0-\omega) \ f_2(\omega_0) \ d\omega_0$$

$$\sigma_y = \int_0^\pi \Sigma_Y \ f_1(\omega_0) \ d\omega_0 \tag{3.11}$$

$$\tau_{ry} = \int_0^\pi T_{XY} \cos(\omega_0-\omega) \ f_1(\omega_0) \ d\omega_0 -$$

$$- \int_0^\pi T_{YZ} \sin(\omega_0-\omega) \ f_2(\omega_0) \ d\omega_0$$

$$\tau_{y\omega} = \int_0^\pi T_{XY} \sin(\omega_0-\omega) \ f_1(\omega_0) \ d\omega_0 +$$

$$+ \int_0^\pi T_{YZ} \cos(\omega_0-\omega) \ f_2(\omega_0) \ d\omega_0$$

$$\tau_{r\omega} = \frac{c_{11}-c_{13}}{2} \int_0^\pi E_X \sin 2(\omega_0-\omega) \ f_1(\omega_0) \ d\omega_0 +$$

$$+ \int_0^\pi T_{XZ} \cos 2(\omega_0-\omega) \ f_2(\omega_0) \ d\omega_0$$

Here, Σ_X, Σ_Y, T_{XY}, T_{XZ}, T_{YZ} denote the stresses and E_X the strain in the X-direction of the two-dimensional problems. It can be seen that σ_y, τ_{ry} and $\tau_{y\omega}$ are formed by a rotational superposition of the two-dimensional

stresses, while the remaining stresses involve additional terms. This is a very important observation because the three quantities σ_y, τ_{ry}, $\tau_{y\omega}$ must be specified on the boundary to define the three-dimensional problem. Thus, by inversion of the three integral equations involved, the two-dimensional quantities can be determined.

The rotational superposition of plane strain and antiplane problems in anisotropic media must be differentiated from the same method as applied in the case of isotropy. There, the medium for each contributing plane or antiplane solution is the same and the superposition of the wave fields is a natural consequence. On the contrary, the solutions that have been superimposed in this study correspond to two quite different materials. It is a remarkable fact that the rotational superposition of the plane displacement fields leads to expressions for the stresses σ_y, τ_{ry}, and $\tau_{y\omega}$ which can be solved easily to define the two-dimensional problems.

3.4 Axisymmetric Problems

A three-dimensional axisymmetric problem can be solved by a rotational superposition of the solution of a unique plane strain problem [12,18]. The determination of the plane problem is simplified by observing that the two-dimensional field must be symmetric. Here, the weighting functions are taken as

$$f_1(\omega_0) = 1$$
$$f_2(\omega_0) = 0$$

(3.12)

44

After introduction of the new variable $W = \omega - \omega_0$, the displacements and stresses are rewritten as

$$u_r = \int_0^\pi U_X [r\cos W, Y, t] \cos W \, dW$$

$$u_\omega = 0$$

$$u_y = \int_0^\pi U_Y [r\cos W, Y, t] \, dW$$

$$\sigma_r = \int_0^\pi \left(\Sigma_X [r\cos W, Y, t] - \right.$$
$$\left. - (c_{11} - c_{13}) \, E_X [r\cos W, Y, t] \sin^2 W \right) dW \qquad (3.13)$$

$$\sigma_\omega = \int_0^\pi \left(\Sigma_X [r\cos W, Y, t] - (c_{11} - c_{13}) \, E_X [r\cos W, Y, t] \cos^2 W \right) dW$$

$$\sigma_y = \int_0^\pi \Sigma_Y [r\cos W, Y, t] \, dW$$

$$\tau_{ry} = \int_0^\pi T_{XY} [r\cos W, Y, t] \cos W \, dW$$

$$\tau_{r\omega} = \tau_{y\omega} = 0$$

An especially convenient form of the boundary tractions σ_y and τ_{ry} on the y=0 plane can be obtained by using the transformation $\upsilon = r\cos W$:

$$\sigma_y(r, 0, t) = 2 \int_0^r \Sigma_Y(\upsilon, 0, t) \frac{d\upsilon}{\sqrt{r^2 - \upsilon^2}}$$

$$\tau_{ry}(r, 0, t) = \frac{2}{r} \int_0^r T_{XY}(\upsilon, 0, t) \frac{\upsilon d\upsilon}{\sqrt{r^2 - \upsilon^2}}$$

$$(3.14)$$

These are integral equations of the Abel type [14]. Their solutions are

$$\Sigma_Y(X, 0, t) = \frac{1}{\pi} \frac{\partial}{\partial X} \int_0^X \sigma_y(\upsilon, 0, t) \frac{\upsilon d\upsilon}{\sqrt{X^2 - \upsilon^2}}$$

$$T_{XY}(X, 0, t) = \frac{1}{\pi X} \frac{\partial}{\partial X} \int_0^X \tau_{ry}(\upsilon, 0, t) \frac{\upsilon^2 d\upsilon}{\sqrt{X^2 - \upsilon^2}}$$

(3.15)

which give the boundary tractions of the plane strain problem in terms of those of the original three-dimensional problem. The methods of Chapter 2 are now applicable to solve the two-dimensional problem. The final three-dimensional case is found by integrating this solution as in Eq. (3.13).

3.4.1 The Vertical Point Force

Consider a transversely isotropic half-space subjected to a normal stress σ_0 applied over a circular region expanding in time. The speed of expansion is α and the center coincides with the origin of the coordinate system. The boundary conditions can be written

$$\left. \begin{array}{lll} \sigma_y = -\sigma_0 & \text{for} & r \le \alpha t \\ \quad = 0 & \text{for} & r > \alpha t \\ \tau_{yr} = \tau_{y\omega} = 0 & \text{for} & 0 \le r < \infty \end{array} \right\} \begin{array}{l} 0 \le \omega < 2\pi \\ y=0 \end{array}$$

(3.16)

and correspond to a loading with a total vertical force $V = \pi\alpha^2 t^2 \sigma_0 = F_v t^2$ where $F_v = \pi\alpha^2 \sigma_0$. By means of Eqs. (3.15) the plane strain problem is defined by the conditions on the $y=0$ plane

$$\Sigma_Y = - \frac{F_V}{\pi^2 \alpha^2} \qquad\qquad \text{for} \qquad |X| \leq \alpha t$$

$$= - \frac{F_V}{\pi^2 \alpha^2} \left[1 - \frac{|X|}{\sqrt{X^2 - \alpha^2 t^2}} \right] \qquad \text{for} \qquad |X| > \alpha t \qquad (3.17)$$

$$T_{XY} = 0 \qquad\qquad \text{for} \qquad -\infty < X < +\infty$$

The complex tractions can be obtained by Eq. (2.22), or in this particular case, by inspection, i.e.

$$\Sigma_Y^* = - \frac{F_V}{\pi^2 \alpha^2} \left[1 - \frac{1}{(1 - \alpha^2 \theta^2)^{\frac{1}{2}}} \right]$$

$$T_{XY}^* = 0 \qquad\qquad\qquad\qquad (3.18)$$

The determination of the potentials from Eqs. (2.26) requires the derivatives of these functions with respect to θ, i.e.

$$\Sigma_Y^{*'} = \frac{F_V \theta}{\pi^2} \frac{1}{(1 - \alpha^2 \theta^2)^{3/2}}$$

$$T_{XY}^{*'} = 0 \qquad\qquad\qquad\qquad (3.19)$$

By a limiting process where $\alpha \to 0$ while F_V remains constant, the prescribed conditions yield the potentials

$$\Omega_1(\theta) = \frac{F_V \theta}{\pi^2 \rho c} \frac{[a\theta^2 + (d-c)\lambda_2^2(\theta) - 1]}{[\lambda_1(\theta) - \lambda_2(\theta)][\theta^2 + \lambda_1^2(\theta)] R(\theta)}$$

$$\Omega_2(\theta) = - \frac{F_V \theta}{\pi^2 \rho c} \frac{[a\theta^2 + (d-c)\lambda_1^2(\theta) - 1]}{[\lambda_1(\theta) - \lambda_2(\theta)][\theta^2 + \lambda_2^2(\theta)] R(\theta)} \qquad (3.20)$$

The complex displacements of the two-dimensional problem of a step force of magnitude F_v can be written from Eqs. (2.23) by differentiating twice with respect to time and multiplying by a factor of $1/2$. Thus,

$$U_X^* = -\frac{F_v}{2\pi^2\rho} \sum_{\kappa=1}^{2} \frac{\theta_\kappa^2 \lambda_\kappa(\theta_\kappa) [a\theta_\kappa^2+(d-c)\lambda_{3-\kappa}^2(\theta_\kappa) - 1]}{\Delta_\kappa' [\lambda_\kappa(\theta_\kappa) - \lambda_{3-\kappa}(\theta_\kappa)] R(\theta_\kappa)}$$

$$U_Y^* = -\frac{F_v}{2\pi^2\rho b} \sum_{\kappa=1}^{2} \frac{\theta_\kappa(a\theta_\kappa^2-1) [(d-c)\theta_\kappa^2+b\lambda_{3-\kappa}^2(\theta_\kappa) - 1]}{\Delta_\kappa' [\lambda_\kappa(\theta_\kappa) - \lambda_{3-\kappa}(\theta_\kappa)] R(\theta_\kappa)}$$

(3.21)

In the three dimensional problems the expressions Δ_κ and Δ_κ', equivalent to the two-dimensional δ_κ and δ_κ' are written

$$\Delta_\kappa \equiv t - r\cos W \, \theta_\kappa - y\lambda_\kappa(\theta_\kappa) = 0 \tag{3.22}$$

$$\Delta_\kappa' = - r\cos W - y\lambda_\kappa'(\theta_\kappa) \tag{3.23}$$

The displacement field can be obtained from Eqs. (3.21) and (3.13). A change of the variable of integration from W to θ_κ results in the following expressions

$$u_r^* = \frac{F_v}{2\pi^2\rho} \sum_{\kappa=1}^{2} \int_{C_\kappa} \frac{\theta_\kappa^2 \lambda_\kappa(\theta_\kappa) [a\theta_\kappa^2+(d-c)\lambda_{3-\kappa}^2(\theta_\kappa) - 1]}{G_\kappa(\theta_\kappa) [\lambda_\kappa(\theta_\kappa) - \lambda_{3-\kappa}(\theta_\kappa)] R(\theta_\kappa)} \, d\theta_\kappa$$

$$u_\omega^* = 0$$

$$u_y^* = \frac{F_v}{2\pi^2\rho b} \sum_{\kappa=1}^{2} \int_{C_\kappa} \frac{\theta_\kappa(a\theta_\kappa^2-1) [(d-c)\theta_\kappa^2+b\lambda_{3-\kappa}^2(\theta_\kappa) - 1]}{G_\kappa(\theta_\kappa) [\lambda_\kappa(\theta_\kappa) - \lambda_{3-\kappa}(\theta_\kappa)] R(\theta_\kappa)} \, d\theta_\kappa$$

(3.24)

where

$$G_\kappa(\theta_\kappa) = r\theta_\kappa \sin W = [r^2\theta_\kappa^2 - [t-y\lambda_\kappa(\theta_\kappa)]^2]^{1/2} \tag{3.25}$$

and C_κ are the contours of integration on the complex plane. The stresses can be determined in a similar manner but will not be given here.

3.5 Certain Non-axisymmetric Problems

The solutions of certain dynamic problems which do not exhibit axial symmetry can be formed by a rotational superposition of solutions for both plane and antiplane problems. The plane strain problem is assumed to be antisymmetric about the y axis, while the antiplane problem is symmetric. Use of the weighting functions $f_1(\omega_0) = \cos\omega_0$ and $f_2(\omega_0) = \sin\omega_0$, and the change of variable $W = \omega - \omega_0$ in Eqs. (3.8) and (3.11) leads to

$$u_r / \cos\omega = \int_0^\pi U_X \cos^2 W dW - \int_0^\pi U_Z \sin^2 W dW$$

$$u_\omega / \sin\omega = -\int_0^\pi U_X \sin^2 W dW + \int_0^\pi U_Z \cos^2 W dW$$

$$u_y / \cos\omega = \int_0^\pi U_Y \cos W dW$$

$$\sigma_r / \cos\omega = \int_0^\pi \Sigma_X \cos W dW + (c_{11}-c_{13}) \int_0^\pi E_X \sin^2 W \cos W dW -$$
$$- \int_0^\pi T_{XZ} \sin^2 W \cos W dW$$

$$\sigma_\omega / \cos\omega = \int_0^\pi \Sigma_X \cos W dW - (c_{11}-c_{13}) \int_0^\pi E_X \cos^3 W dW + \qquad (3.26)$$
$$+ \int_0^\pi T_{XZ} \sin^2 W \cos W dW$$

$$\sigma_y / \cos\omega = \int_0^\pi \Sigma_Y \cos W dW$$

$$\tau_{yr} / \cos\omega = \int_0^\pi T_{YX} \cos^2 W dW - \int_0^\pi T_{YZ} \sin^2 W dW$$

$$\tau_{y\omega} / \sin\omega = - \int_0^\pi T_{YX} \sin^2 W dW + \int_0^\pi T_{YZ} \cos^2 W dW$$

$$\tau_{r\omega} / \sin\omega = - (c_{11}-c_{13}) \int_0^\pi E_X \sin^2 W \cos W dW +$$
$$+ \int_0^\pi T_{XZ} \cos W(\cos^2 W - \sin^2 W) \, dW$$

The three integral equations which express the tractions σ_y, τ_{yr} and $\tau_{y\omega}$ can be transformed by using the new variable $\upsilon = r \cos W$ and the condition $T_{XY} = -T_{YZ} = T$ to the following expressions on the $y=0$ plane

$$\frac{\sigma_y(r,0,t)}{\cos\omega} = \frac{2}{r} \int_0^r \Sigma_Y(\upsilon, 0, t) \frac{\upsilon d\upsilon}{\sqrt{r^2-\upsilon^2}}$$

$$\frac{\tau_{yr}(r,0,t)}{\cos\omega} = -\frac{\tau_{y\omega}(r,0,t)}{\sin\omega} = 2 \int_0^r T(\upsilon,0,t) \frac{d\upsilon}{\sqrt{r^2-\upsilon^2}}$$

(3.27)

The relation between the stresses T_{XY} and T_{YZ} which produces the second of Eqs. (3.27) holds true for the problems of this study (see next section). The boundary tractions of the plane and antiplane problems are given from the solution of Eq. (3.27) as

$$\Sigma_Y(X,0,t) = \frac{1}{\pi X} \frac{\partial}{\partial X} \int_0^X \frac{\sigma_y(\upsilon,0,t)}{\cos\omega} \frac{\upsilon^2 d\upsilon}{\sqrt{X^2-\upsilon^2}}$$

$$T(X,0,t) = \frac{1}{\pi} \frac{\partial}{\partial X} \int_0^X \frac{\tau_{yr}(\upsilon,0,t)}{\cos\omega} \frac{\upsilon d\upsilon}{\sqrt{X^2-\upsilon^2}} =$$

$$= -\frac{1}{\pi} \frac{\partial}{\partial X} \int_0^X \frac{\tau_{y\omega}(\upsilon,0,t)}{\sin\omega} \frac{\upsilon d\upsilon}{\sqrt{X^2-\upsilon^2}}$$

(3.28)

3.5.1 The Tangential Point Force

The same procedure is used as in section 3.4.1. The horizontal traction $\tau_0 = \frac{F_h}{\pi\alpha^2}$ acts over an expanded circular area $r \leq \alpha t$ resulting in a total horizontal force $F_h t^2$. The boundary conditions can be written on the $y=0$ plane as

50

$$\sigma_y = 0 \qquad \text{for} \qquad 0 \leq r < \infty$$

$$\left.\begin{array}{l} \tau_{yr} = -\tau_0 \cos\omega \\[6pt] \tau_{y\omega} = \tau_0 \sin\omega \end{array}\right\} \quad \text{for} \quad r \leq \alpha t \qquad \left.\begin{array}{l} 0 \leq \omega < 2\pi \\[6pt] y=0 \end{array}\right\} \qquad (3.29)$$

$$\tau_{yr} = \tau_{y\omega} = 0 \qquad \text{for} \qquad r > \alpha t$$

The self-similar tractions of the plane strain problem are given from Eqs. (3.28). Following the same steps as in section 3.4.1 the solution for a step horizontal force of magnitude F_h can be written

$$\left.\begin{array}{l} U_X^* = -\dfrac{c}{2} \displaystyle\sum_{\kappa=1}^{2} \dfrac{\theta_\kappa \lambda_\kappa(\theta_\kappa) \, [\theta_\kappa^2 + \lambda_\kappa^2(\theta_\kappa)] \, \Omega_\kappa(\theta_\kappa)}{\Delta_\kappa'} \\[18pt] U_Y^* = \dfrac{1}{2} \displaystyle\sum_{\kappa=1}^{2} \dfrac{[\theta_\kappa^2 + \lambda_\kappa^2(\theta_\kappa)] \, [a\theta_\kappa^2 + d\lambda_\kappa^2(\theta_\kappa) - 1] \, \Omega_\kappa(\theta_\kappa)}{\Delta_\kappa'} \end{array}\right\} \qquad (3.30)$$

where

$$\left.\begin{array}{l} \Omega_1(\theta) = -\dfrac{F_h \theta}{\pi^2} \, \dfrac{\lambda_2(\theta) \, S_2(\theta)}{\Pi(\theta)} \\[18pt] \Omega_2(\theta) = \dfrac{F_h \theta}{\pi^2} \, \dfrac{\lambda_1(\theta) \, S_1(\theta)}{\Pi(\theta)} \end{array}\right\} \qquad (3.31)$$

It is not difficult to show that the solution of the antiplane problem is given by

$$U_Z^* = -\frac{F_h}{2\pi^2 \rho d} \frac{\theta_3}{\Delta_3' \, \lambda_3(\theta_3)} \qquad (3.32)$$

where

$$\Delta_3 \equiv t - \theta_3 r \cos W - y\lambda_3(\theta_3) = 0 \qquad (3.33)$$

and

$$\Delta_3' = -\, r\cos W - y\lambda_3'(\theta_3) \tag{3.34}$$

Here, $\lambda_3(\theta_3)$ is given by Eq. (2.32) while

$$\lambda_3'(\theta_3) = -\, \sqrt{e/d}\ \frac{\theta_3}{(e^{-1} - \theta_3^2)^{\frac{1}{2}}} \tag{3.35}$$

Direct substitution of Eqs. (3.30) and (3.32) to Eqs. (3.26) with a change of the variable of integration from W to θ_κ yields

$$u_r^*/\cos\omega = \frac{F_h}{2\pi^2\rho dr^2}\left[-\sum_{\kappa=1}^{2}\int_{C_\kappa} \frac{\lambda_\kappa(\theta_\kappa)\,\lambda_{3-\kappa}(\theta_\kappa)\,[t-y\lambda_\kappa(\theta_\kappa)]^2}{\theta_\kappa\,G_\kappa(\theta_\kappa)\,[\lambda_\kappa(\theta_\kappa)-\lambda_{3-\kappa}(\theta_\kappa)]R(\theta_\kappa)} \times \right.$$

$$\times\ [b\{a\theta_\kappa^2+d\lambda_{3-\kappa}^2(\theta_\kappa)-1\} - c(c-d)\,\theta_\kappa^2]\,d\theta_\kappa -$$

$$\left. -\int_{C_3}\frac{G_3(\theta_3)}{\theta_3\,\lambda_3(\theta_3)}\,d\theta_3\right]$$

$$u_\omega^*/\sin\omega = \frac{F_h}{2\pi^2\rho dr^2}\left[\sum_{\kappa=1}^{2}\int_{C_\kappa} \frac{\lambda_\kappa(\theta_\kappa)\lambda_{3-\kappa}(\theta_\kappa)\,G_\kappa(\theta_\kappa)}{\theta_\kappa\,[\lambda_\kappa(\theta_\kappa)-\lambda_{3-\kappa}(\theta_\kappa)]\,R(\theta_\kappa)} \times \right. \tag{3.36}$$

$$\times\ [b\{a\theta_\kappa^2+d\lambda_{3-\kappa}^2(\theta_\kappa) - 1\} - c(c-d)\,\theta_\kappa^2]\,d\theta_\kappa +$$

$$\left. +\int_{C_3}\frac{[t-y\,\lambda_3(\theta_3)]^2}{\theta_3\,G_3(\theta_3)\,\lambda_3(\theta_3)}\,d\theta_3\right]$$

$$u_y^*/\cos\omega = \frac{F_h}{2\pi^2\rho r}\ \sum_{\kappa=1}^{2}\int_{C_\kappa} \frac{\theta_\kappa\,\lambda_{3-\kappa}(\theta_\kappa)\,[a\theta_\kappa^2+(d-c)\,\lambda_\kappa^2(\theta_\kappa) - 1]}{G_\kappa(\theta_\kappa)\,[\lambda_\kappa(\theta_\kappa)-\lambda_{3-\kappa}(\theta_\kappa)]\,R(\theta_\kappa)}\ \times$$

$$\times\ [t-y\lambda_\kappa(\theta_\kappa)]\,d\theta_\kappa$$

where

$$G_3(\theta_3) = \theta_3 r sinW = [r^2\theta_3^2 - [t-y\lambda_3(\theta_3)]^2]^{\frac{1}{2}} \qquad (3.37)$$

The contours of integration C_1, C_2 and C_3 are traced on the complex plane in a manner to be described in Chapter 5.

4. THE REPRESENTATION OF THE WAVE FIELDS ONTO THE COMPLEX PLANES. GEOMETRY OF THE WAVE FRONTS

4.1 General Remarks

The numerical computation of the dynamic response of an anisotropic medium caused by an applied step force requires the evaluation of the real part of the complex displacements and stresses given in the preceding two chapters. In the process, the need arises for an accurate representation of the physical space on the complex domain composed of a four-sheeted Riemann surface (Appendix B). The present chapter attempts to clarify the regions on this surface which represent the quasi-longitudinal and quasi-transverse wave fields. The discussion concerns the solutions of the two-dimensional wave propagation problems which form the basis for developing the transversely isotropic solutions.

The correspondence between points of the (x, y) space and the complex domain is given by Eqs. (2.16) which parametrize the characteristic surfaces of the solutions to the wave equations by means of the complex variable θ_κ. The major difference from the isotropic case is caused by the behavior of the multi-valued function $\lambda_\kappa(\theta_\kappa)$ which, in turn, depends upon certain inequalities among the elastic parameters. In has been found convenient to separate orthotropic materials into a number of different cases, which greatly facilitates the total exposition.

No real conceptual difficulties are introduced by anisotropy in wave propagation problems. The system of partial differential equations that describe the motion has two solutions corresponding to two types of propagating waves. The wave associated with the larger velocity is "nearly" longitudinal while the wave which travels with the smaller velocity

is "nearly" transverse with the displacement vector polarized in the plane of deformation. It is only along preferential directions, such as the axes of material symmetry, that the wave equations uncouple, thus producing purely longitudinal and purely transverse displacements.

4.2 The Geometry of the Wave Fronts

A peculiarity of wave propagation in anisotropic media is the existence, if certain relations are satisfied by the elastic parameters, of quasi-transverse wave fronts not strictly convex but with double points and cusps. This fact has been established from analytical investigations as well as from experimental observations [1, 25].

Consider the dimensionless form of Eq. (2.16) in the self-similar coordinate system $\xi = x/t$, $\eta = y/t$

$$\delta_\kappa \equiv 1 - \xi\theta_\kappa - \eta\lambda_\kappa(\theta_\kappa) = 0 \tag{4.1}$$

The (ξ, η) coordinates of the wave fronts at any time can be obtained by eliminating the parameter θ_κ from Eqs. (4.1) and from

$$\delta_\kappa' = \frac{\partial\delta_\kappa}{\partial\theta_\kappa} = -\xi - \eta\lambda_\kappa'(\theta_\kappa) = 0 \tag{4.2}$$

where

$$\lambda_\kappa'(\theta_\kappa) = \frac{\theta_\kappa\psi_\kappa(\theta_\kappa)}{2bd\lambda_\kappa(\theta_\kappa)} \tag{4.3}$$

and

$$\psi_\kappa(\theta_\kappa) = -L + (-1)^\kappa \frac{K_1 K_2 \theta_\kappa^2 - M}{\sqrt{Q(\theta_\kappa)}} \tag{4.4}$$

These functions are sufficiently involved to discourage any attempt to express the general equation of the wave fronts in the form $f(\xi, \eta) = 0$.

Instead, the curves will be traced in terms of the parameter θ_κ.

Let α_κ be the angle that the normal vector $\bar{n}_\kappa$ to the tangent plane at point P (ξ_p, η_p) makes with the positive η-axis (Fig. 2), and β_κ the angle that the ray OP makes with the same axis. The following relations can be easily verified

$$\tan\alpha_\kappa = \frac{\theta_\kappa}{\lambda_\kappa(\theta_\kappa)} \tag{4.5}$$

$$\tan\beta_\kappa = -\lambda_\kappa'(\theta_\kappa) \tag{4.6}$$

The half plane $\eta \geq 0$ will be represented on the upper half of the complex plane $\text{Im}\theta_\kappa \geq 0$. It is important to note that this choice in the mapping determines a corresponding choice of the sign of the outside radical of the function $\lambda_\kappa(\theta_\kappa)$. This is equivalent to selecting the two sheets of the four-sheeted Riemann surface on which the functions giving the solution will be defined. In this study, sheets S_1 and S_2 are chosen to represent the domain of the complex solutions. The index κ will assume the values 1 or 2 according to which sheet of the Riemann surface contains the argument of the functions under consideration.

Let S_1 indicate initially that complex domain of the quasi-longitudinal wave which possesses a branch cut between points $\pm 1/\sqrt{a}$ on the real axis of θ_1 (Fig. 3). Every point along the sides of the branch cut is the image of all points lying on a half plane tangent to the wave front. Thus, the functions that express the complex solutions remain constant on these half planes which are chosen in such a way that they do not cross each other in each of the $\eta \geq 0$ or $\eta \leq 0$ half planes. Consequently, the same expressions that give the solution for every point inside the wave front can be used to give the solution for points

56

outside the wave front provided that the continuation is taken along the previously mentioned half tangent planes [41, § 53]. The mapping of the space outside the quasi-longitudinal wave front on the branch cut $(- 1/\sqrt{a}, 1/\sqrt{a})$ is given in Fig. 3. No point located in the region $|\eta| > \sqrt{b}$ has a representation on the complex plane. Similar remarks can be made for the quasi-transverse wave field although the presence of cusps needs some extended analysis. Any further discussion will concentrate on the $\xi \geq 0$, $\eta \geq 0$ quarter plane since the indicated symmetry makes the remaining quarter planes equivalent.

The parametric variation of the angles $\alpha_\kappa(\theta_\kappa)$ and $\beta_\kappa(\theta_\kappa)$ can be examined by means of Eqs. (4.5) and (4.6) and the derivatives of the tangents with respect to θ_κ; i.e.

$$(\tan\alpha_\kappa)' = \frac{\phi_\kappa(\theta_\kappa)}{2bd\lambda_\kappa^3(\theta_\kappa)} \tag{4.7}$$

$$(\tan\beta_\kappa)' = \frac{D_\kappa(\theta_\kappa)}{4b^2d^2\lambda_\kappa^3(\theta_\kappa)} \tag{4.8}$$

where

$$\phi_\kappa(\theta_\kappa) = b + d + (-1)^\kappa \frac{(b-d)^2 - M\theta_\kappa^2}{\sqrt{Q(\theta_\kappa)}} \tag{4.9}$$

$$D_\kappa(\theta_\kappa) = \phi_\kappa(\theta_\kappa)\psi_\kappa(\theta_\kappa) + 2bd\theta_\kappa\lambda_\kappa^2(\theta_\kappa)\psi_\kappa'(\theta_\kappa) =$$

$$= 2bd\left[\psi_\kappa(\theta_\kappa)+\theta_\kappa\psi_\kappa'(\theta_\kappa)\right]\lambda_\kappa^2(\theta_\kappa) - \theta_\kappa^2\psi_\kappa^2(\theta_\kappa) \tag{4.10}$$

and

$$\psi_\kappa'(\theta_\kappa) = (-1)^\kappa \frac{8bdc^2N_1\theta_\kappa}{\sqrt{Q^3(\theta_\kappa)}} \tag{4.11}$$

Consider also the following expressions

$$\phi_K'(\theta_K) = - \frac{(-1)^K \, 8bdc^2 N_1 \theta_K^3}{\sqrt{Q^3(\theta_K)}} \tag{4.12}$$

$$D_K'(\theta_K) = (-1)^K \, 48b^2 d^2 c^2 N_1 \theta_K \lambda_K^2(\theta_K) \, \frac{(b-d)^2 - K_1 K_2 \theta_K^4}{\sqrt{Q^5(\theta_K)}} \tag{4.13}$$

An examination of the behavior of α_1 and β_1 in the interval $0 \le \theta_1 \le 1/\sqrt{a}$ leads to the conclusion that both angles vary continuously and are monotonically increasing in the interval $(0, \pi/2)$ [30]. Therefore, the shape of the quasi-longitudinal wave front is always a strictly convex, closed curve.

A complete analysis of the variation of the angles α_2 and β_2 associated with the quasi-transverse wave is given in Appendix C. Table 1 presents a summary of this investigation. It can be seen that the orthotropic materials under consideration can be separated into five distinct cases, indicated by the letters A, B, C, D and E, according to the existence or nonexistence of cuspidal edges and the orientation of the cusps relative to the coordinate axes [Table 1]. The inequalities involving the elastic parameters associated with each material case are not always compatible with the conditions which accompany each of the four types of complex planes I, II, III or IV (see Appendix B). An examination of the range of validity of each inequality results in the following table.

Material Case	Compatible Complex Plane
A	I, II, III, IV
B	I
C	II
D	II, III
E	II, IV

In this chapter and the next, a given material will be classified by a letter indicating the material case followed by a Roman numeral indicating the type of the complex plane. For example, material A-IV has elastic parameters that satisfy the conditions associated with material case A and type of complex plane IV, i.e. $N_1 < 0$, $N_2 > 0$, $N_3 > 0$, $N_4 > 0$, $K_2 > 0$, $M > 0$.

4.3 The Representation of the Wave Fields

It has been mentioned that the functions determining the complex solutions for the two types of propagating waves will be defined on the sheets S_1 and S_2 of the Riemann surface. In anisotropic materials, each sheet does not, in general, exclusively represent the field of a single type of wave. A careful examination is needed to define the areas on each sheet that correspond to the wave field of the quasi-longitudinal or the quasi-transverse type of disturbance. Before proceeding any further on this subject, it is useful to consider briefly Eq. (4.1) written in an equivalent form where the radicals of function λ_K (θ_K) have been eliminated, i.e.,

$$[bd\xi^4 + L\xi^2\eta^2 + ad\eta^4]\,\theta_\kappa^4 - 2\xi(2bd\xi^2 + L\eta^2)\,\theta_\kappa^3 -$$

$$- [(a + d)\eta^4 + (b + d)\xi^2\eta^2 - 6bd\xi^2 - L\eta^2]\,\theta_\kappa^2 +$$

$$+ 2\xi[(b + d)\eta^2 - 2bd]\theta_\kappa + [\eta^4 - (b + d)\eta^2 + bd] = 0 \qquad (4.14)$$

This equation, in general, possesses four roots in θ_κ for every point (ξ,η). When the point is located in the interior of both wave fronts, the roots form two pairs of complex conjugate numbers. The value of θ_κ for each pair which represents the solution must be located in the appropriate section of the complex plane in agreement with the mapping convention. The existence of real roots for θ_κ is equivalent to saying that real tangents can be drawn from the given point to the wave front. In accordance with the method of the preceding section for continuing the solution along half tangent planes, the real roots must be chosen appropriately. Any point located outside both wave fronts has four real roots for θ_κ while any point between the two wave fronts has two real roots for θ_κ. Consider now points located inside the triangularly shaped area of a cusped quasi-transverse wave front (Fig. 4). It can be seen that four real tangents can be drawn to the wave front indicating the existence of four real roots θ_κ of Eq. (4.14). The solution is represented now by the two real roots which are associated with the half tangent planes in the chosen direction. One interpretation of this fact is that there are no roots associated with the quasi-longitudinal wave. In other words, the inside of the cusped region is a "hole" in the quasi-longitudinal wave.

The correpsondence between points of the wave fields and points on sheets S_1 and S_2 of the Riemann surface is expressed by Eq. (4.1).

Let

$$\theta_\kappa = \varepsilon_\kappa + i\zeta_\kappa$$

$$\lambda_\kappa(\theta_\kappa) = E_\kappa + iZ_\kappa \tag{4.15}$$

then, the following expressions can be obtained

$$\xi = \frac{Z_\kappa}{\varepsilon_\kappa Z_\kappa - \zeta_\kappa E_\kappa}$$

$$\eta = -\frac{\zeta_\kappa}{\varepsilon_\kappa Z_\kappa - \zeta_\kappa E_\kappa} \tag{4.16}$$

These will be used in the next sections to discuss each type of complex Riemann surface separately.

4.3.1 Type I Riemann Surface

A typical configuration of the complex domain of Type I is given by two sheets of the Riemann surface shown in Fig. 5. The branch cut $(-1/\sqrt{a}, 1/\sqrt{a})$ of the S_1 sheet represents the quasi-longitudinal wave front and the branch cut $(-1/\sqrt{d}, 1/\sqrt{d})$ represents the quasi-transverse wave front. Sheets S_1' and S_2 are interconnected along branch cuts parallel to the imaginary θ_κ - axis from points $\pm\,\theta_{01}$ and $\pm\,\theta_{02}$ to $\pm\,\infty$ (Appendix B).

Let θ_κ assume real values not located on the branch cuts. Then, from Eqs. (4.15) and (4.16) it can be seen that

$$\xi = \frac{1}{\varepsilon_\kappa}$$

$$\eta = 0 \tag{4.17}$$

i.e. as θ_κ varies from $1/\sqrt{a}$ (or $1/\sqrt{d}$) to infinity, the corresponding points of the wave field lie on the ξ-axis from the intersection with the wave front $\xi = \sqrt{a}$ (or $\xi = \sqrt{d}$) to the origin. For purely imaginary values of

θ_κ (i.e. $\theta_\kappa = i\zeta_\kappa$) the function $\lambda_\kappa(\theta_\kappa)$ can be written

$$\lambda_\kappa(i\zeta_\kappa) = \left[\frac{b+d+L\zeta_\kappa^2 + (-1)^\kappa \sqrt{Q(i\zeta_\kappa)}}{2bd}\right]^{1/2} \tag{4.18}$$

where

$$Q(i\zeta_\kappa) = (b+d+L\zeta_\kappa^2)^2 - 4bd(1+a\zeta_\kappa^2)(1+d\zeta_\kappa^2) =$$

$$= (b-d)^2 + 2M\zeta_\kappa^2 + K_1K_2\zeta_\kappa^4 \tag{4.19}$$

The polynomial $Q(i\zeta_\kappa)$ does not have any real roots in ζ_κ and as a result remains always real and positive in the range of ζ_κ. It is obvious from Eq. (4.19) that

$$Q(i\zeta_\kappa) < (b+d+L\zeta_\kappa^2)^2 \tag{4.20}$$

Then, from Eq. (4.18) it can be seen that $\lambda_\kappa(i\zeta_\kappa)$ is a real quantity. Equations (4.16) now can be written

$$\xi = 0$$

$$\eta = \frac{1}{E_\kappa} \tag{4.21}$$

It is not difficult to show that $\lambda_\kappa(i\zeta_\kappa)$ is a monotonically increased function of ζ_κ. Therefore, every point along the imaginary θ_κ axis in the interval $(0, \infty)$ corresponds to a single point on the η-axis which lies in the interval defined from the intersection with the wave front (i.e. $\eta = \sqrt{b}$ for the quasi-longitudinal and $\eta = \sqrt{d}$ for the quasi-transverse) and the origin ($\xi = 0$, $\eta = 0$).

It is interesting to examine what points of the wave fields correspond to the sides of the branch cut from Θ_{02} to infinity. Direct

application of Eqs. (4.16) yields the curves shown in Fig. 6 for an A-I material and Fig. 7 for a B-I material. The branch point Θ_{02} is the image of point A_{02} while the point at infinity of the complex plane corresponds to the origin of the (ξ, η) plane. These curves and their images in Fig. 5 are plotted with lines of the same type for easy recognition.

Imagine now that the quasi-longitudinal effect at a given point can be determined by a sequence of values of the parameter θ_1 which forms a path on the S_1 sheet. When the path encounters a branch cut, the continuation of the functions require a transfer from sheet S_1 to S_2. Therefore, the curves traced on the ξ-η plane separate the regions of the wave fields which are mapped onto different sheets of the Riemann surface. It should be noticed, however, that the sections of the curves located outside the quasi-transverse wave front (see Fig. 7) do not have any effect on the quasi-transverse wave field, since that region either does not have a representation or is mapped on the real axis of the S_2 sheet (see section 4.2).

4.3.2 Type II Riemann Surface

Four of the five material cases satisfy conditions of the elastic parameters that are in agreement with the inequalities associated with the existence of the Type II Riemann surface. The study of the Riemann surface will be separated in two parts according to whether the quantity N_2 is positive or negative. This has a direct effect on whether the branch points Θ_D are located on the S_2 or the S_1 sheet (Appendix B).

4.3.2.1 The Condition $N_2 > 0$

The complete configuration of branch cuts in the case under examination is given in Fig. 8. For all real values of θ_κ the discussion in section 4.3.1 is directly applicable. Every point of the region inside the wave front is represented, in general, by a complex value of θ_κ. Particular attention will be given to purely imaginary values $\theta_\kappa = i\zeta_\kappa$, specifically the part of the imaginary axis $(0, \zeta_{02})$ which lies between the origin and the branch point $\theta_{02} = i\zeta_{02}$ on each of the sheets S_1 and S_2. In that range of values of ζ_κ the polynominal $Q(i\zeta_\kappa)$ is a real positive quantity, smaller in magnitude than $(b+d+L\zeta_\kappa^2)^2$. It becomes zero at $\zeta_\kappa = \zeta_{02}$. The number of local extrema, determined from the expression

$$\frac{dQ(i\zeta_\kappa)}{d\zeta_\kappa} = 4\zeta_\kappa(M+K_1K_2\zeta_\kappa^2) = 0 \tag{4.18}$$

depends on whether M is positive or negative.

Let $M<0$. Then $Q(i\zeta_\kappa)$ has one local maximum at $\zeta_\kappa=0$ and is monotonically decreasing. The calculation of the derivative of $\lambda_\kappa(i\zeta_\kappa)$ with respect to ζ_κ gives the expression

$$\frac{d\,\lambda_\kappa(i\zeta_\kappa)}{d\zeta_\kappa} = \frac{\zeta_\kappa\tilde{\psi}_\kappa(\zeta_\kappa)}{2bd\lambda(i\zeta_\kappa)} \tag{4.19}$$

where

$$\tilde{\psi}_\kappa(\zeta_\kappa) = L + (-1)^\kappa \frac{K_1K_2\zeta_\kappa^2+M}{\sqrt{Q(i\zeta_\kappa)}} \tag{4.20}$$

Since the Type II complex plane satisfies the conditions $K_2 < 0$, $N_1 < 0$ (Table B.1), it can be immediately seen that $\tilde{\psi}_1(\zeta_1) > 0$, i.e. $\lambda_1(i\zeta_1)$ is a monotonically increasing function. Moreover,

$$\tilde{\psi}_2(0) = \frac{2bN_3}{b-d}$$

(4.21)

$$\tilde{\psi}_2(\zeta_{02}) = - \infty$$

For $N_3 < 0$ (i.e. material case D), $\tilde{\psi}_2(\zeta_2)$ is negative in $(0, \zeta_{02})$. As a result, $\lambda_2(i\zeta_2)$ is monotonically decreasing. The sides of the branch cuts on the imaginary axis are the images of the closed curves through the origin (see Fig. 9). Each side of the branch cut and the corresponding curves in Fig. 9 are plotted with the same type of line.

The foregoing considerations *lead to the following* interpretations. Every point of the interval $(0, \zeta_{02})$ of the imaginary axis of sheet S_1 corresponds to a single point of the interval $(\sqrt{b}, A_{02})$ of the η-axis (Figs. 8 and 9). The points of the quasi-longitudinal wave field between $\eta=A_{02}$ and $\eta=\sqrt{d}$ have a representation on the interval $(\zeta_{02}, 0)$ of the imaginary axis of sheet S_2. It was mentioned in section 4.3 that there are no values on the complex plane to represent a quasi-longitudinal wave field contained in the triangularly shaped area of the quasi-transverse wave front. Let n^* denote the η-coordinate of the double point of the quasi-transverse wave front and θ^* the corresponding value of parameter θ_2 (see Table 1). Then, every point of the interval $(\sqrt{d}, \eta^*)$ of the quasi-transverse wave field has a double representation on the real axis of the S_2 sheet in the intervals $(0, \theta^*)$ and $(0, -\theta^*)$. It can be seen from Eqs. (4.15) and (4.16) that every point of the η-axis in the interval

$(\eta^*, 0)$ requires $\lambda_\kappa(\theta_\kappa)$ to be a real quantity. The complex values of θ_κ for which $\lambda_\kappa(\theta_\kappa)$ becomes real form a curve on the sheet S_2. In fact there are two such curves, denoted as A_θ and B_θ in Fig. 8, which emanate respectively from points $-\theta^*$ and θ^*. The continuity of the wave fields makes the curve A_θ represent points of the quasi-longitudinal wave which lie on the interval $(\eta^*, 0)$ when this interval is considered as the limit of the $\xi > 0$ half plane. For the quasi-transverse wave the same limit yields the curve B_θ. In effect, curves A_θ and B_θ represent the boundaries in the complex domain which separate the regions of mapping the quasi-longitudinal and quasi-transverse wave fields.

When condition $N_3 > 0$ is satisfied (i.e. material case A) the function $\tilde{\psi}_2(\zeta_2)$ (Eq. 4.20) changes sign from positive to negative at a point located inside the interval $(0, \zeta_{02})$. This point can be determined as the root of the equation $\tilde{\psi}_2(\zeta_2) = 0$. The elimination of the radical transforms this equation to

$$K_1 K_2 \zeta_2^4 - 2M\zeta_2^2 + \frac{L^2(b-d)^2 - M^2}{4abd^2} = 0 \qquad (4.22)$$

The product of the squares of the two roots in ζ_2 is written as

$$\frac{[L(b-d) + M][L(b-d) - M]}{4abd^2 K_1 K_2} \qquad (4.23)$$

and is a negative quantity under the existing values of M, K_2 and N_3. The positive real root in ζ_2 is

$$\zeta_2^* = \left[-\left[\sqrt{ad}\, M + L\, \sqrt{-c^2 N_1} \right] / \sqrt{ad}\, K_1 K_2 \right]^{\frac{1}{2}} \qquad (4.24)$$

which can be shown to satisfy $\zeta_2^* < \zeta_{02}$. Consequently, $\lambda_2(i\zeta_2)$ is monotonically increasing in the interval $(0, \zeta_2^*)$ and monotonically decreasing in (ζ_2^*, ζ_{02}). If $\theta_2^* = i\zeta_2^*$, and η^* is the point which is mapped by θ_2^* in the complex domain, the interval $(\eta^*, 0)$ of the η-axis has a double representation shown by curves C_θ and D_θ, depending on whether it is considered as the limit of positive or negative values of ξ. The curves C_θ and D_θ on the Riemann surface (Fig. 8) separate the regions of mapping the two types of wave fields (Fig. 10).

The case $M > 0$ is now examined. In this case a second local extremum of the function $Q(i\zeta_\kappa)$ exists in the interval $(0, \zeta_{02})$ at point

$$\zeta_{\kappa 0} = (-M/K_1 K_2)^{\frac{1}{2}}$$

where $\zeta_{\kappa 0} < \zeta_{02}$. However, the general behavior of $\lambda_\kappa(i\zeta_\kappa)$ is not altered and the separation of the regions of the complex domain corresponding to the quasi-longitudinal and quasi-transverse wave fields is similar to the case $N_3 > 0$, $M < 0$ which was discussed in this section. The inequalities $M > 0$ and $N_3 < 0$ cannot be simultaneously satisfied.

4.3.2.2 The Condition $N_2 < 0$

The branching of the Riemann surface in this case is given in Fig. 11. The branch cut $(-1 / \sqrt{a}, 1 / \sqrt{a})$ of the S_1 sheet represents the quasi-longitudinal wave front while the branch cuts $(-\theta_{01}, \theta_{01})$ of the S_2 sheet and $(\theta_{01}, 1 / \sqrt{d})$, $(-\theta_{01}, -1 / \sqrt{d})$ of the S_1 sheet represent the quasi-transverse wave front. Equations (4.15) and (4.16) are employed again to show that real values of θ_1 in the intervals $(1 / \sqrt{a}, 1 / \sqrt{d})$ and (θ_{01}, ∞) represent points of the quasi-longitudinal wave field in the sections

($\sqrt{a}$, $\sqrt{d}$) and (ξ_{01}, 0) of the ξ-axis (Fig. 12). There is no representation of this wave field for points of the ξ-axis between $\xi = \sqrt{d}$ and $\xi = \xi_{01}$. Correspondingly, real values of θ_2 in the interval (θ_{01}, ∞) of the S_2 sheet are the images of points (ξ_{01}, 0) of the quasi-transverse wave field. On the Riemann surface, the interval (ξ_{01}, $\sqrt{d}$) of the ξ-axis has a double representation which includes the upper side of the branch cut (θ_{01}, $1 / \sqrt{d}$) on the sheet S_1 and the section (θ_{01}, θ_ξ) of sheet S_2. Here, θ_ξ is the point on the S_2 plane corresponding to that half tangent plane which passes through ($\xi = \sqrt{d}$, $\eta = 0$) and which is not parallel to the η-axis.

For purely imaginary values on sheets S_1 and S_2 the discussion is analogous to that given for the case $N_2 > 0$. The separation of the complex domain for either $N_3 > 0$ or $N_3 < 0$ is given in Fig. 11 while the corresponding wave fields for material cases C-II and E-II are shown in Figs. 12 and 13.

4.3.3 Type III Riemann Surface

Figure 14 shows the two sheets of the Type III Riemann surface. For real values of θ_κ the discussion in section 4.3.1 is directly applicable. Let $\theta_{01} = i\zeta_{01}$ and $\theta_{02} = i\zeta_{02}$ be the branch points on the imaginary θ_κ-axis. They represent the images of points A_{01} and A_{02} of the wave fields (Figs. 15, 16). Each side of the branch cut (θ_{01}, θ_{02}) corresponds to a curve connecting points A_{01} and A_{02}. The side of the branch cut drawn with a dashed line (Fig. 14) corresponds to the curve which is plotted with the same type of dashed line between points A_{01} and A_{02} (Figs. 15, 16). It can be shown that in the intervals (0, ζ_{02}) and (ζ_{01}, ∞) of sheet S_1 the function $\tilde{\psi}_1(\zeta_1)$ is positive, thus

making $\lambda_1(i\zeta_1)$ a real monotonically increasing function. In the same intervals of sheet S_2, when $N_3 > 0$, the function $\tilde{\psi}_2(\zeta_2)$ possesses two real roots as a solution to Eq. (4.22):

$$\zeta^{1*} = \left[\frac{-M-L\sqrt{-c^2 N_1/ad}}{K_1 K_2}\right]^{\frac{1}{2}}, \quad \text{and} \quad \zeta^{2*} = \left[\frac{-M+L\sqrt{-c^2 N_1/ad}}{K_1 K_2}\right]^{\frac{1}{2}} \tag{4.25}$$

where $\zeta^{1*} < \zeta^{2*}$. The points $\theta^{1*} = i\zeta^{1*}$ and $\theta^{2*} = i\zeta^{2*}$ are the images of points η^{1*} and η^{2*} of the η-axis which define a section with a double representation on the complex domain. The curves A_θ and B_θ (Fig. 14) map the section (η^{1*}, η^{2*}) of the quasi-longitudinal wave field when this section is taken as the limit of positive ξ values (curve A_θ) or negative ξ values (curve B_θ). For the quasi-transverse wave field curve A_θ maps the section (η^{1*}, η^{2*}) when it is taken as the limit of negative ξ values and curve B_θ maps the same section as the limit of positive ξ values. The region enclosed by A_θ and B_θ on the S_2 sheet (Fig. 14) maps part of the quasi-longitudinal wave field.

It is not difficult to verify the following correspondence between sections of the η-axis of the wave fields and intervals on the Riemann surface (see Figs. 14 and 15).

Wave Field	Interval on η-axis	Image on Riemann Surface	Sheet
Quasi-Longitudinal	$(\sqrt{b}, A_{02})$	$(0, \zeta_{02})$	S_1
	(A_{02}, η^{1*})	(ζ_{02}, ζ^{1*})	S_2
	(η^{1*}, η^{2*})	Curve A_θ	S_2
	(η^{2*}, A_{01})	(ζ^{2*}, ζ_{01})	S_2
	$(A_{01}, 0)$	(ζ_{01}, ∞)	S_1
Quasi-Transverse	$(\sqrt{d}, \eta^{1*})$	$(0, \zeta^{1*})$	S_2
	(η^{1*}, η^{2*})	Curve B_θ	S_2
	$(\eta^{2*}, 0)$	(ζ^{2*}, ∞)	S_2

The case $N_3 < 0$ (i.e. material case D-III) provides one real root of
Eq. (4.22) which is larger in absolute value than ζ_{01}. Curves C_θ and D_θ
of Fig. 14 are now the boundaries of the regions of mapping the two types
of wave fields which are shown in Fig. 16.

4.3.4 Type IV Riemann Surface

The branch points $\pm\Theta_{01}$ and $\pm\Theta_{02}$ in this case are located on the real
θ_κ axis (Fig. 17). When condition $N_2 > 0$ is satisfied it can be shown
that the quasi-longitudinal wave field is mapped entirely on the S_1 sheet
and the quasi-transverse entirely on the S_2 sheet (see Fig. 18). The
same thing holds true when $N_2 < 0$ except for point located on and inside

the triangularly shaped area of the quasi-transverse wave adjacent to
the ξ-axis which is mapped on the branch cut $(\Theta_{01}, 1 / \sqrt{d})$ of the S_1 sheet
(see Figs. 19 and 20).

5.   NUMERICAL METHODS AND RESULTS

5.1   General Remarks

The expressions for the displacements and stresses given in
Chapters 2 and 3 determine the dynamic response in an anisotropic medium
as functions of the complex parameter θ_κ. As time increases, the value
of θ_κ for a given point traces a path on the Riemann surface. A
particular value of θ_κ on this path determines the dynamic solution at the
corresponding time. The stresses are evaluated by direct substitution
of θ_κ in the given expressions, while the displacements involve a
quadrature in θ_κ. The result of these operations is, in general, a complex
quantity the real part of which represents the answer sought.

The principal objectives of this chapter are:

  a) to focus attention on certain numerical problems which
     appear in the solution of anisotropic wave propagation
     problems by the method of self-similar potentials and to
     explain the techniques which have been used to overcome
     them; and

  b) to provide numerical results in the form of time histories
     of displacements and stresses for the specific dynamic
     problems solved in this study and to discuss the most
     characteristic variations arising from different classes
     of anisotropy as compared to the isotropic case.

Two-dimensional problems are treated first in the various anisotropic
media. The elastic constants and density that were used to obtain
numerical results were taken from references [2, 17]. The paths of θ_κ on

sheets S_1 and S_2 of the Riemann surface are shown for typical points, in particular those located inside the sector formed from the cusps and the origin. Subsequently, the numerical techniques that are applicable in obtaining the displacements for a sudden application of a point force in transversely isotropic materials are discussed to the extent that they differ from the two-dimensional case.

The contributions of the quasi-longitudinal and the quasi-transverse wave fields at points not near the wave fronts are quantities of opposite sign. Their superposition often turns out to involve small differences of large quantities. Therefore, in order to avoid erroneous final results, the quantities corresponding to individual waves must often be calculated much more accurately than might at first be thought necessary.

5.2 Two-Dimensional Problems

The discussion of the two-dimensional case concentrates solely on the plain strain problems in orthotropic materials excluding the much simpler antiplane problem which is briefly mentioned in section 5.3.2. The methodology presented in the next three sections not only applies to all the two-dimensional problems of this study, but also forms the core of the three-dimensional case.

5.2.1 The Determination of θ_κ

The determination of the complex parameter θ_κ as a function of the point coordinates (x, y) and the time variable t, given implicitly by Eq. (2.16), requires the solution of a complete fourth degree equation (see Eq. (4.14)). It is convenient to use a numerical procedure for this

calculation.

As time increases, the given point will first have a representation on the Riemann surface when the tangent parallel to the horizontal axis passes through the point. The corresponding value of θ_κ is zero. Consider now that at time t_n the value of the parameter is known and given by θ_κ^n. A numerical solution of the differential equation

$$\frac{\partial \theta_\kappa}{\partial t} = - \frac{1}{\delta_\kappa'(\theta_\kappa)} = \frac{1}{x + y \lambda_\kappa'(\theta_\kappa)} \tag{5.1}$$

yields the new value θ_κ^{n+1} at time $t_{n+1} = t_n + \Delta t$. A predictor-corrector iterative method is used to solve this equation. The number of iterations required to achieve a certain number of identical significant digits in the predicted and the corrected value of θ_κ^{n+1} is a criterion for deciding what value of time interval Δt should be used. For example, when convergence is not attained after a preset maximum number of iterations, it is an indication that the rate of change of θ_κ is very large and it is convenient to reduce the time interval. It is reduced by a factor of 2 in the program. On the other hand, if the convergence criterion is satisfied in less than a preset minimum number of iterations, the rate of change of θ_κ is very small and the time interval is increased by a factor of 2. In this process, in order to avoid excessively large time intervals, an upper limit of Δt is imposed. However, if θ_κ is approaching a singular point, Δt would assume values smaller than any preset lower limit. In the neighborhood of such a singularity the values of θ_κ are obtained by a modified method to be explained in the next section.

Since the evaluation of θ_K^{n+1} depends on the previously calculated value θ_K^n, the errors of approximation accumulate causing an increasing drift of the calculated values from the exact ones. To eliminate this effect, the use of the Newton-Raphson method [36] with a higher convergence criterion is employed at selected time instances. Thus, the desired values θ_K are evaluated with better accuracy and the accumulation of error is canceled.

The combined use of the predictor-corrector and the Newton-Raphson iterative methods provides a very efficient technique for the numerical solution of Eq. (2.16). Direct application of only the latter method could fail to converge or even might converge to the wrong value if the initial guess was not good enough. The predictor-corrector method provides a fast means of obtaining a sufficiently good approximation in addition to the criterion for an approaching singularity.

Particular care should be exercised in the computation of the numerical value of the function $\lambda_K(\theta_K)$. The double radical expression of Eq. (2.19) is calculated in two steps. In the first step, the value of the square root of the polynomial $Q(\theta_K)$ is computed by means of a special routine as shown in Appendix D.1. Since the term $(-1)^K$ assumes a definite value on each of sheets S_1 and S_2 of the Riemann surface, every value of θ_K yields a unique value for the expression under the outside radical on the right hand side of Eq. (2.19). In the second step, the calculation of the square root of this last quantity is now straightforward (see Appendix D.2).

5.2.2 The Behavior Near the Wave Fronts

In Chapter 4 it has been mentioned that the condition satisfied by points on the wave fronts can be expressed by the equation

$$\delta_\kappa'(\theta_{\kappa 0}) = -x -y \; \lambda_\kappa'(\theta_{\kappa 0}) = 0 \tag{5.2}$$

where $\theta_{\kappa 0}$ is the value of the parameter θ_κ corresponding to point (x, y) on the wave front at time t_0. The differential equation (5.1) becomes singular at this point. At times very close to t_0 the rate of change of θ_κ is very large. As a result, the time interval Δt required for convergence in the predictor-corrector method becomes very small. In such a case it is convenient to use a modified version of the method to obtain a better approximation of the predicted value by taking account of the behavior of Eq. (5.1) at points near the wave fronts.

Consider the power series expansion of the function $\delta_\kappa'(\theta_\kappa)$ about the value $\theta_{\kappa 0}$, i.e.:

$$\delta_\kappa'(\theta_\kappa) = \delta_\kappa'(\theta_{\kappa 0}) + (\theta_\kappa - \theta_{\kappa 0})\delta_\kappa''(\theta_{\kappa 0}) + (\theta_\kappa - \theta_{\kappa 0})^2 \frac{\delta_\kappa'''(\theta_{\kappa 0})}{2!} + \ldots \tag{5.3}$$

Since $\delta_\kappa'(\theta_{\kappa 0}) = 0$ it can be rewritten as follows:

$$\delta_\kappa'(\theta_\kappa) = (\theta_\kappa - \theta_{\kappa 0})\left[-y\lambda_\kappa''(\theta_{\kappa 0}) - (\theta_\kappa - \theta_{\kappa 0}) \; y \; \frac{\lambda_\kappa'''(\theta_{\kappa 0})}{2!} - \ldots\right] \tag{5.4}$$

Equation (5.1) can now be integrated between t_0 and t to give

$$(t - t_0) = (\theta_\kappa - \theta_{\kappa 0})^2 \left[-\frac{y\lambda_\kappa''(\theta_{\kappa 0})}{2!} - (\theta_\kappa - \theta_{\kappa 0}) \frac{y\lambda_\kappa'''(\theta_{\kappa 0})}{3!} - \ldots \right] \tag{5.5}$$

This last equation suggests that for points near the wave fronts the change of the parameter θ_κ can be closely approximated as being proportional to the square root of the change of time. Based on this result, the right part of Eq. (5.1) can be expressed approximately as a linear function in time divided by the term $\sqrt{t-t_0}$, which gives rise to the singularity at $t=t_0$. The evaluation of the integral of this quantity is a simple matter (see Appendix D.3) and provides a very good first estimate of θ_κ. There is need for only a small number of subsequent iterations to determine θ_κ to the desired level of accuracy.

The application of the Newton-Raphson method at points near the wave fronts is also ineffective. The reason is the existence of a double root of the equation $\delta_\kappa(\theta_\kappa) = 0$ at $\theta_{\kappa 0}$, which makes it almost impossible to apply the correction term $-\dfrac{\delta_\kappa(\theta_\kappa^n)}{\delta_\kappa'(\theta_\kappa^n)}$ to go from iteration to iteration. The problem can be bypassed by seeking the root of a new function $g(\theta_\kappa) = \dfrac{\delta_\kappa(\theta_\kappa)}{\delta_\kappa'(\theta_\kappa)}$ since $\theta_{\kappa 0}$ is a single root of $g(\theta_\kappa)$ [36, section 8.6].

5.2.3 The Description of the Paths of θ_κ

Let the coordinates (x_R, y_R) define a point on the $x \geq 0$, $y \geq 0$ quarter plane for which displacements and stresses are to be found. From the discussion of Chapter 4 it becomes obvious that, for a given material, the path of the complex variable θ_κ traced on the complex domain as time increases depends entirely on the ratio $\gamma = \dfrac{x_R}{y_R}$. Let $t_?$ denote the arrival time of the quasi-longitudinal wave and t_s the arrival time of the inside convex part of the quasi-transverse wave front. For points inside the sector formed from the cusps and the origin, t_{s1} indicates the arrival time

of the external, concave part of the quasi-transverse wave front between the two cusps and t_{s2} the arrival time of the section between one of the cusps and the double point $B \equiv E$ of the same front (Fig. 4). Consider now the tangents, parallel to the x-axis at the intersection of each wave front with the positive axis. Let $t_{p0} = y_R / \sqrt{b}$ and $t_{s0} = y_R / \sqrt{d}$ be the corresponding times that these tangents pass through point (x_R, y_R). It is always true that $t_{p0} \leq t_p < t_{s1} \leq t_{s2} \leq t_s$ and $t_{s0} \leq t_s$.

Since different values of γ correspond to points with different locations relative to the cusps (Fig. 7), the shape of the curves that represent the paths of θ_κ varies accordingly. A number of such curves is shown in Figs. 21-27 for different material cases and different values of γ. It is of interest to observe that for values of γ corresponding to points inside the sector included between the cusps and the origin and for times after the arrival of the first wave, the complex value of θ_κ which represents the quasi-longitudinal wave field eventually approaches a real value as time approaches t_{s1} (Figs. 22, 25, 27). Moreover, at times after t_{s2} the parameter θ_κ assumes complex values again. It is not difficult to show that at these two instants Eq. (5.1) is singular while at times just before t_{s1} or just after t_{s2} the behavior is as described in section 5.2.2. The conclusion that seems to suggest itself is that the boundary of the triangularly shaped area of the cusped front is not only part of the quasi-transverse wave front but is also a front of the quasi-longitudinal wave. The enclosed area does not experience any disturbances of the quasi-longitudinal type.

5.2.4 The Computation of Displacements and Stresses

Selected time histories of displacements and stresses are given
for the following two-dimensional problems (Fig. 28):

    a) Horizontal load in a full-space (FS-H)

    b) Vertical load on the surface of a half-space (HS-V)

    c) Horizontal load in the interior of a half-space (HS-IH)

The load consists of a suddenly applied line force. It is instructive to
include in certain cases the displacements for the impulsive application of
the load. At every time t_n the corresponding value of the parameter
θ_κ^n on the path described is substituted in a straightforward manner to
calculate the values of the stresses for the suddenly applied force and
the two displacements for the impulsive load. The displacements for the
suddenly applied force are found by performing a quadrature along a path
with end points $\theta_\kappa = 0$ and $\theta_\kappa = \theta_\kappa^n$. Any path between these two points can be
used provided the conditions for the Cauchy-Goursat theorem [9] are
fulfilled. However, it is convenient to use the path that θ_κ traces on
the complex domain as time increases. Then, the displacements at time t_{n+1}
are computed from the values at time t_n and the contribution of the integral
between values θ_κ^n and θ_κ^{n+1}. The latter may be obtained by use of any
numerical integration scheme. In the present study satisfactory answers
have been found from the application of the trapezoidal rule of integration.
This may be due to the fact that the time interval, which in effect sets
the integration interval, has been proportioned in accordance with the
rate of change of θ_κ (and all functions of θ_κ) with time.

All results are plotted against the dimensionless quantity t/t_s. It can be seen that in all cases the displacement in the direction of the suddenly applied force is not bounded. The displacement in the direction perpendicular to the loading, as well as the stresses, asymptotically approach constant values for large times. For the vertical force on the surface of the half space these constant values are in agreement with the static solutions of reference [20]. Solutions to dynamic problems in isotropic materials can be obtained from the expressions of Chapter 2 by imposing the conditions of Appendix G. For sufficiently large values of the ratio (t/t_s) the dynamic quantities are, as expected, in agreement with the static solutions of references [21, 22, 24].

The basic features of the dynamic response at a point of an orthotropic material can best be exemplified by considering the full space problem where the effects from the head and Rayleigh waves are absent. Let Γ_c indicate any value of γ such that the corresponding point encounters the concave part of the cuspidal front and let Γ_0 be any other value of γ. Consider also an anisotropic medium of the classes A-II, B-I or C-II. The time histories for points with $\gamma=0.5$, $\gamma=0.8$ and $\gamma=10$ are given in Figs. 29 to 33. Whenever $\gamma=\Gamma_0$, the arrival of each of the two wave fronts is clearly apparent from the resulting singularities[*] in the diagrams of stresses as well as in the diagrams of the displacements caused by the impulsive load. When $\gamma=\Gamma_c$ there are four such singularities corresponding to the four encounters with sections of the wave fronts. While the point under consideration is inside the triangularly shaped

---

[*]In the diagrams of the time histories of the displacements and stresses, these singularities are denoted by an arrow.

area or "lacuna" of the quasi-transverse wave front no elastic vibrations
are experienced, as can be seen from the vanishing of the stresses
(Figs. 31b and 33b) and the displacements for the impulsive load
(Figs. 31c and 33c). The effect on the displacements for the step force
is best described as "zero change" shown as the flat part of the response
in Figs. 31a and 33a. The comparison of the time histories for the same
value of γ but for different materials shows that any differences occur
for $t/t_s < 1$. It is interesting to point out the rapid change in the
response before the arrival of the quasi-transverse wave shown in
Figs. 30b and 30c. Such a change could be confused with the arrival of
the second wave front, but it is merely caused by the nearness to the
singularity at the cusp. If the response is parametrically examined in
terms of γ it can be seen that this change becomes more pronounced as γ
increases and eventually evolves into the two singularities that correspond
to the encounter of the boundary of the lacuna, which was discussed
previously. All classes of plane strain orthotropic media with cuspidal
fronts exhibit this kind of behavior in the time histories of the stresses.
On the other hand, the dynamic response of materials with strictly convex
fronts (Fig. 29) is very similar to the response observed in isotropic media.

The half space solutions where the load is applied on the surface are
presented in Figs. 34-38 for the same classes of orthotropic materials as
in the previous problem (i.e. A-II, B-I and C-II). Displacements and
stresses are given for points with $\gamma = 0.8$, $\gamma = 2.2$ and $\gamma = 10.0$. It is a
well known fact that the presence of a free boundary causes the generation
of head waves and surface (Rayleigh) waves which may influence the dynamic
response depending on the location of the point. The head wave regions for

materials with strictly convex fronts are defined in exactly the same way
as in the case of isotropy. The presence of cusps alters the geometry of
these regions as can be shown by the shaded areas in Fig. 39. It is
interesting to remark that for materials in the classes C-II, E-II and
E-IV, which have lacunas crossed by the x-axis, there exists a leading and
a trailing wave front (Fig. 39(b)). This is a result of the absence of
any quasi-longitudinal type disturbances in the section of the $y = 0$ plane
contained inside the lacuna of the quasi-transverse wave front, thus making
the existence of head wave disturbances unnecessary. The effect of the
Rayleigh waves becomes quite noticeable, as expected, for points close to
the free surface (i.e. for large values of γ). This effect is shown in
Fig. 38 by the rapid change in the response just after the arrival of the
quasi-transverse wave.

The time histories of the surface displacements u_{x0}, u_{y0} and the
surface stress σ_{x0} for the third problem of a subsurface horizontal force
are given in Figs. 40-44. In this case, a head wave is present in order
to satisfy boundary conditions on the free surface prior to the arrival of
the reflected quasi-transverse and after the passage of the reflected
quasi-longitudinal wave. Here, both of these two reflected waves are
generated after an incident quasi-transverse wave encounters the $y = 0$
plane. The presence of cusps in the incident wave front will, of course,
complicate the geometry of the head wave regions. However, any con-
tribution that may affect the response is included automatically in the
general solutions by the Smirnov-Sobolev method and consequently in the
given time histories. The effect of the Rayleigh waves becomes more
pronounced at points sufficiently far from the origin (Fig. 44).

5.3 Three-Dimensional Problems

The numerical solution of the problem of the sudden application of a point force on the surface of a transversely isotropic medium incorporates the same techniques used for the two-dimensional plane strain problems, up to the point that the path of θ_K is defined on the Riemann surface. In order to show how the antiplane problem is treated, the more complicated case of a tangential force will be considered instead of the simpler axisymmetric case of a normal force.

5.3.1 The Contours of Integration C_K

The formal solution of the dynamic Cerruti problem for a transversely isotropic medium is given by Eqs. (3.36) which were derived from Eqs. (3.26) by changing the variable of integration from W to θ_K. As W varies in the closed interval $(0,\pi)$ the variable θ_K assumes complex values which satisfy Eq. (3.22). These values trace a contour on the Riemann surface along which the integration indicated by Eq. (3.3f) must be performed. The end points of the contour are determined as the solutions of Eq. (3.22) for values W = 0 and W = π. Every value of θ_K on the contour C_K determines the contribution to the three-dimensional wave field of a two-dimensional wave field located at the corresponding angular position W. The numerical computation of the values θ_K on contours C_K is performed in exactly the same way as in two-dimensional problems since for every value of W an equivalent x may be taken as x = rcos W.

5.3.2 The Numerical Treatment of the Three-Dimensional Solutions

The considerations of the previous section suggest that the approach to be followed in the numerical treatment of the three-dimensional

solutions may be divided into three steps.

In the first step, the paths of θ_κ for the plane strain and antiplane problems at the angular position W=0 are determined as time increases. The numerical solution of Eq. (3.22) is required to achieve this task for the plane strain problem. However, the complex parameter θ_3, which defines the contribution of the antiplane problem, can be explicitly expressed as a function of x, y and t, i.e.

$$\theta_3 = \frac{tx + y\sqrt{e/d}\sqrt{(x^2 + ey^2/d)/e - t^2}}{(x^2 + ey^2/d)} \tag{5.6}$$

The sign of the y-term is chosen to correspond with the mapping of the $y \geq 0$ half plane to the $\mathrm{Im}\theta_3 \geq 0$ complex plane.[*]

In the second step, the effect of the rotational superposition on the displacement field at every value of time is found by performing the quadratures along the contours C_κ (κ=1, 2, 3). It is important to determine whether the contours C_1 and C_2 are composed of sections that lie entirely on a single sheet of the Riemann surface or not. The reason is that in the numerical computation of the quadratures it is often convenient by use of the Cauchy-Goursat theorem [9] to deform the actual contour into a number of straight line segments. Contour C_3 lies entirely on the θ_3-complex plane. Notice also that the singularity of the integrand expressions of Eqs. (3.36) at $\theta_\kappa = 0$ must be avoided by the deformed contours.

Finally in the third step, a numerical integration scheme is used to perform the quadratures over suitably deformed contours C_κ. The

---

[*]The θ_3-complex plane has a branch cut determined from the function $\lambda_3(\theta_3)$ (see Eq. (2.32)). In this study it is taken along the real axis connecting branch points $\pm 1/\sqrt{e}$.

displacements are calculated by adding the contributions of the quasi-longitudinal wave (contour C_1),the quasi-transverse wave (contour C_2) and the shear wave of the antiplane problem (contour C_3).   In this study Simpson's rule is used except for a short segment at each end of the contour.   There, the singularities introduced by the function $G_\kappa(\theta_\kappa)$ require special consideration, which is the subject of the next section.

5.3.3   The Behavior at the Ends of the Contours C_κ

Let the function $G_\kappa(\theta_\kappa)$ (see Eq. (3.25)) be written in the form

$$G_\kappa(\theta_\kappa) = \left[r\theta_\kappa - t + y\,\lambda_\kappa(\theta_\kappa)\right]^{\frac{1}{2}} \left[r\theta_\kappa + t - y\,\lambda_\kappa(\theta_\kappa)\right]^{\frac{1}{2}} \tag{5.7}$$

The first radical in the product contains the left-hand side of Eq. (3.22) for $W = 0$ and the second radical contains the same expression for $W = \pi$. That is, the ends of the contour C_κ are the zeros of the function $G_\kappa(\theta_\kappa)$. If θ_κ^ℓ indicate the initial point of the contour it is not difficult to show that a power series expansion about θ_κ^ℓ transforms Eq. (5.7) to the expression

$$G_\kappa(\theta_\kappa) = \left(\theta_\kappa - \theta_\kappa^\ell\right)^{\frac{1}{2}} \tilde{G}_\kappa(\theta_\kappa) \tag{5.8}$$

where $\tilde{G}_\kappa(\theta_\kappa^\ell) \neq 0$. As a result, the integrands of Eqs. (3.36) can be written in terms of the radical $(\theta_\kappa - \theta_\kappa^\ell)^{\frac{1}{2}}$ which behaves nonanalytically at θ_κ^ℓ and a function which is analytic at θ_κ^ℓ. The latter can be approximated by its linear part and integrated as shown in sections 4.1 and 4.2 of Appendix D to obtain an integration formula. This formula is used for the numerical computation of the quadrature along a small section at the ends of the contours.

9476

1.0

4.5
5.0
5.6

2.8

2.5

3.2

2.2

3.6

1.1

4.0

2.0

1.8

1.25

1.4

1.6
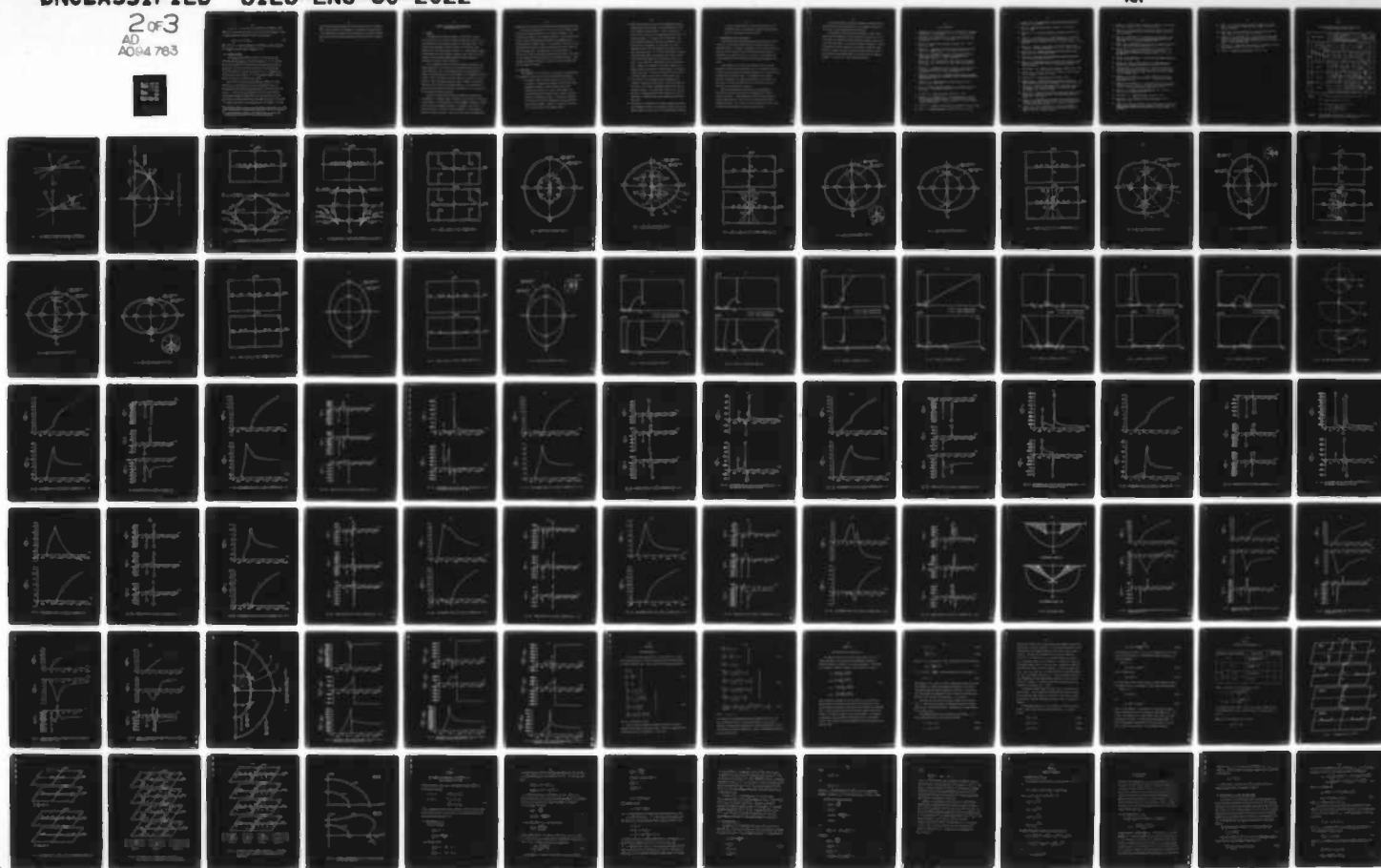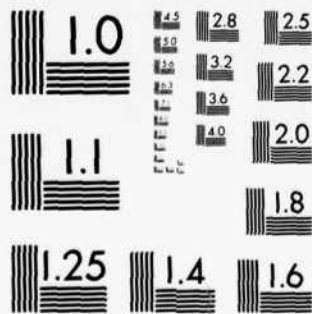
MICROCOPY RESOLUTION TEST CHART
NATIONAL BUREAU OF STANDARDS-1963-A

If the particular value of the time variable corresponds to the passage of one of the wave fronts at the point under consideration, then it can be shown that the function $G_\kappa(\theta_\kappa)$ can be written as

$$G_\kappa(\theta_\kappa) = (\theta_\kappa - \theta_\kappa^\ell)\, \tilde{G}^*(\theta_\kappa) \tag{5.9}$$

where $\tilde{G}_\kappa^*(\theta_\kappa^\ell) \neq 0$. The same procedure as previously is used to develop the integration formula given in Appendix D.4.3.

5.3.4 Sample Problems

The methodology described in section 5.3.2 has been used to calculate the time histories of the displacements u_r, u_ω, u_y when the applied load consists of a suddenly applied tangential point force at the origin. The wave-front pattern generated for a transversely isotropic material of class B-I[*] is shown in Fig. 45. Sample dynamic responses for various values of γ[**] in transversely isotropic media of classes B-I and A-I are given in Figs. 46-48.

The arrival of the quasi-longitudinal wave results in a step discontinuity of the radial and vertical displacements while the circumferential displacement behaves continuously starting from a value of zero. A similar step discontinuity in the radial and vertical displacements appears also upon the arrival of the quasi-transverse wave front, while the arrival of the shear type (antiplane) wave results in a step discontinuity of the circumferencial displacement. At large

---

[*] Transversely isotropic materials are designated in this study by the class which characterizes the corresponding plane-strain orthotropic material.

[**] In three-dimensional problems $\gamma = r_R / y_R$, where (r_R, ω_R, y_R) are the cylindrical coordinates of the point under consideration.

times the displacements approach the static solutions found in reference [48]. When the conditions of Appendix G are applied, the time histories of the displacements correspond to the solutions for an isotropic material. These solutions at large times approach the static solutions of reference [24].

6. SUMMARY, CONCLUSIONS AND RECOMMENDATIONS
FOR FURTHER STUDY

6.1 Summary

The method of self-similar potentials or functional invariant
solutions was used in this study to obtain solutions for certain two- and
three-dimensional wave propagation problems in anisotropic media. The
solutions were expressed in terms of analytic functions which were
determined from the given boundary conditions in a straightforward manner.
In the process only simple algebraic operations were required, a distinct
advantage over alternative methods employing the more complicated
techniques of multiple inverse transforms.

The two-dimensional cases solved wave propagation problems for the
sudden application of a line force in an orthotropic medium under plane
strain conditions. Each of the propagating waves was parametrized by a
complex variable which was used as the argument of a corresponding potential
function. Thus, the problem of reflection was easily handled by forming a
system of linear simultaneous equations, equal in number to the boundary
conditions, and solving for the unknown potentials. Any singularities in
the wave fields could be inferred from the examination of the singularities
of the associated potential functions.

Solutions of appropriately defined two-dimensional problems were
superimposed in a rotational manner to obtain the wave field in transversely
isotropic media. The displacements for the axisymmetric problem of a normal
force and the non-axisymmetric problem of a tangential force on the $y = 0$
surface were given in the form of simple quadratures. The technique of
rotational superposition made it possible to solve these three-dimensional

problems with little additional difficulty than the two-dimensional cases.

The correct representation of the wave fields in the complex domain proved to be extremely important in the numerical treatment of the solutions and, therefore, was thoroughly examined. It was shown that wave fields in plane strain othotropic materials can be mapped onto four different types of Riemann surfaces. In the numerical calculation of the displacements and stresses efficient techniques were used to locate the existing singularities. The quadratures of the displacements in transversely isotropic media were performed by using Simpson's rule except for small segments at the end points of the integration contours. There, the dominant nonanalytic behavior was taken into account by employing special integration formulas.

6.2 Conclusions

The development of the solutions, the discussion of the mapping and the presentation of the results lead to the following conclusions:

1) The method of the self-similar potentials can also be used to provide a straightforward approach in the solution of wave propagation problems in certain anisotropic materials. Isotropy can be treated as a special case; however, the computational effort to develop the more general anisotropic solution is significantly larger. Of particular importance is the fact that the quasi-longitudinal and quasi-transverse wave fields are mapped, in general, in regions which do not lie on a single sheet of the Riemann surface.

2) Under certain conditions on the elastic parameters the quasi-transverse wave front possesses cusps and double points which form triangularly shaped lacunas. Elastic stresses do not exist for points inside the lacunas except when the lacuna is in a head wave region. In a sense, then, the sections of the quasi-transverse wave front which form the boundary of the lacunas can also be thought of as being part of a quasi-longitudinal wave front even though they are moving out at quasi-transverse speeds. As a result, points which are located so that they experience four encounters with various sections of the wave fronts present four singularities in the stress field. At all other point locations only two such encounters occur. However, rapid changes in the stress responses are observed which are affected to a varying degree by the nearness to any of the cusps. The behavior of materials with no cusps in the wave fronts is very similar to the isotropic case.

3) The solutions of the half-space problems demonstrate the existence of head wave regions which, in the case of materials with cusps in the fronts, are somewhat different than those in isotropic materials. In certain cases there exists a trailing as well as a leading head wave front in contrast to a single front which is formed when the quasi-transverse wave does not have cusps.

4) The extension of the method of rotational superposition permits wave propagation problems in transversely isotropic media to be treated almost as easily as any of the two-dimensional problems.

It should be emphasized that in this case solutions for two
different materials are superposed to obtain the displacement
field in a transversely isotropic medium.

6.3 Recommendations for Further Study

The solutions which have been developed in this study can be used
directly for a more detailed examination of the dynamic behavior of
anisotropic media. For example, a parametric study of the time histories
where the elastic constants vary continuously may make possible the
recognition of the characteristics, if any exist, in the response that
may be associated with the conditions for the initial formation of the
cusps.

A more general time variation of the applied force in the two-
dimensional problems can be constructed by use of a convolution integral.
In such a process solutions for different magnitudes of an impulsive load
are superposed at different times. In seismology and in fracture
mechanics the problem of an expanding dislocation in the interior of a
half-space is of great importance and can be solved for anisotropic
materials by the methodology of Chapter 2.

Another interesting application concerns the development of
solutions for two bonded half-spaces each representing a different
anisotropic material. The generated reflected and refracted waves are
associated with potentials which can be easily determined from the
boundary conditions. The solution to this problem may be the first step
in formulating a more general layered anisotropic space.

A challenging question is posed as to whether a modified Smirnov-Sobolev method could be developed to solve the problems worked out in this study for a more general anisotropic material.

In transversely isotropic media the problems of a point force, a double force with moment or a point dislocation in the interior of a half space can be obtained from the solutions of Chapters 2 and 3 with little additional effort. The case of two bonded transversely isotropic half-spaces can also be treated by the technique of rotational super-position. However, the latter may require some modification before it can be applied to more general types of anisotropy than the hexagonal symmetry. This point still needs further exploration.

92

LIST OF REFERENCES

1. Aleksandrov, K.S., "The Wave Surfaces for Elastic Waves in Crystals," Soviet Physics - Crystallography, Vol. 3, No. 5, 1958, pp. 627-629.

2. Aleksandrov, K.S. and Ryzhova, T.V., "The Elastic Properties of Crystals," Soviet Physics - Crystallography, Vol. 6, No. 2, 1961, pp. 228-252.

3. Auld, B.A., Acoustic Fields and Waves in Solids, Vols. I and II, John Wiley, 1973.

4. Backus, G.E., "Long-Wave Elastic Anisotropy Produced by Horizontal Layering," J. Geophys. Res., 67 (11), 1962, pp. 4427-4440.

5. Budaev, V.S., "Boundary-Value Problem in the Dynamical Theory of Elastic Anisotropic Media," Zhurnal Prikladnoi Mekhaniki i Tekhnicheskoi Fiziki, No. 3, 1974, pp. 121-125.

6. Budaev, V.S., "The Two-Dimensional Lamb's Problem in Anisotropic Half-Space", Bull. (Izv) Acad. Sci. USSR, Mech. of Solid Bodies, No. 3, 1975.

7. Budaev, V.S., "Propagation of Vibrations from a Point Pulse Source in Elastic Anisotropic Half-Space," Izvestiya, Physics of the Solid Earth, Vol. 13, No. 2, 1977, pp. 102-107.

8. Chadwick, P. and Smith, G.D., Foundations of the Theory of Surface Waves in Anisotropic Elastic Materials, Advances in Applied Mechanics, Academic Press, 1977.

9. Churchill, R.V., Complex Variables and Applications, 2nd Ed., McGraw-Hill, New York, 1960.

10. De, S., "Problem on the Wave Propagation in an Anisotropic Elastic Half-Space," Acta Geophysica Polonica, Vol. XXI, No. 1, 1973, pp. 11-26.

11. Evgrafov, M.A., Analytic Functions, Dover Publ., 1978.

12. Farewell, T.E. and Robinson, A.R., "Wave Propagation in an Elastic Half Space due to Couples Applied at a Point Beneath the Surface," Civil Engineering Studies, SRS 411, University of Illinois, Urbana, Illinois, August 1974.

13. Fedorov, F.I., Theory of Elastic Waves in Crystals, Plenum Press, 1968.

14. Hamel, G., Integralgleichungen, Springer-Verlag, Berlin, 1949.

15. Hearmon, R.F.S., _An Introduction to Applied Anisotropic Elasticity_, Oxford Univ. Press, 1961.

16. Hille, E., _Analytic Function Theory_, Volumes I, II, Ginn & Co., New York, 1959.

17. Huntington, H.B., _The Elastic Constants of Crystals_, Academic Press, 1958.

18. Johnson, J.J. and Robinson, A.R., "Wave Propagation in a Half Space Due to an Interior Point Load Parallel to the Surface," Civil Engineering Studies, _SRS 388_, University of Illinois, Urbana, Illinois, July 1972.

19. Kraut, E.A., "Advances in the Theory of Anisotropic Elastic Wave Propagation," _Reviews of Geophysics_, Vol. 1, No. 3, 1963, pp. 401-448.

20. Lekhnitskii, S.G., _Theory of Elasticity of an Anisotropic Elastic Body_, Holden-Day, San Francisco, 1963.

21. Love, A.E.H., _A Treatise on the Mathematical Theory of Elasticity_, Dover Publications, New York, 1944.

22. Melan, E., "Der Spannungszustand der durch eine Einzelkraft im Innern beanspruchten Halbscheibe," _Zeits. fur angew. Math. und Mech._, 12, 1932, pp. 343-346.

23. Milne-Thomson, L.M., _Antiplane Elastic Systems_, Academic Press, 1962.

24. Mindlin, R.D., "Force at a Point in the Interior of a Semi-Infinite Solid," _Physics_, 7, 1936, pp. 195-202.

25. Musgrave, M.J.P., _Crystal Acoustics_, Holden-Day, 1970.

26. Musgrave, M.J.P., "Progressive Waves in Anisotropic Media," in _Modern Problems in Elastic Wave Propagation_, Wiley-Interscience, 1978.

27. Osipov, I.O., "Reflection and Refraction of Plane Elastic Waves at the Boundary of Two Anisotropic Media," _Izv. Akad. Nauk. SSSR, ser. geofiz._, No. 5, 1961, pp. 424-431.

28. Osipov, I.O., "Features of the Variation of Propagation Velocities of Elastic Waves in Anisotropic Media," _Izv. Akad. Nauk. SSSR, ser. geofiz_, No. 1, 1962, pp. 5-9.

29. Osipov, I.O., "The Method of Functionally Invariant Solutions for Problems in the Dynamic Theory of Elasticity for Anisotropic Media," _Izv. Akad. Nauk. SSSR, ser. geofiz._ No. 3, 1963, pp. 245-248.

30. Osipov, I.O., "On the Two-Dimensional Problem of Propagation of Elastic Waves due to a Point Source in an Anisotropic Medium," _PMM_, Vol. 33, No. 3, 1969, pp. 534-542.

31. Osipov, I.O., "On the Theory of Rayleigh Type Waves in an Anisotropic Half-Space," PMM, Vol. 34, No. 4, 1970, pp. 729-731.

32. Osipov, I.O., "On Wave Fields and Acute-Angled Edges on Wave Fronts in an Anisotropic Medium from a Point Source," PMM, Vol. 36, No. 5, 1972, pp. 874-882.

33. Paul, S.L., and Robinson, A.R., "Interaction of Plane Elastic Waves with a Cylindrical Cavity," Technical Documentary Report No. RTD TDR-63-3021, Air Force Weapons Laboratory, 1963.

34. Payton, R.G., "Symmetry-Axis Elastic Waves for Transversely Isotropic Media," Quarterly of Applied Mathematics, April 1977, pp. 63-73.

35. Payton, R.G., "Plane Strain Displacement and Stress Waves Induced in a Tranversely Isotropic Elastic Solid by a Line Source," Journal of Applied Mathematics and Physics (ZAMP), Vol. 29, 1978, pp. 262-272.

36. Ralston, A. and Rabinowitz, P., A First Course in Numerical Analysis, 2nd Ed., McGraw-Hill, 1978.

37. Schwartz, M., Green, S. and Rutledge, W.A., Vector Analysis with Applications to Geometry and Physics, Harper, New York, 1960.

38. Seyyedian-Choobi, M. and Robinson, A.R., "Motion on the Surface of a Layered Elastic Half Space Produced by a Buried Dislocation Pulse," Civil Engineering Studies, SRS 421, University of Illinois, Urbana, Illinois, November 1975.

39. Smirnov, V.I. and Sobolev, S.L., "Sur une méthode nouvelle dans le problème plan des vibrations élastiques," Trud. Inst. Seism. Akad. Nauk. SSSR, 20, 1932.

40. Smirnov, V.I. and Sobolev, S.L., "On the Application of a New Method of Investigation of the Elastic Vibrations in the Space with Axial Symmetry," Trud. Inst. Seism. Akad. Nauk. SSSR, 29, 1933.

41. Smirnov, V.I., A Course of Higher Mathematics, Vol. III, Part 2, Addison-Wesley, Reading, Mass, 1964.

42. Sokolnikoff, I.S., Advanced Calculus, McGraw-Hill, 1939.

43. Sokolnikoff, I.S., Mathematical Theory of Elasticity, 2nd Ed., McGraw-Hill, 1956.

44. Sveklo, V.A., "Elastic Vibrations of Anisotropic Bodies" (in Russian), Uchenye Zapiski Leningr. Univ. Ser. Matem. N. (Scientific Memoirs of Leningrad Univ., Mathematical Sciences Series), No. 17, 1949, pp. 28-71.

45. Sveklo, V.A., "On the Solution of Dynamic Problems in the Plane Theory of Elasticity for Anisotropic Media," PMM, Vol. 25, No. 5, 1961, pp. 1324-1339.

46. Sveklo, V.A., "The Mixed Problem for the Elastic Anisotropic Half-Plane," PMM, Vol. 26, No. 5, 1962, pp. 1354-1368.

47. Thompson, J.C. and Robinson, A.R., "Exact Solutions of Some Dynamic Problems of Identation and Transient Loadings of an Elastic Half Space," Civil Engineering Studies, SRS 350, University of Illinois, Urbana, Illinois, September 1969.

48. Toneatto, G.M., "Concentrated Force Problems in Transverse Isotropy," Ph.D. Thesis, University of Illinois, Urbana, 1978.

49. Voigt, W., Lehrbuch der Kristallphysik, Leipzig, 1910.

TABLE 1

RELATIONS BETWEEN ELASTIC CONSTANTS AND THE SHAPE OF THE QUASI-TRANSVERSE WAVE FRONT

Elastic Conditions					(Values of Angle β_2) / (Values of θ_κ) / S_κ Sheet of Riemann Surface	Shape of Quasi-Transverse Wave Front	Material Case
$N_2 > 0$	$N_3 > 0$	$N_4 > 0$			$0 \vdash\!\!\!\!\longrightarrow\!\!\!\!\longrightarrow\!\!\!\!\dashv\ \pi/2$ / $1/\sqrt{d}$; S_2	(circle)	A
		$N_4 < 0$	$N_1 < 0$	$N_5 < 0$			
			$N_1 > 0$	$N_5 > 0$	$0 \vdash\ \beta^{1*}\ \beta^{2*}\ \pi/2$; $\theta^{1*}\ \theta^{2*}\ 1/\sqrt{d}$; S_2	(rounded square)	B
	$N_3 < 0$				$0 \vdash\ -\beta^*\ 0\ \pi/2$; $\theta^*\ \theta^{**}\ 1/\sqrt{d}$; S_2	(lens/eye shape)	D
$N_2 < 0$	$N_3 < 0$				$0 \vdash\ -\widetilde{\beta}^{1*}\ 0\ \pi/2\ \widetilde{\beta}^{3*}\ \pi/2$; $\widetilde{\theta}^{1*}\ \widetilde{\theta}^{2*}\ \Theta_{01}\ \widetilde{\theta}^*\ 1/\sqrt{d}$; S_2 S_1	(crossing shape)	C
	$N_3 > 0$				$0 \vdash\ \pi/2\ \widetilde{\beta}^*\ \pi/2$; $\Theta_{01}\ \widetilde{\theta}^*\ 1/\sqrt{d}$; S_2 S_1	(crossing shape)	E

<u>Note 1.</u> θ^{1*}, θ^{2*} and θ^* are roots of function $D_2(\theta)$ in $(0, 1/\sqrt{d})$

$\widetilde{\theta}^{1*}$ is the root of $D_2(\theta)$ in $(0, \Theta_{01})$

$\widetilde{\theta}^*$ is the root of $D_1(\theta)$ in $(\Theta_{01}, 1/\sqrt{\bar{d}})$

$$\theta^{**} = \widetilde{\theta}^{2*} = \left[\frac{M - L\sqrt{-c^2 N_1/ad}}{K_1 K_2}\right]^{1/2}$$

<u>Note 2.</u> Arrow indicates monotonically increasing (↗) or monotonically decreasing (↘) values in the specified interval.
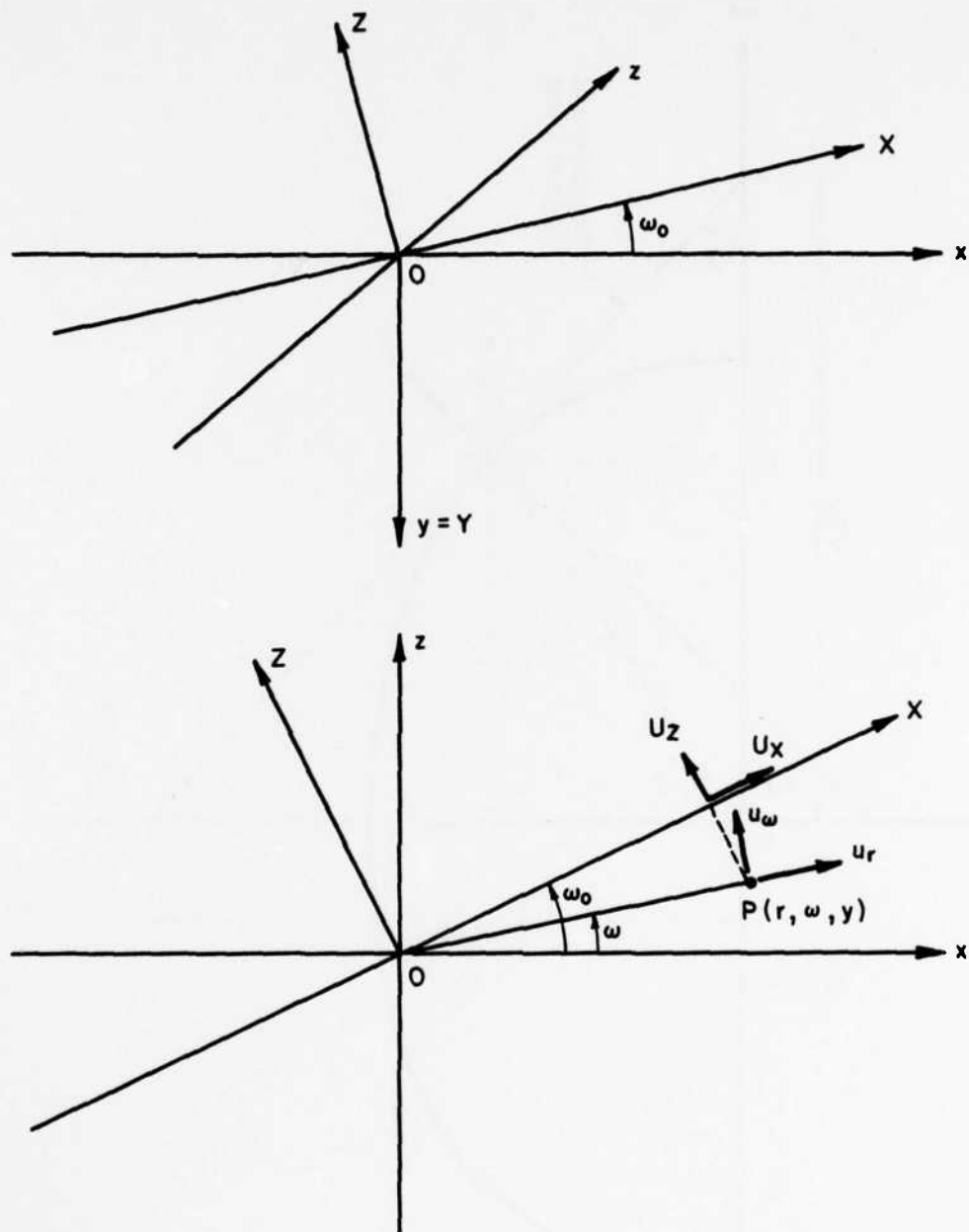
FIG. 1   THE COORDINATE SYSTEMS FOR ROTATIONAL SUPERPOSITION
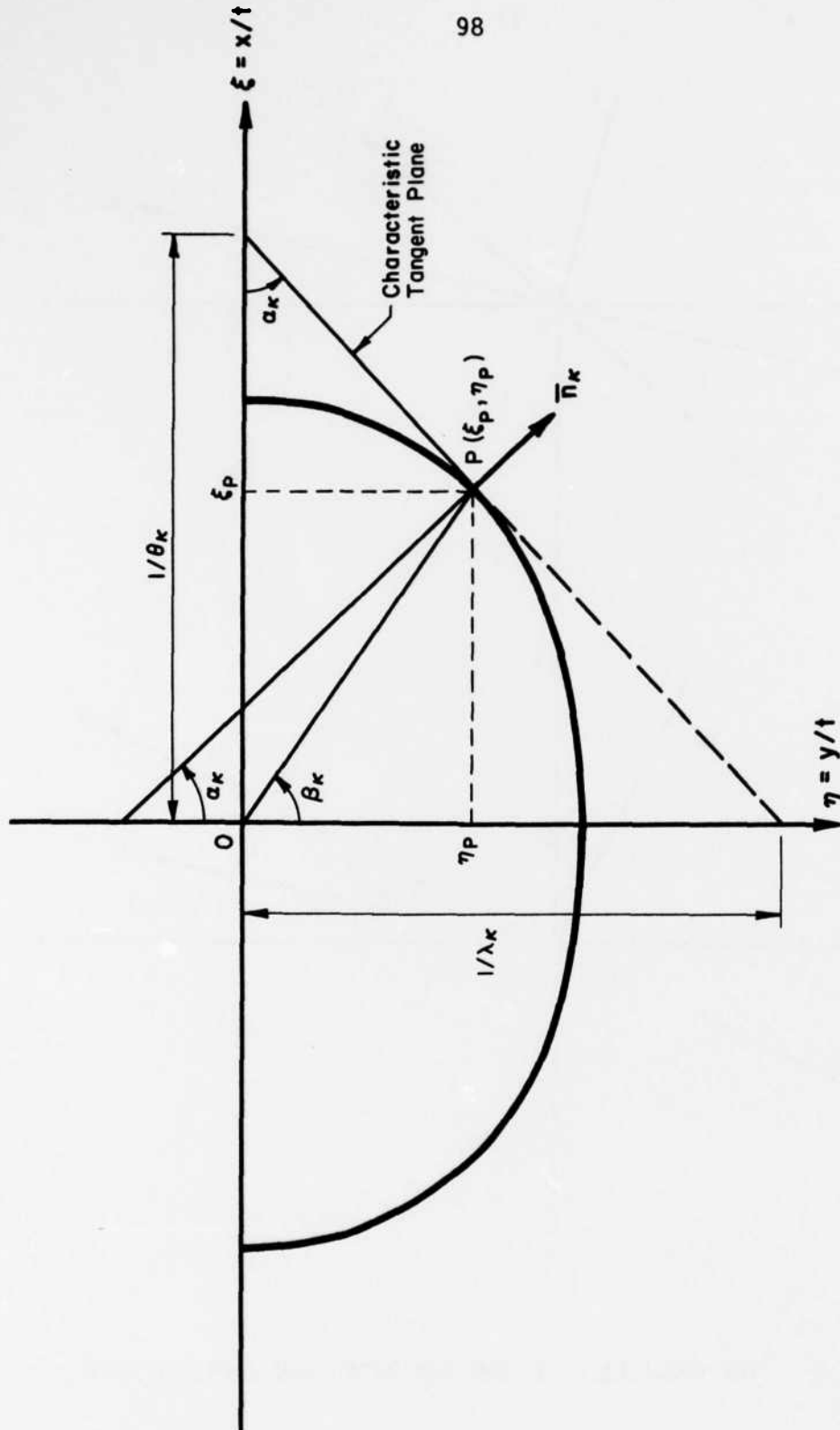
FIG. 2   WAVE FRONT WITH DEFINITION OF α_κ AND β_κ
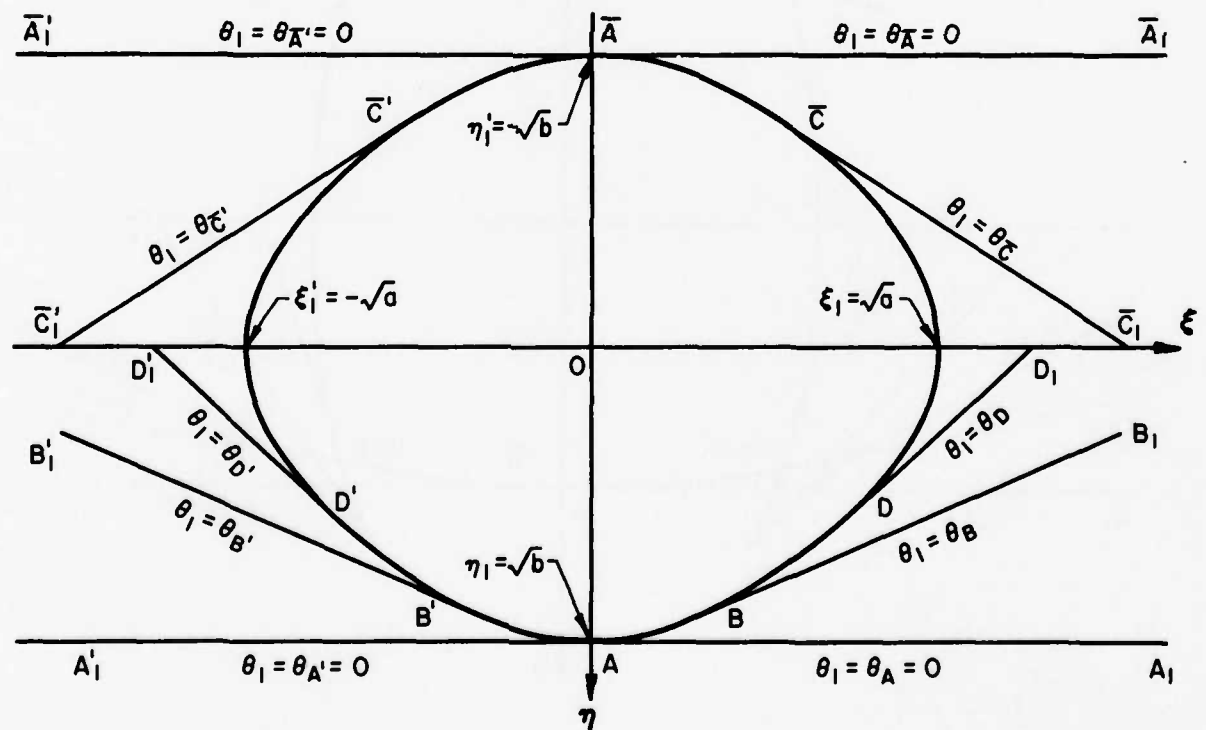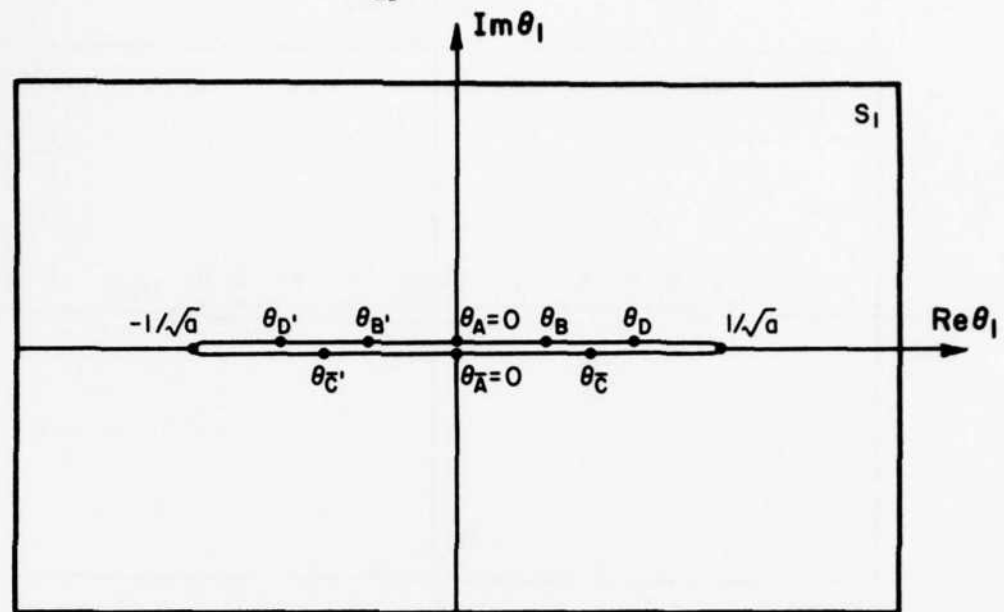
FIG. 3   THE REPRESENTATION OF THE QUASI-LONGITUDINAL WAVE ON SHEET S_1
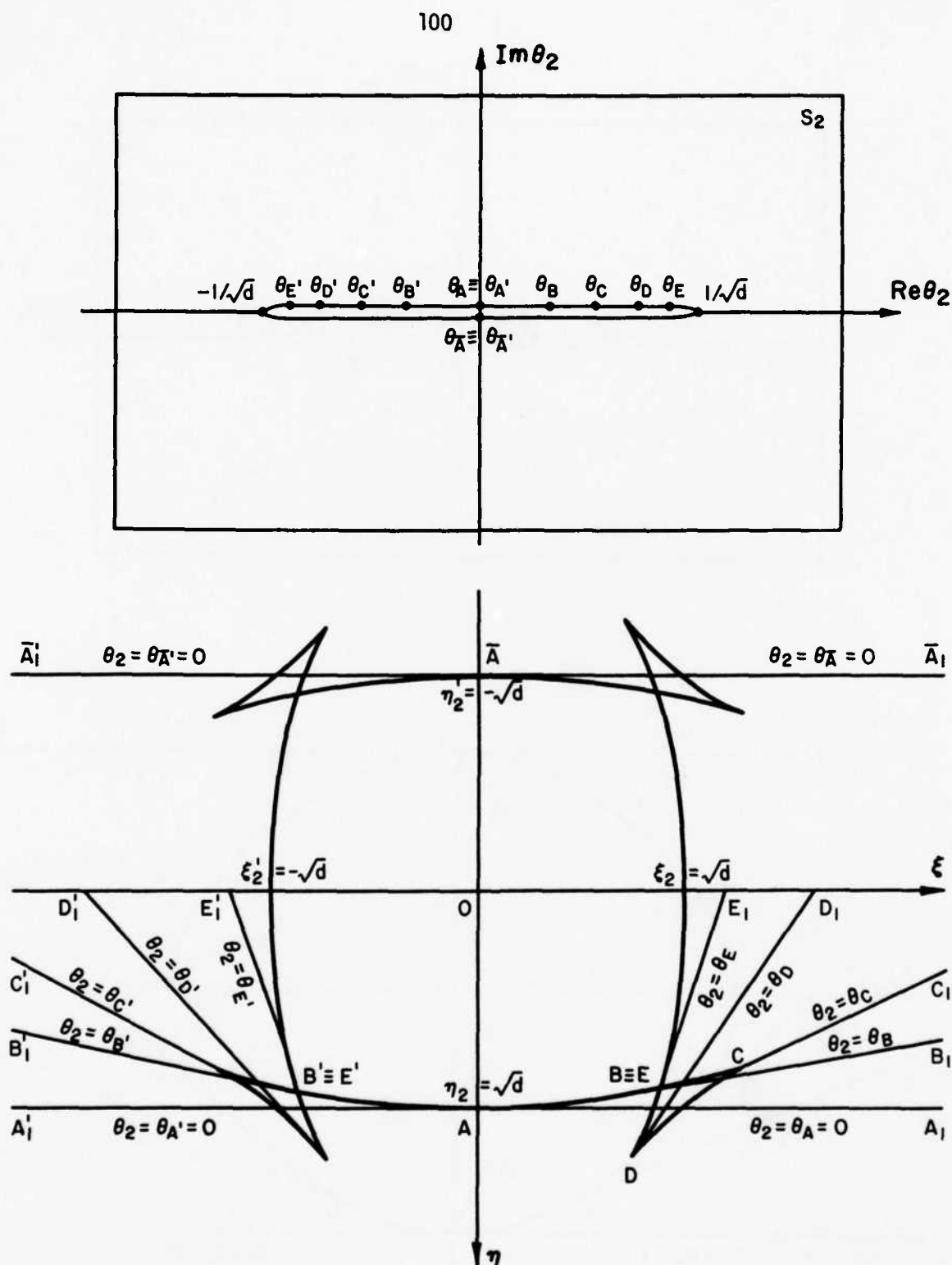
FIG. 4   THE REPRESENTATION OF A CUSPED QUASI-TRANSVERSE WAVE ON SHEET S_2
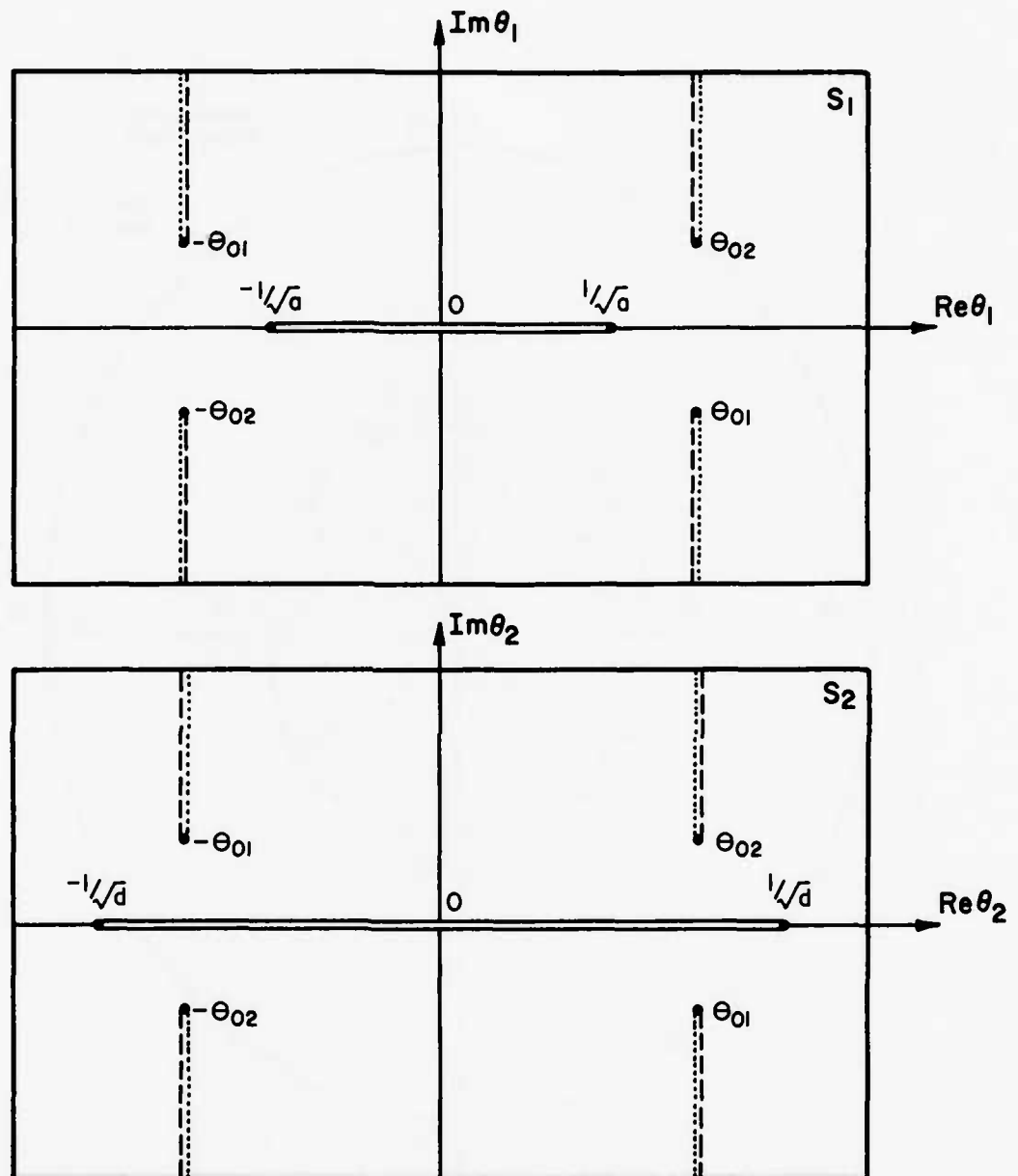
FIG. 5   SHEETS S_1 AND S_2 OF TYPE I RIEMANN SURFACE

102
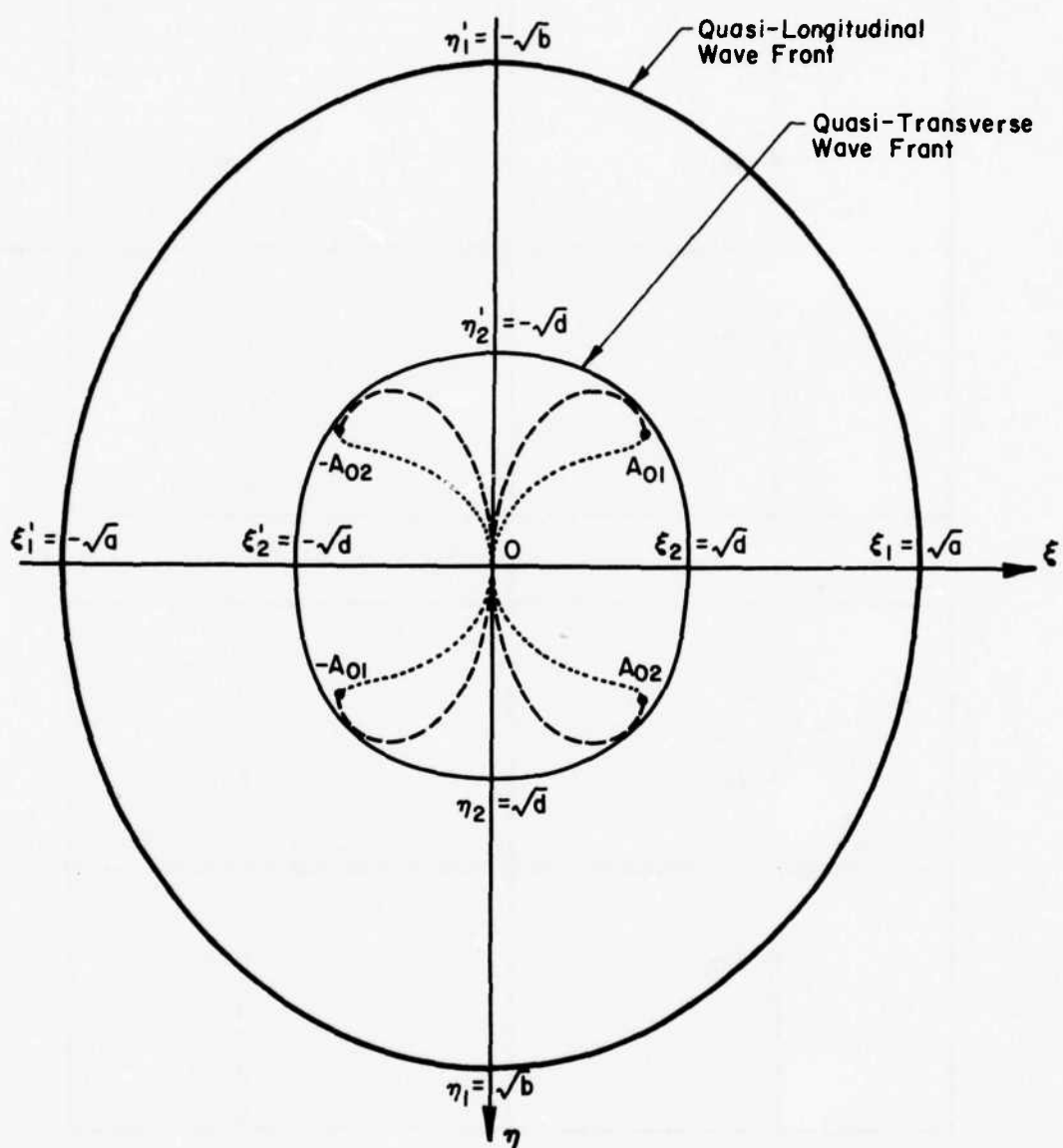
FIG. 6   WAVE FIELDS FOR MATERIAL CASE A-I
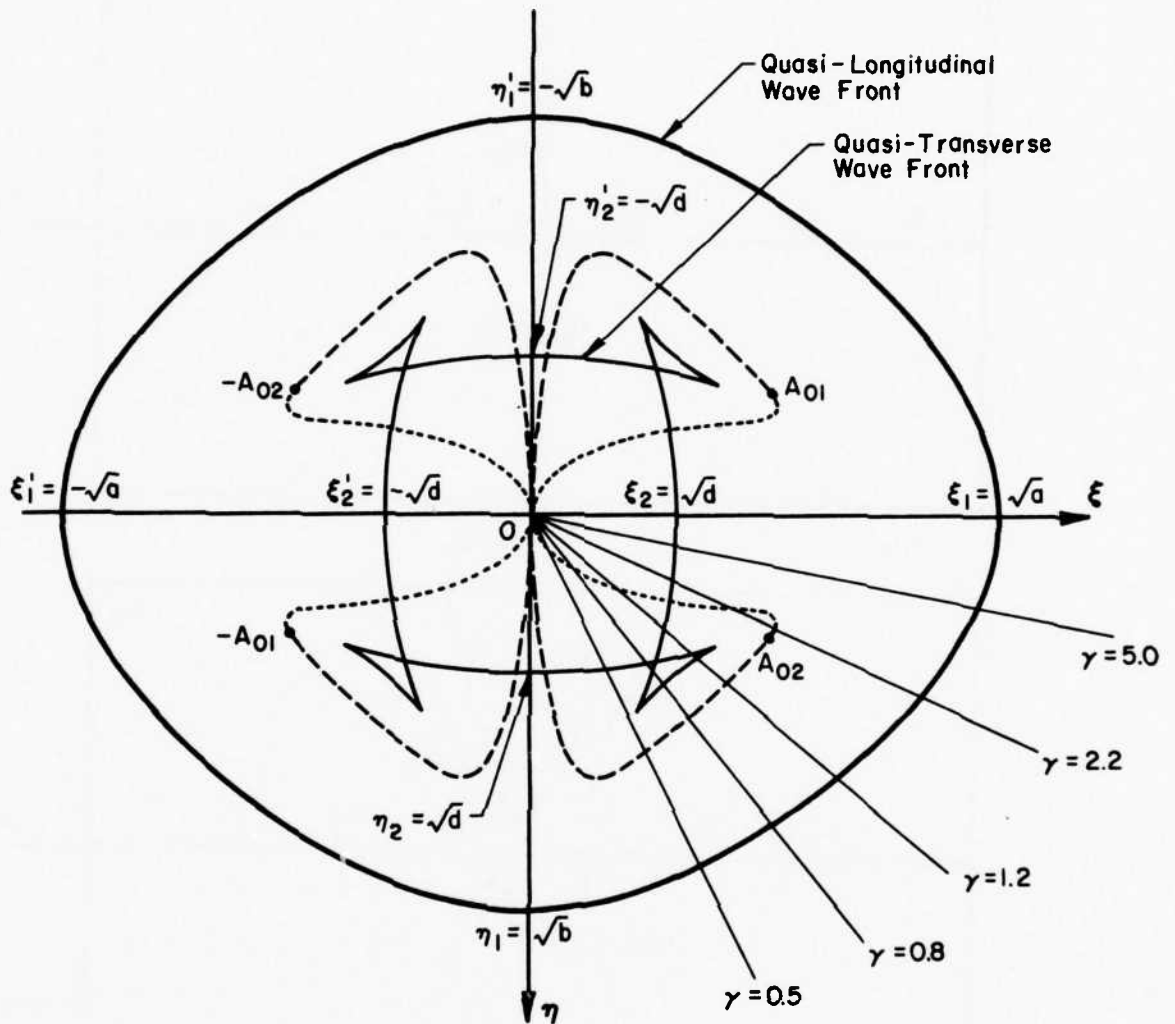
FIG. 7   WAVE FIELDS FOR MATERIAL CASE B-I
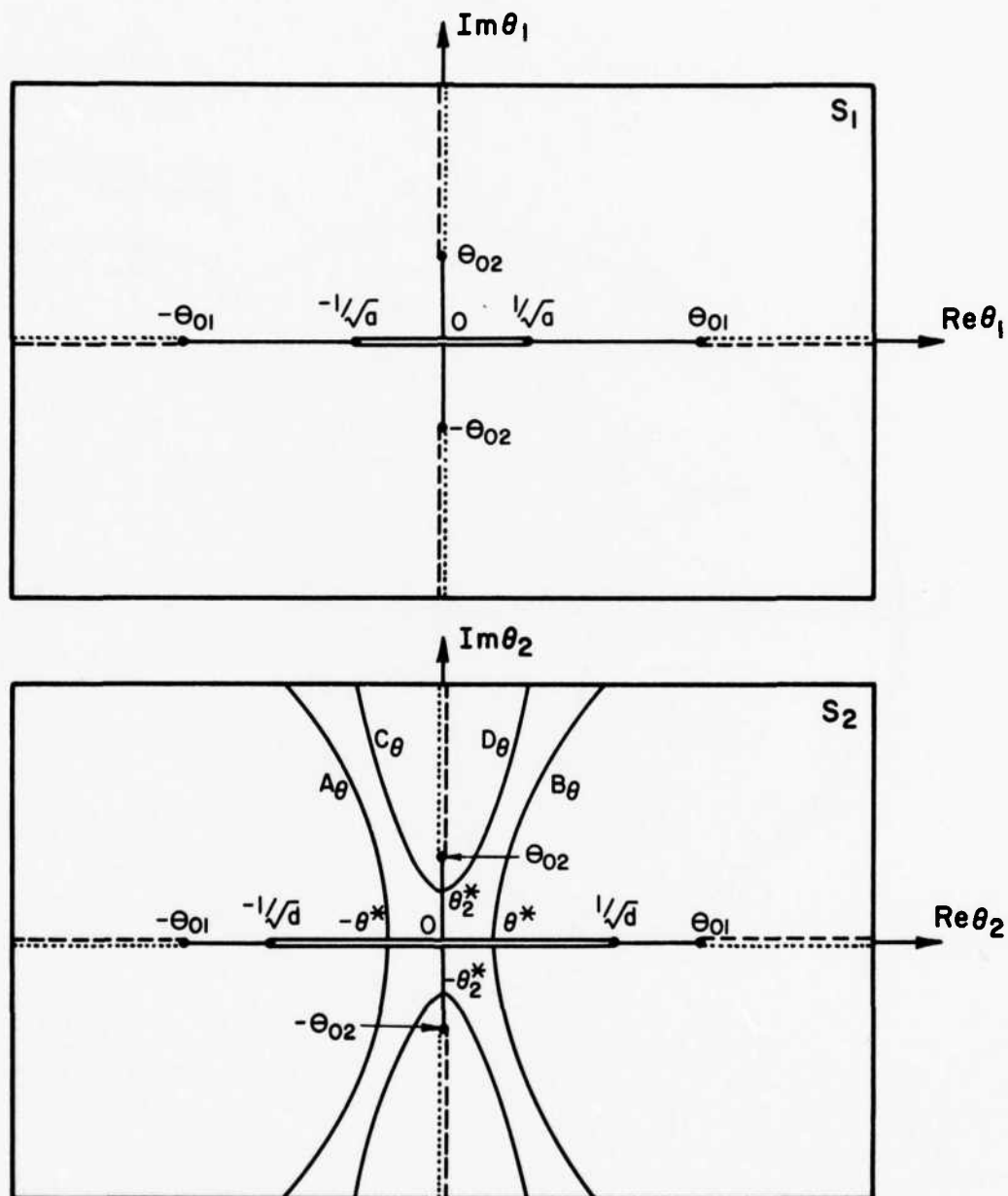
FIG. 8   SHEETS S_1 AND S_2 OF TYPE II RIEMANN SURFACE ($N_2 > 0$)
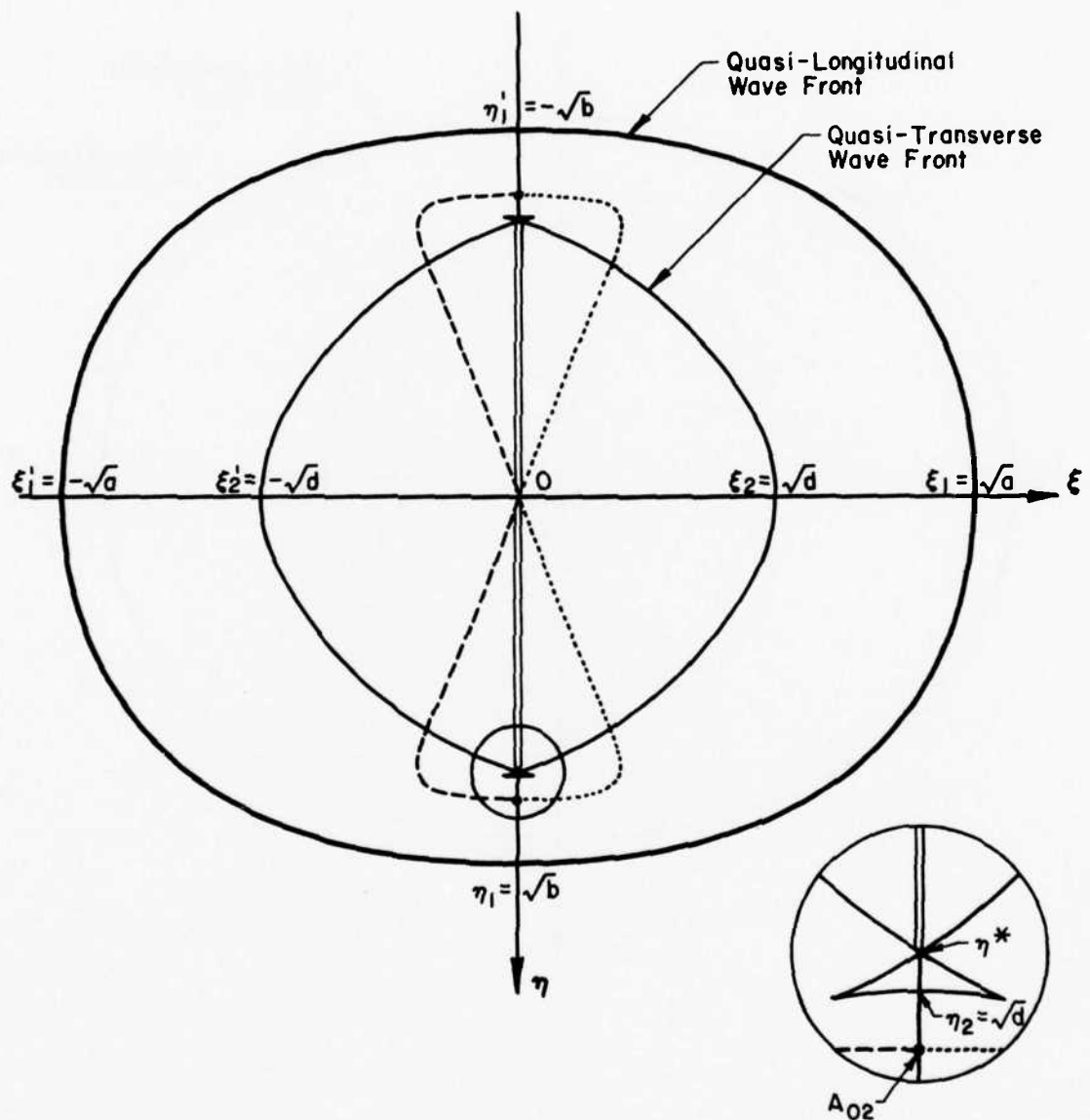
FIG. 9   WAVE FIELDS FOR MATERIAL CASE D-II

106
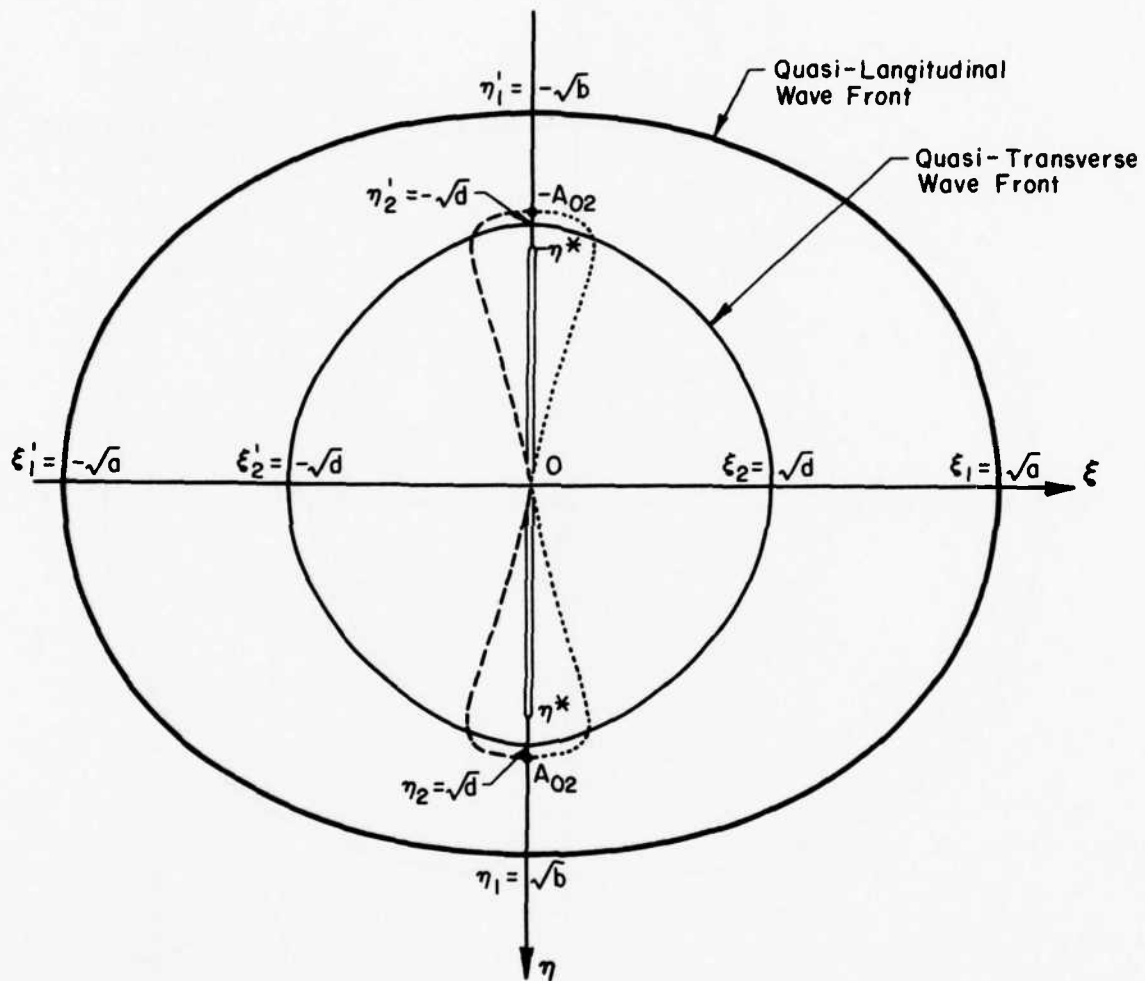
FIG. 10   WAVE FIELDS FOR MATERIAL CASE A-II
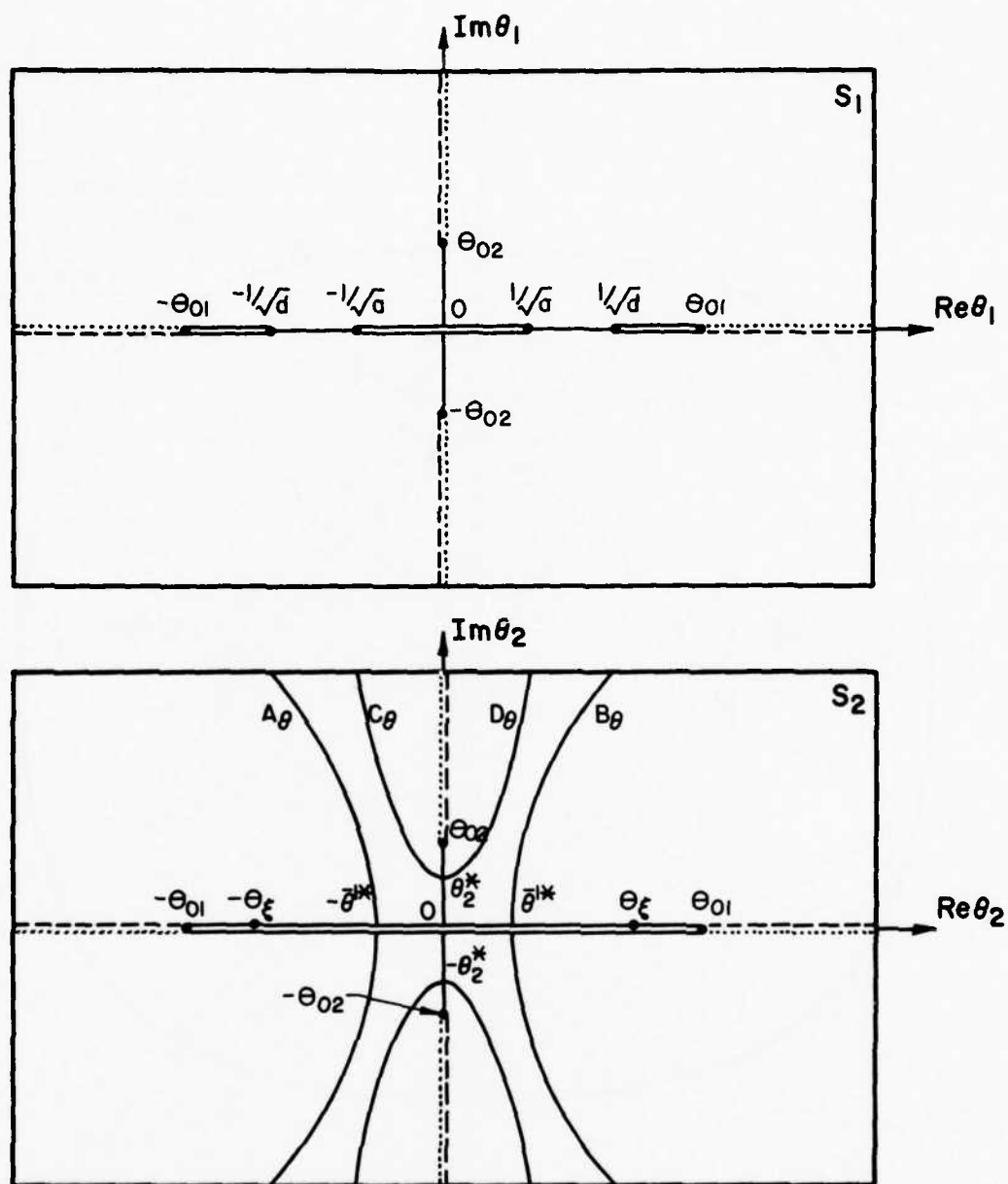
FIG. 11   SHEETS S_1 AND S_2 OF TYPE II RIEMANN SURFACE ($N_2 < 0$)
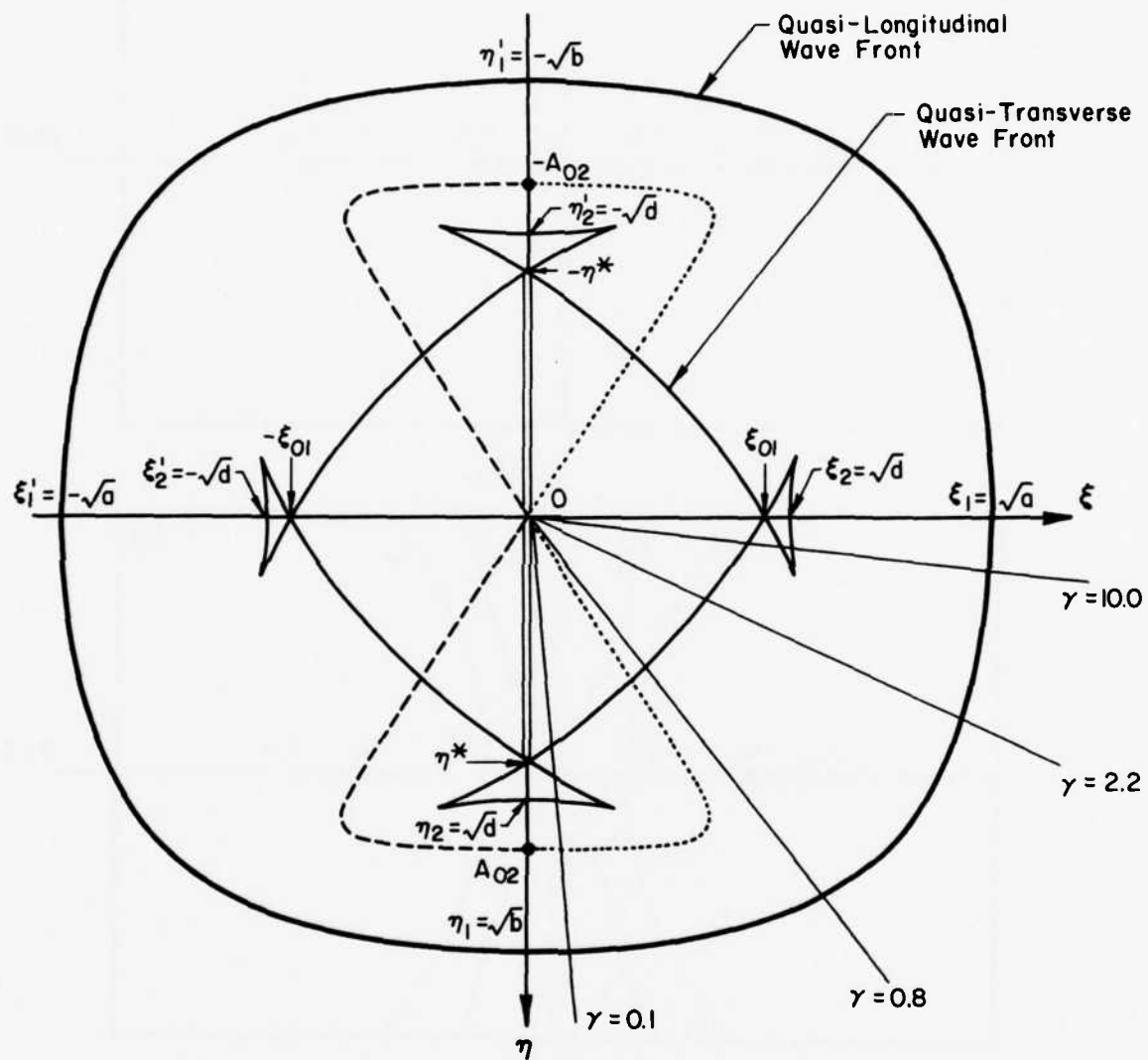
FIG. 12   WAVE FIELDS FOR MATERIAL CASE C-II
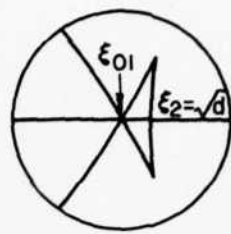
FIG. 13   WAVE FIELDS FOR MATERIAL CASE E-II
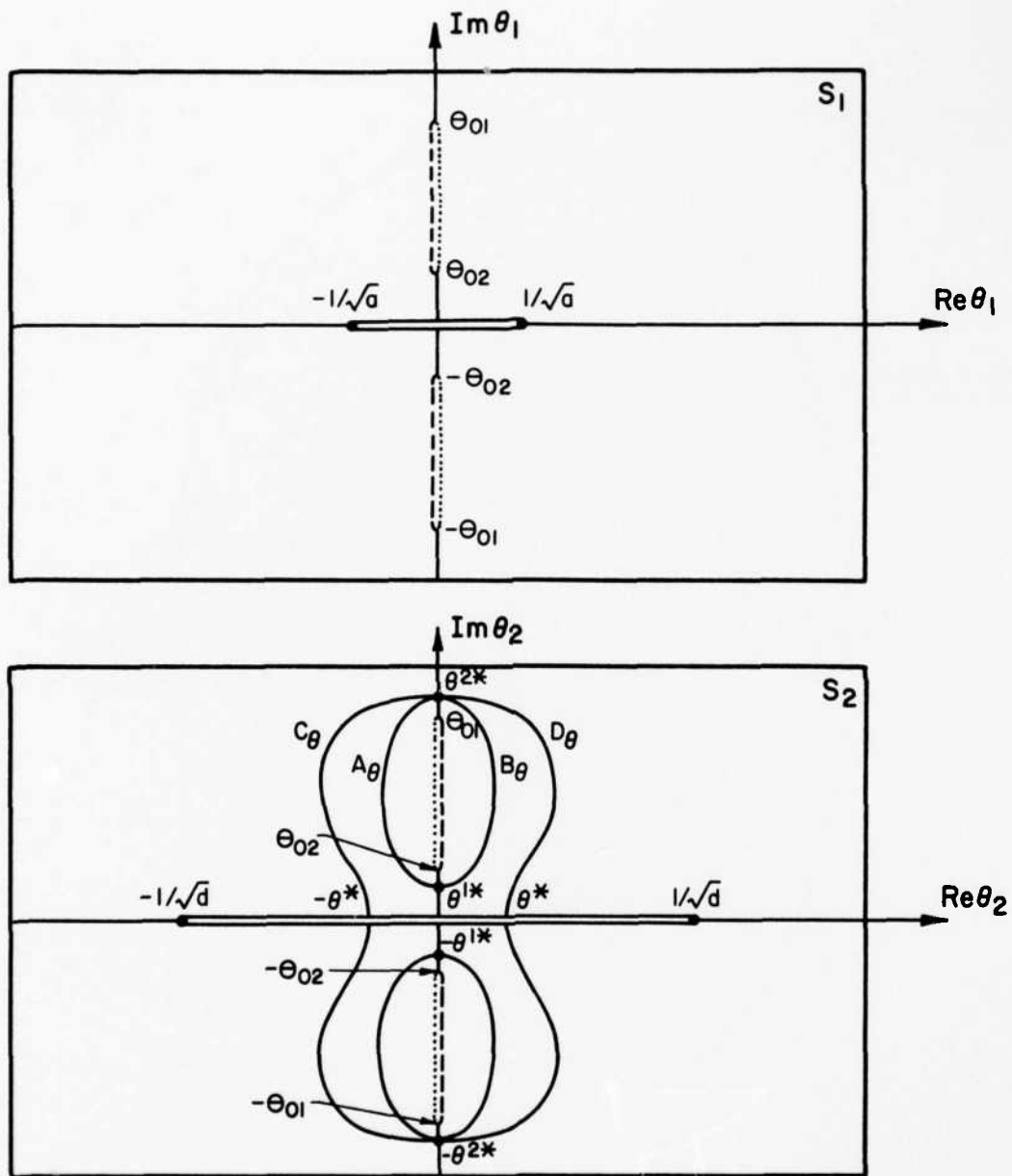
FIG. 14   SHEETS S_1 AND S_2 OF TYPE III RIEMANN SURFACE
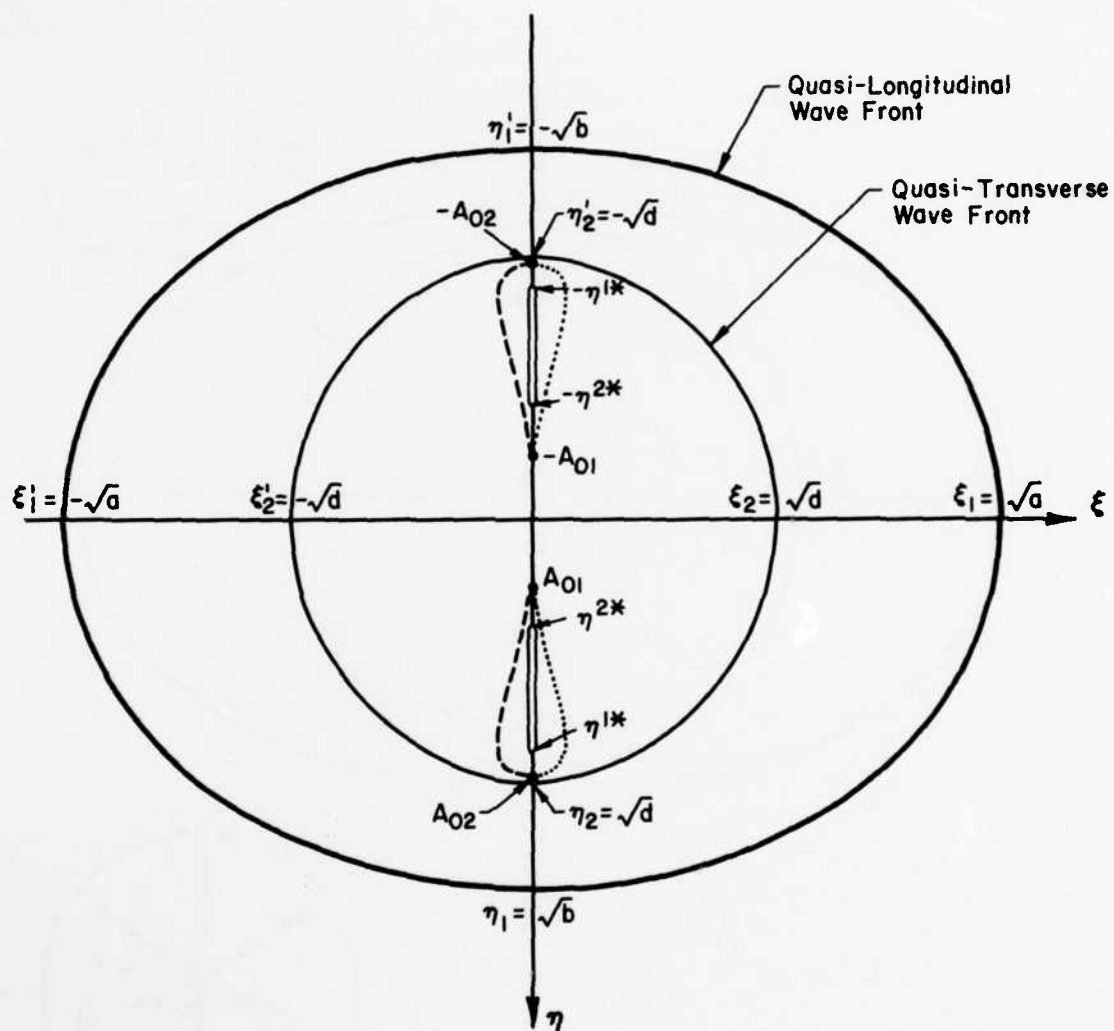
FIG. 15   WAVE FIELDS FOR MATERIAL CASE A-III
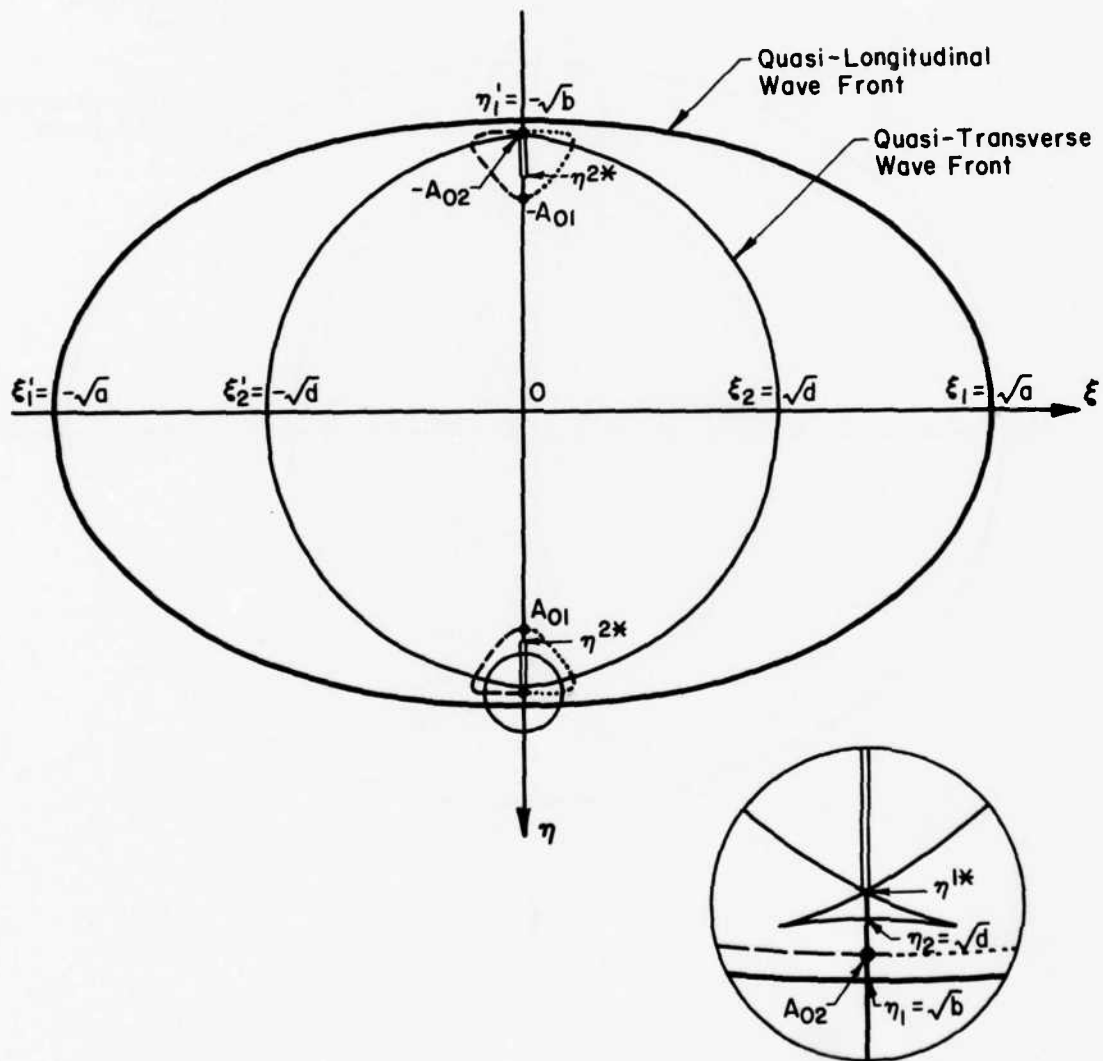
FIG. 16   WAVE FIELDS FOR MATERIAL CASE D-III
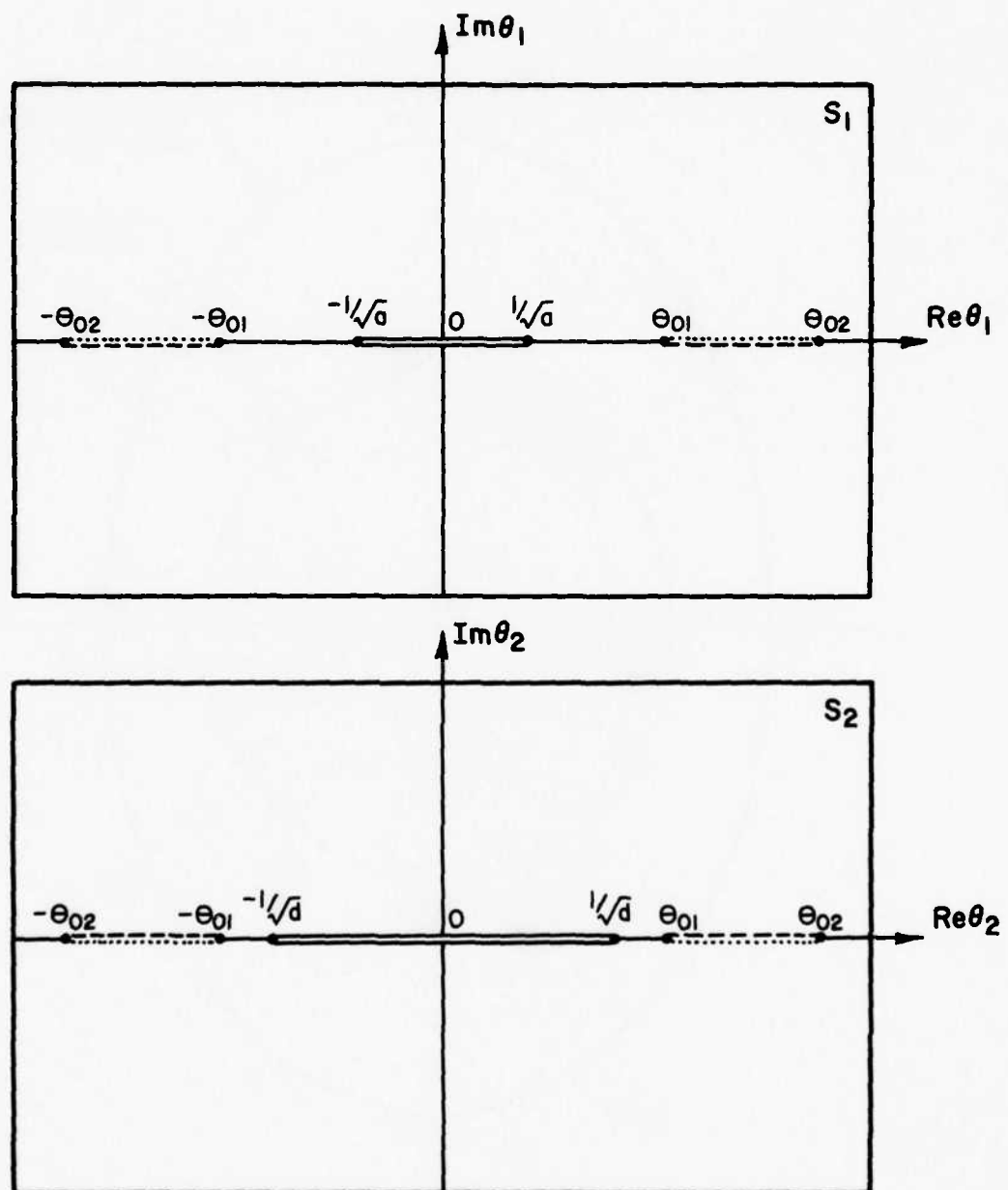
FIG. 17   SHEETS S_1 AND S_2 OF TYPE IV RIEMANN SURFACE ($N_2 > 0$)
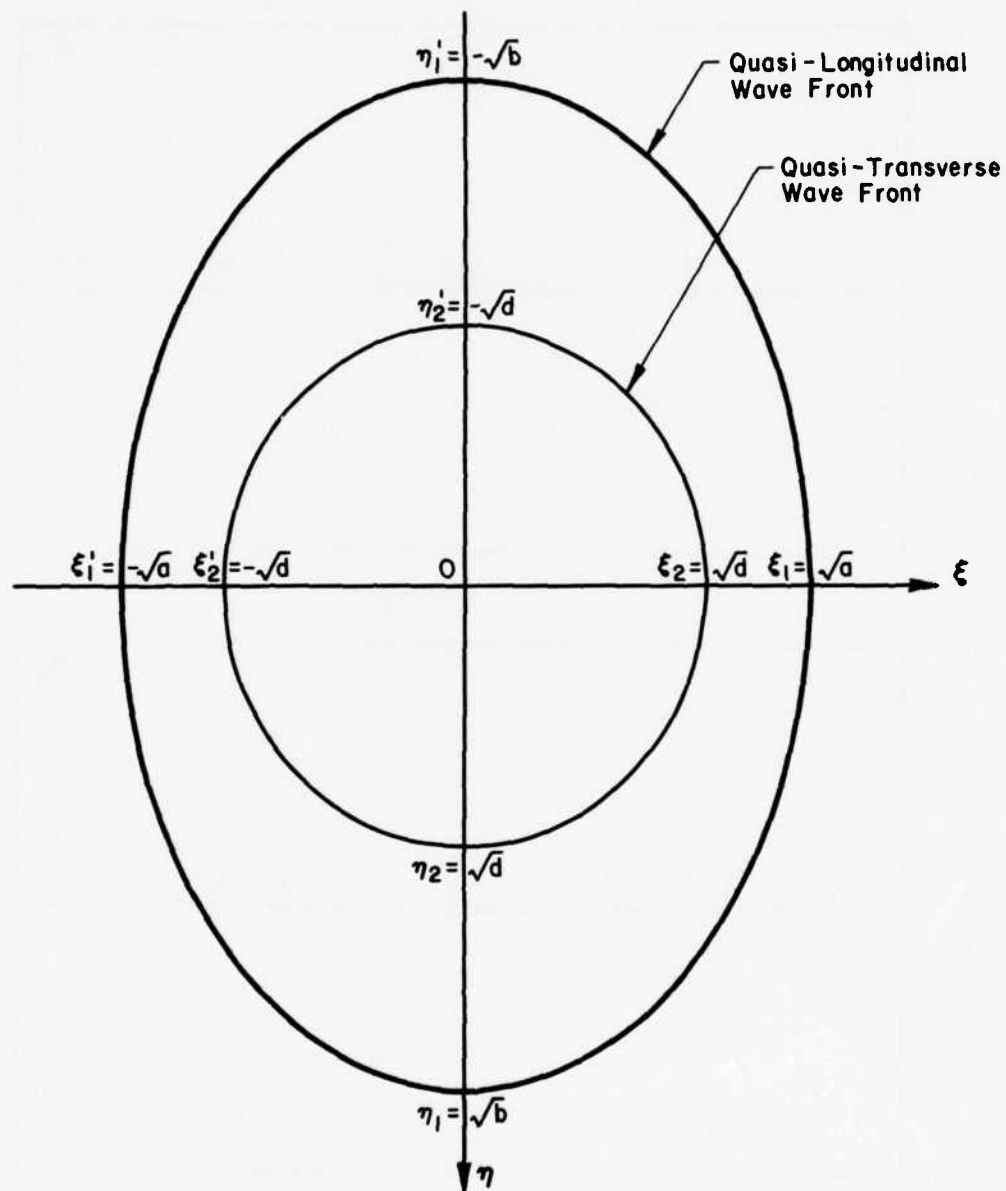
FIG. 18   WAVE FIELDS FOR MATERIAL CASE A-IV

Imθ_1

S_1

$-\Theta_{02}$ $-\Theta_{01}$ $-1/\sqrt{d}$ $-1/\sqrt{a}$ 0 $1/\sqrt{a}$ $1/\sqrt{d}$ Θ_{01} Θ_{02} Reθ_1

Imθ_2

S_2

$-\Theta_{02}$ $-\Theta_{01}$ 0 Θ_{01} Θ_{02} Reθ_2
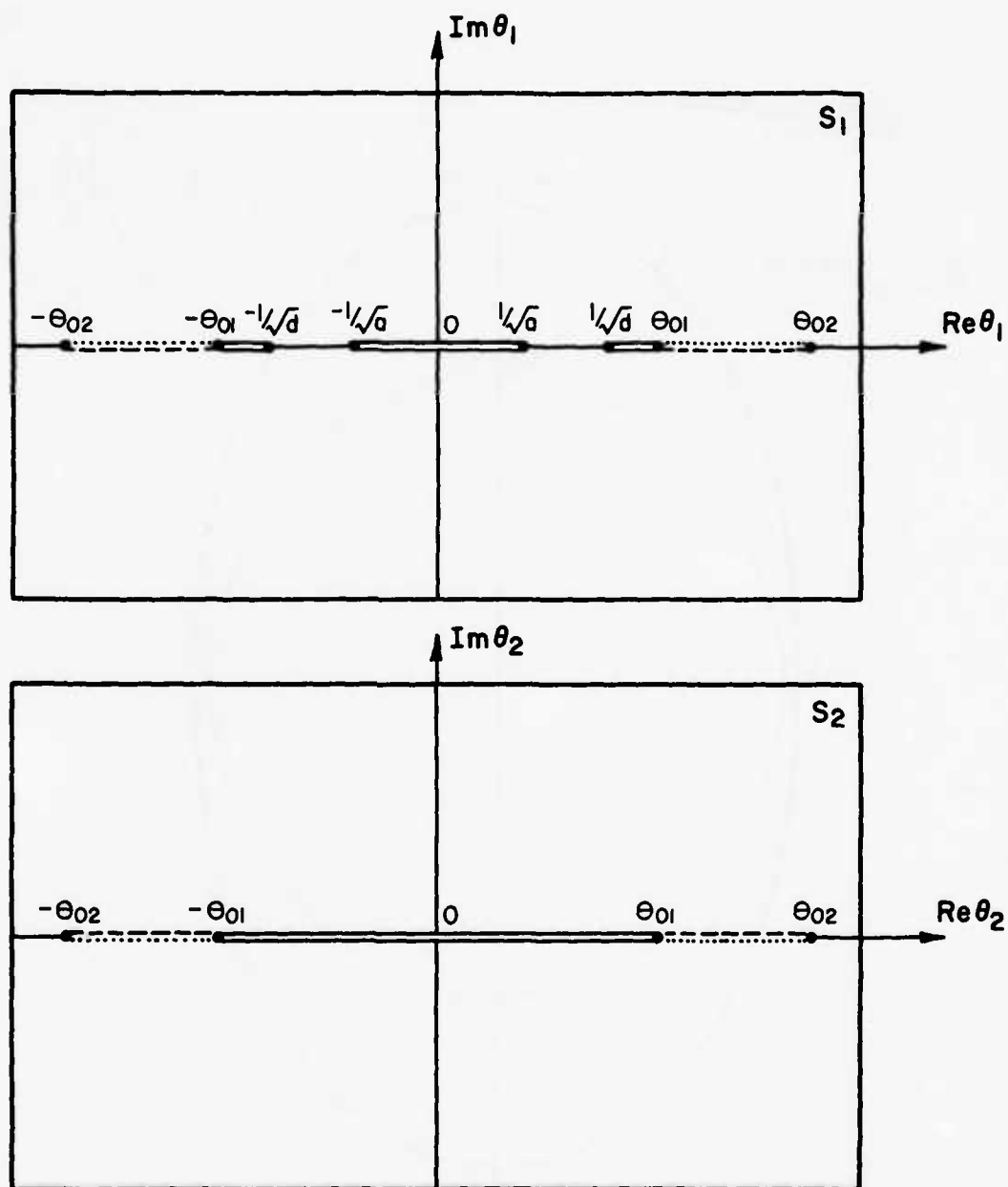
FIG. 19   SHEETS S_1 AND S_2 OF TYPE IV RIEMANN SURFACE ($N_2 < 0$)
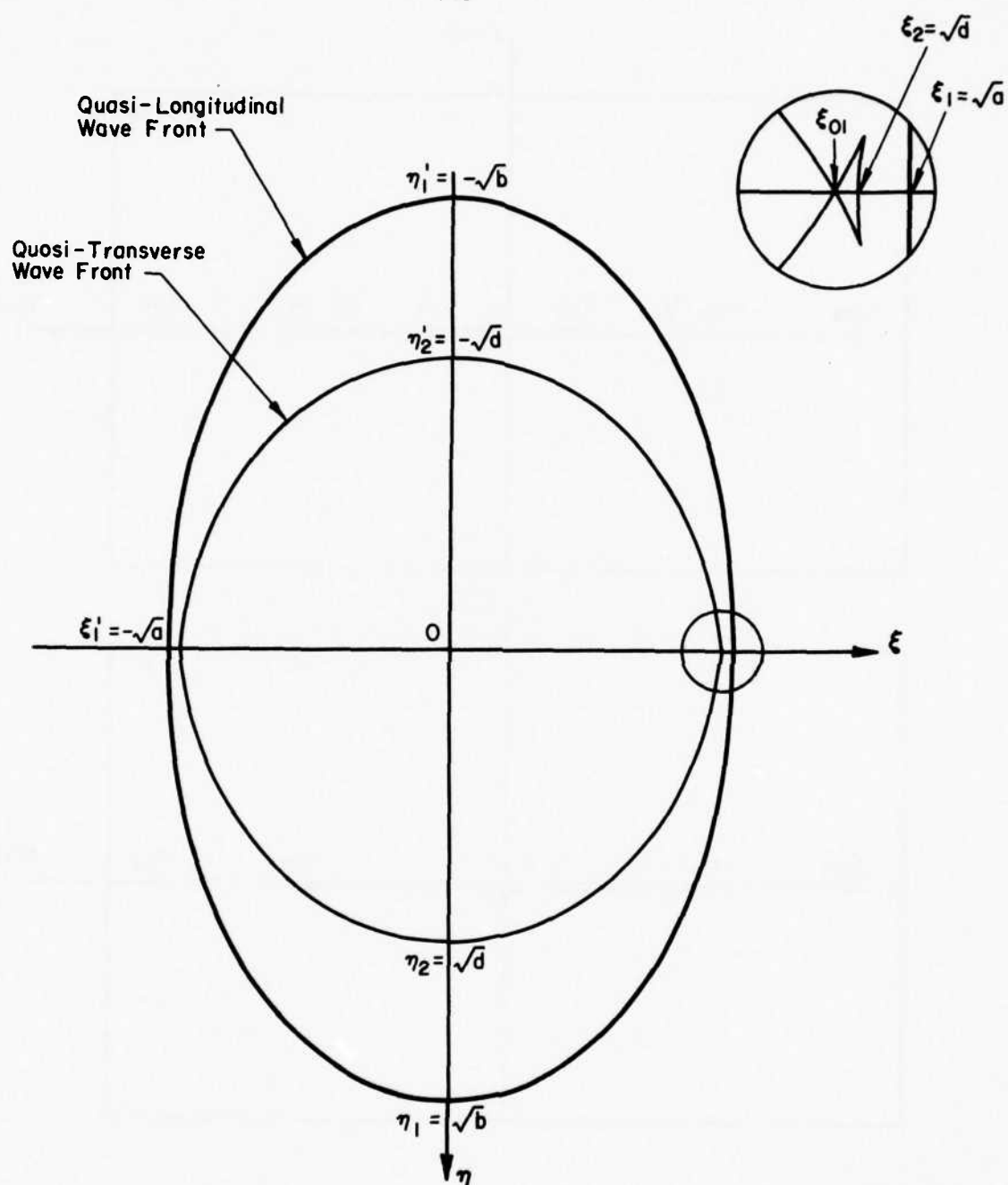
FIG. 20 WAVE FIELDS FOR MATERIAL CASE E-IV
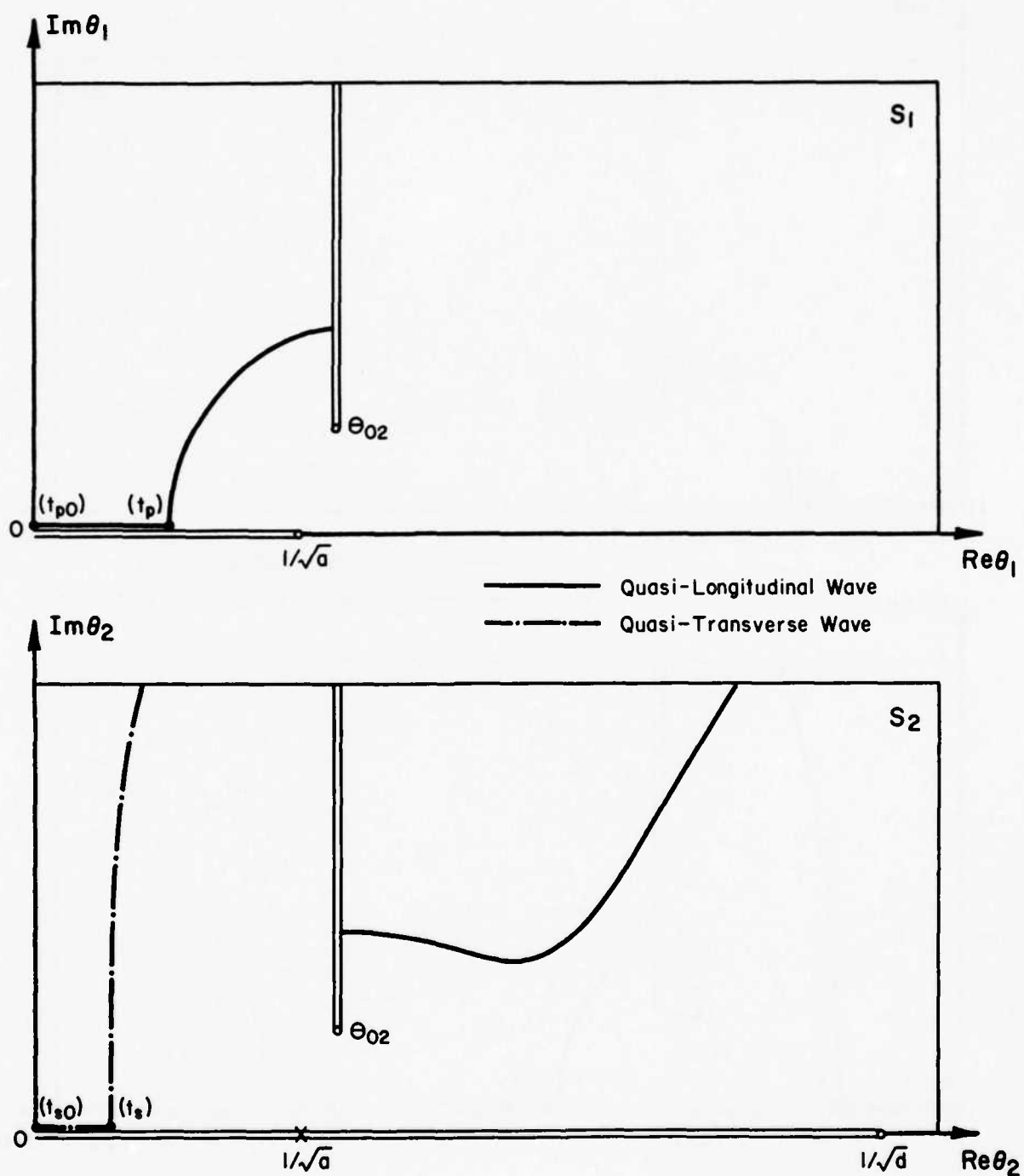
FIG. 21   PATHS OF θ_κ FOR CASE B-I AND $\gamma=0.5$
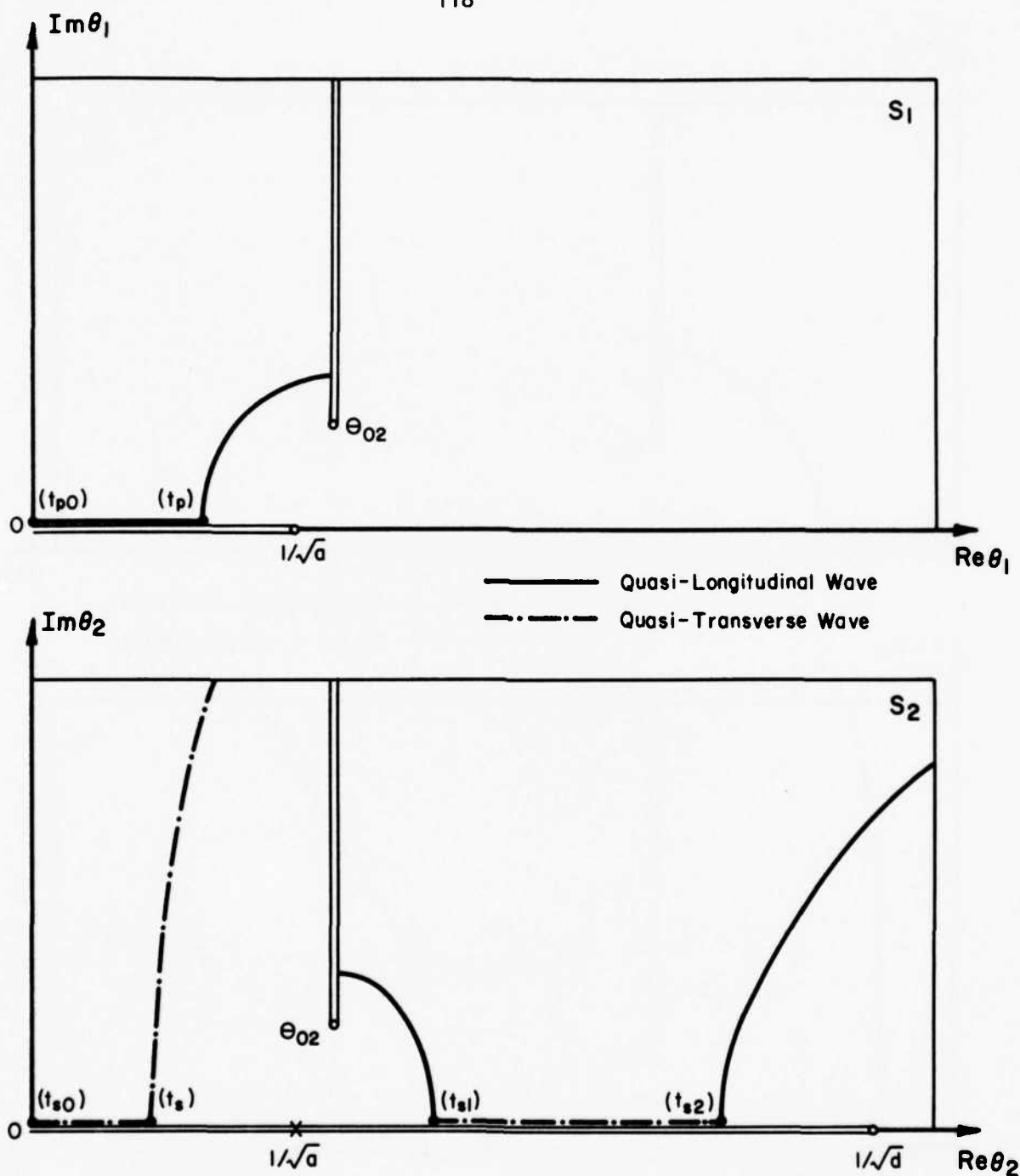
FIG. 22   PATHS OF θ_K FOR CASE B-I AND $\gamma = 0.8$
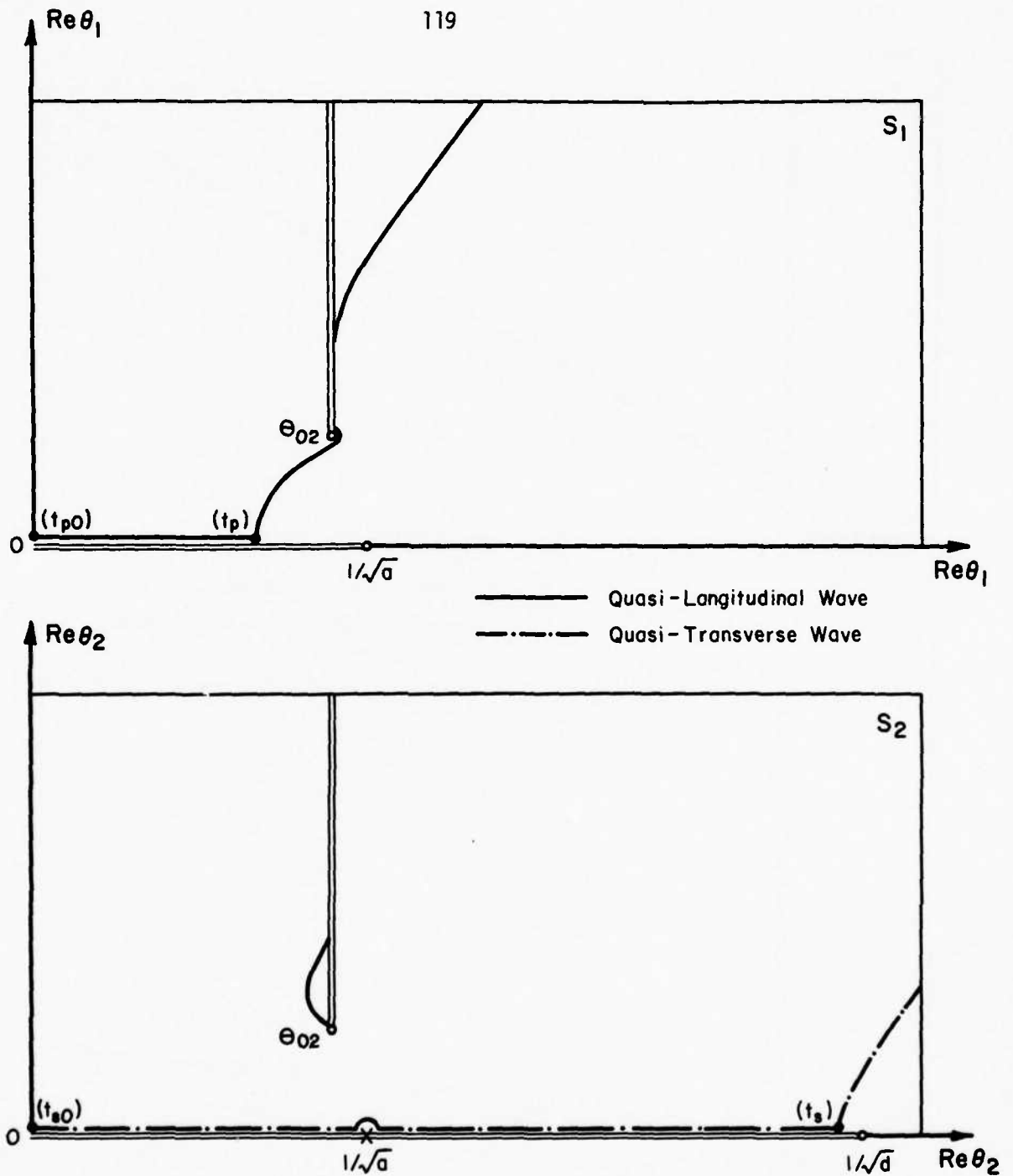
FIG. 23   PATHS OF θ_K FOR CASE B-I AND $\gamma=2.2$
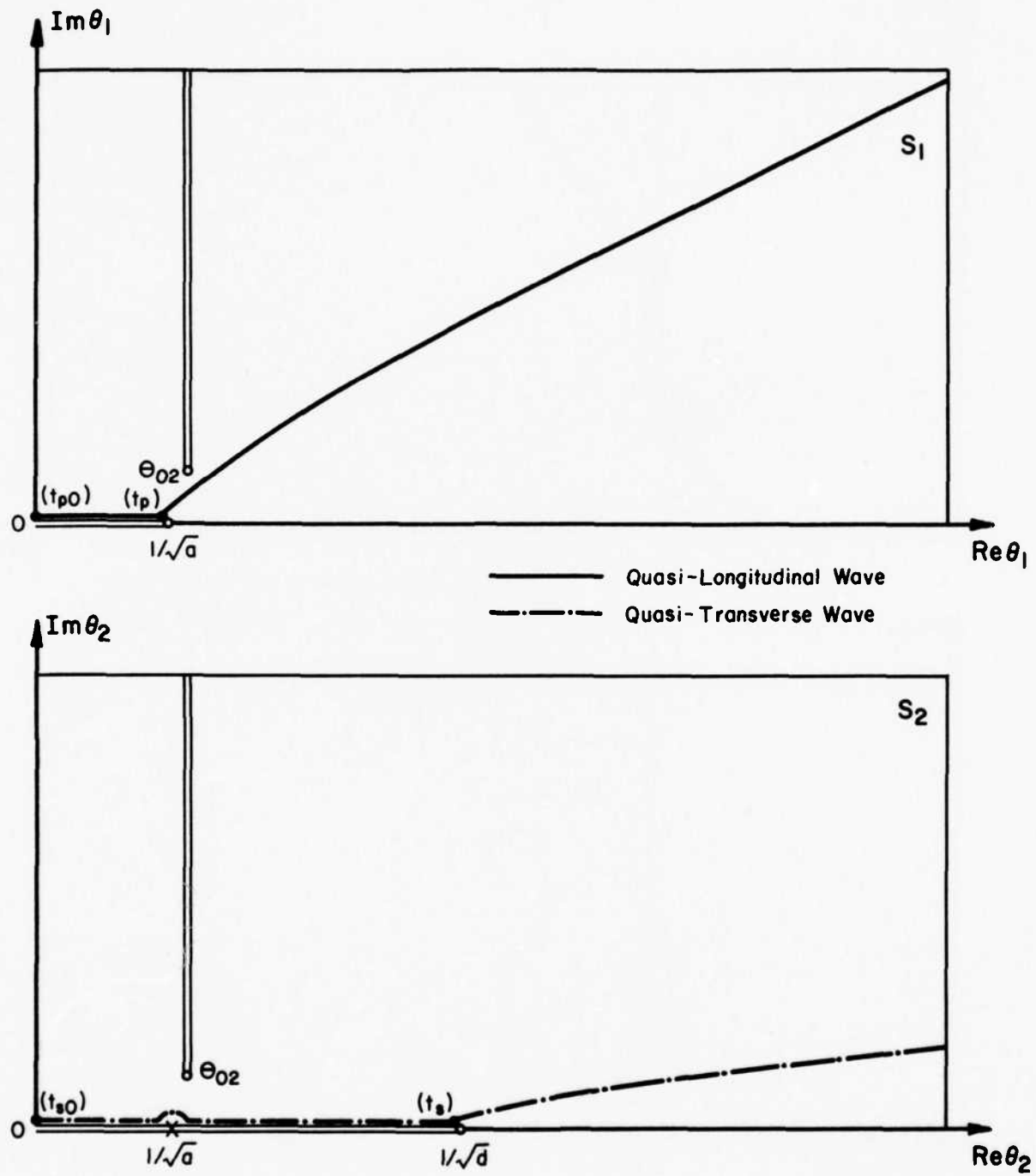
FIG. 24   PATHS OF θ_K FOR CASE B-I AND $\gamma = 5.0$
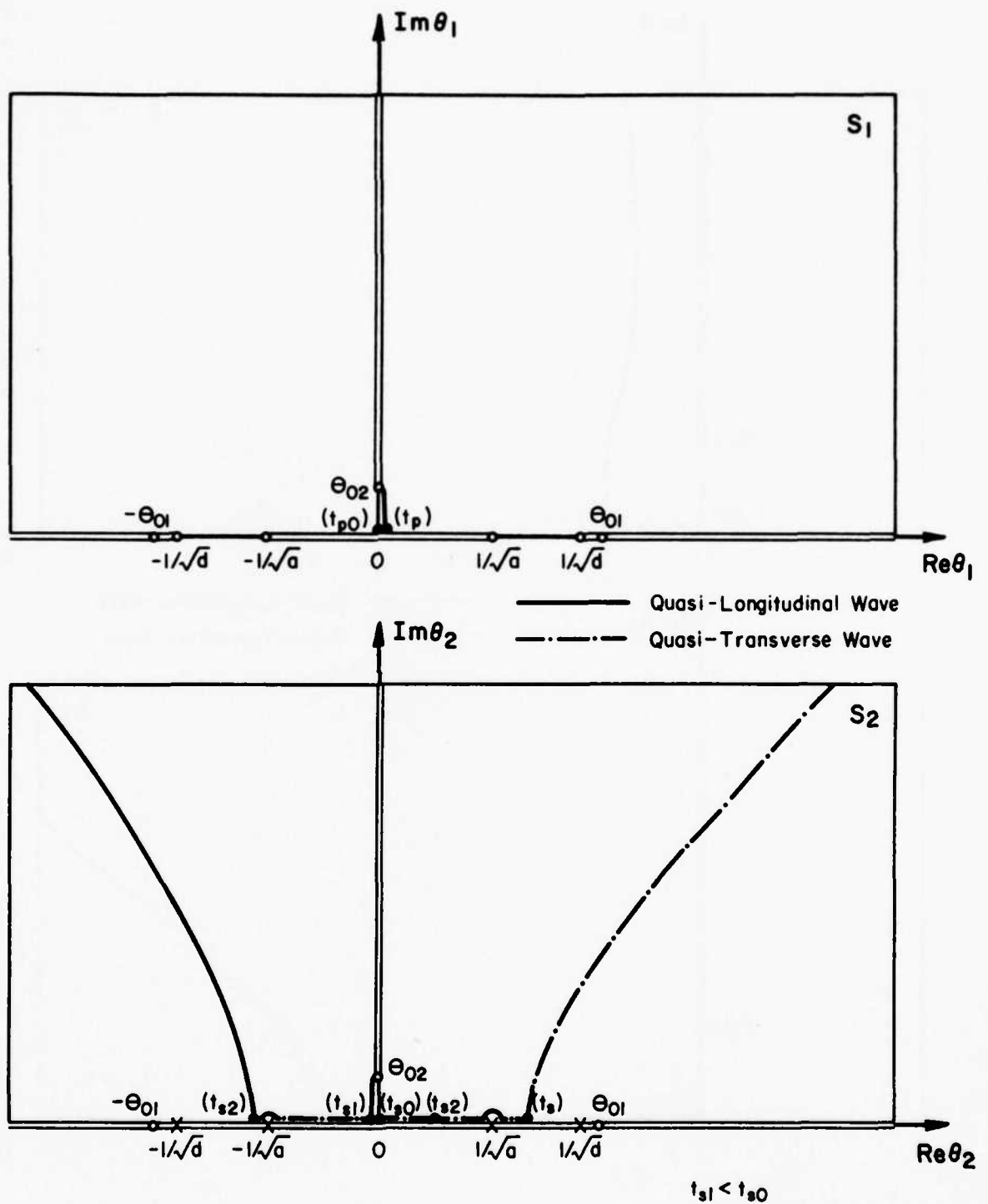
FIG. 25   PATHS OF θ_K FOR CASE C-II AND $\gamma = 0.1$
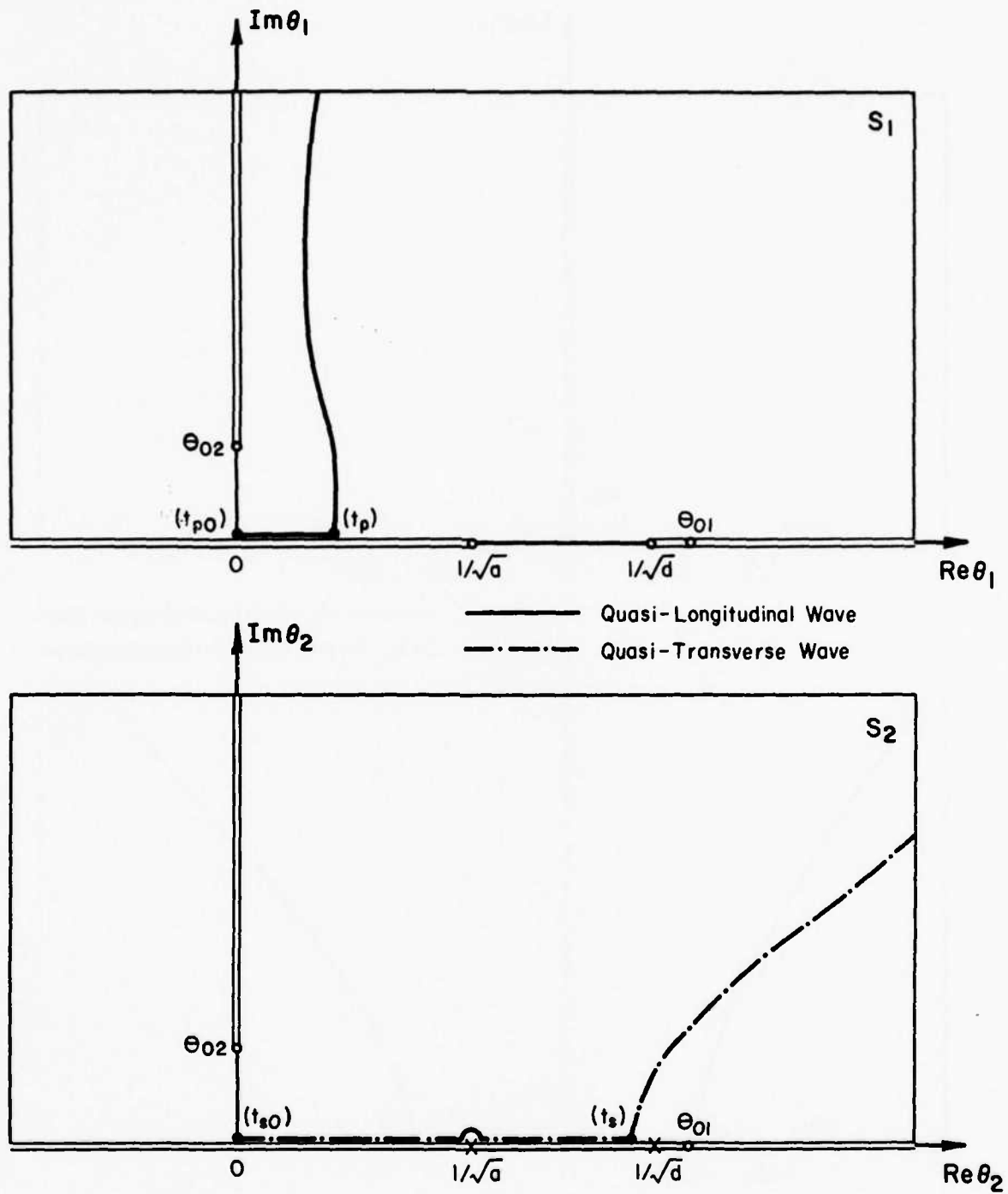
FIG. 26   PATHS OF θ_κ FOR CASE C-II AND $\gamma = 0.8$
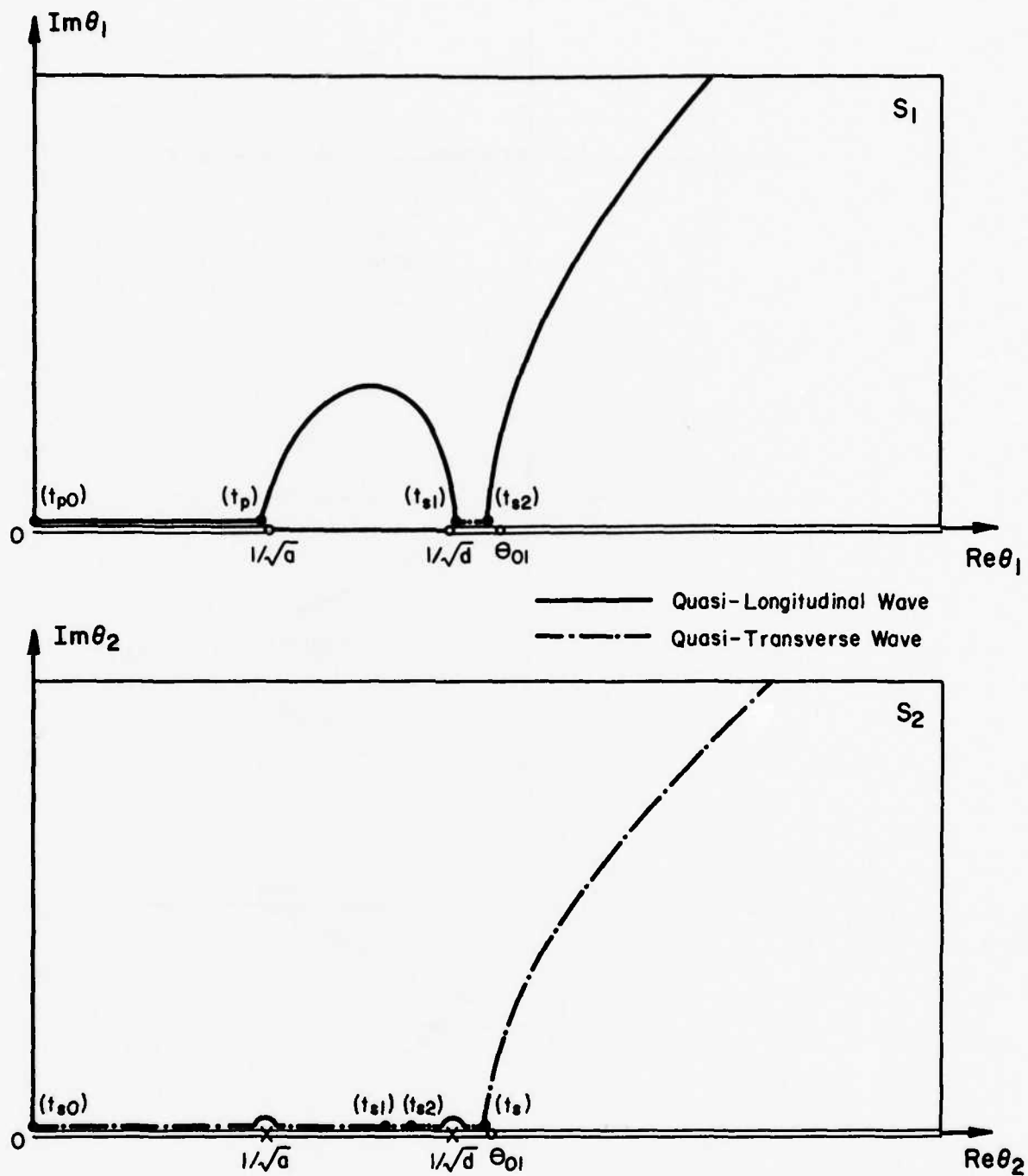
FIG. 27   PATHS OF θ_κ FOR CASE C-II AND $\gamma=10.0$
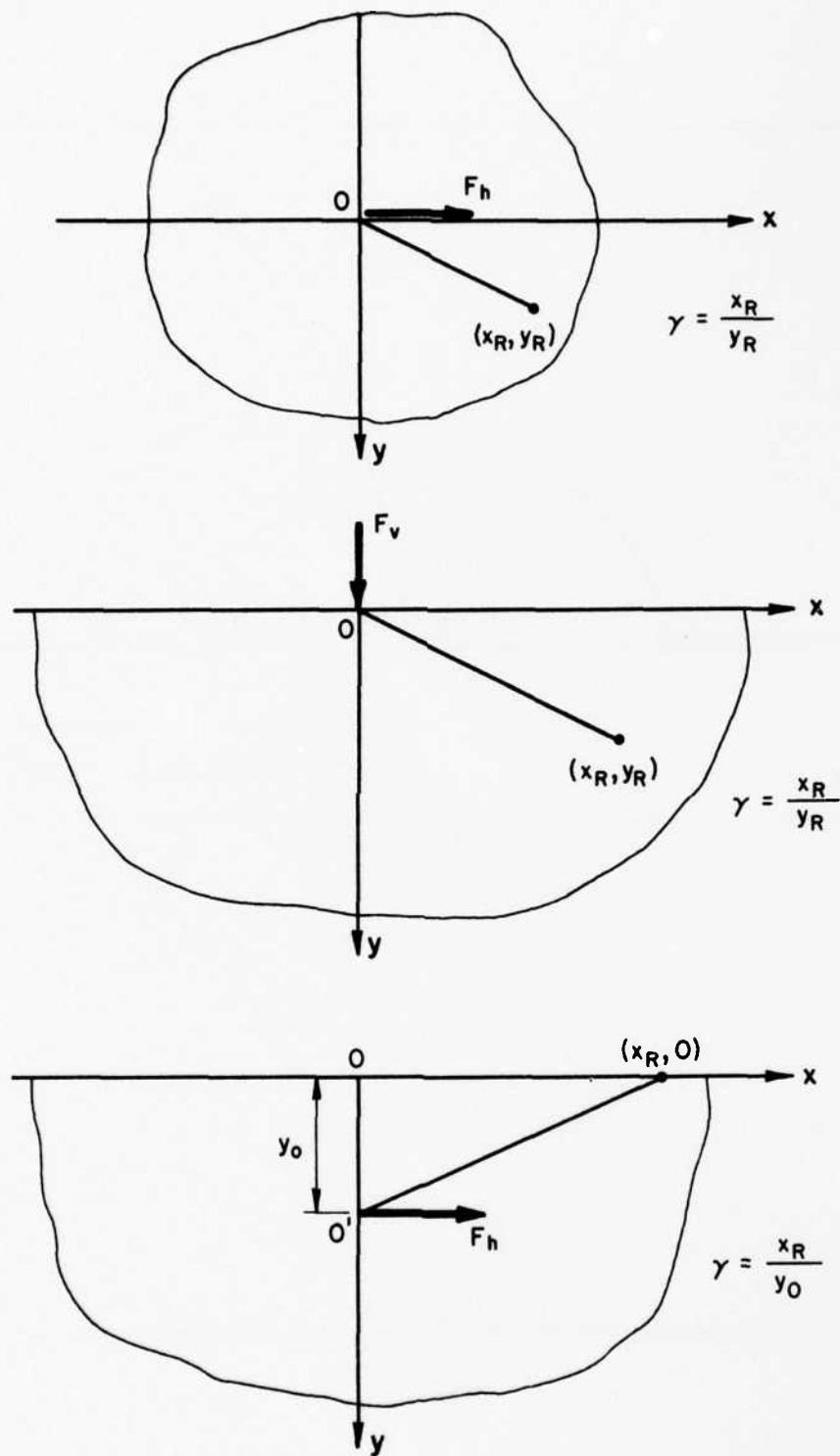
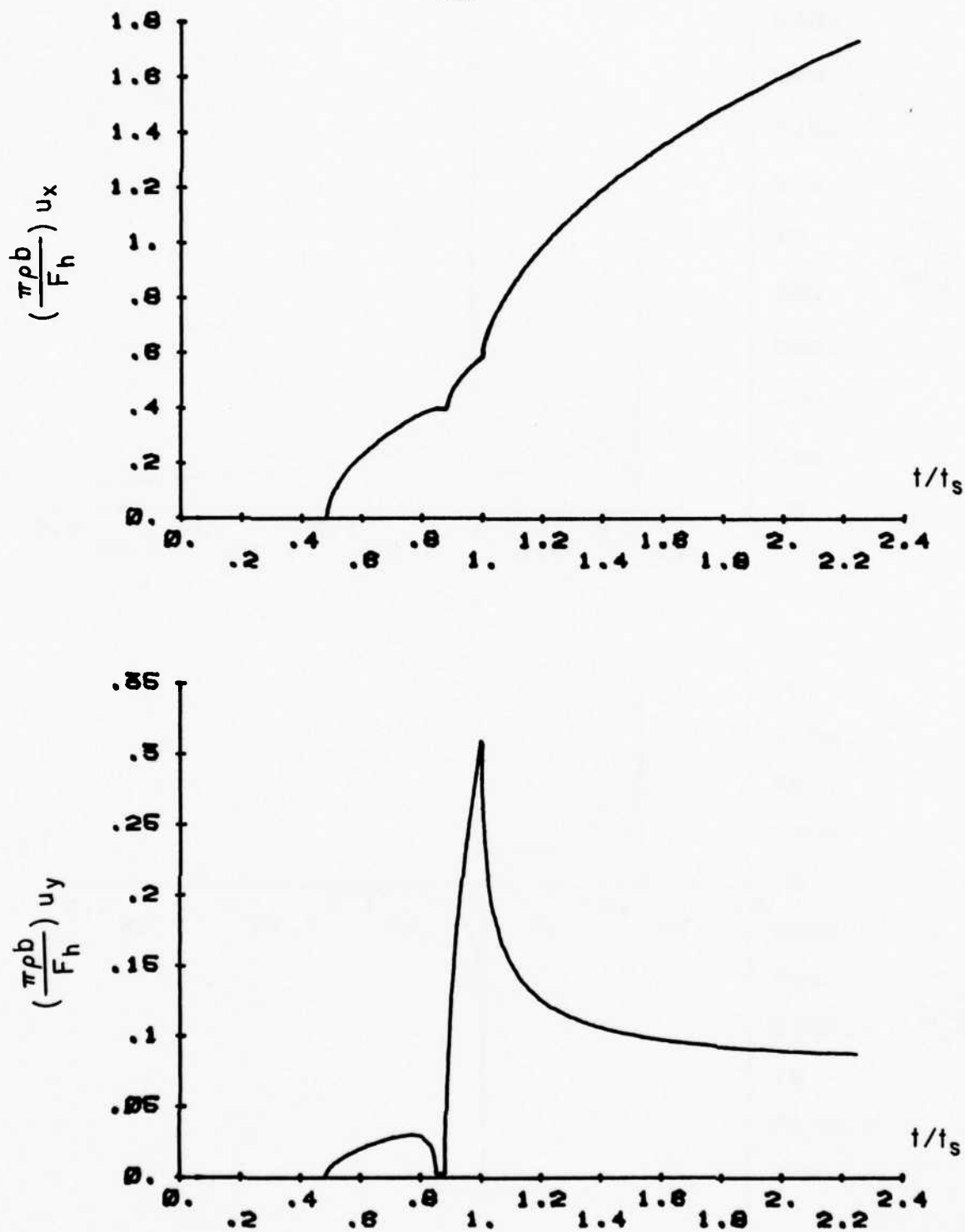FIG. 28   THE THREE TYPES OF LOADING FOR THE PLANE STRAIN PROBLEMS
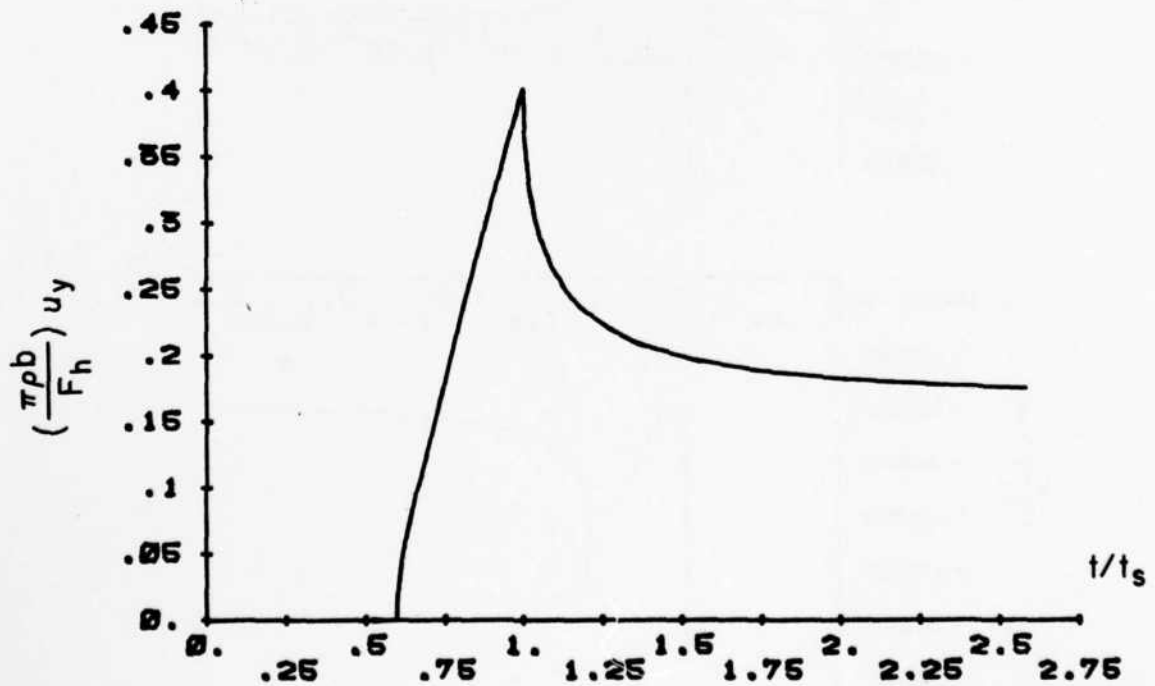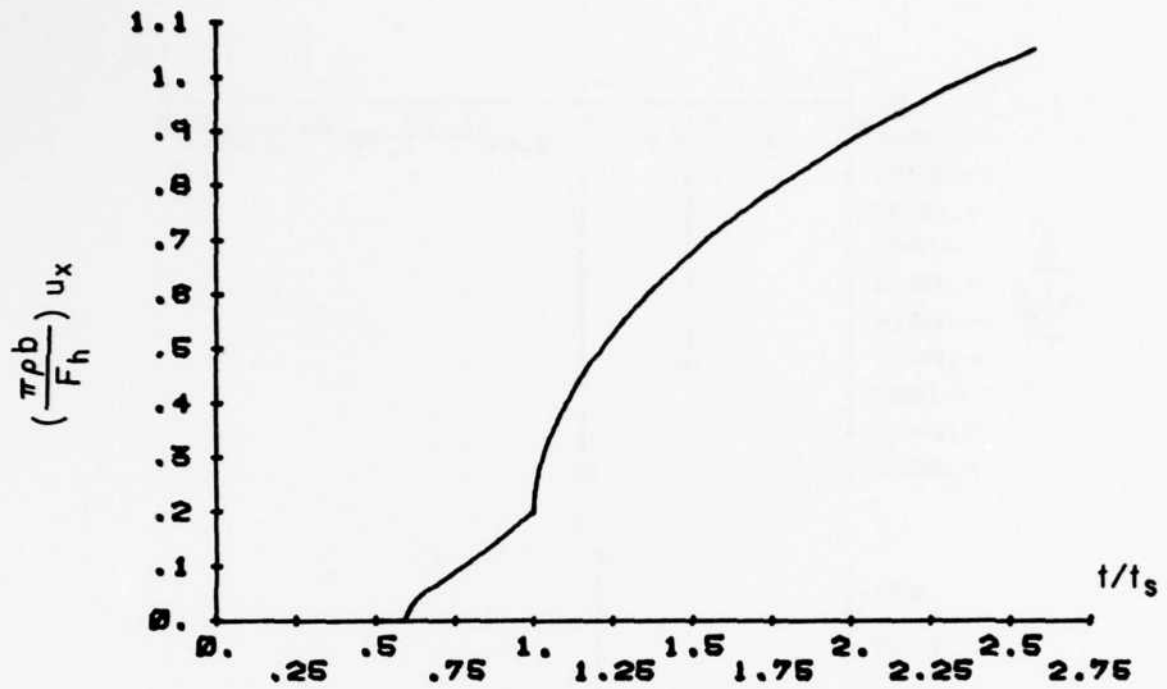
FIG. 29a   DISPLACEMENTS FOR FS-H IN A CLASS A-II MATERIAL WITH $\gamma = 0.8$
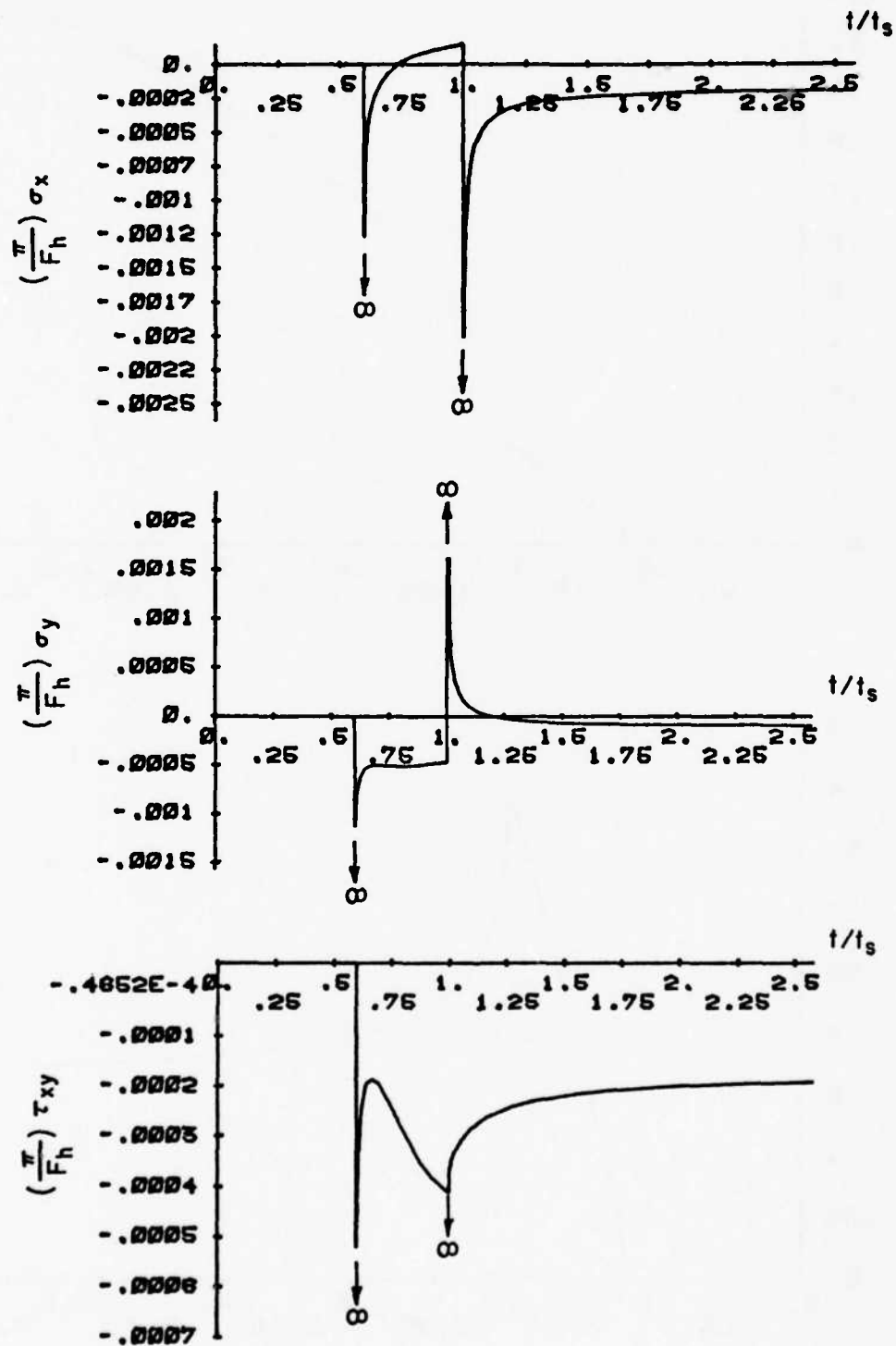
FIG. 29b   STRESSES FOR FS-H IN A CLASS A-II MATERIAL WITH γ = 0.8
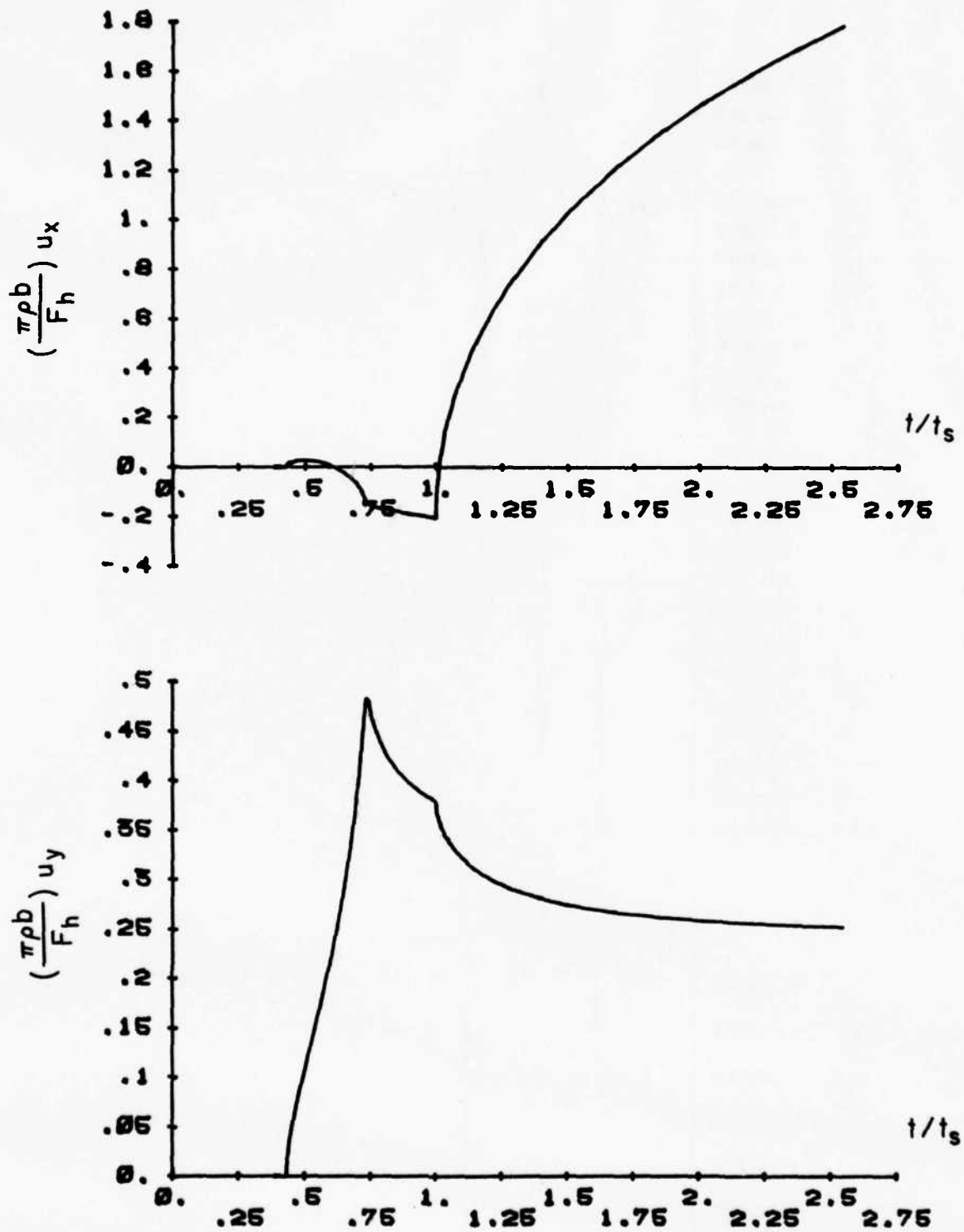
FIG. 30a   DISPLACEMENTS FOR FS-H IN A CLASS B-I MATERIAL WITH γ = 0.5

128
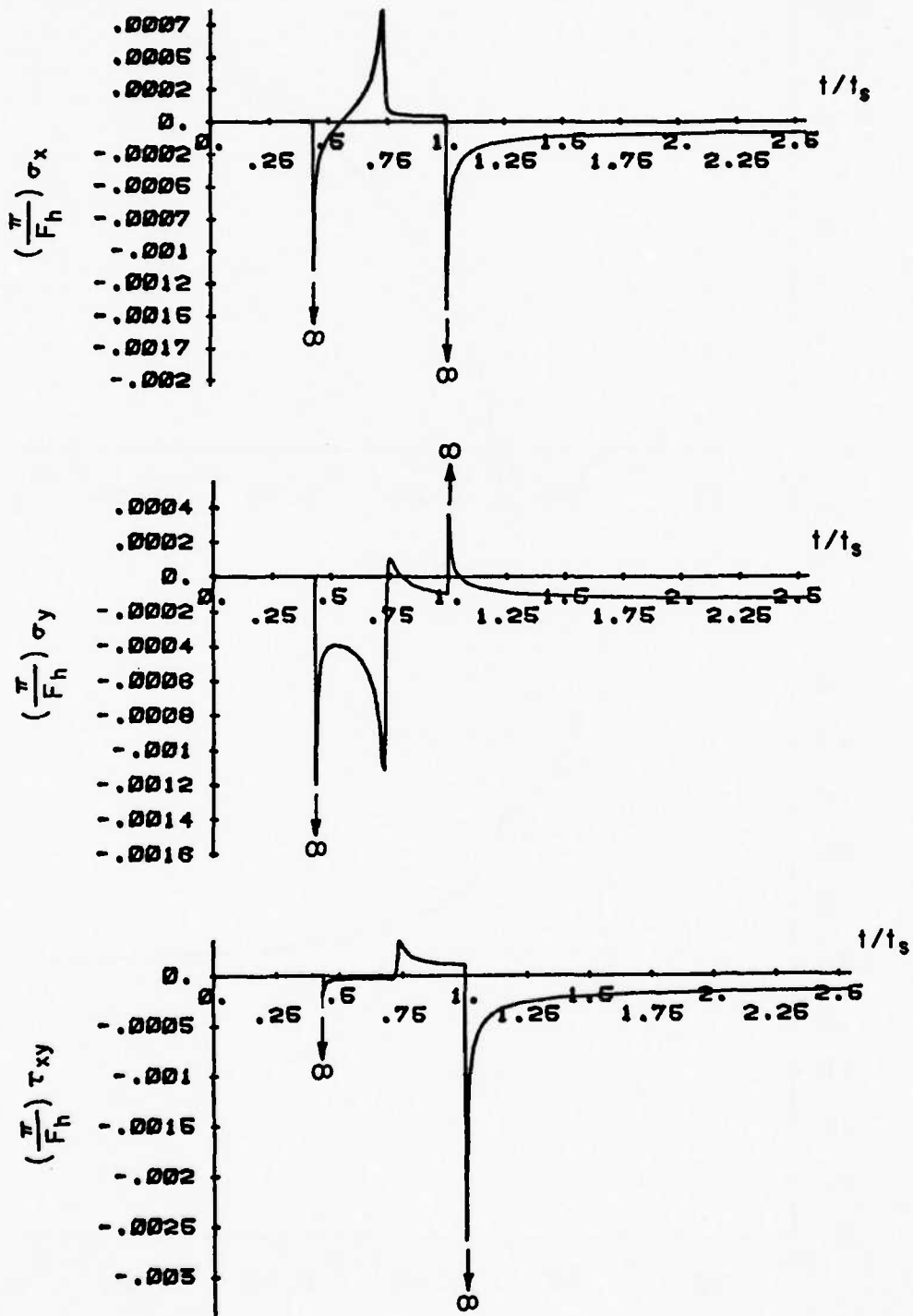
FIG. 30b   STRESSES FOR FS-H IN A CLASS B-I MATERIAL WITH γ = 0.5
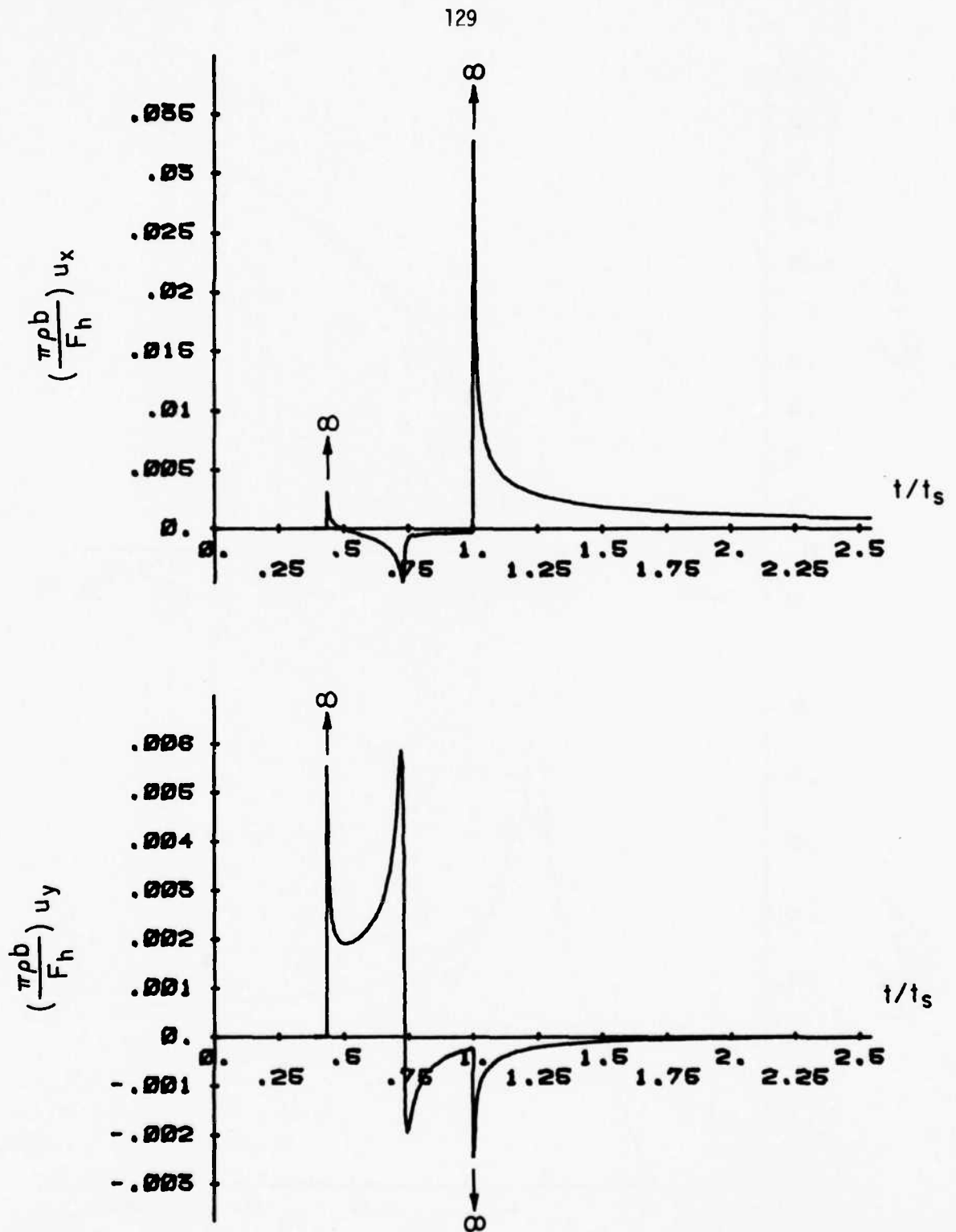
FIG. 30c   DISPLACEMENTS FOR FS-H IN A CLASS B-I MATERIAL WITH $\gamma = 0.5$ AND IMPULSIVE APPLICATION OF THE LOAD
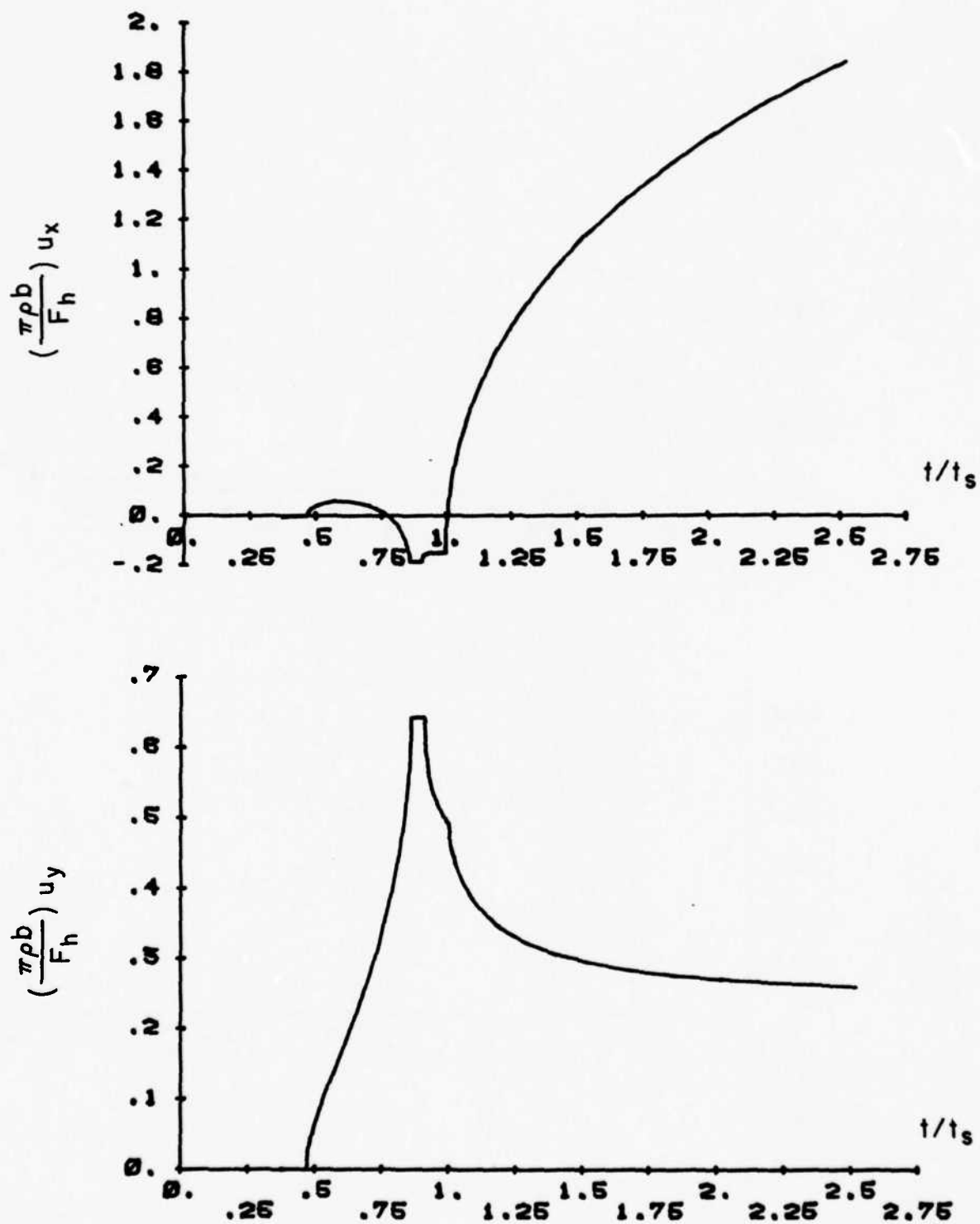
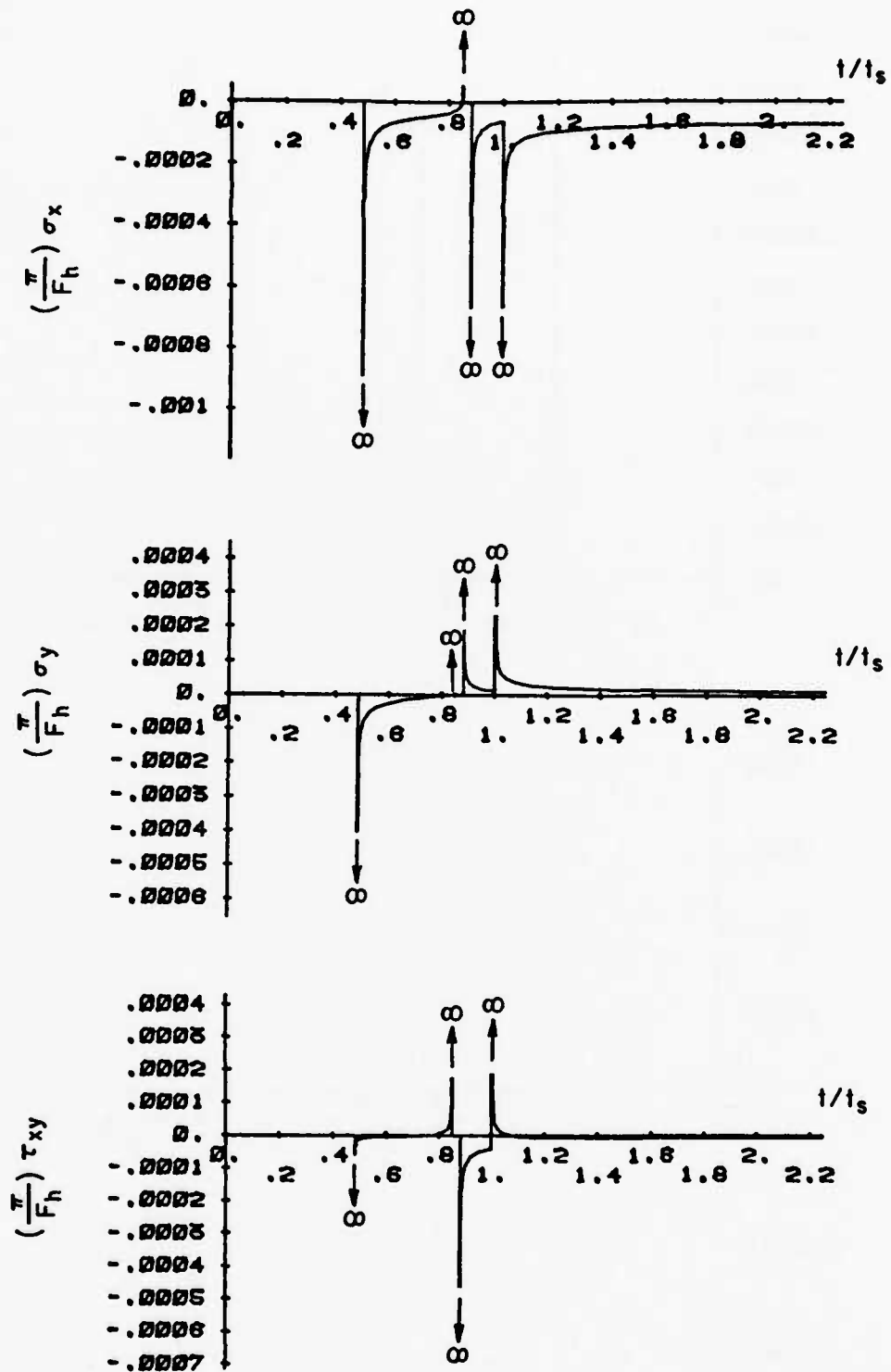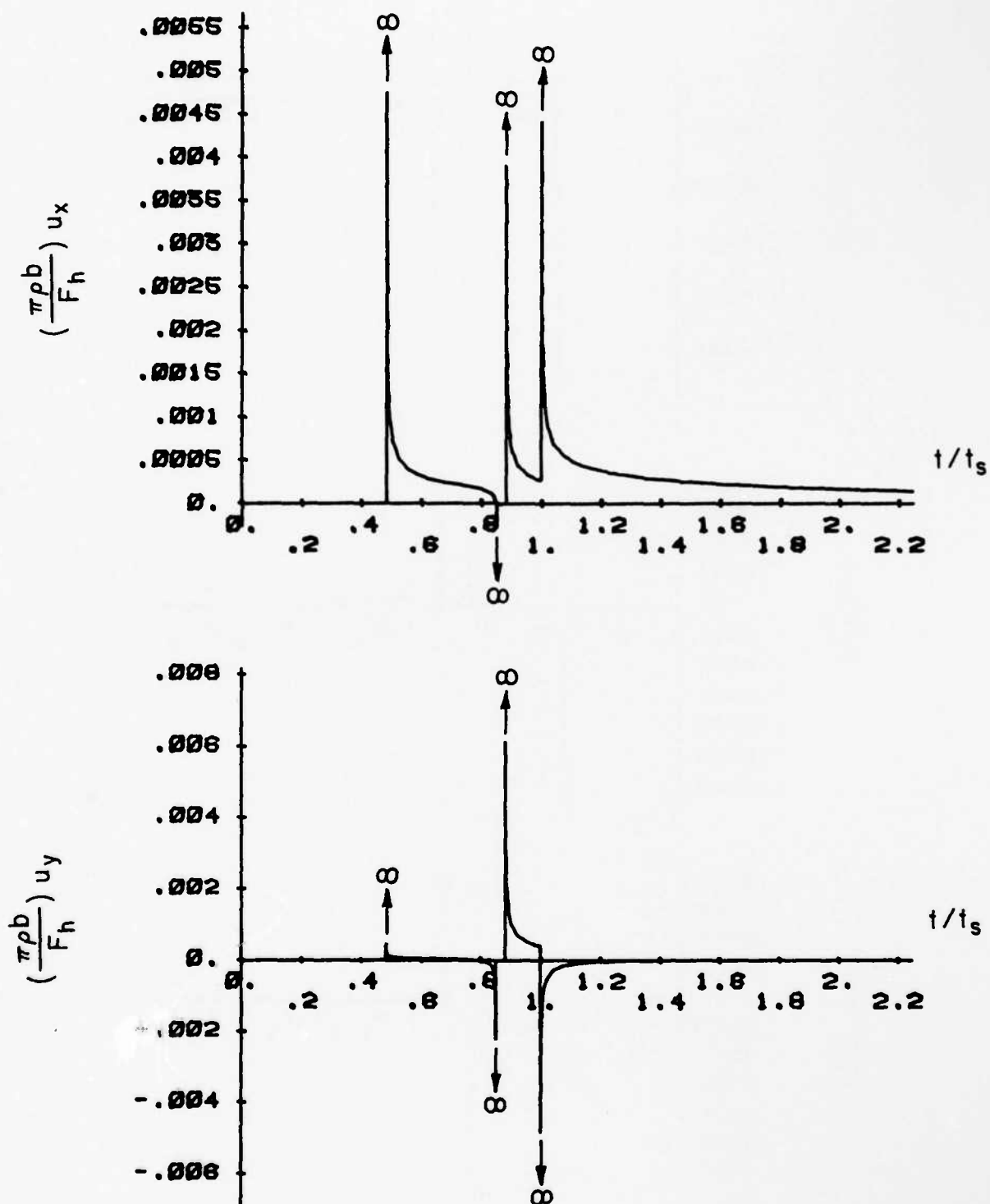FIG. 31a   DISPLACEMENTS FOR FS-H IN A CLASS B-I MATERIAL WITH $\gamma = 0.8$

131
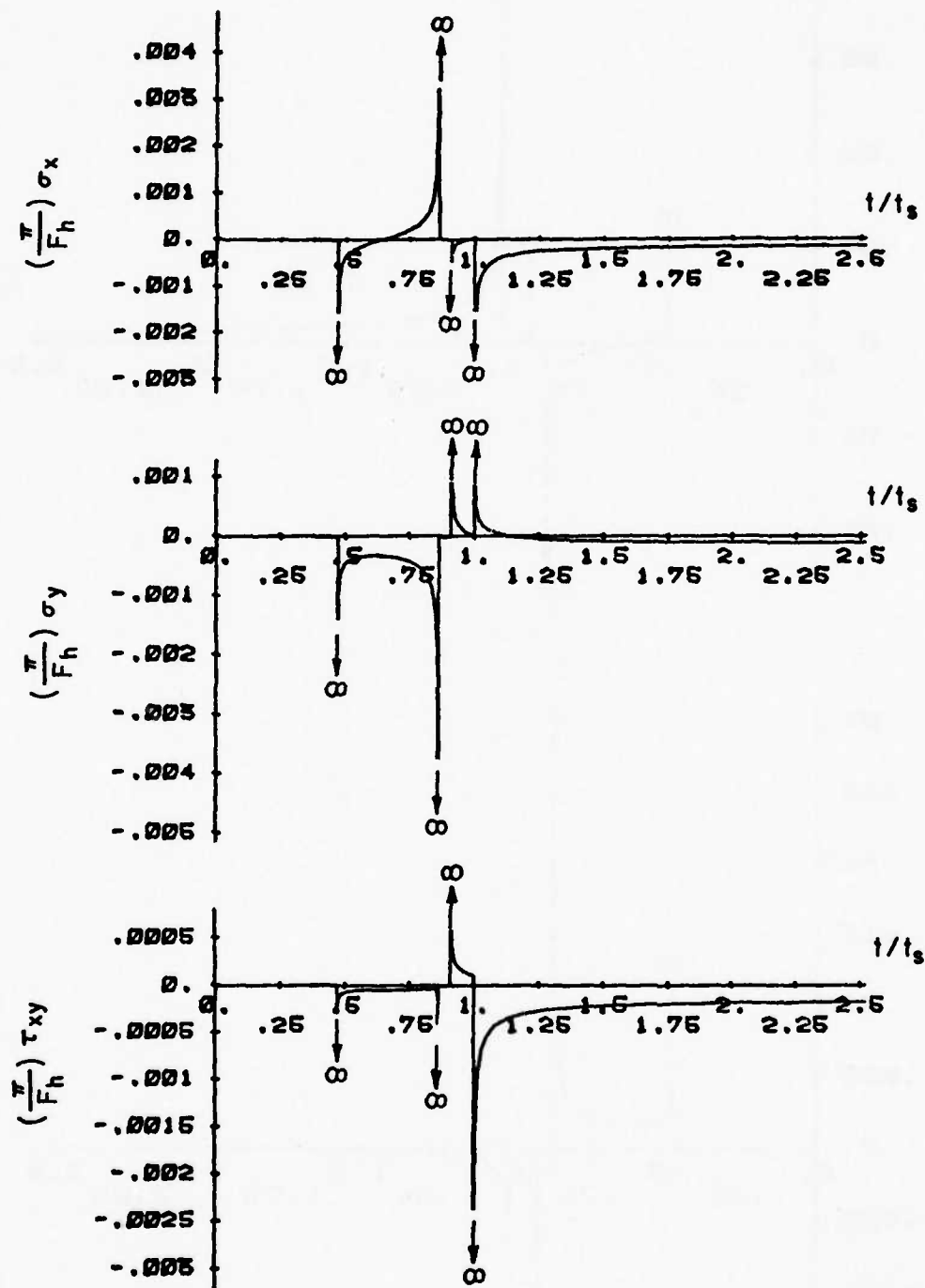
FIG. 31b   STRESSES FOR FS-H IN A CLASS B-I MATERIAL WITH $\gamma = 0.8$
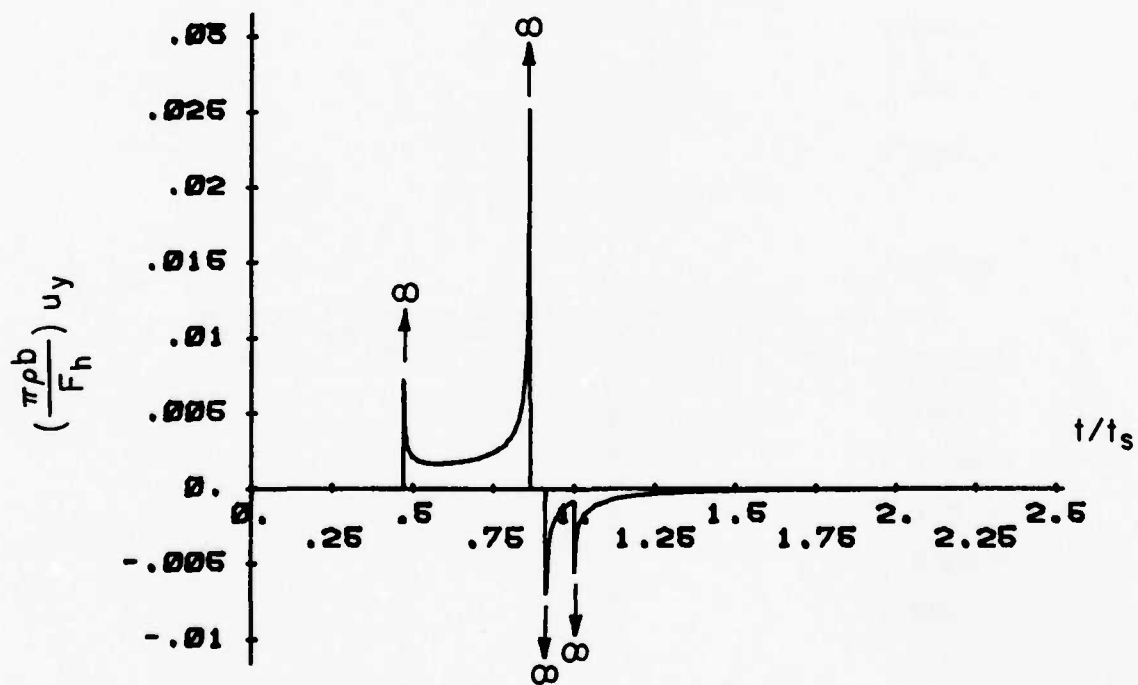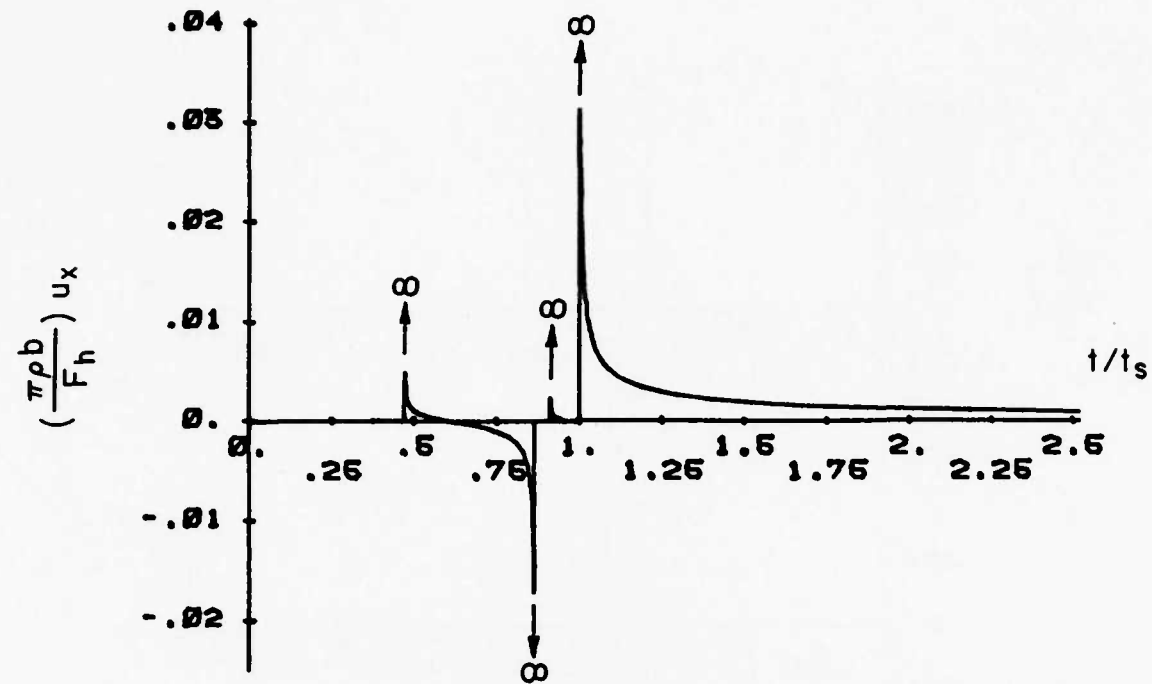
FIG. 31c   DISPLACEMENTS FOR FS-H IN A CLASS B-I MATERIAL WITH $\gamma = 0.8$
AND IMPULSIVE APPLICATION OF THE LOAD
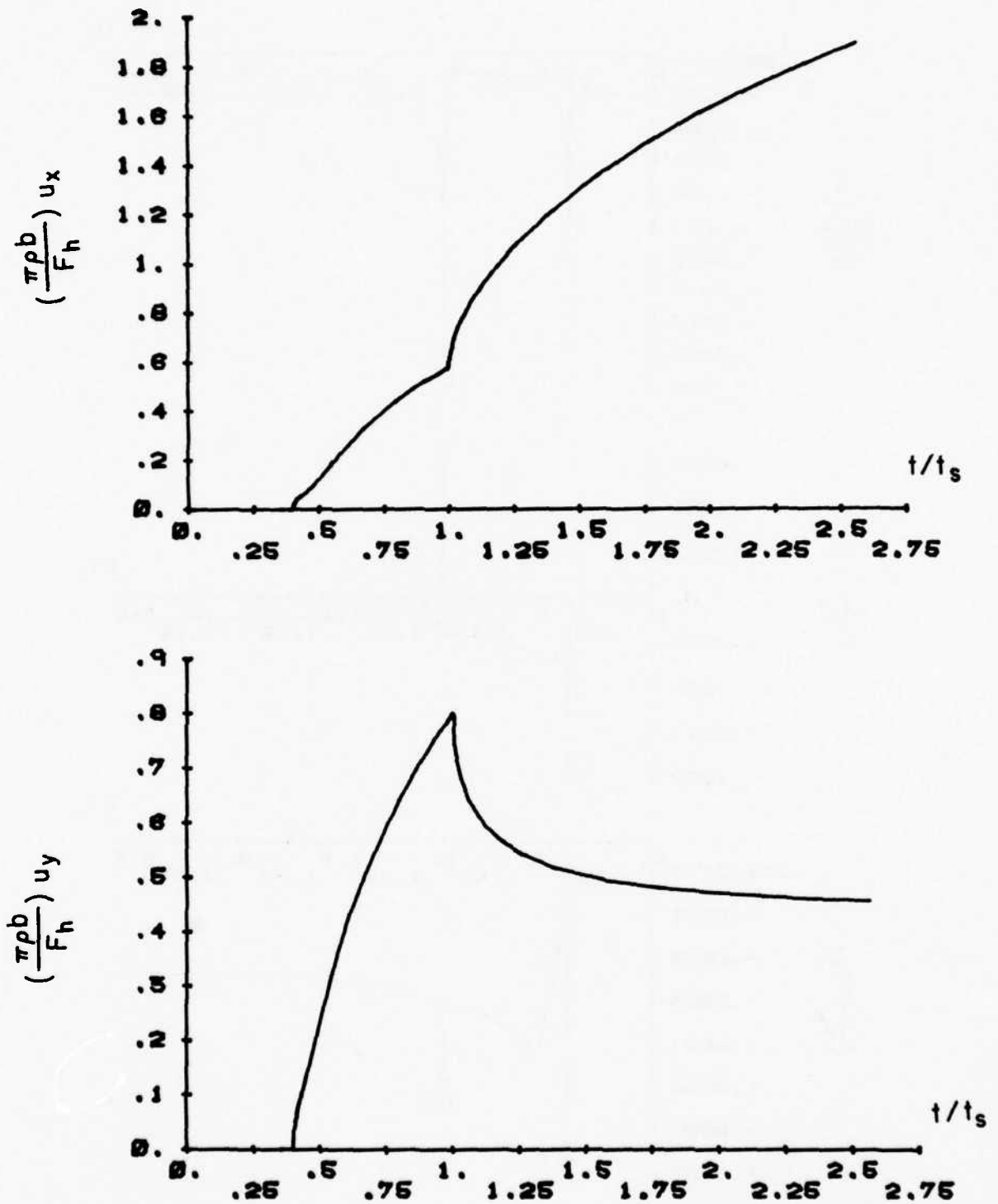
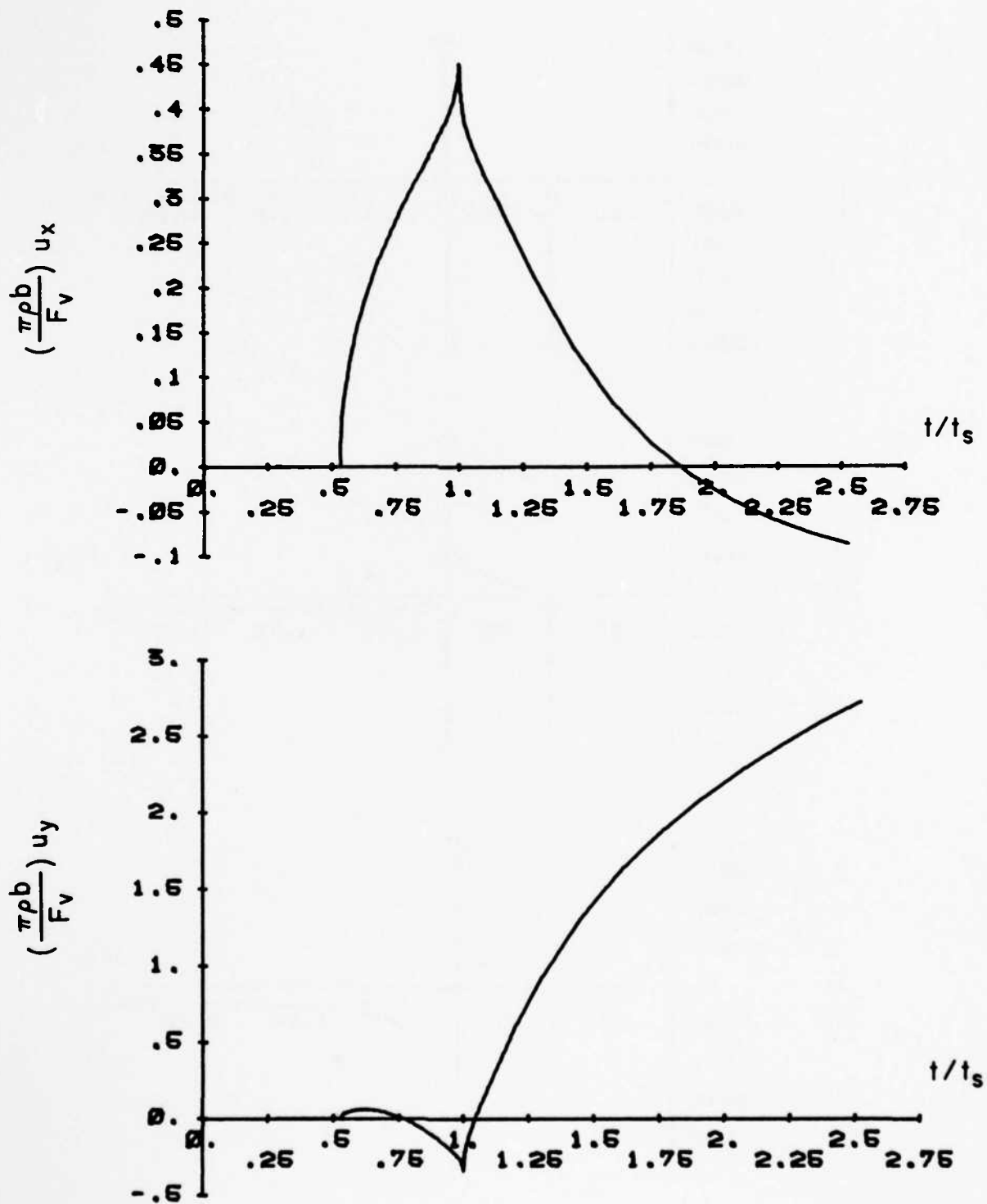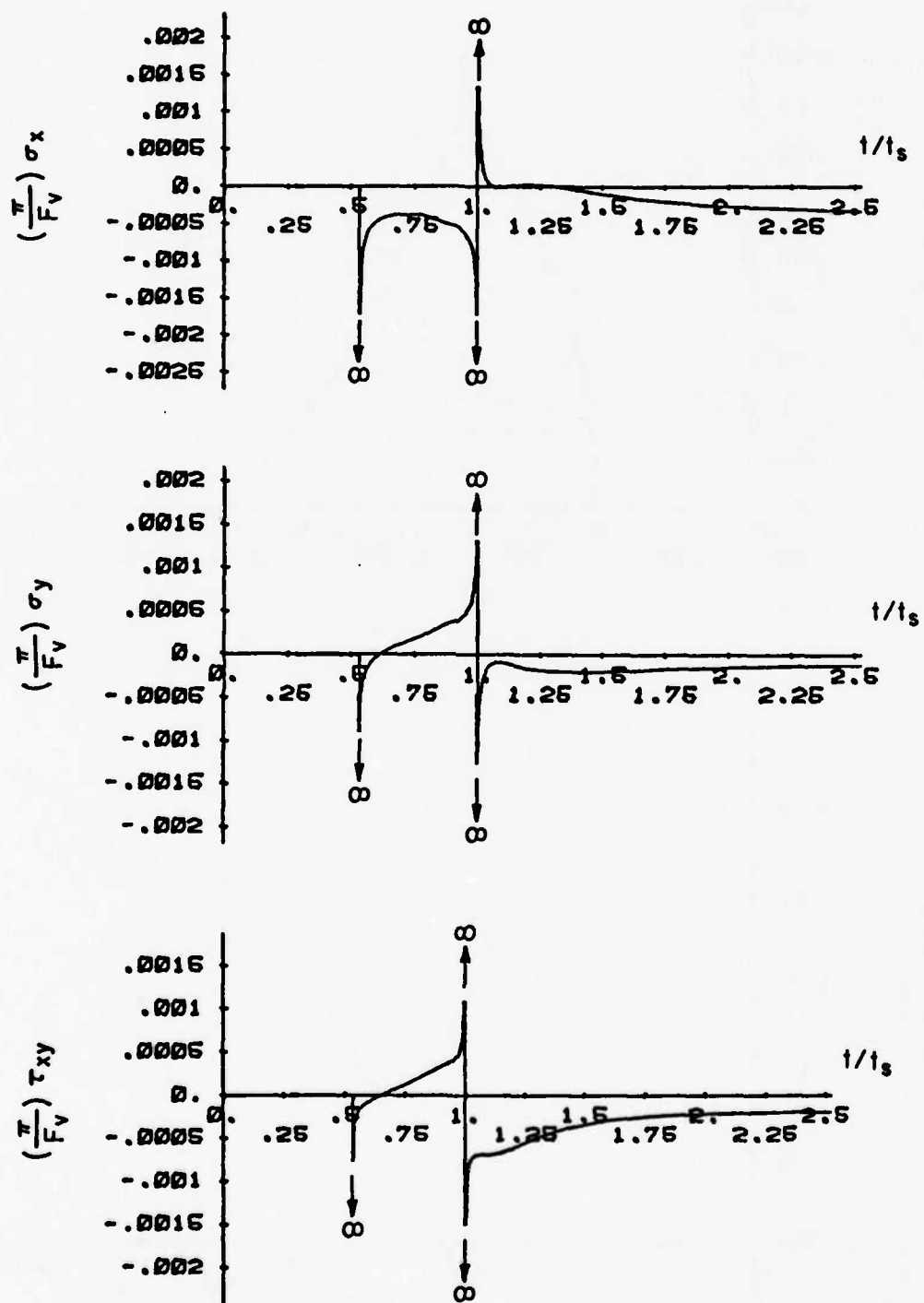FIG. 32a   DISPLACEMENTS FOR FS-H IN A CLASS C-II MATERIAL WITH $\gamma = 0.8$
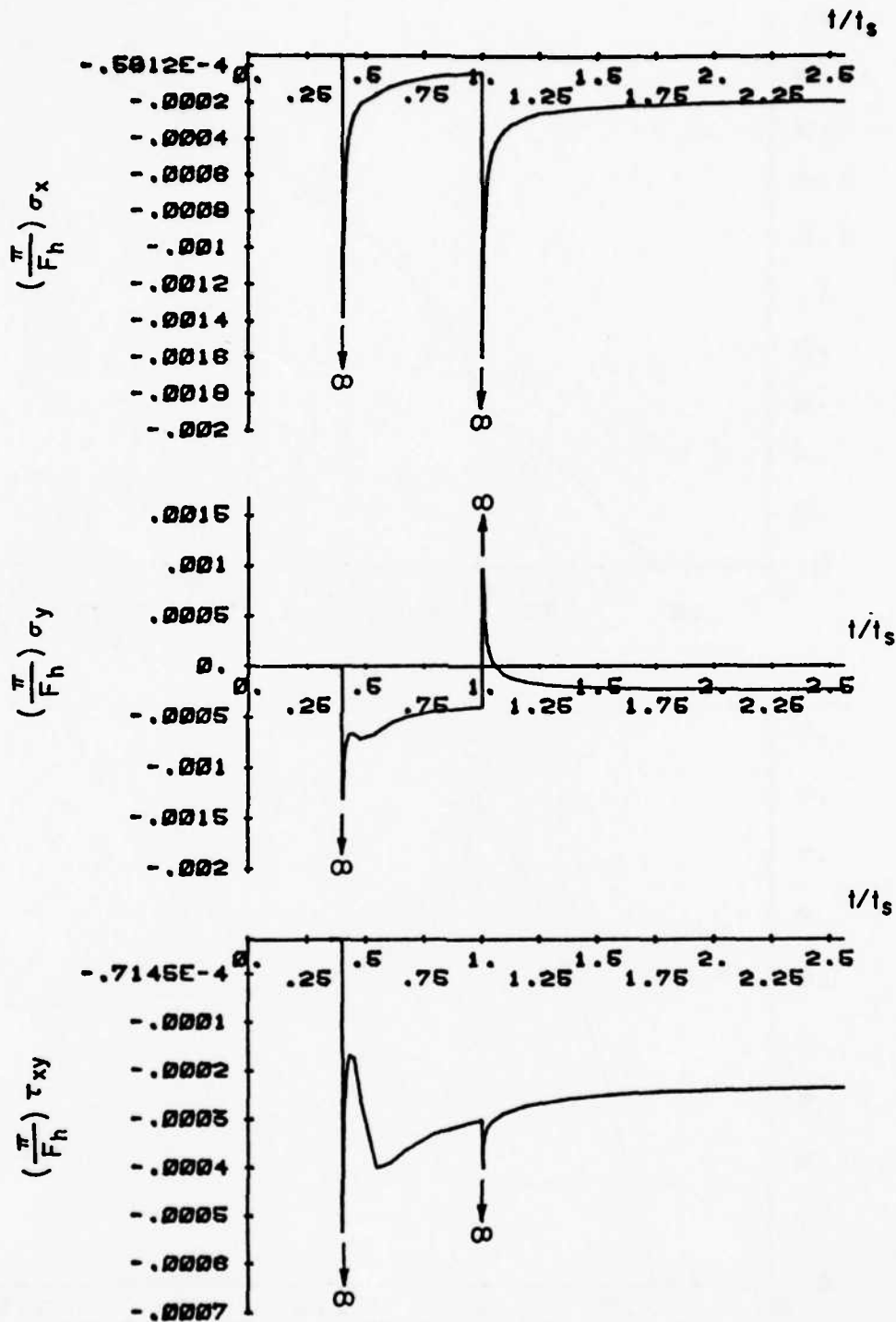
FIG. 32b   STRESSES FOR FS-H IN A CLASS C-II MATERIAL WITH Y = 0.8
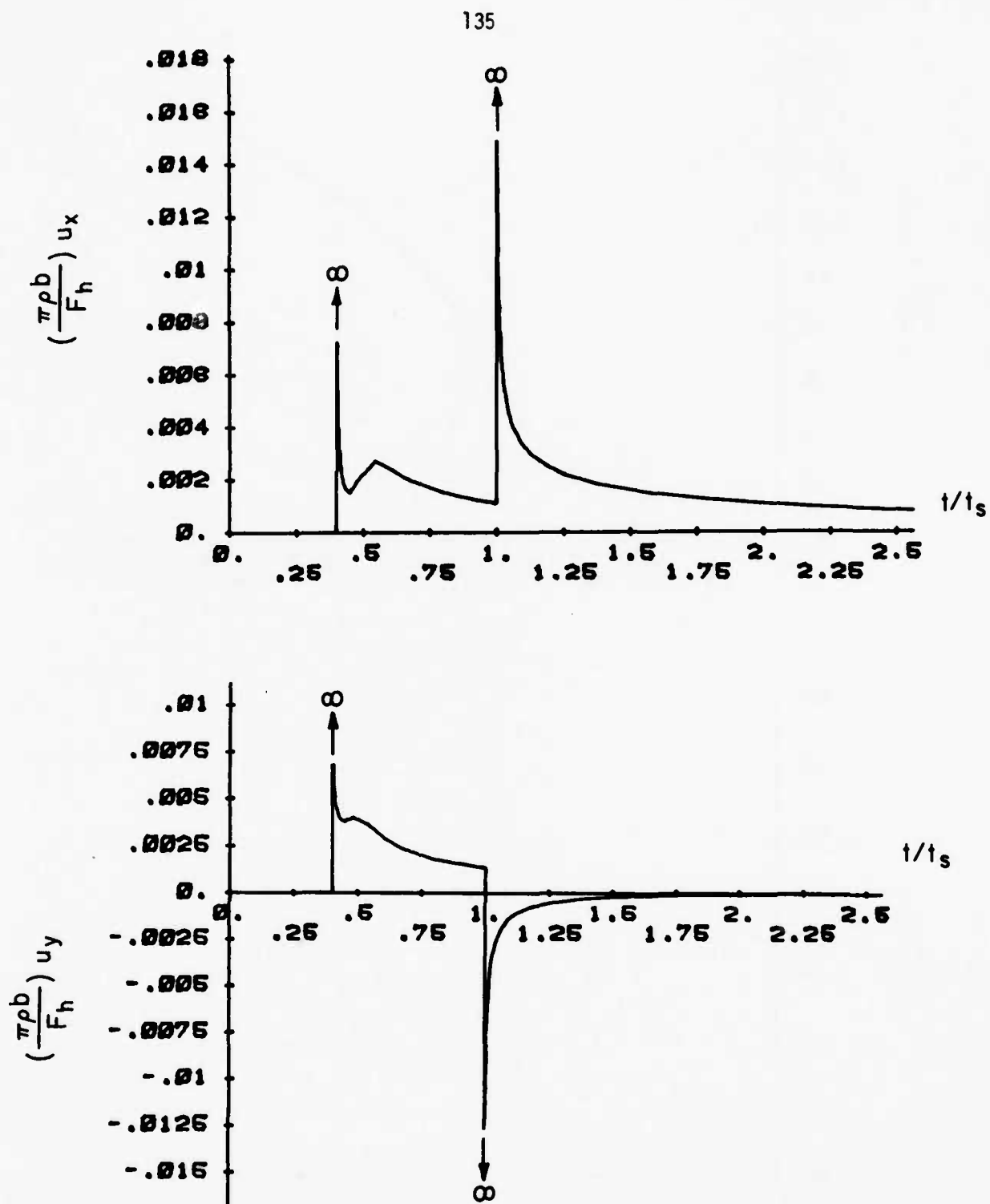
FIG. 32c   DISPLACEMENTS FOR FS-H IN A CLASS C-II MATERIAL WITH γ = 0.8
AND IMPULSIVE APPLICATION OF THE LOAD

FIG. 33a   DISPLACEMENTS FOR FS-H IN A CLASS C-II MATERIAL WITH $\gamma = 10.0$

FIG. 33b   STRESSES FOR FS-H IN A CLASS C-II MATERIAL WITH $\gamma = 10.0$

FIG. 33c   DISPLACEMENTS FOR FS-H IN A CLASS C-II MATERIAL WITH $\gamma = 10.0$ AND IMPULSIVE APPLICATION OF THE LOAD

FIG. 34a   DISPLACEMENTS FOR HS-V IN A CLASS A-II MATERIAL WITH $\gamma = 2.2$

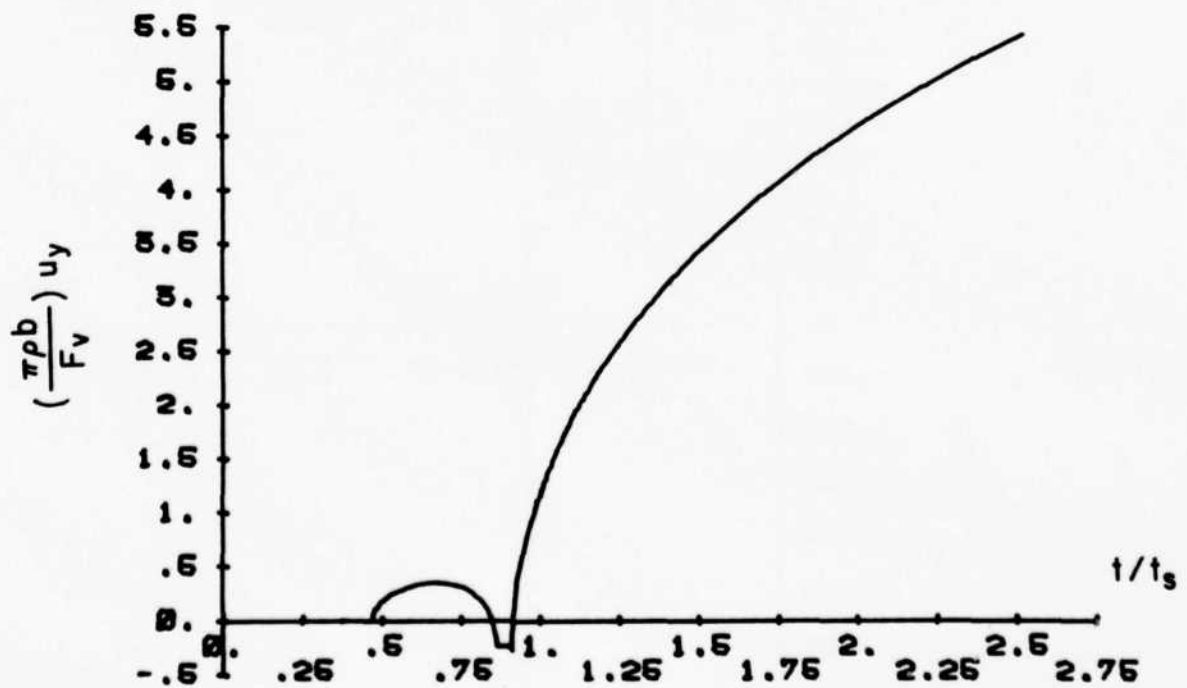FIG. 34b   STRESSES FOR HS-V IN A CLASS A-II MATERIAL WITH $\gamma = 2.2$
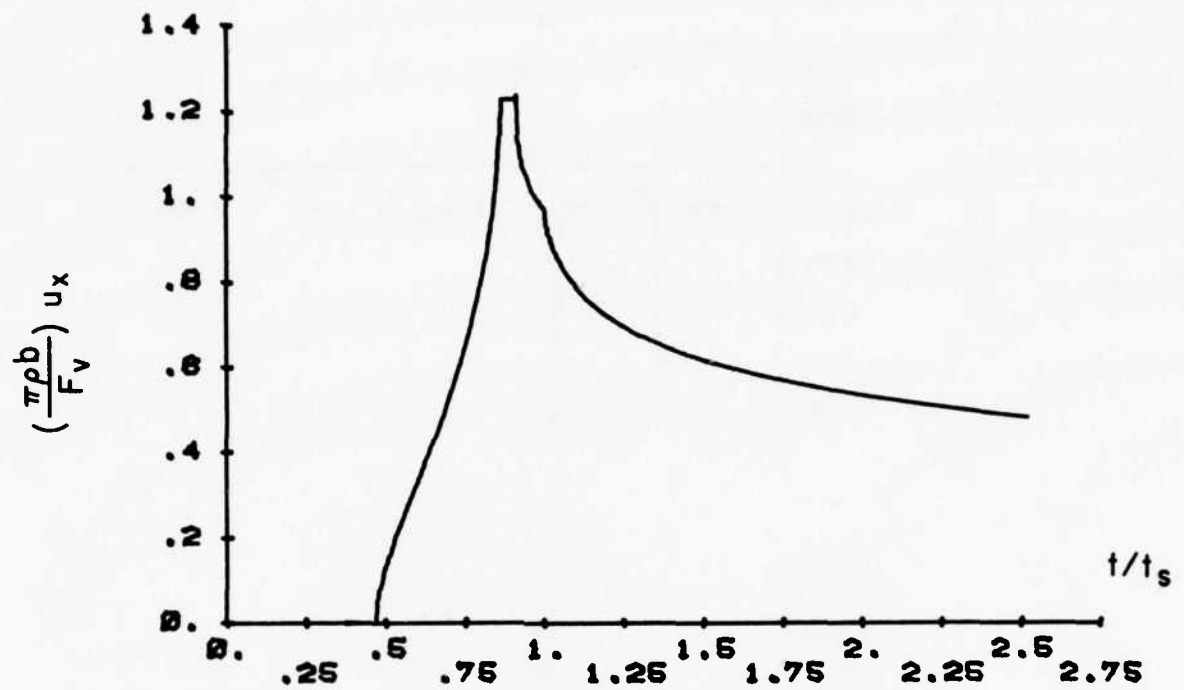
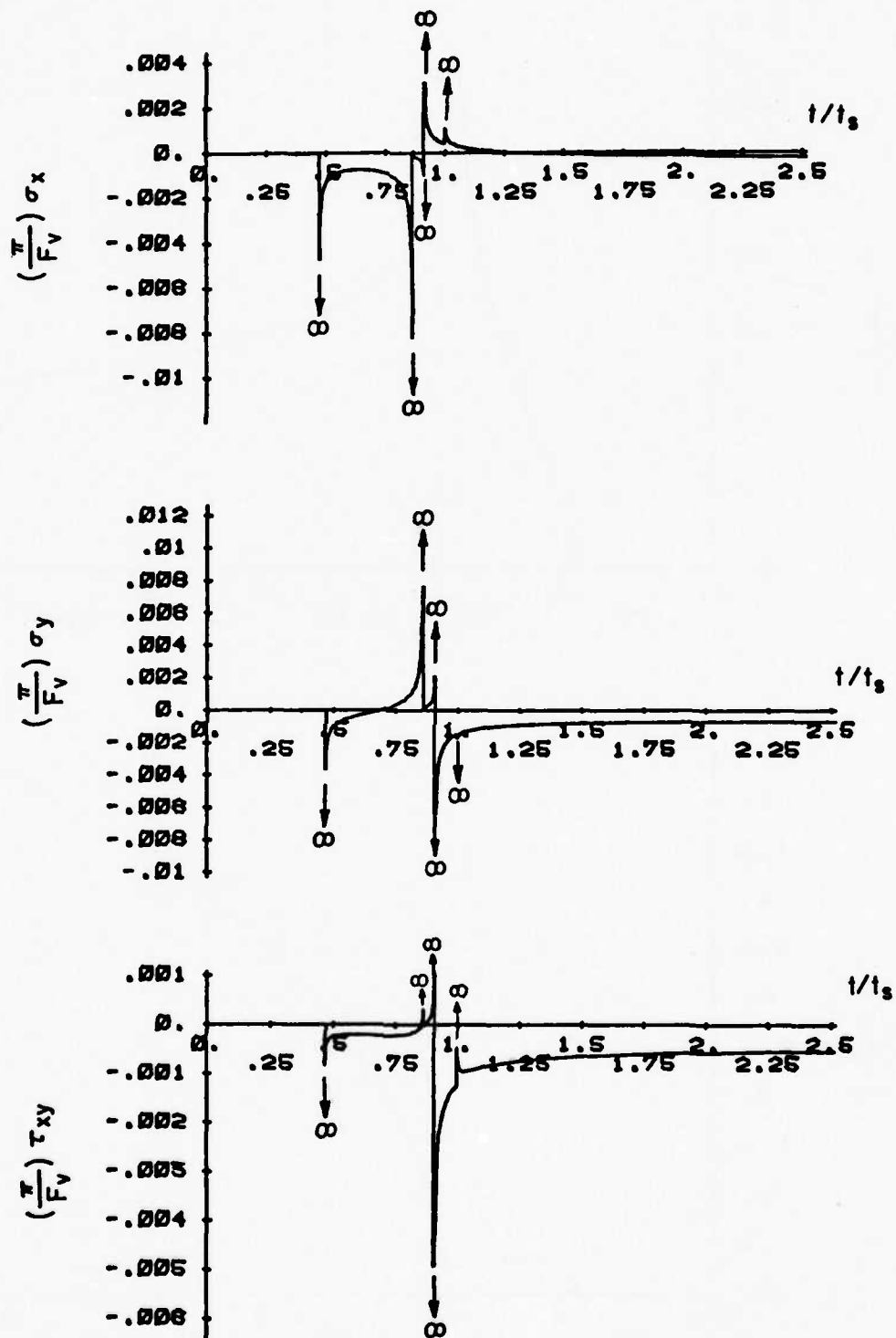FIG. 35a   DISPLACEMENTS FOR HS-V IN A CLASS B-I MATERIAL WITH $\gamma = 0.8$

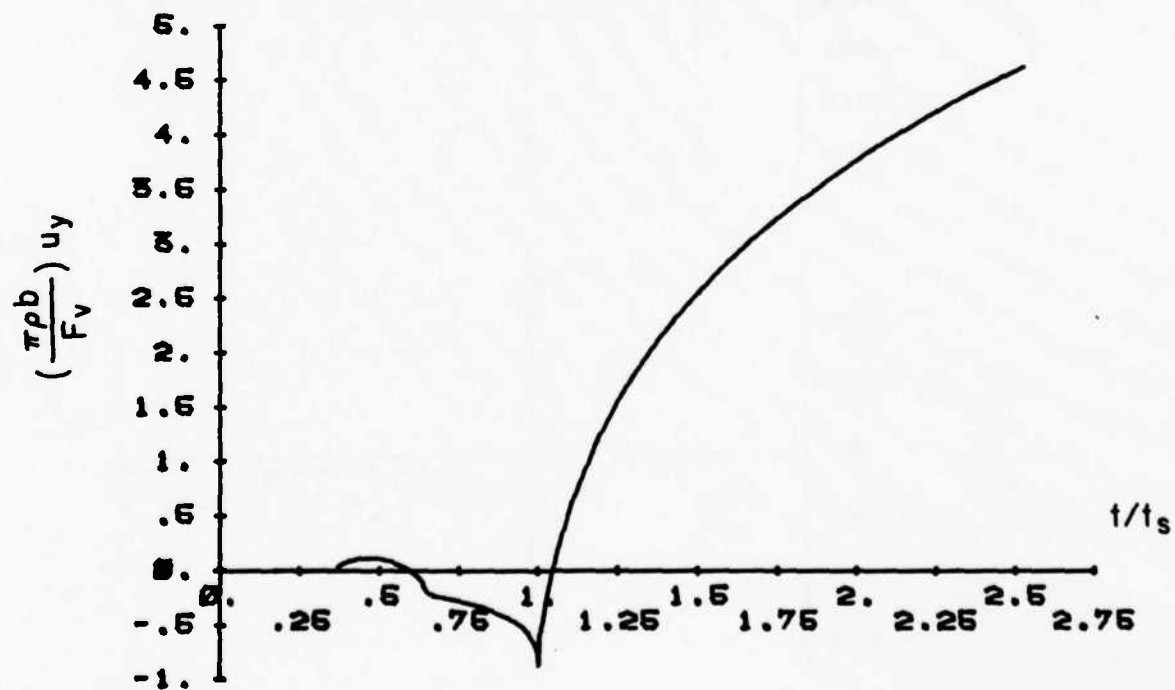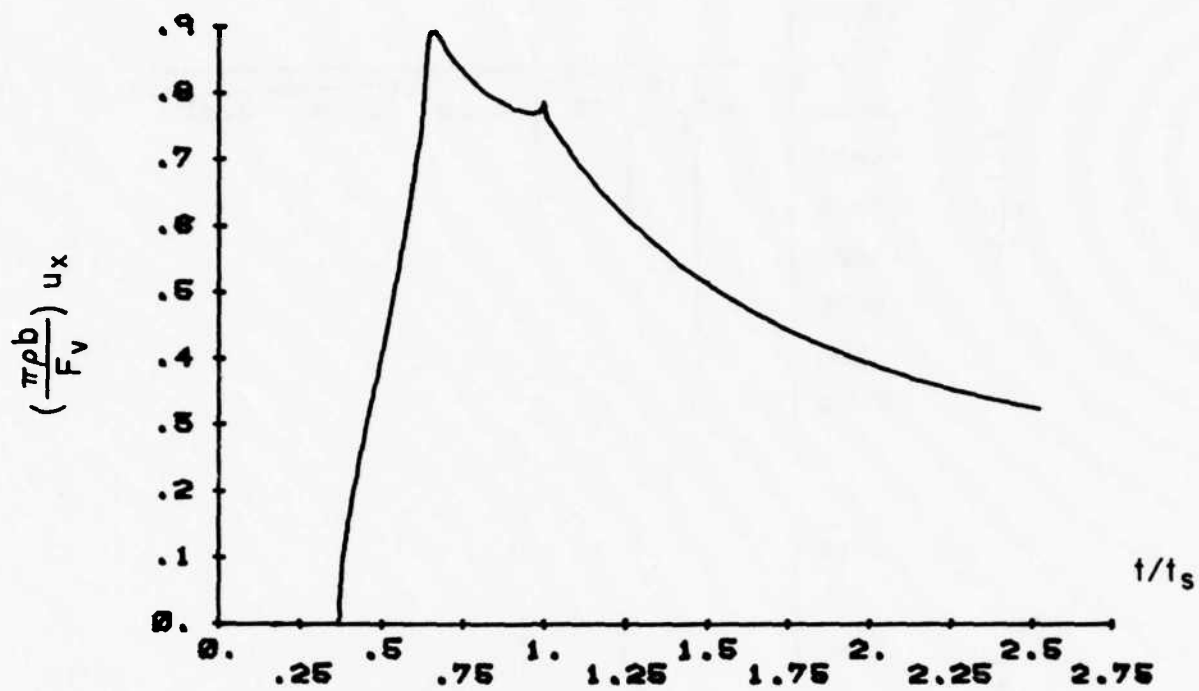FIG. 35b STRESSES FOR HS-V IN A CLASS B-I MATERIAL WITH $\gamma = 0.8$

FIG. 36a   DISPLACEMENTS FOR HS-V IN A CLASS B-I MATERIAL WITH $\gamma = 2.2$
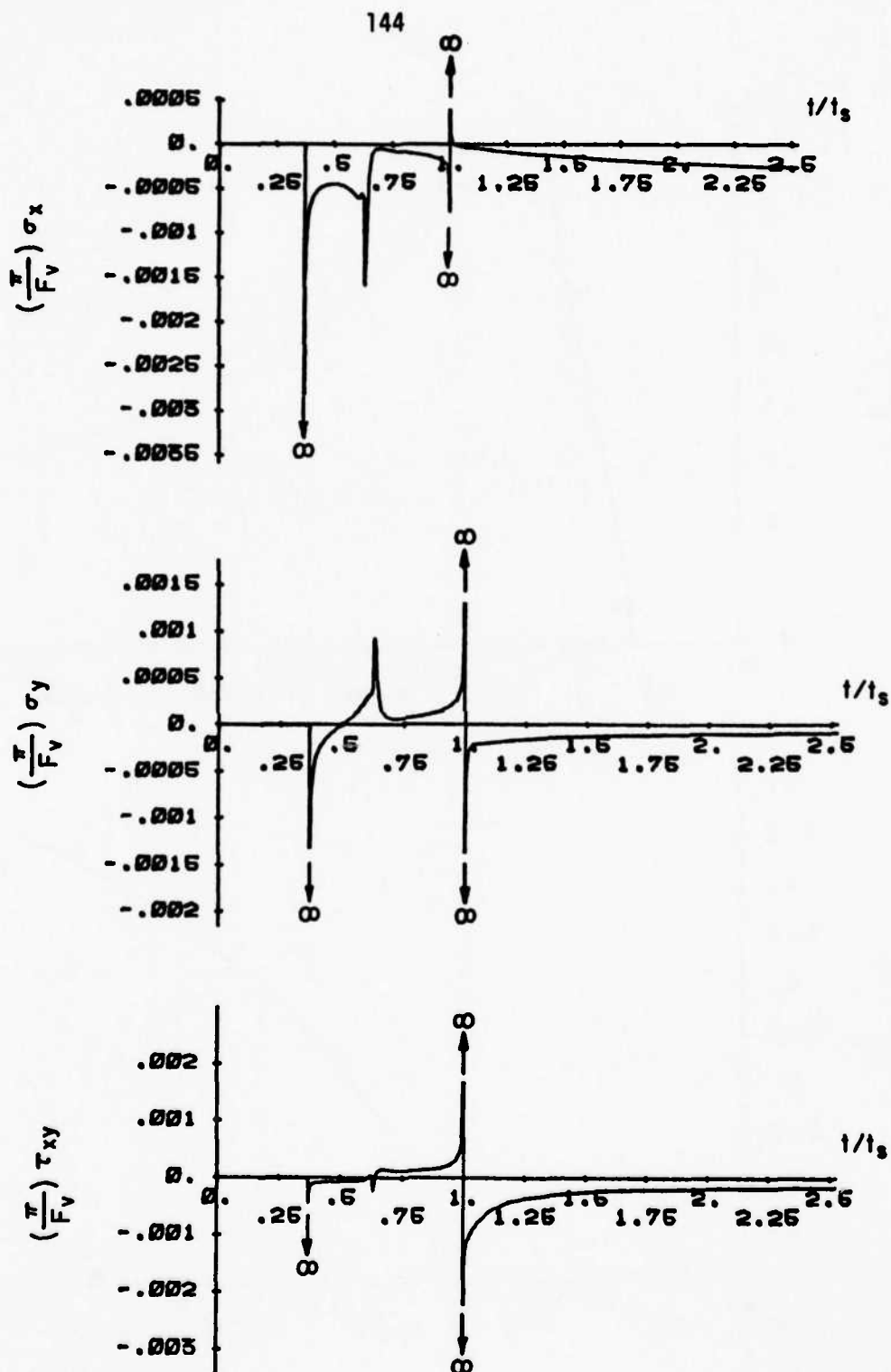
144

FIG. 36b   STRESSES FOR HS-V IN A CLASS B-I MATERIAL WITH $\gamma = 2.2$
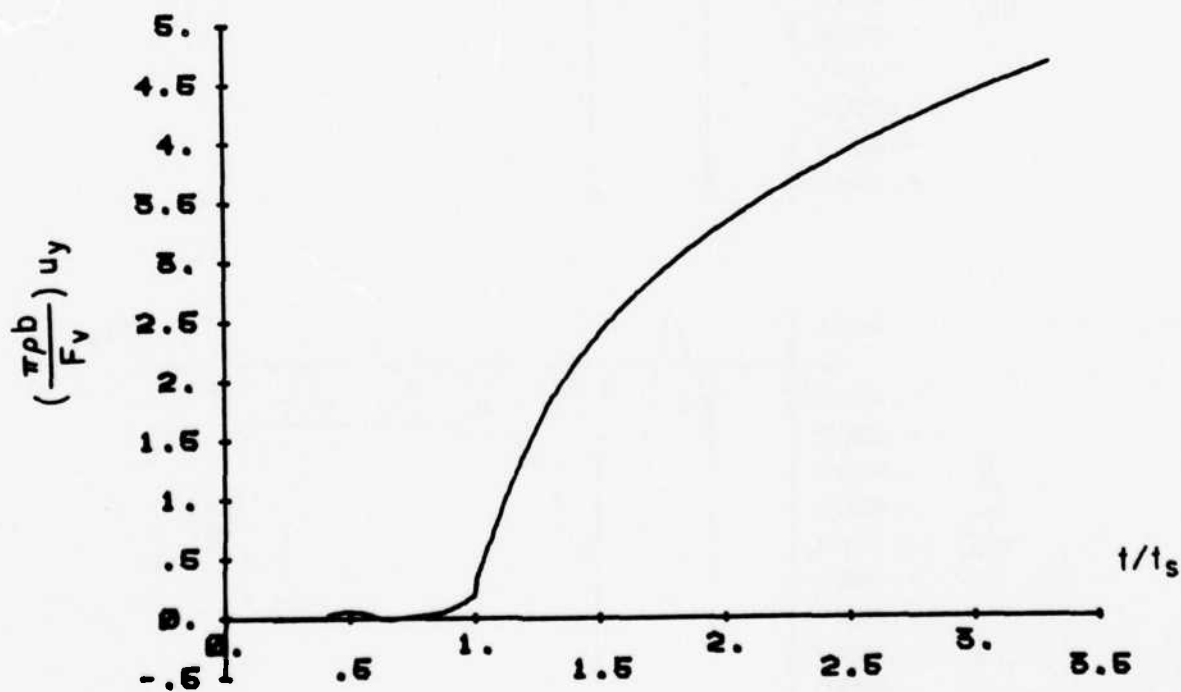
FIG. 37a   DISPLACEMENTS FOR HS-V IN A CLASS C-II MATERIAL WITH $\gamma = 2.2$

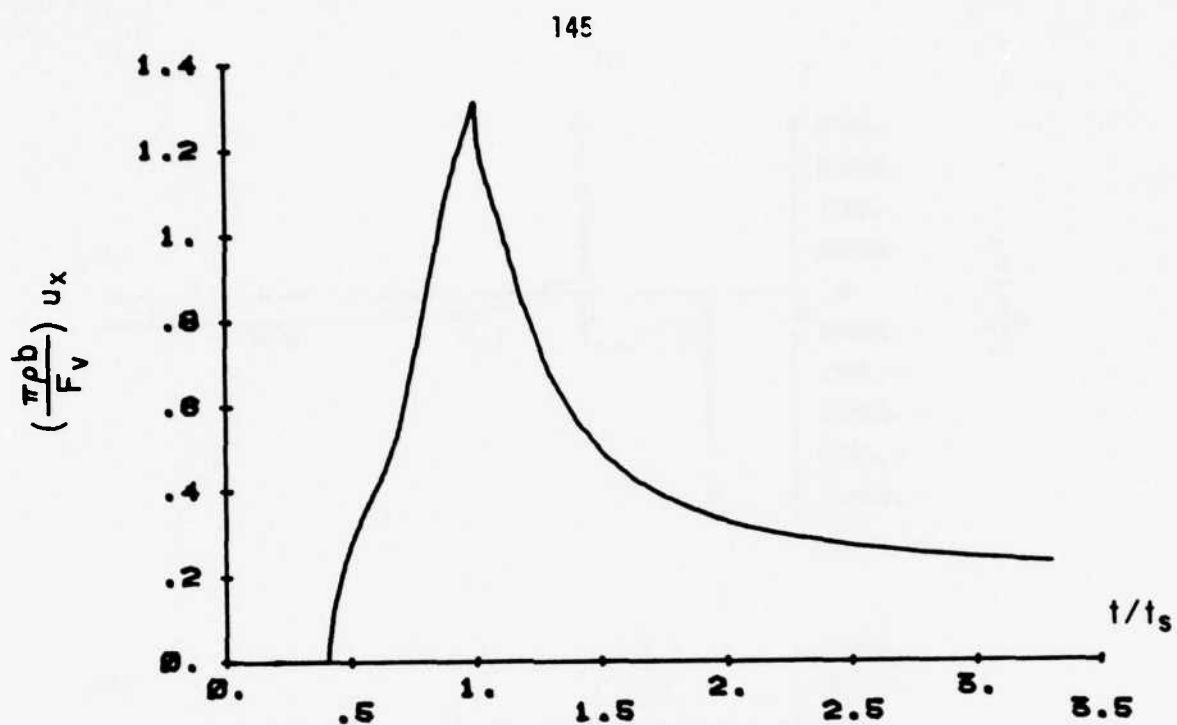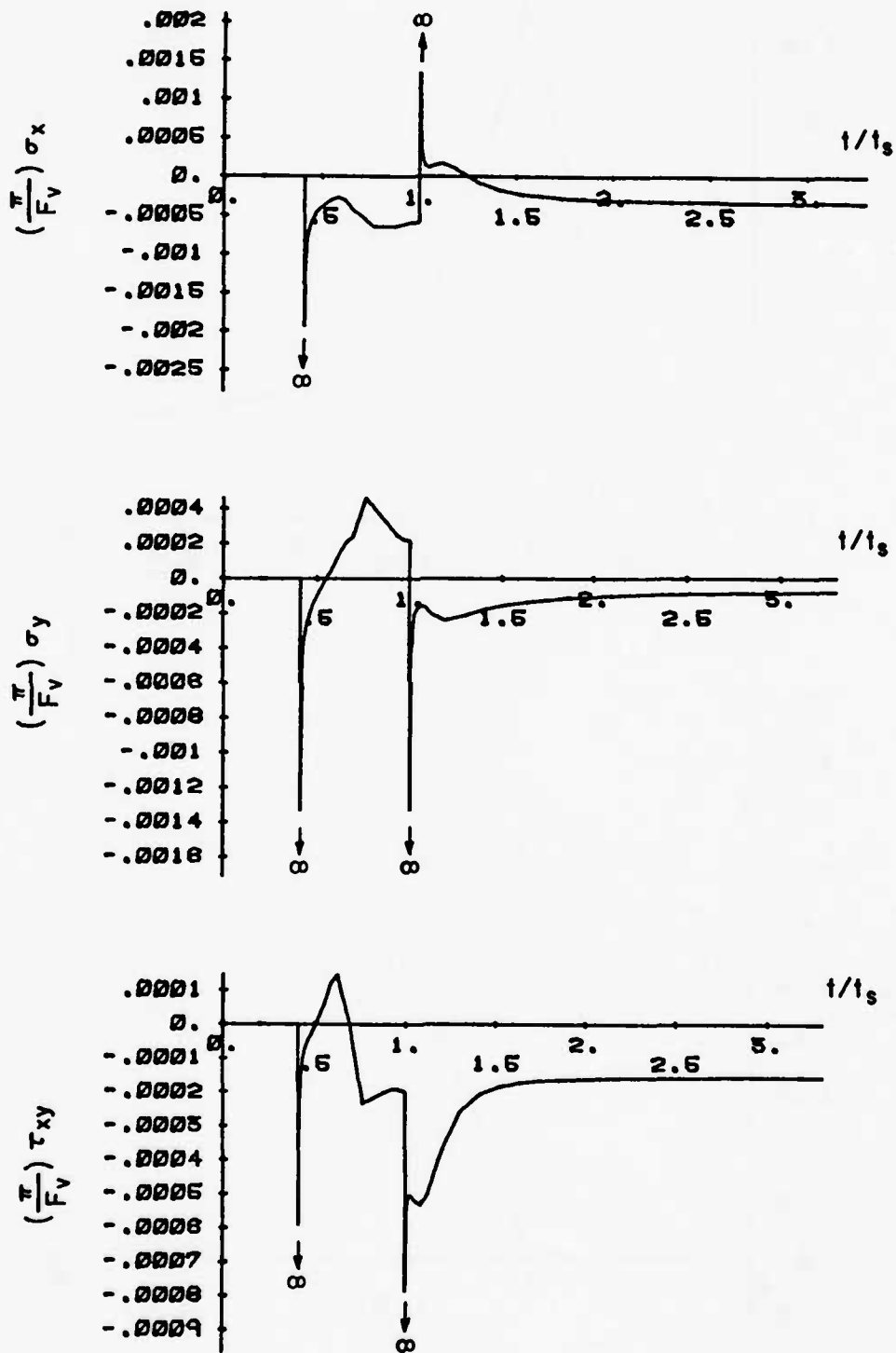FIG. 37b   STRESSES FOR HS-V IN A CLASS C-II MATERIAL WITH $\gamma = 2.2$
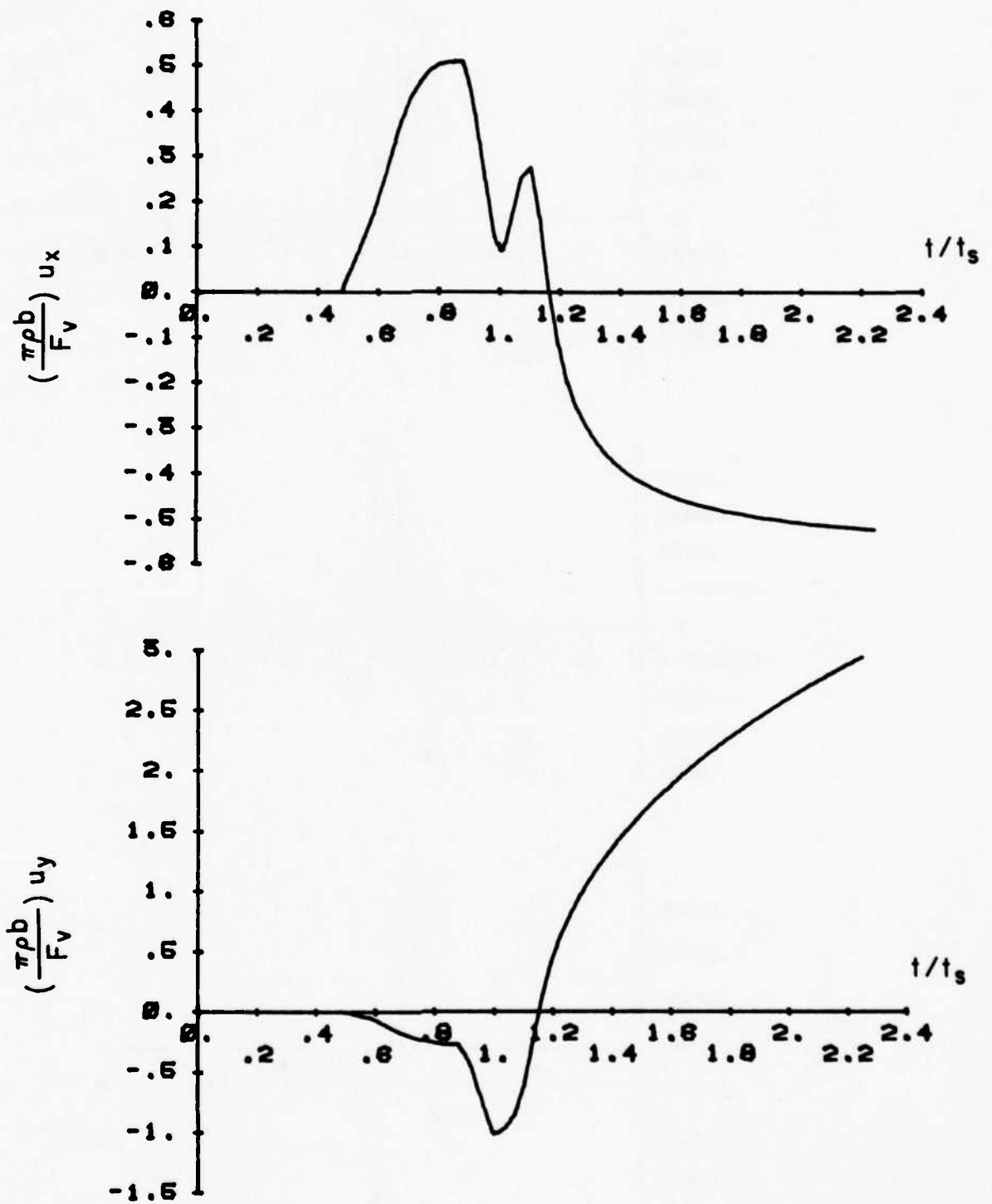
FIG. 38a   DISPLACEMENTS FOR HS-V IN A CLASS C-II MATERIAL WITH $\gamma = 10.0$

148
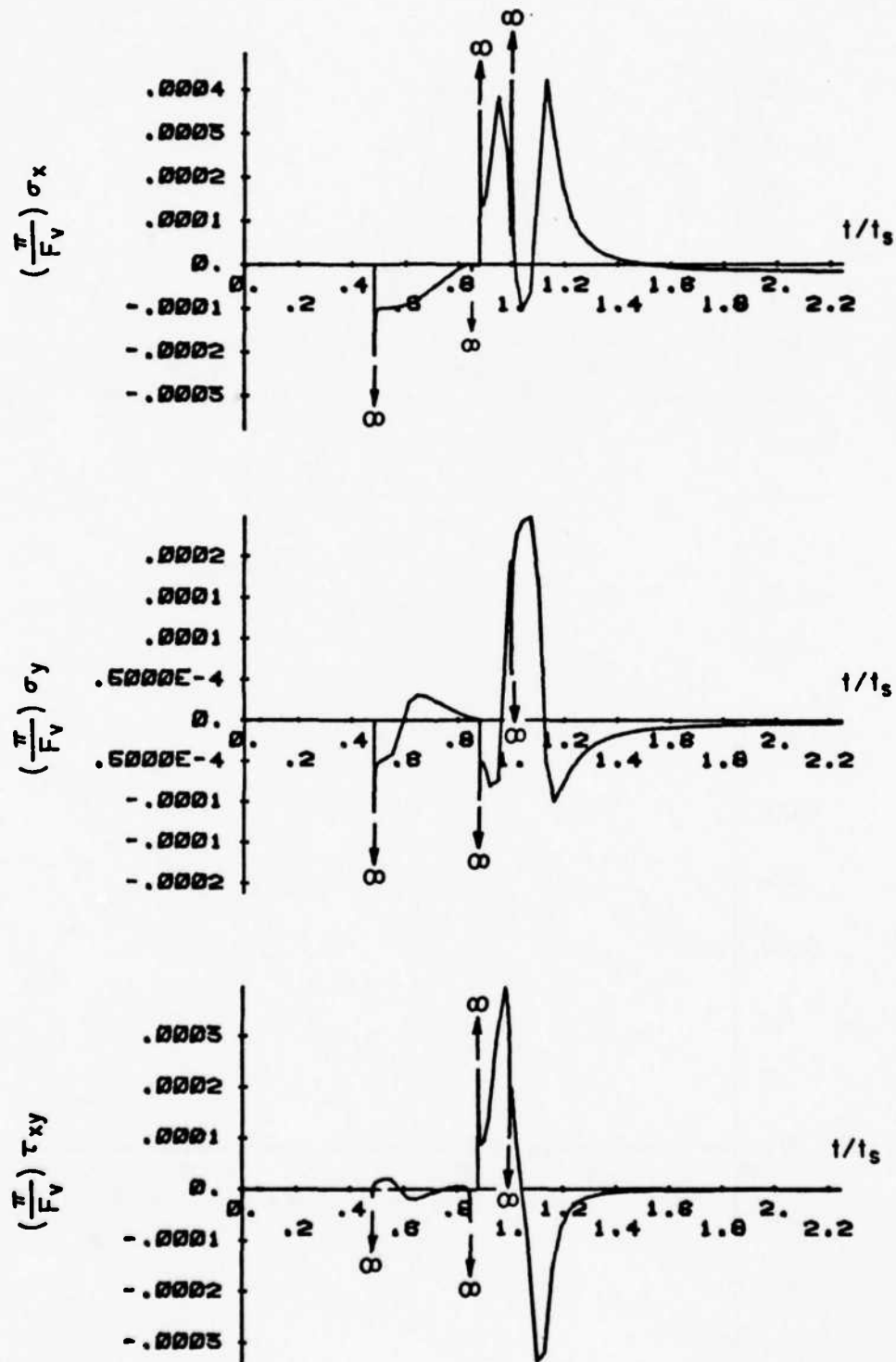
FIG. 38b   STRESSES FOR HS-V IN A CLASS C-II MATERIAL WITH γ = 10.0
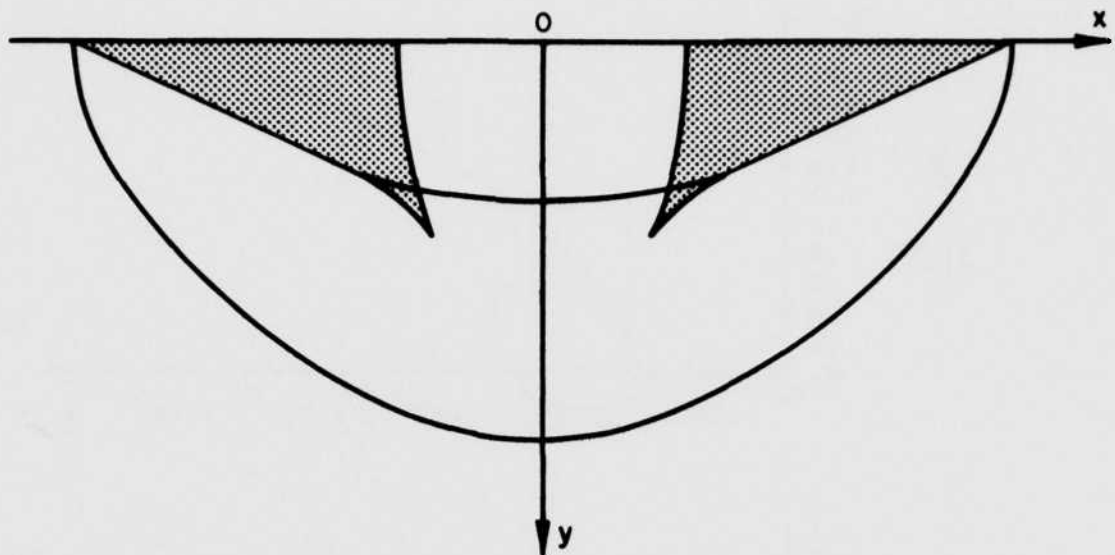
a) MATERIAL CASE B-I
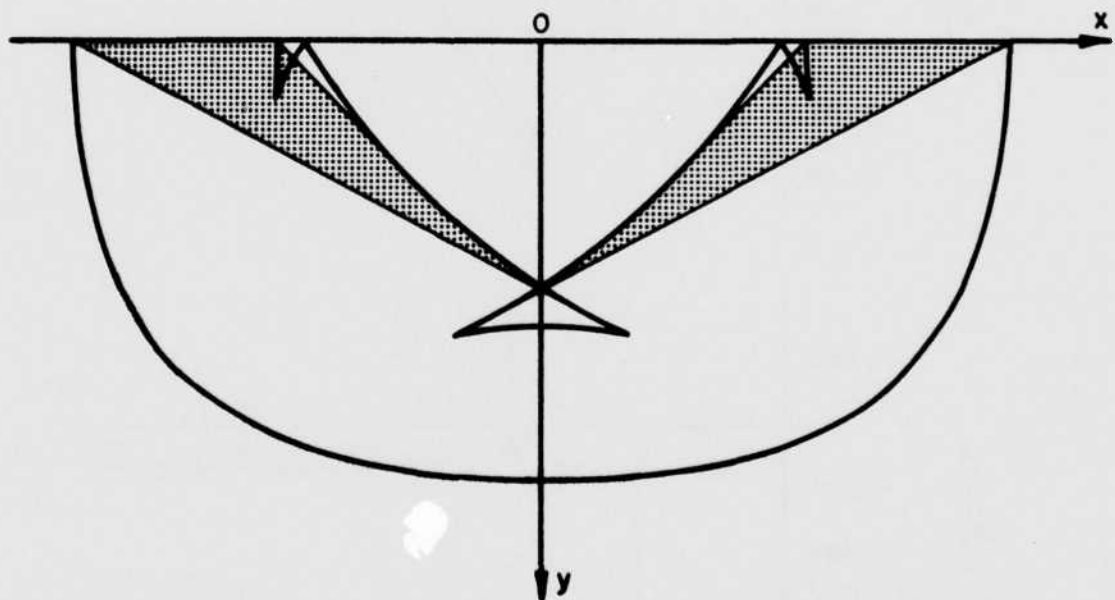
b) MATERIAL CASE C-II

FIG. 39   THE HEAD WAVE REGIONS
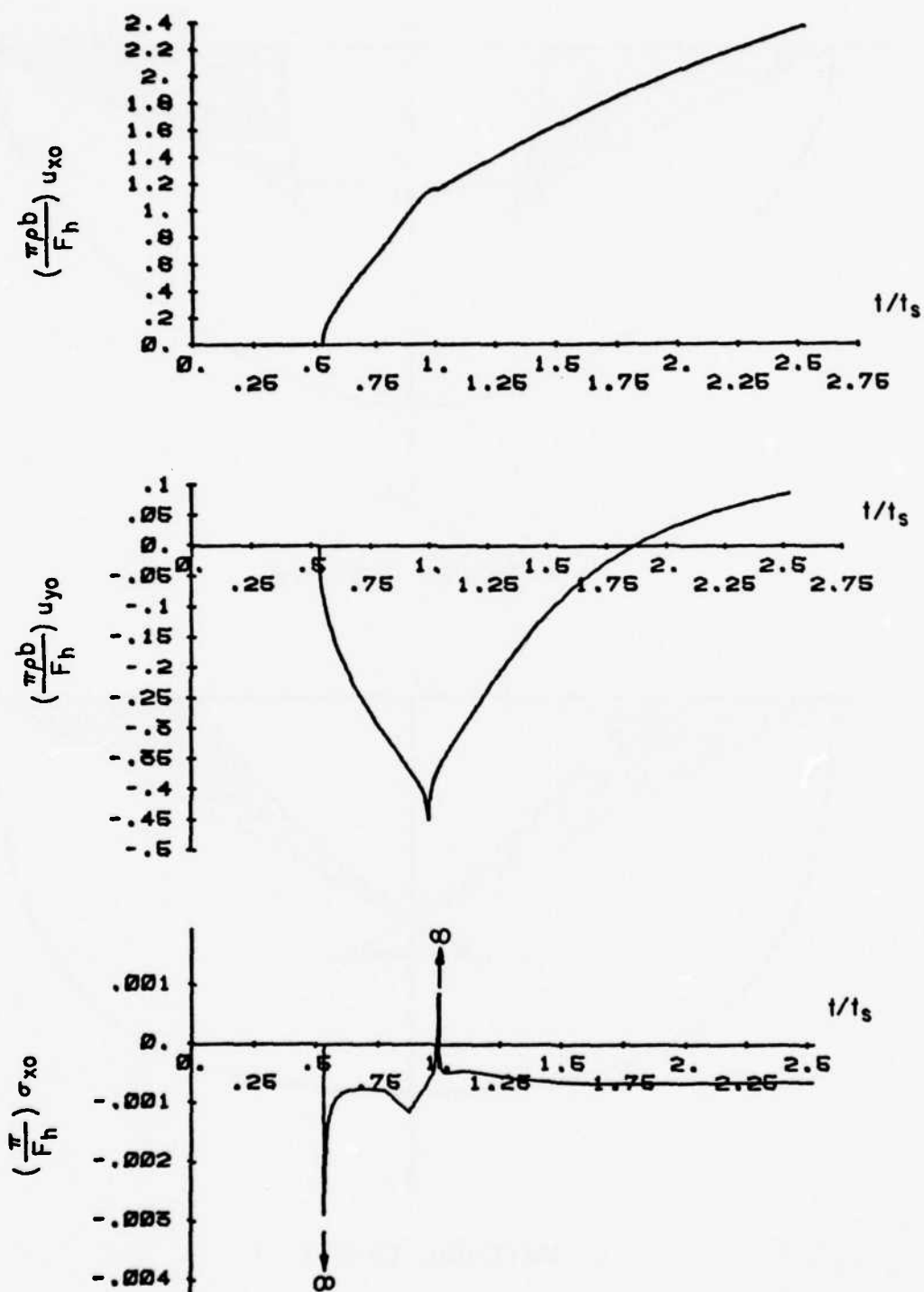
FIG. 40 SURFACE DISPLACEMENTS AND STRESS FOR HS-IH IN A CLASS A-II MATERIAL WITH $\gamma = 2.2$
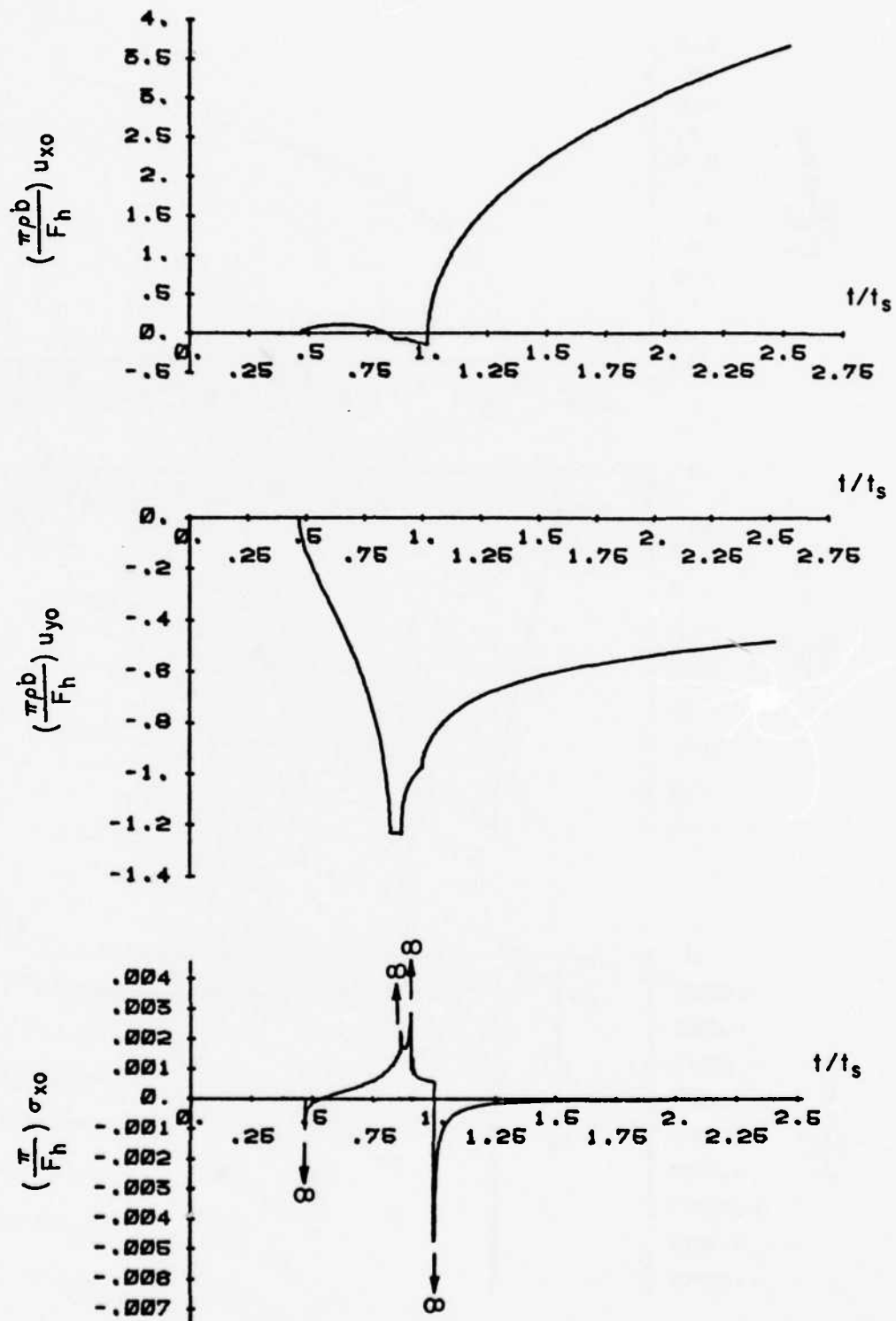
FIG. 41 SURFACE DISPLACEMENTS AND STRESS FOR HS-IH IN A CLASS B-I
MATERIAL WITH $\gamma = 0.8$
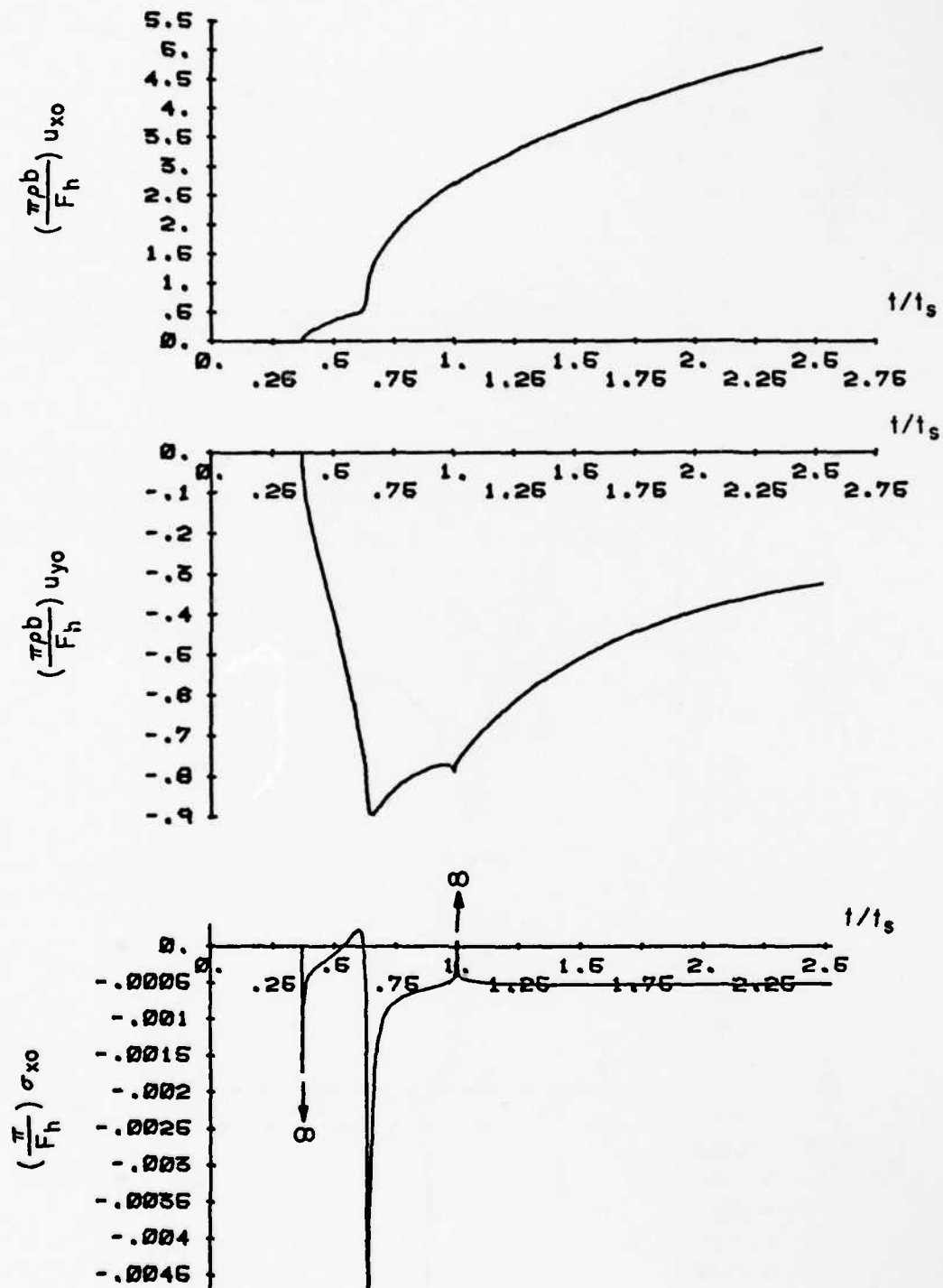
FIG. 42   SURFACE DISPLACEMENTS AND STRESS FOR HS-IH IN A CLASS B-I
           MATERIAL WITH γ = 2.2
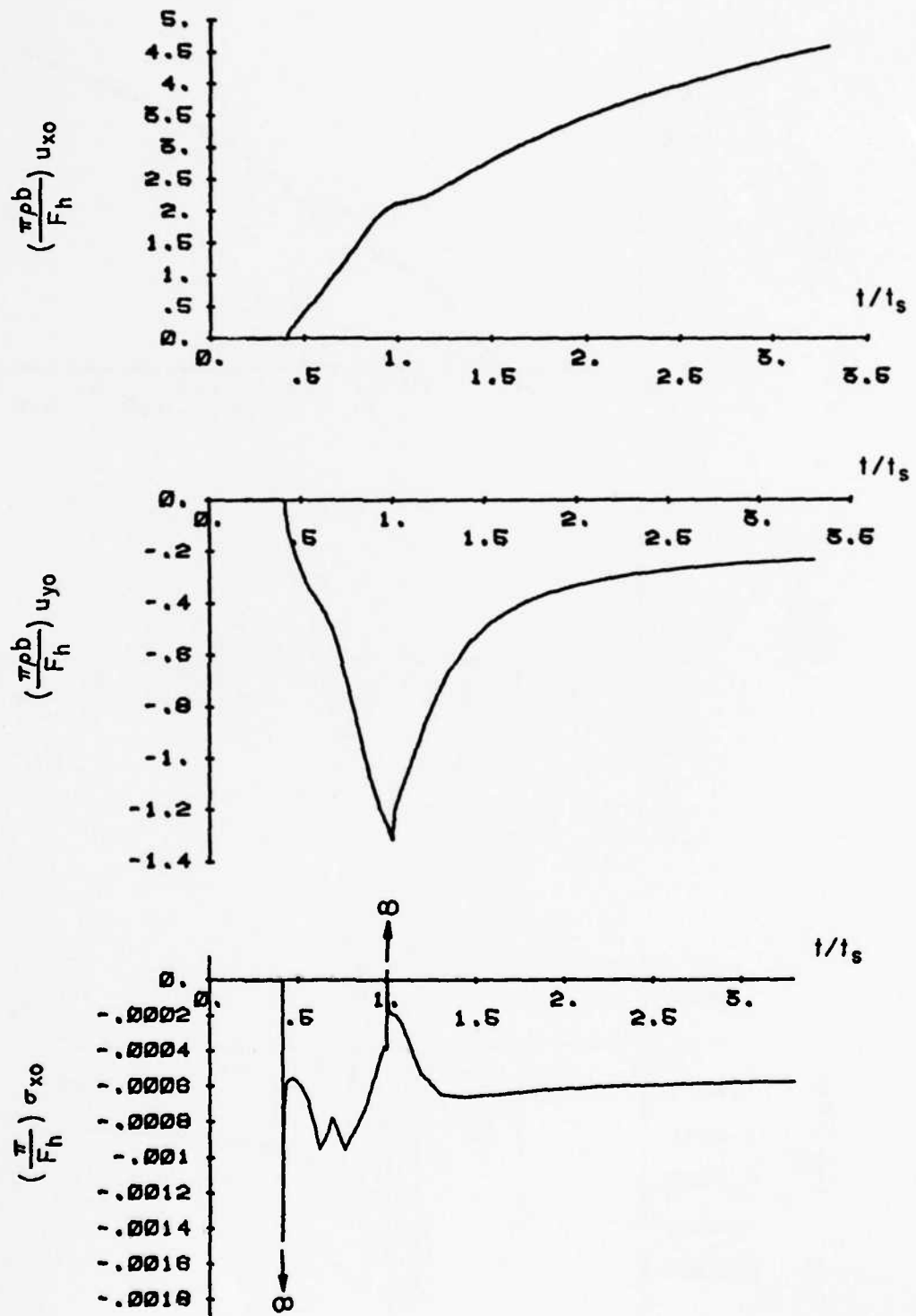
FIG. 43   SURFACE DISPLACEMENTS AND STRESS FOR HS-IH IN A CLASS C-II
          MATERIAL WITH $\gamma = 2.2$

154
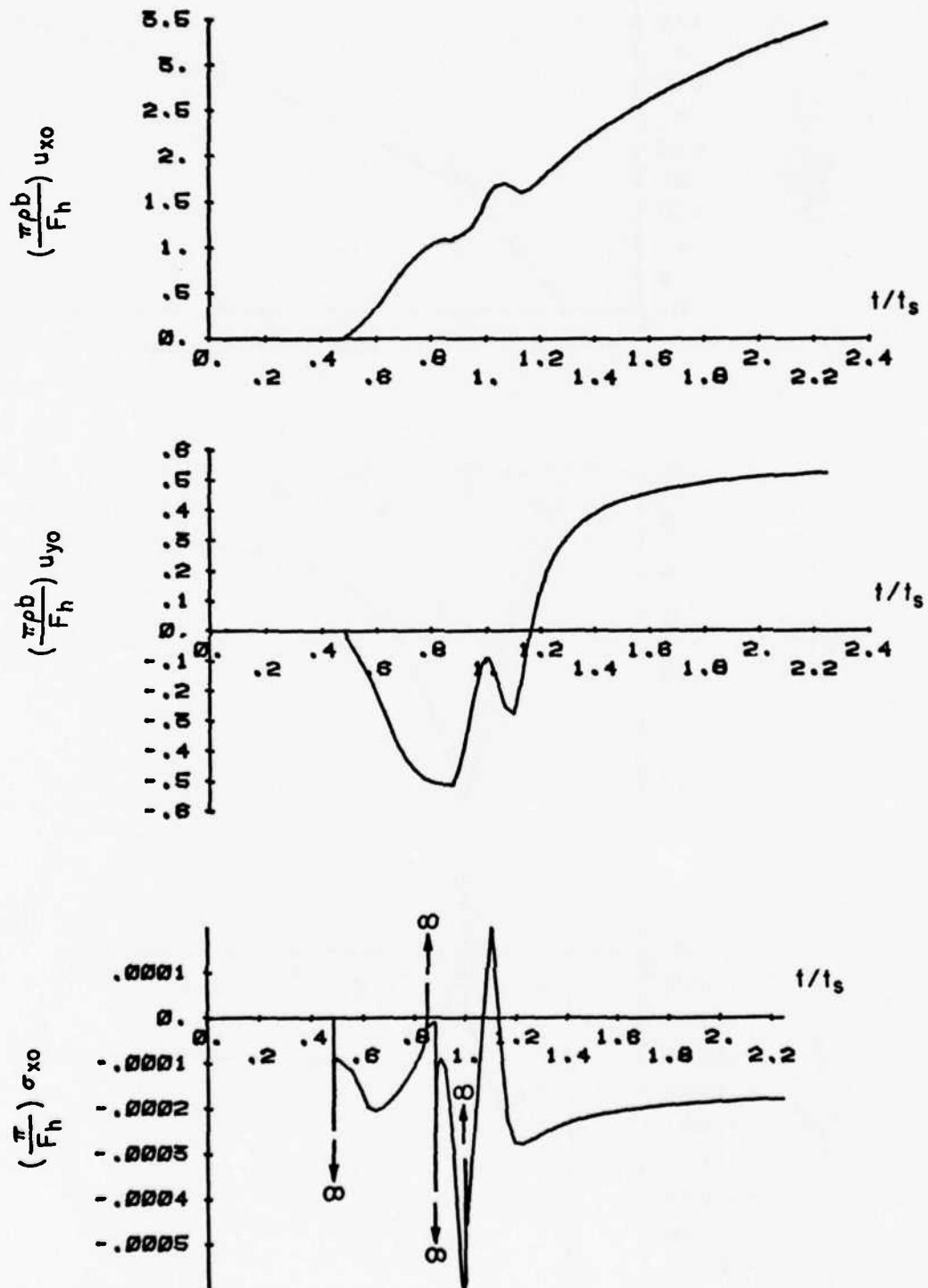
FIG. 44   SURFACE DISPLACEMENTS AND STRESS FOR HS-IH IN A CLASS C-II
MATERIAL WITH $\gamma = 10.0$

155
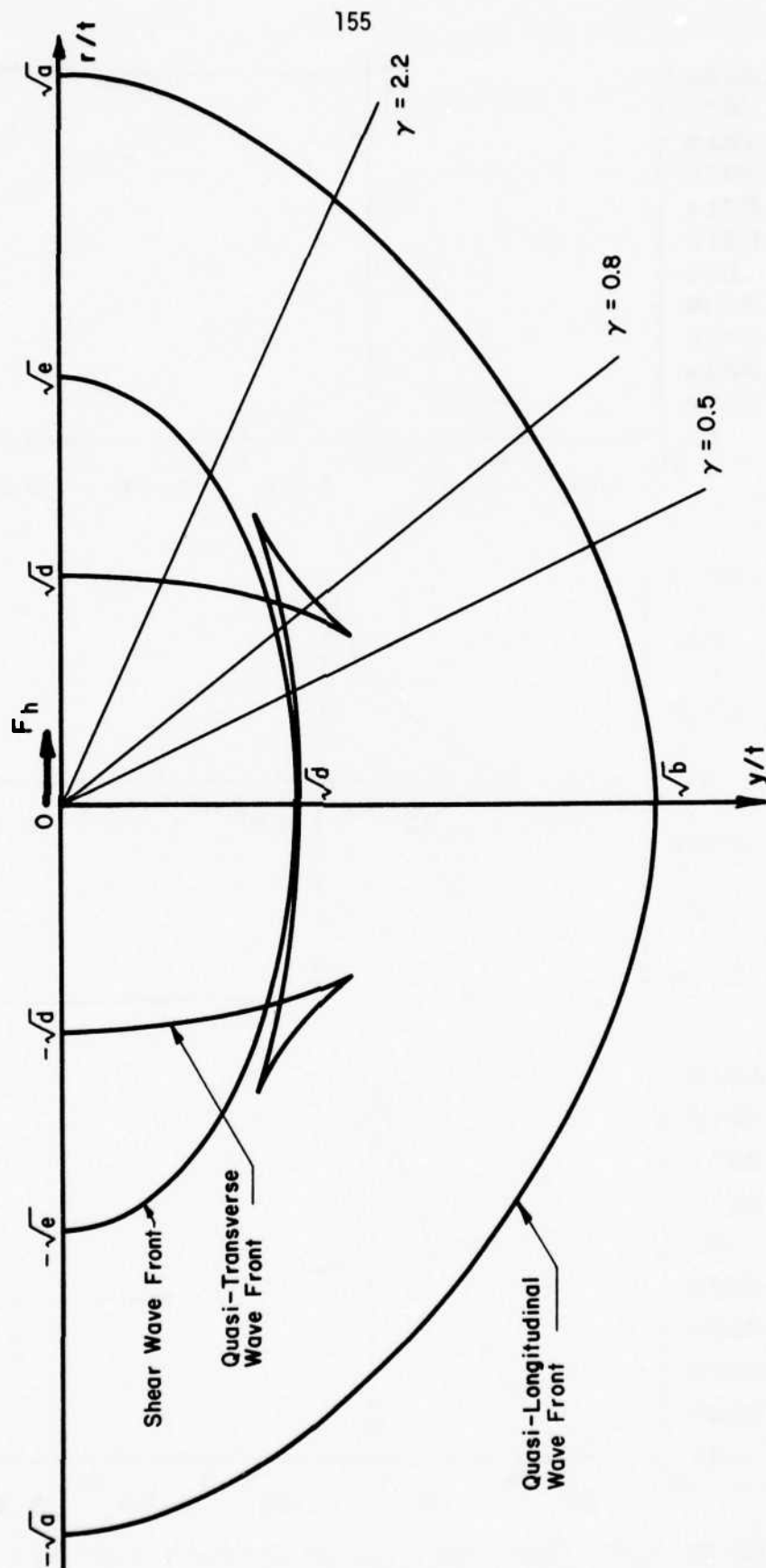
FIG. 45   THE PATTERN OF WAVE FRONTS IN A CLASS B-I
TRANSVERSELY ISOTROPIC MATERIAL
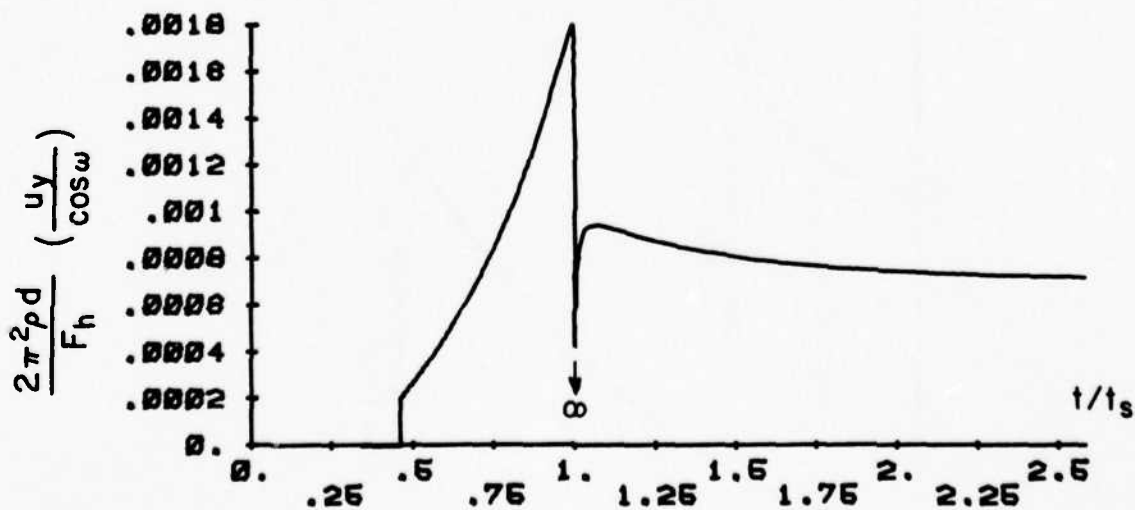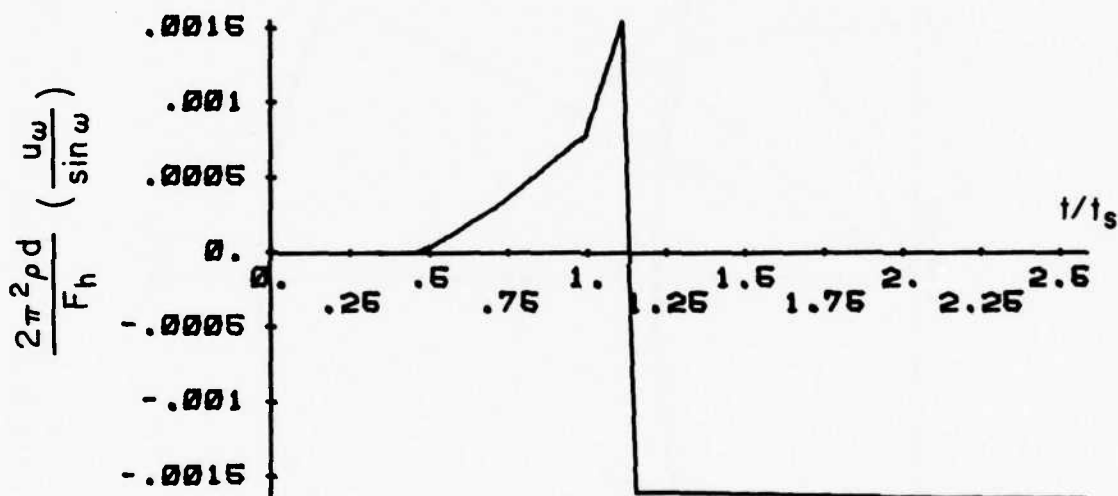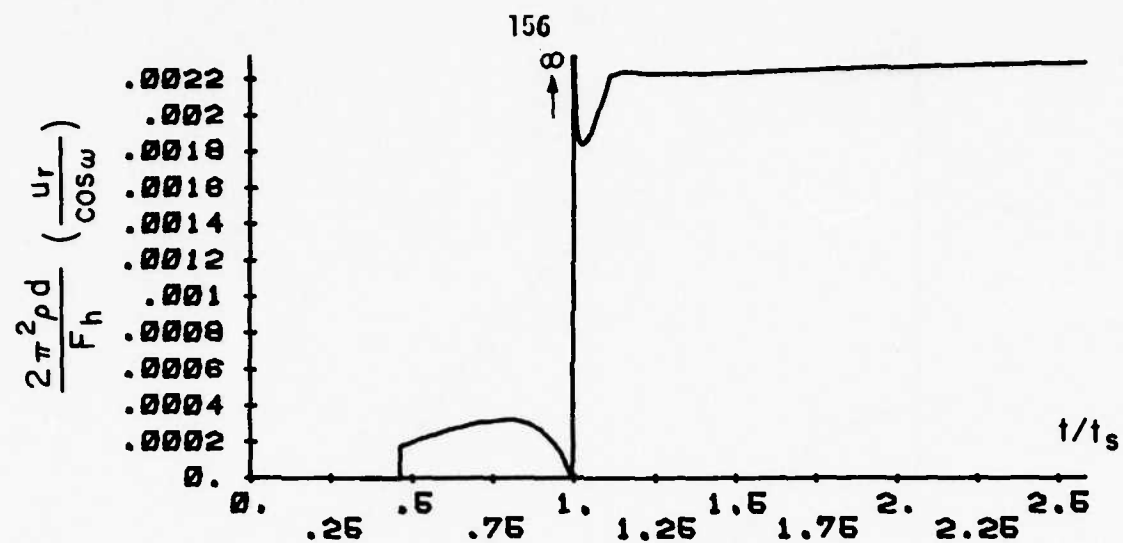
FIG. 46   DISPLACEMENTS FOR A SURFACE HORIZONTAL FORCE IN A CLASS A-I
TRANSVERSELY ISOTROPIC MATERIAL WITH $\gamma = 0.8$
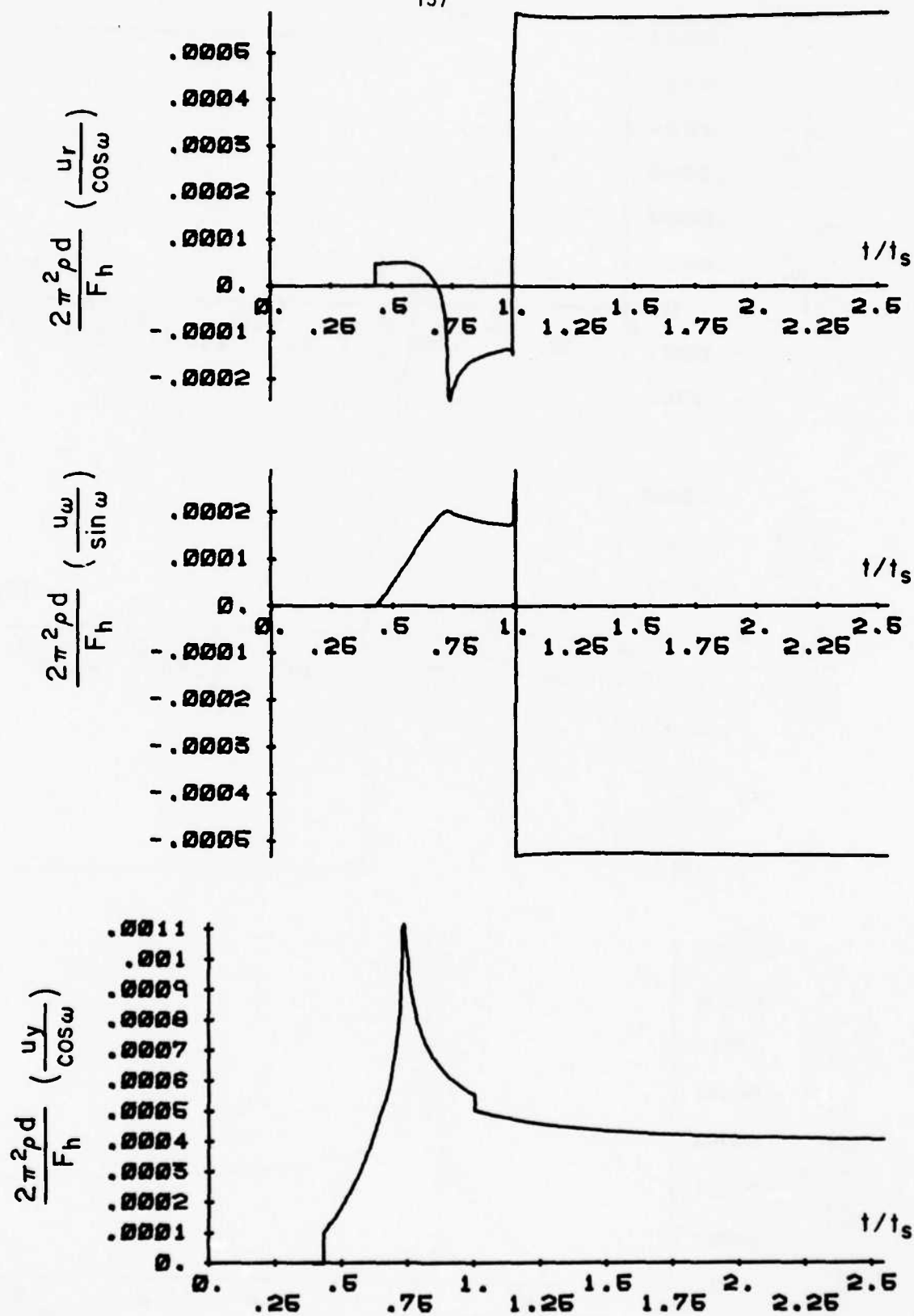
FIG. 47   DISPLACEMENTS FOR A SURFACE HORIZONTAL FORCE IN A CLASS B-I
TRANSVERSELY ISOTROPIC MATERIAL WITH γ = 0.5
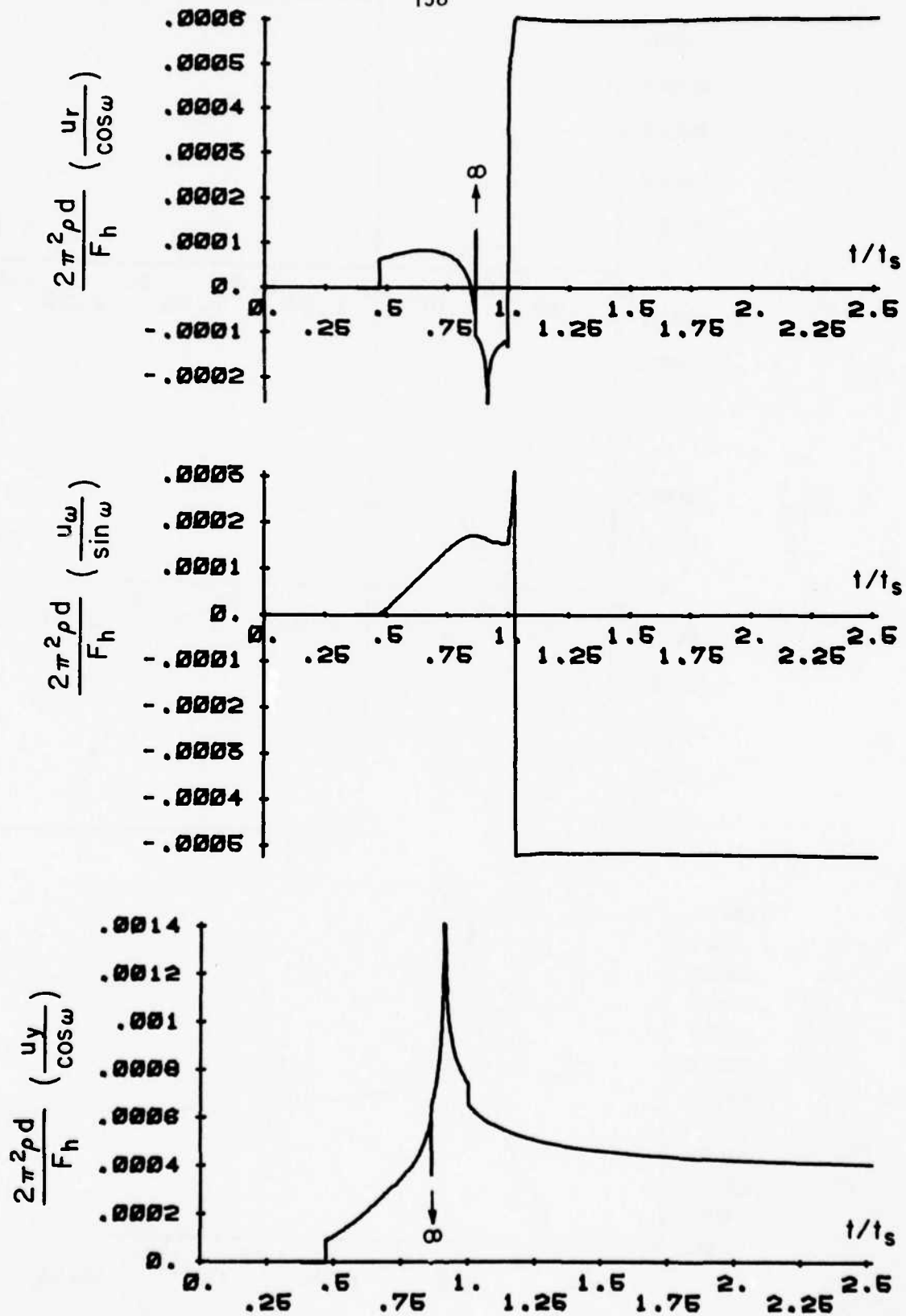
FIG. 48 DISPLACEMENTS FOR A SURFACE HORIZONTAL FORCE IN A CLASS B-I
TRANSVERSELY ISOTROPIC MATERIAL WITH $\gamma = 0.8$

APPENDIX A

THE DERIVATIVES OF θ_κ

The first and second derivatives of θ_κ with respect to x, y and t can be obtained from Eq. (2.16) by following the rules of differentiation for implicit functions [42]. They are given by the following expressions

$$\left.\begin{aligned}
\frac{\partial \theta_\kappa}{\partial x} &= \frac{\theta_\kappa}{\delta'_\kappa} \\
\frac{\partial \theta_\kappa}{\partial y} &= \frac{\lambda_\kappa(\theta_\kappa)}{\delta'_\kappa} \\
\frac{\partial \theta_\kappa}{\partial t} &= -\frac{1}{\delta'_\kappa}
\end{aligned}\right\} \qquad (A.1)$$

$$\left.\begin{aligned}
\frac{\partial^2 \theta_\kappa}{\partial x^2} &= \frac{1}{\delta'_\kappa} \frac{\partial}{\partial \theta_\kappa}\left[\frac{\theta_\kappa^2}{\delta'_\kappa}\right] \\
\frac{\partial^2 \theta_\kappa}{\partial y^2} &= \frac{1}{\delta'_\kappa} \frac{\partial}{\partial \theta_\kappa}\left[\frac{\lambda_\kappa^2(\theta_\kappa)}{\delta'_\kappa}\right] \\
\frac{\partial^2 \theta_\kappa}{\partial t^2} &= \frac{1}{\delta'_\kappa} \frac{\partial}{\partial \theta_\kappa}\left[\frac{1}{\delta'_\kappa}\right] \\
\frac{\partial^2 \theta_\kappa}{\partial x \partial y} &= \frac{1}{\delta'_\kappa} \frac{\partial}{\partial \theta_\kappa}\left[\frac{\theta_\kappa \lambda_\kappa(\theta_\kappa)}{\delta'_\kappa}\right]
\end{aligned}\right\} \qquad (A.2)$$

where δ'_κ is given by Eq. (2.37).

Let $f(\theta_\kappa)$ and $f'(\theta_\kappa)$ denote any analytic function of θ_κ and its derivative with respect to the same variable. The first, second and third derivatives of $f(\theta_\kappa)$ with respect to x, y and t are

160

$$\frac{\partial f(\theta_\kappa)}{\partial x} = \frac{\theta_\kappa}{\delta'_\kappa} f'(\theta_\kappa)$$

$$\frac{\partial f(\theta_\kappa)}{\partial y} = \frac{\lambda_\kappa(\theta_\kappa)}{\delta'_\kappa} f'(\theta_\kappa) \tag{A.3}$$

$$\frac{\partial f(\theta_\kappa)}{\partial t} = -\frac{1}{\delta'_\kappa} f'(\theta_\kappa)$$

$$\frac{\partial^2 f(\theta_\kappa)}{\partial x^2} = \frac{1}{\delta'_\kappa} \frac{\partial}{\partial \theta_\kappa}\left[\frac{\theta_\kappa^2}{\delta'_\kappa} f'(\theta_\kappa)\right]$$

$$\frac{\partial^2 f(\theta_\kappa)}{\partial y^2} = \frac{1}{\delta'_\kappa} \frac{\partial}{\partial \theta_\kappa}\left[\frac{\lambda_\kappa^2(\theta_\kappa)}{\delta'_\kappa} f'(\theta_\kappa)\right] \tag{A.4}$$

$$\frac{\partial^2 f(\theta_\kappa)}{\partial x \partial y} = \frac{1}{\delta'_\kappa} \frac{\partial}{\partial \theta_\kappa}\left[\frac{\theta_\kappa \lambda_\kappa(\theta_\kappa)}{\delta'_\kappa} f'(\theta_\kappa)\right]$$

$$\frac{\partial^2 f(\theta_\kappa)}{\partial t^2} = \frac{1}{\delta'_\kappa} \frac{\partial}{\partial \theta_\kappa}\left[\frac{1}{\delta'_\kappa} f'(\theta_\kappa)\right]$$

$$\frac{\partial^3 f(\theta_\kappa)}{\partial x^p \partial y^q \partial t^r} = \frac{(-1)^{p+1}}{\delta'_\kappa} \frac{\partial}{\partial \theta_\kappa}\left[\frac{1}{\delta'_\kappa} \frac{\partial}{\partial \theta_\kappa}\left(\frac{\theta_\kappa^p[-\lambda_\kappa(\theta_\kappa)]^q}{\delta'_\kappa} f'(\theta_\kappa)\right)\right] \tag{A.5}$$

where $p + q + r = 3$

In the case of the reflected waves the same formulas can be used. The only differences are that $\lambda_\kappa(\theta_\kappa)$ must be replaced by $-\lambda_\kappa(\theta_\kappa)$, which indicates a reflected wave as opposed to an incident wave (see Eqs. 2.40 to 2.44) and that θ_κ must be replaced by $\theta_{\kappa j}$, which is the parameter associated with the reflected wave.

APPENDIX B

THE DEFINITION OF THE FUNCTION $\lambda_\kappa(\theta)$

The complete definition of the multi-valued function $\lambda_\kappa(\theta)$ is of extreme importance in the solution of wave propagation problems in orthotropic media by the method of self-similar potentials. The solution of the algebraic biquadratic equation (2.18) yields the four values

$$\lambda_1(\theta) = \left[\frac{b+d-L\theta^2 - \sqrt{Q(\theta)}}{2bd}\right]^{\frac{1}{2}}$$

$$\lambda_2(\theta) = \left[\frac{b+d-L\theta^2 + \sqrt{Q(\theta)}}{2bd}\right]^{\frac{1}{2}}$$

$$\lambda_3(\theta) = -\left[\frac{b+d-L\theta^2 - \sqrt{Q(\theta)}}{2bd}\right]^{\frac{1}{2}}$$

$$\lambda_4(\theta) = -\left[\frac{b+d-L\theta^2 + \sqrt{Q(\theta)}}{2bd}\right]^{\frac{1}{2}}$$

(B.1)

which correspond respectively to the four sheets S_1, S_2, S_3 and S_4 of a Riemann surface as the domain of definition of the function $\lambda_\kappa(\theta)$ [11]. The four sheets are connected along branch cuts in a manner to be described later. Since the ends of the branch cuts are the singular points of the function $\lambda_\kappa(\theta)$ which are common to more than one branch, it is necessary to determine first the position of these branch points on the Riemann surface. Their values are found by considering the following system of two equations [16]:

$$F(\theta, \lambda_\kappa) = 0 \tag{B.2a}$$

$$\frac{\partial F(\theta, \lambda_\kappa)}{\partial \lambda_\kappa} = 0 \tag{B.2b}$$

where $F(\theta, \lambda_\kappa)$ is given by Eq. (2.18). Equation (B.2b) can be written as

$$\lambda_\kappa \left[\lambda_\kappa^2 - \frac{b+d-L\theta^2}{2bd} \right] = 0 \tag{B.3}$$

If $\lambda_\kappa \neq 0$ then $\lambda_\kappa^2 = \frac{b+d-L\theta^2}{2bd}$ and back-substitution to (B.2a) results in

$$Q(\theta) = 0 \tag{B.4}$$

The polynomial $Q(\theta)$ (see Eq. 2.20) has in general four roots which assume real, imaginary or complex values depending on whether or not certain inequalities among the elastic parameters are satisfied. The results of this investigation are summarized in Table B.1 where it can be seen that there exist four different cases denoted by I, II, III and IV.

The choice of the branch cuts for each of these cases is shown in Fig. B.1. Each of the four sheets of the Riemann surface has the same branch cuts for the function $[Q(\theta_\kappa)]^{\frac{1}{2}}$. These branch cuts connect sheets S_1 to S_2 and S_3 to S_4.

The remaining branch points are defined by the condition $\lambda_\kappa = 0$. Direct substitution into Eq. (B.2a) yields the values

$$\theta = \pm \theta_A = \pm 1/\sqrt{a} \tag{B.5a}$$

$$\theta = \pm \theta_D = \pm 1/\sqrt{d} \tag{B.5b}$$

The location of these points on the Riemann surface depends on whether the quantity N_2 is positive or negative. It can be shown that when $N_2 > 0$ the branch points Θ_A are located on sheets S_1 and S_3 while Θ_D are on sheets S_2 and S_4. The choice of the branch cuts in this case is shown in Fig. B.2 (a). The branch cut $(-\Theta_A, \Theta_A)$ connects sheet S_1 to S_3 while $(-\Theta_D, \Theta_D)$ connects sheet S_2 to S_4. When $N_2 < 0$, both pairs $\pm \Theta_A$ and $\pm \Theta_D$ are singular points common to S_1 and S_3 sheets. Figure B.2 (b) shows the selection of the branch cuts for the case $N_2 < 0$. Again the branch cuts $(-\Theta_{01}, -\Theta_D), (-\Theta_A, \Theta_A)$ and (Θ_D, Θ_{01}) connect sheet S_1 to S_3 while the branch cut $(-\Theta_{01}, \Theta_{01})$ connects sheet S_2 to S_4. It must be noted here that $N_2 < 0$ is not compatible with the inequalities associated with cases I and III (Table B.1). When $N_2 < 0$, there are always two real branch points $\pm \Theta_{01}$ satisfying the condition $|\Theta_{01}| \geq |1/\sqrt{d}|$.

The complete Riemann surface is given in Figs. B.3 and B.4 for two distinct cases. The construction and interconnection of the four sheets for the remaining cases is made in a similar way. Only sheets S_1 and S_2 are required to represent the mapping of the wave fields as discussed in Chapter 4.

The important behavior of $\lambda_\kappa(\theta)$ for values of θ on the real axis of the Im$\theta \geq 0$ half complex plane will now be considered. It is easy to see that

$$\lambda_1(0) = 1/\sqrt{b} \tag{B.6a}$$

$$\lambda_2(0) = 1/\sqrt{d} \tag{B.6b}$$

$$\lambda_1(\pm 1/\sqrt{a}) = 0 \tag{B.6c}$$

$$\lambda_2(\pm\ 1/\sqrt{a}) = \left[\ \frac{d(a-d)\ +\ c^2}{abd}\ \right]^{\frac{1}{2}} \tag{B.6d}$$

In the interval $1/\sqrt{a} < |Re\theta| < 1/\sqrt{d}$, $\lambda_1(\theta)$ is imaginary and $\lambda_2(\theta)$ is real. For any values with $|Re\theta| \geq 1/\sqrt{d}$ the behavior depends on whether N_2 is positive or negative.

When $N_2 > 0$

$$\lambda_1(\pm\ 1/\sqrt{d}) = (-N_2/bd^2)^{\frac{1}{2}} \tag{B.7a}$$

which is imaginary and

$$\lambda_2(\pm\ 1/\sqrt{d}) = 0 \tag{B.7b}$$

For larger values of $Re\theta$, both $\lambda_1(\theta)$ and $\lambda_2(\theta)$ remain imaginary unless a real branch point θ_{01} is encountered, in which case they become complex.

When $N_2 < 0$

$$\lambda_1(\pm\ 1/\sqrt{d}) = 0 \tag{B.8a}$$

and

$$\lambda_2(\pm\ 1/\sqrt{d}) = (-N_2/bd^2)^{\frac{1}{2}} \tag{B.8b}$$

which is a real quantity. The existence of at least one real branch point on the positive real axis is necessary if the inequality $N_2 < 0$ is to hold. For any values of θ in the interval $1/\sqrt{d} \leq |Re\theta| \leq \theta_{01}$, both $\lambda_1(\theta)$ and $\lambda_2(\theta)$ are real. For larger values they become complex. In Fig. B.5 the graphical representation of the real values of $\lambda_1(\theta)$ and $\lambda_2(\theta)$ is shown for real values of θ in the indicated intervals.

TABLE B.1

THE ROOTS OF THE POLYNOMIAL Q (θ)

Conditions of Elastic Parameters			Type of Roots	Case of Cut Complex Plane
$N_1 > 0$			Four complex (in two conjugate pairs)	I
$N_1 < 0$	$K_2 < 0$		Two real + two imaginary	II
	$K_2 > 0$	$M < 0$	Four imaginary	III
		$M > 0$	Four real	IV

<u>Note 1.</u> The roots of Q (θ) are given by the values

$$\theta = \pm \ \Theta_{01} = \pm \left[\frac{M - \sqrt{-4bdc^2N_1}}{K_1K_2} \right]^{1/2}$$

$$\theta = \pm \ \Theta_{02} = \pm \left[\frac{M + \sqrt{-4bdc^2N_1}}{K_1K_2} \right]^{1/2}$$

Θ_{01} represent the real values in case II, the largest in absolute value of the imaginary part in case III, and the smaller in absolute value in case IV.

<u>Note 2.</u> It can be shown that for real roots

$$\frac{1}{d} \leq \ \Theta_{01}^2 \ < \Theta_{02}^2$$
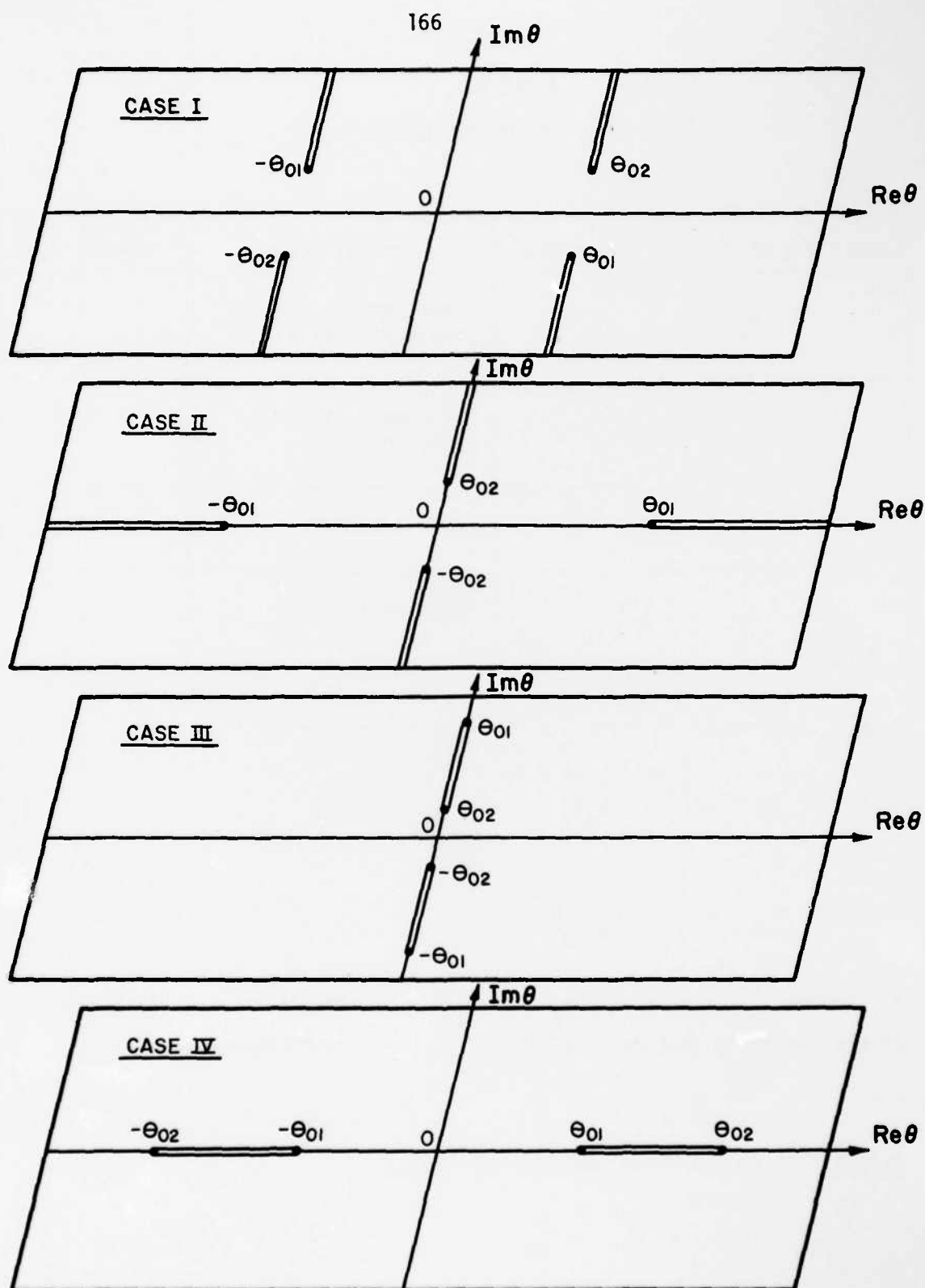
FIG. B.1 THE BRANCH CUTS OF $[Q(\theta)]^{1/2}$
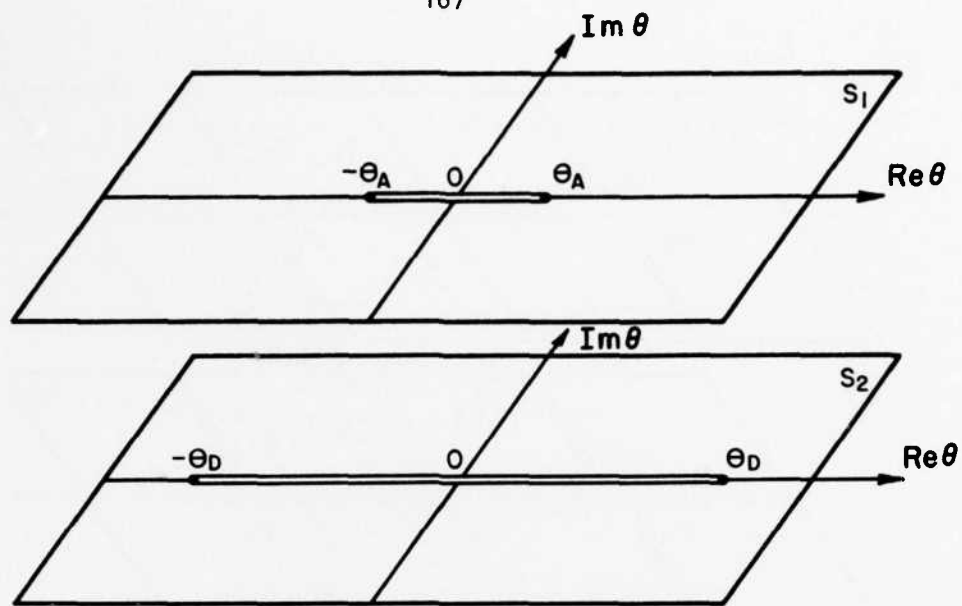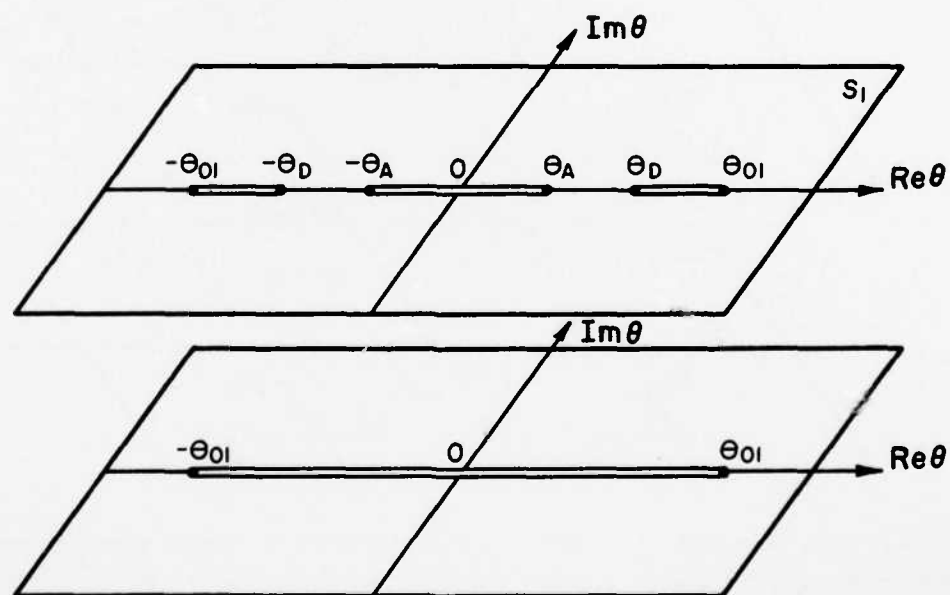
FIG. B.2   THE BRANCH POINTS Θ_A AND Θ_D, AND THE CORRESPONDING BRANCH CUTS

168
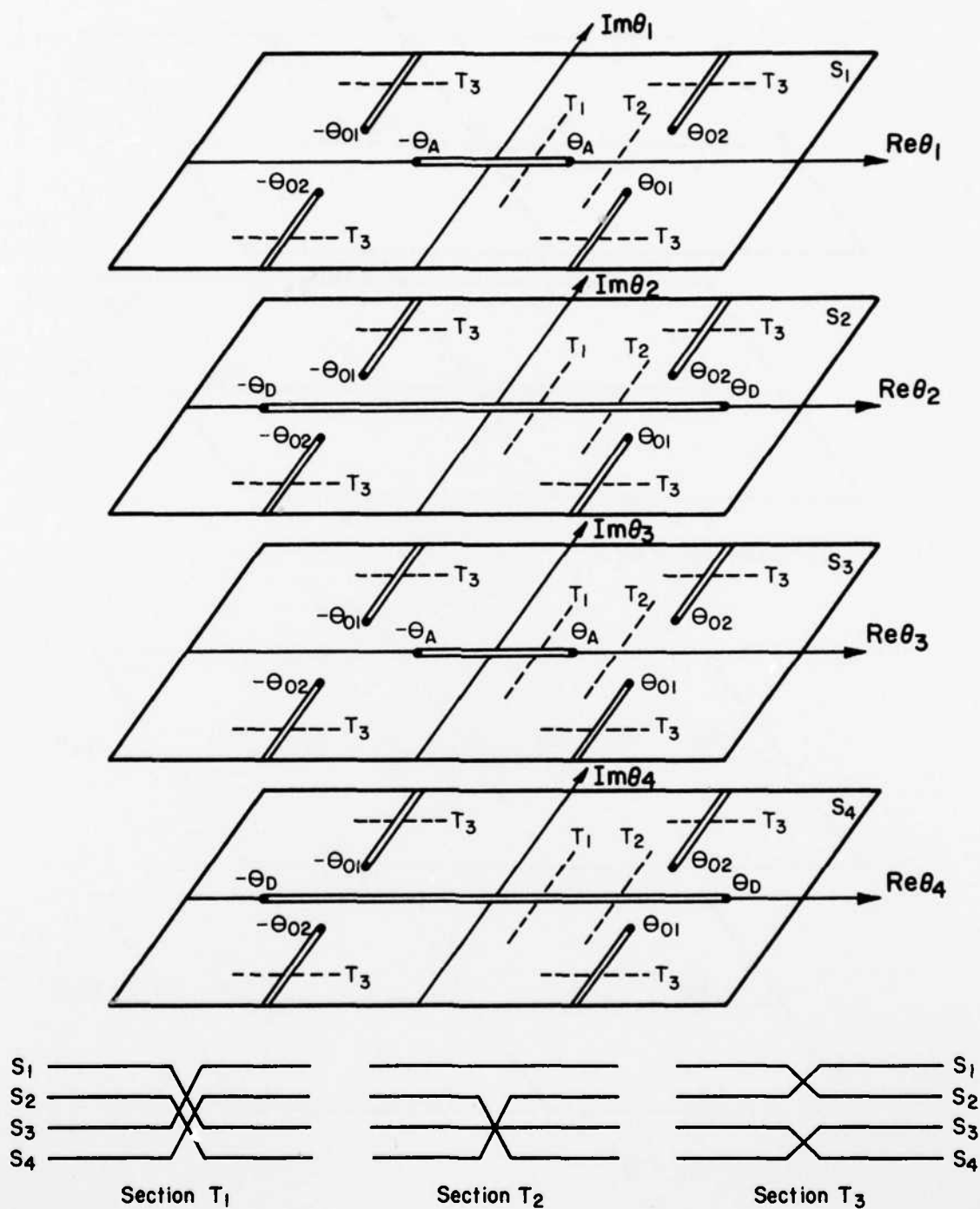
FIG. B.3   THE COMPLETE TYPE I RIEMANN SURFACE (SECTIONS T_1, T_2, AND T_3 INDICATE THE INTERCONNECTION OF THE FOUR SHEETS)
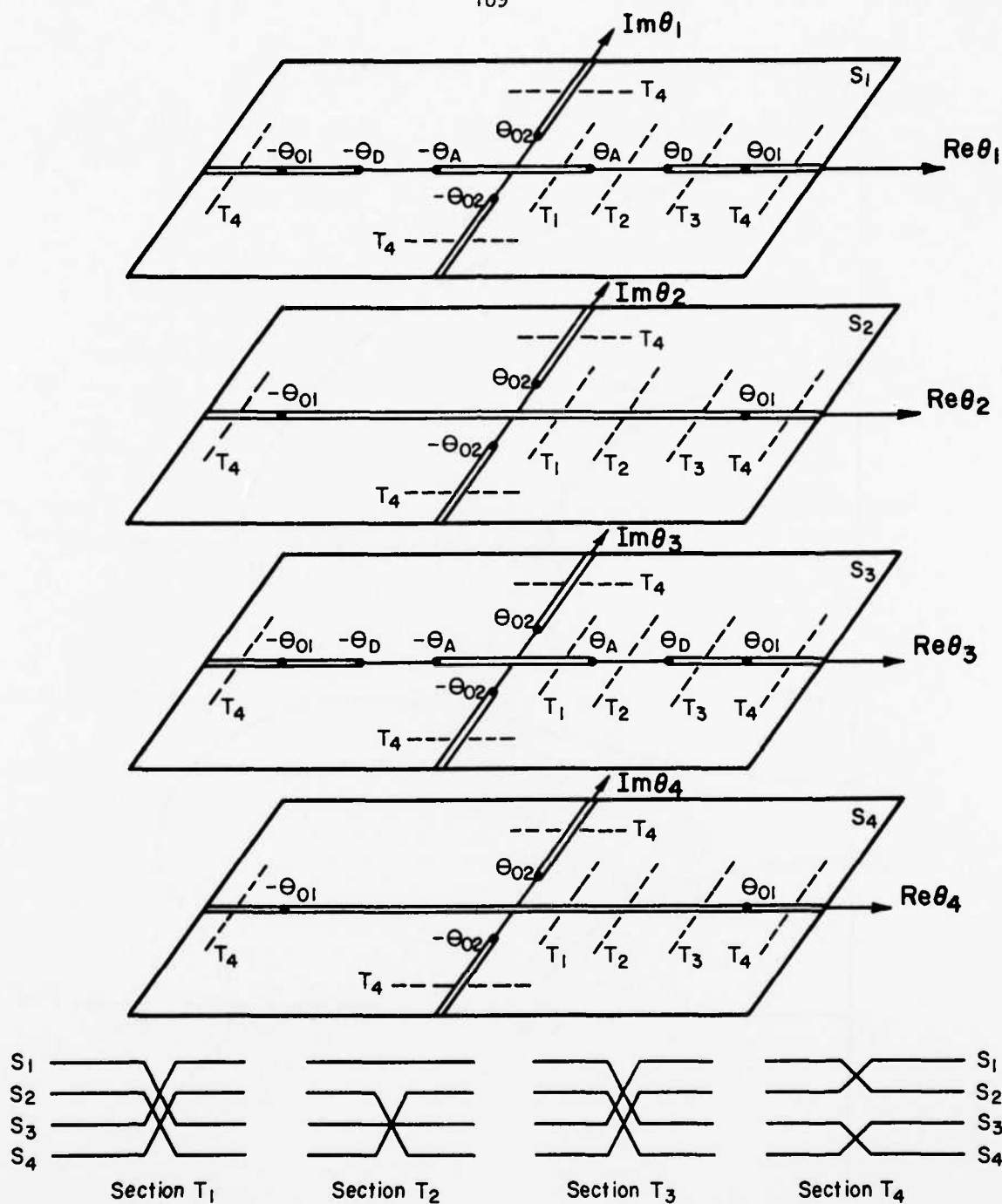
FIG. B.4 THE COMPLETE TYPE II RIEMANN SURFACE FOR $N_2 < 0$ (SECTIONS T_1, T_2, T_3, AND T_4 INDICATE THE INTERCONNECTION OF THE FOUR SHEETS)
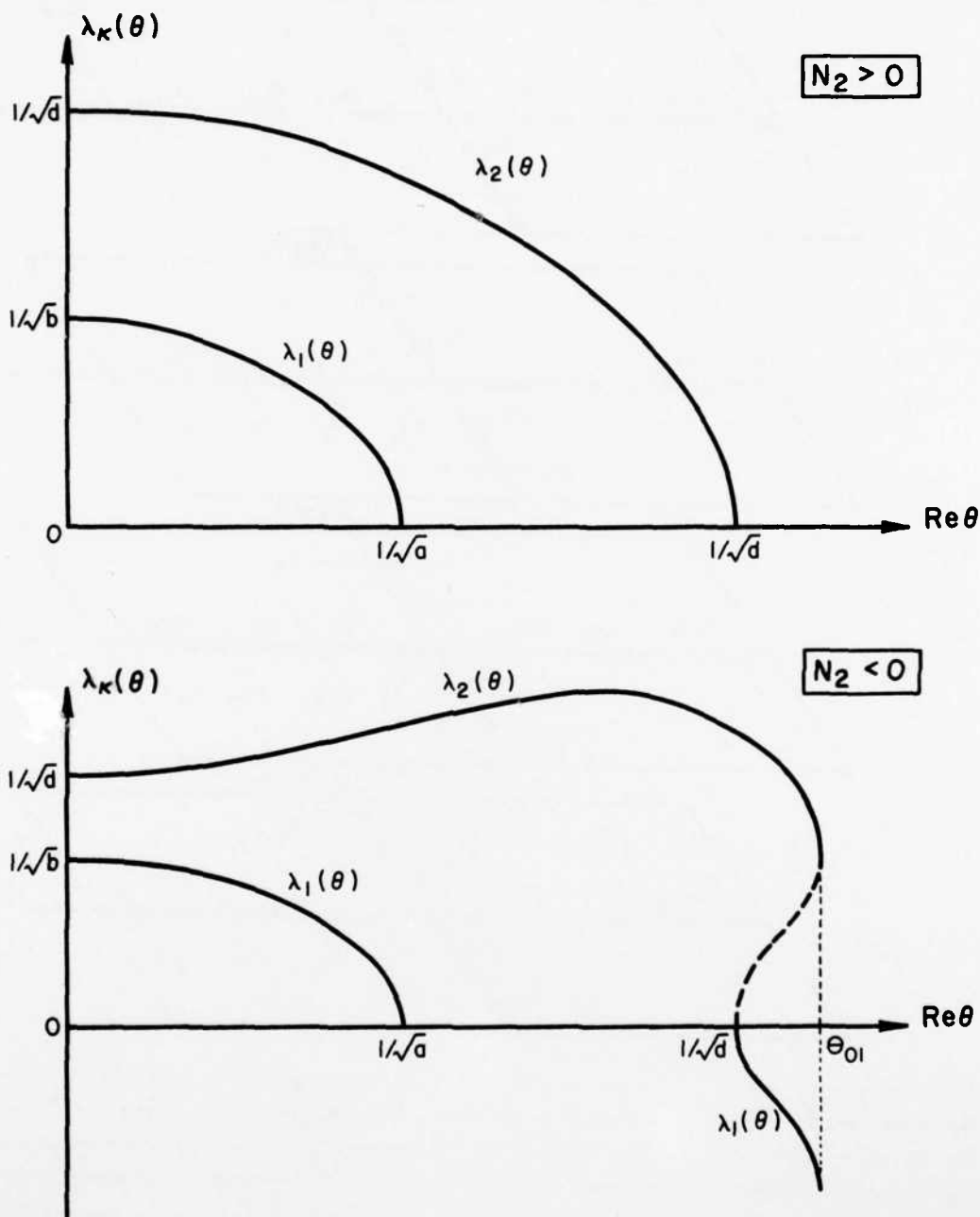
FIG. B.5   SCHEMATIC REPRESENTATION OF THE REAL VALUES OF FUNCTION
$\lambda_\kappa(\theta)$ FOR REAL VALUES OF θ

APPENDIX C

THE PARAMETRIC EXAMINATION OF THE GEOMETRY OF THE
QUASI-TRANSVERSE WAVE FRONT

The quasi-transverse wave front is parametrized by real values of θ_κ in the following intervals

a) $N_2 > 0$ $\qquad$ $-1/\sqrt{d} \leq \theta_2 \leq 1/\sqrt{d}$ $\qquad\qquad$ (C.1a)

b) $N_2 < 0$ $\qquad$ $-\Theta_{01} \leq \theta_2 \leq \Theta_{01}$

$$1/\sqrt{d} \leq |\theta_1| \leq \Theta_{01}$$

(C.1b)

where θ_2 represents values on the S_2 sheet and θ_1 values on the S_1 sheet of the Riemann surface. The two cases will be examined separately and only for the positive values of θ_κ.

C.1 The Condition $N_2 > 0$

It can be seen that

$$\phi_2(0) = 2b > 0$$

(C.2)

$$\phi_2(1/\sqrt{d}) = \frac{2bd(a-d)}{N_2} > 0$$

while from Eqs. (4.12)

$$\phi_2'(\theta_2) < 0 \qquad \text{for} \qquad N_1 > 0$$

(C.3)

$$\phi_2'(\theta_2) > 0 \qquad \text{for} \qquad N_1 < 0$$

As a result $\phi_2(\theta_2)$ is positive throughout the interval $(0, 1/\sqrt{d})$ and thus, α_2 increases monotonically in the interval $(0, \pi/2)$. It can be seen also that

$$\tan\beta_2(\theta_2 = 0) = -\lambda_2'(0) = 0$$

$$\tan\beta_2(\theta_2 = 1/\sqrt{d}) = -\lambda_2'(1/\sqrt{d}) = \infty$$

i.e. β_2 varies continuously in the interval $(0, \pi/2)$. Since $\lambda_2(\theta_2)$ varies monotonically in the specified interval, the behavior of β_2 depends directly on the function $\psi_2(\theta_2)$ which at the ends of the interval $(0, 1/\sqrt{d})$ assumes the values

$$\psi_2(0) = -\frac{2bN_3}{b-d}$$

$$\psi_2(1/\sqrt{d}) = -\frac{2bd^2(a-d)}{N_2} < 0 \tag{C.4}$$

while for every value of θ_2 in the same interval

$$\psi_2'(\theta_2) = \frac{8bdc^2N_1\theta_2}{[Q^3(\theta_2)]^{\frac{1}{2}}} \tag{C.5}$$

It can be seen from Eqs. (C.4) and (C.5) that for $N_1 > 0$ or $N_1 < 0$ and $N_3 > 0$ the function $\psi_2(\theta_2)$ remains negative throughout the interval while for $N_1 < 0$, $N_3 < 0$ changes from positive to negative at

$$\theta_\psi = \left[\frac{M-L \sqrt{-c^2N_1/ad}}{K_1K_2}\right]^{\frac{1}{2}} \tag{C.6}$$

Using the equations of section 4.2 the following values can be found.

$$D_2(0) = -\frac{4b^2 N_3}{b-d}$$

$$D_2(1/\sqrt{d}) = -\frac{1}{d}\left[\psi_2(1/\sqrt{d})\right]^2 < 0$$

$$D_2'(0) = 0 \tag{C.7}$$

$$D_2'(1/\sqrt{d}) = 0$$

Let

$$F(\theta) = (b-d)^2 - K_1 K_2 \theta^4 \tag{C.8}$$

which becomes zero at

$$\theta_F = (b-d)^{\frac{1}{2}} / (K_1 K_2)^{\frac{1}{4}} \tag{C.9}$$

For $\theta = 1/\sqrt{d}$ the function $F(\theta)$ becomes the quantity N_4 (see Eq. (2.10)).

Let first N_3 be positive. In this case $D_2(\theta_2)$ remains negative in the interval $(0, 1/\sqrt{d})$ provided one of the following three cases holds

a) $N_4 > 0$

b) $N_1 < 0$ and $N_4 < 0$ $\qquad$ (C.10)

c) $N_1 > 0$ and $D_2(\theta_F) \equiv N_5 < 0$

As a result, the angle β_2 increases monotonically in the interval $(0, \pi/2)$ and the quasi-transverse wave front is a strictly convex curve.

If conditions $N_1 > 0$ and $N_5 > 0$ are satisfied, then $D_2(\theta_2)$ has two roots in the interval $(0, 1/\sqrt{d})$ denoted by θ^{1*} and θ^{2*}. The values of these roots can be conveniently evaluated by using a numerical solution.

It is not difficult to see then that, if $\theta^{1*} < \theta^{2*}$ the function $D_2(\theta_2)$ is negative in the interval $(0, \theta^{1*})$, positive in the interval $(\theta^{1*}, \theta^{2*})$ and negative in the interval $(\theta^{2*}, 1/\sqrt{d})$. Therefore, the angle β_2 increases monotonically from 0 to β^{1*} (i.e. the value of β_2 which corresponds to θ^{1*}), decreases monotonically from β^{1*} to β^{2*} and increases monotonically from β^{2*} to $\pi/2$. The quasi-transverse wave front in this case possesses cusps in each quarter plane.

Consider now $N_3 < 0$ which implies $N_1 < 0$. In such a case $D_2(\theta_2)$ changes from positive to negative values at a point θ^* which is the root of $D_2(\theta_2)$ in the specified interval. The angle β_2 decreases monotonically from 0 to a negative value $-\beta^*$ corresponding to θ^* and then increases monotonically from $-\beta^*$ to $\pi/2$. It becomes zero for a value $\theta^{**} = \theta_\psi$ (Eq. C.6) which is the root of function $\psi_2(\theta_2)$. Thus, the quasi-transverse wave front has cusps located adjacent to the η-axis.

C.2 The Condition $N_2 < 0$

The functions will be examined in the interval $(0, \Theta_{01})$ of the S_2 sheet and $(\Theta_{01}, 1/\sqrt{d})$ of the S_1 sheet. The index of each function indicates the appropriate sheet with the corresponding interval. It can be seen that

$$\phi_1(1/\sqrt{d}) = \frac{2bd(a-d)}{N_2} < 0$$

$$\phi_1(\Theta_{01}) = -\infty$$

$$\phi_2(0) = 2b > 0 \tag{C.11}$$

$$\phi_2(\Theta_{01}) = +\infty$$

while

$$\phi_1' (\theta_1) < 0$$

and

$$\phi_2' (\theta_2) > 0$$

Therefore, α_2 increases monotonically from 0 to $\pi/2$ for a continuous change of θ_κ from 0 to θ_{01} on S_2 sheet and from θ_{01} to $1/\sqrt{d}$ on S_1 sheet.

Consider the following quantities

$$\psi_2 (0) = - \frac{2bN_3}{b-d}$$

$$\psi_2 (\theta_{01}) = - \infty$$

$$\psi_1 (1/\sqrt{d}) = - \frac{2bd^2(a-d)}{N_2} > 0 \tag{C.12}$$

$$\psi_1 (\theta_{01}) = \infty$$

while

$$\psi_2'(\theta_2) < 0 \quad \text{and} \quad \psi_1'(\theta_1) > 0$$

In addition

$$D_2(0) = - \frac{4b^2 N_3}{b-d}$$

$$D_2(\theta_{01}) = - \infty$$

$$D_1(\theta_{01}) = + \infty \tag{C.13}$$

$$D_1 (1/\sqrt{d}) = - \frac{1}{d} [\psi (1/\sqrt{d})]^2 < 0$$

while

$$D_2'(\theta_2) < 0 \qquad \text{and} \qquad D_1'(\theta_1) > 0$$

Let $N_3 > 0$. Then functions $\psi_2(\theta_2)$ and $D_2(\theta_2)$ are negative, $\psi_1(\theta_1)$ is positive and $D_1(\theta_1)$ changes from positive to negative at a root $\tilde{\theta}^*$. The angle β_2 increases monotonically from 0 to $\pi/2$, continues to increase monotonically from $\pi/2$ to $\tilde{\beta}^*$ corresponding to the value $\tilde{\theta}^*$ and then decreases monotonically from that value to $\pi/2$. The quasi-transverse wave front has cusps adjacent to the ξ-axis.

When $N_3 < 0$ the behavior of $\psi_1(\theta_1)$ and $D_1(\theta_1)$ is not altered. However, $\psi_2(\theta_2)$ and $D_2(\theta_2)$ change from positive to negative values at the root $\tilde{\theta}^{2*} = \theta_\psi$ (see Eq. (C.6)) for $\psi_2(\theta_2)$ and at $\tilde{\theta}^{1*}$ for $D_2(\theta_2)$. As a result the angle β_2 decreases monotonically from 0 to a negative value $-\tilde{\beta}^{1*}$ (corresponding to $\tilde{\theta}^{1*}$), increases monotonically from $-\tilde{\beta}^{1*}$ to $\tilde{\beta}^{3*}$ ($> \frac{\pi}{2}$) passing through $\beta_2 = 0$ at $\tilde{\theta}^{2*}$ and $\beta_2 = \frac{\pi}{2}$ at θ_{01}, and then decreases monotonically from $\tilde{\beta}^{3*}$ (corresponding to $\tilde{\theta}^*$) to a value of $\pi/2$ at $\theta_1 = 1/\sqrt{d}$. The quasi-transverse wave front possesses cusps adjacent to both ξ and η axis. A summary of this investigation is given in Table 1.

APPENDIX D

NUMERICAL TECHNIQUES

D.1 The Square Root of $Q(\theta_\kappa)$

The polynomial $Q(\theta_\kappa)$ given in Eq. (2.20) can be written in the form

$$Q(\theta_\kappa) = K_1 K_2 (\theta_\kappa - \theta_{01})(\theta_\kappa + \theta_{01})(\theta_\kappa - \theta_{02})(\theta_\kappa + \theta_{02}) \tag{D.1}$$

where $\pm\,\theta_{01}$ and $\pm\,\theta_{02}$ are its four roots. Let

$$\theta_\kappa - \theta_{01} = r_{11}\, e^{i\phi_{11}}$$

$$\theta_\kappa + \theta_{01} = r_{12}\, e^{i\phi_{12}}$$

$$\tag{D.2}$$

$$\theta_\kappa - \theta_{02} = r_{21}\, e^{i\phi_{21}}$$

$$\theta_\kappa + \theta_{02} = r_{22}\, e^{i\phi_{22}}$$

The square root of $Q(\theta)$ is then given by the expression

$$q(\theta_\kappa) = [Q(\theta_\kappa)]^{1/2} = \pm\sqrt{K_1 K_2}\,(\theta_\kappa - \theta_{01})^{1/2}(\theta_\kappa + \theta_{01})^{1/2}\,\times$$

$$\times\,(\theta_\kappa - \theta_{02})^{1/2}(\theta_\kappa + \theta_{02})^{1/2} = \pm\sqrt{K_1 K_2}\,r_q\, e^{i\phi_q} \tag{D.3}$$

where

$$r_q = [r_{11} \cdot r_{12} \cdot r_{21} \cdot r_{22}]^{1/2}$$

and

$$\phi_q = \frac{\phi_{11} + \phi_{12} + \phi_{21} + \phi_{22}}{2} \qquad (D.4)$$

The range of the arguments ϕ_{11}, ϕ_{12}, ϕ_{21}, ϕ_{22}, depends on the relative position of the roots $\pm\Theta_{01}$ and $\pm\Theta_{02}$ and is different for each of the four types of Riemann surface. The sign in Eq. (D.3) is fixed for each case in such a manner as to yield a positive value of $q(\theta_K)$ for $\theta_K = 0$. Figure D.1 shows the polar rays and arguments to determine $q(\theta_K)$ on a complex plane with the branch cuts of a Type II Riemann surface. Note that in this particular case $K_2 < 0$, therefore, $\sqrt{K_1 K_2} = i \sqrt{|K_1 K_2|}$. In accordance with the previously mentioned condition, Eq. (D.3) must be chosen with the minus sign.

D.2 The Square Root of $\lambda_K(\theta_K)$

For every value of the variable θ_K, the quantity

$$\Lambda_K(\theta_K) = \frac{b + d - L\theta_K^2 + (-1)^K q(\theta_K)}{2bd} \qquad (D.5)$$

assumes values in a complex domain S_{Λ_K}. The function $q(\theta_K)$ is given in Appendix D.1. The complex domain S_{Λ_K} has a branch cut along the real Λ_K axis from point 0 to infinity. It is convenient to choose this branch cut in such a way that for all values of θ_K in the upper half S_K sheet (i.e. $\text{Im}\theta_K \geq 0$) the values of $\Lambda_K(\theta_K)$ lie on a single sheet of the S_{Λ_K} domain. It turns out that for certain cases the branch cut may most conveniently be taken along the positive real Λ_K axis while in the

remaining cases it is to be taken along the negative real Λ_κ axis of the domain S_{Λ_κ}. Once this choice has been made appropriately, the evaluation of the function

$$\lambda_\kappa(\theta_\kappa) = \sqrt{\Lambda_\kappa(\theta_\kappa)} \tag{D.6}$$

is a simple matter. The sign in Eq. (D.6) has been fixed from the mapping procedure which is presented in Chapter 4.

D.3 The Evaluation of θ_κ near the Wave Fronts

In section 5.2.2 it has been shown that for points near the wave fronts the rate of change of θ_κ with time is very large. The increased curvature of the surface that is formed from the values of the right hand side of Eq. (5.1) in this range of values of θ_κ calls for a more accurate evaluation of the predicted value in the predictor-corrector iterative method than the one obtained from the utilization of the trapezoidal rule. This is achieved by using an integration formula which is obtained as follows.

From the discussion of section 5.2.2 it can be written that

$$\theta_\kappa - \theta_\kappa 0 \cong \sqrt{t-t_0} \tag{D.7}$$

Using this equation as well as Eq. (5.3) the differential equation given in Eq. (5.1) can be expressed approximately as

$$\frac{\partial \theta_\kappa}{\partial t} \cong \frac{1}{\sqrt{t-t_0}} [A(\theta_\kappa)+(t-t_0) B(\theta_\kappa)] \tag{D.8}$$

The result of the integration of Eq. (D.8) between $t_m = t_0 + m \, \Delta t$ and $t_{m+1} = t_0 + (m+1) \Delta t$ is written by the integration formula [33, Appendix A]

$$\Delta\theta_\kappa = \sqrt{\Delta t} \left(g_m \left[2(1+m) \left[(m+1)^{1/2} - m^{1/2} \right] - \frac{2}{3} \left[(m+1)^{3/2} - m^{3/2} \right] \right] + \right.$$
$$\left. + g_{m+1} \left[\frac{2}{3} \left[(m+1)^{3/2} - m^{3/2} \right] - 2m \left[(m+1)^{1/2} - m^{1/2} \right] \right] \right) \qquad (D.9)$$

Here, m is an integer and

$$g_m = \sqrt{t_m - t_0} \; \lambda'_\kappa (\theta_\kappa) \cong A(\theta_\kappa) + B(\theta_\kappa) \; (t_m - t_0)$$

$$g_{m+1} = A(\theta_\kappa) + B(\theta_\kappa) \; (t_{m+1} - t_0) \qquad (D.10)$$

where θ_κ is the known value at time t_m.

The procedure to be followed in applying the predictor-corrector method in its modified form is now briefly explained. Let the known value of θ_κ at time t_m be written as $\theta_{\kappa, \, m}$. A first approximation at time t_{m+1} is given by

$$\theta^1_{\kappa, \, m+1} = \theta_{\kappa, \, m} + \Delta\theta^1_{\kappa, \, m} \qquad (D.11)$$

where $\Delta\theta^1_{\kappa, \, m}$ is obtained from Eq. (D.9) and g^1_m, g^1_{m+1} are given by Eq. (D.10). Subsequent iterations yield

$$\theta^n_{\kappa, m+1} = \theta_{\kappa, m} + \Delta\theta^n_{\kappa, m} \qquad (D.12)$$

where $\Delta\theta^n_{\kappa, \, m}$ is evaluated from the integration formula given in Eq. (D.9) and

$$g^n_m = \sqrt{t_m - t_0} \; \delta'_\kappa \; (\theta_{\kappa, m}) = g^1_m$$

$$g^n_{m+1} = \sqrt{t_{m+1} - t_0} \; \delta'_\kappa \; (\theta^{n-1}_{\kappa, \, m+1}) \qquad (D.13)$$

09476
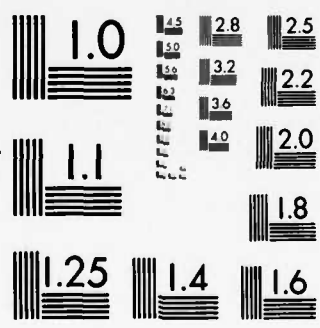
MICROCOPY RESOLUTION TEST CHART
NATIONAL BUREAU OF STANDARDS-1963-A

At m=0 the procedure requires special attention. It can be shown that

$$g_0 = A(\theta_{\kappa 0}) = - \frac{i}{\sqrt{2\delta_\kappa''(\theta_{\kappa 0})}} \qquad (D.14)$$

A first approximation of the value of θ_κ at t_1 can be obtained by integrating Eq. (5.1) written as

$$\frac{\partial \theta_\kappa}{\partial t} = \frac{A(\theta_{\kappa 0})}{\sqrt{t-t_0}} \qquad (D.15)$$

between t_0 and t_1, i.e.

$$\theta_{\kappa,1}^1 = \theta_{\kappa 0} + \Delta\theta_{\kappa,0}^1 \qquad (D.16)$$

where

$$\Delta\theta_{\kappa,\,0}^1 = 2\sqrt{t_1-t_0}\, A\,(\theta_{\kappa 0}) \qquad (D.17)$$

The second of Eq. (D.13) can now be used to obtain g_{m+1}^2 which when substituted in Eq. (D.9) together with the value from Eq. (D.14) yields a new value of $\Delta\theta_\kappa$, and so on.

The advantage of this numerical technique lies on the fact that it produces a very good first approximation resulting in   very fast convergence.

D.4 Integration Formulas for Points Near the Ends of the Contours C_κ

Three integration formulas will be given. Which of these should be applied depends on whether the point under consideration lies on a wave front or not and on the nature of the singularity caused by the expression $G_\kappa(\theta_\kappa)$. These are cases in which a standard numerical integration technique, such as Simpson's rule, cannot be directly applied.

D.4.1 First Integration Formula

Consider the integrands of Eq. (3.36) which contain the function $G_\kappa(\theta_\kappa)$ in the denominator. Assume also that the end values of the contour C_κ do not represent points on the wave fronts. Then, these integrands at values of θ_κ very close to the ends of the contour C_κ can be approximated by expressions of the form

$$F(\theta_\kappa) = \frac{A_n + B_n(\theta_\kappa - \theta_\kappa^n)}{\sqrt{\theta_\kappa - \theta_{\kappa 0}}} = \frac{\tilde{F}(\theta_\kappa^n)}{\sqrt{\theta_\kappa - \theta_{\kappa 0}}} \tag{D.18}$$

where $\theta_{\kappa 0}$ represents the end of the contour and θ_κ^n the beginning of the integration interval. The constants A_n and B_n are to be determined. The contribution of the integral between values θ_κ^n and θ_κ^{n+1} can now be written

$$
\begin{aligned}
I_1 &= \int_{\theta_\kappa^n}^{\theta_\kappa^{n+1}} \frac{A_n + B_n(\theta_\kappa - \theta_\kappa^n)}{\sqrt{\theta_\kappa - \theta_{\kappa 0}}}\, d\theta_\kappa = \\
&= 2\left[A_n - \frac{B_n}{3}\left[2(\theta_\kappa^n - \theta_{\kappa 0}) - h\right]\right]\sqrt{\theta_\kappa^{n+1} - \theta_{\kappa 0}} - \\
&\quad - 2\left[A_n - \frac{2B_n}{3}(\theta_\kappa^n - \theta_{\kappa 0})\right]\sqrt{\theta_\kappa^n - \theta_{\kappa 0}}
\end{aligned}
\tag{D.19}
$$

where $\quad h = \theta_\kappa^{n+1} - \theta_\kappa^n$

The quantities A_n and B_n can be defined for each interval of integration from the relations

$$A_n = \tilde{F}(\theta_\kappa^n)$$

$$B_n = \frac{1}{h}\left[\tilde{F}(\theta_\kappa^{n+1}) - \tilde{F}(\theta_\kappa^n)\right] \tag{D.20}$$

D.4.2 Second Integration Formula

This formula is used with the integrand expressions that contain the function $G_\kappa(\theta_\kappa)$ in the numerator. It is applicable for points not on the wave fronts. In this case the integrand is approximated by the expression

$$F(\theta_\kappa) = [A_n + B_n(\theta_\kappa - \theta_\kappa^n)] \sqrt{\theta_\kappa - \theta_{\kappa 0}} = \tilde{F}(\theta_\kappa) \sqrt{\theta_\kappa - \theta_{\kappa 0}} \tag{D.21}$$

and the contribution of the integral between θ_κ^n and θ_κ^{n+1} is given by

$$I_2 = \int_{\theta_\kappa^n}^{\theta_\kappa^{n+1}} [A_n + B_n(\theta_\kappa - \theta_\kappa^n)] \sqrt{\theta_\kappa - \theta_{\kappa 0}} \, d\theta_\kappa =$$

$$= \frac{2}{3} [A_n - (\theta_\kappa^n - \theta_{\kappa 0})B_n] [(\theta_\kappa^{n+1} - \theta_{\kappa 0})^{3/2} - (\theta_\kappa^n - \theta_{\kappa 0})^{3/2}] +$$

$$+ \frac{2B_n}{5} [(\theta_\kappa^{n+1} - \theta_{\kappa 0})^{5/2} - (\theta_\kappa^n - \theta_{\kappa 0})^{5/2}] \tag{D.22}$$

Here, the constants A_n and B_n can be determined by Eq. (D.20) for each interval of integration.

D.4.3 Third Integration Formula

This is a variation of the first integration formula for points on the wave fronts. In such a case the function $G_\kappa(\theta_\kappa)$ is expressed as in Eq. (5.9). The same integrands that were given by Eq. (D.18) can now be written as

$$F(\theta_\kappa) = \frac{A_n + B_n(\theta_\kappa - \theta_\kappa^n)}{\theta_\kappa - \theta_{\kappa 0}} = \frac{\tilde{F}(\theta_\kappa)}{\theta_\kappa - \theta_{\kappa 0}} \tag{D.23}$$

The result of the integration between θ_κ^n and θ_κ^{n+1} is

$$I_3 = \int_{\theta_\kappa^n}^{\theta_\kappa^{n+1}} \frac{A_n + B_n(\theta_\kappa - \theta_\kappa^n)}{\theta_\kappa - \theta_{\kappa 0}} \, d\theta_\kappa =$$

184

$$= [A_n - B_n(\theta_\kappa^n - \theta_{\kappa 0})] [\log(\theta_\kappa^{n+1} - \theta_{\kappa 0}) - \log(\theta_\kappa^n - \theta_{\kappa 0})] + B_n h \qquad (D.24)$$

where $h = \theta_\kappa^{n+1} - \theta_\kappa$, and A_n, B_n are determined by Eq. (D.20).

$$0 \leq \phi_{11} < 2\pi$$

$$-\pi < \phi_{12} \leq \pi$$

$$-\frac{3\pi}{2} < \phi_{21} \leq \frac{3\pi}{2}$$

$$-\frac{\pi}{2} \leq \phi_{22} < \frac{3\pi}{2}$$
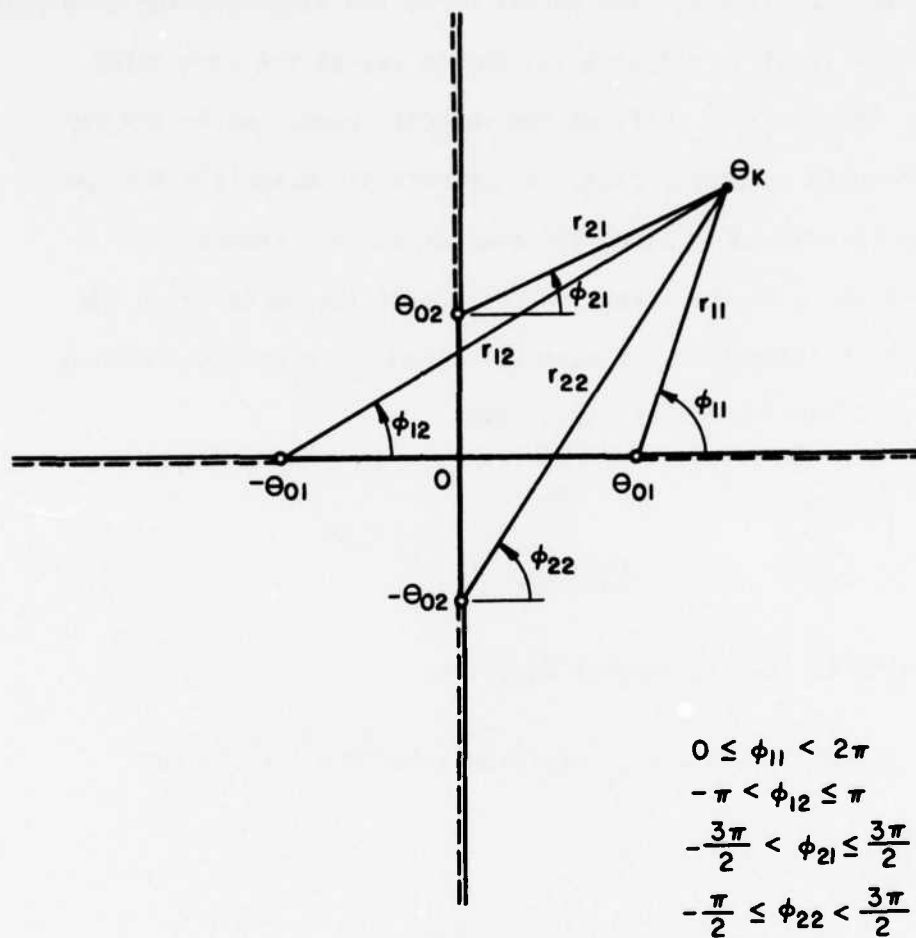
FIG. D.1   THE ARGUMENTS FOR THE DEFINITION OF $q = [Q(\theta_K)]^{1/2}$
ON THE TYPE II RIEMANN SURFACE

APPENDIX E

THE VELOCITIES OF THE WAVES

In anisotropic media the normal $\bar{n}_\kappa$ to the tangent plane at a point P of the wave front is not parallel to the ray at the same point (Fig. 2). The normal $\bar{n}_\kappa$ defines the velocity vector while the ray defines the path of energy flux. In orthotropic materials the two directions coincide only along the axes of elastic symmetry.

Let ℓ and m be the direction cosines of the vector $\bar{n}_\kappa$. The equation which determines the wave velocities υ_κ associated with $\bar{n}_\kappa$ is given from the determinant [21, §208]

$$\begin{vmatrix} a\ell^2+dm^2-\upsilon_\kappa^2 & c\ell m \\ c\ell m & d\ell^2+bm^2-\upsilon_\kappa^2 \end{vmatrix} = 0 \qquad (E.1)$$

which results in the biquadratic equation

$$\upsilon_\kappa^4 - [(a+d)\ell^2+(b+d)m^2] \, \upsilon_\kappa^2 + (a\ell^2+dm^2)(d\ell^2+bm^2)-c^2\ell^2 m^2 = 0 \qquad (E.2)$$

The solution can be written as

$$\upsilon_\kappa^2 = \frac{1}{\theta_\kappa^2 + \lambda_\kappa^2(\theta_\kappa)} \qquad (\kappa=1,2) \qquad (E.3)$$

Every point P of the wave fronts is uniquely determined by a real value of the parameter θ_κ. By Eq. (E.3) this value determines the magnitude of the velocity of propagation of the corresponding wave in the direction specified by $\bar{n}_\kappa$.

In transversely isotropic media the velocities associated with the

vector $\bar{N}$ which has direction cosines ℓ, m and n are given by the determinant

$$\begin{vmatrix} \gamma_{11} - \upsilon^2 & \gamma_{12} & \gamma_{13} \\ \gamma_{12} & \gamma_{22} - \upsilon^2 & \gamma_{23} \\ \gamma_{13} & \gamma_{23} & \gamma_{33} - \upsilon^2 \end{vmatrix} = 0 \qquad (E.4)$$

where

$$\gamma_{11} = a\ell^2 + dm^2 + en^2$$

$$\gamma_{22} = bm^2 + d(\ell^2 + n^2)$$

$$\gamma_{33} = e\ell^2 + dm^2 + an^2$$

$$\gamma_{12} = c\ell m \qquad\qquad (E.5)$$

$$\gamma_{13} = (a-e)\,\ell n$$

$$\gamma_{23} = cmn$$

When the vector $\bar{N}$ lies in the (x, y) plane (i.e. $n = 0$), Eq. (E.5) is equivalent to Eq. (E.3) which gives the velocities of the quasi-longitudinal and quasi-transverse wave, and to the equation

$$\upsilon_3^2 = e\ell^2 + dm^2 \qquad (E.6)$$

which determines the velocity of the third wave.

APPENDIX F

SPECIAL RELATIONS

In the development of the solutions of the present study, the algebraic work may be reduced by the observation that certain functions can be written in equivalent forms which are more convenient to manipulate. Some of these relations are given here:

$$\lambda_1^2(\theta) + \lambda_2^2(\theta) = (b+d-L\theta^2)/bd \tag{F.1}$$

$$\lambda_1^2(\theta) - \lambda_2^2(\theta) = -\sqrt{Q(\theta)}/bd \tag{F.2}$$

$$\lambda_1^2(\theta) \ \lambda_2^2(\theta) = (1-a\theta^2) \ (1-d\theta^2)/bd \tag{F.3}$$

$$[a\theta^2 + d\lambda_\kappa^2(\theta)-1] \ [a\theta^2+d\lambda_{3-\kappa}^2(\theta)-1] = c^2\theta^2(a\theta^2-1)/b \tag{F.4}$$

$$[a\theta^2 + d\lambda_\kappa^2(\theta)-1] \ [d\theta^2+b\lambda_\kappa^2(\theta)-1] = c^2\theta^2 \ \lambda_\kappa^2(\theta) \tag{F.5}$$

$$[d\lambda_\kappa^2(\theta)-1] \ [a\theta^2+d\lambda_{3-\kappa}^2(\theta)-1] = \theta^2[ad\{d\theta^2+b\lambda_\kappa^2(\theta)-1\}-c^2]/b \tag{F.6}$$

$$d[a\theta^2+b\lambda_\kappa^2(\theta)-1] \ [d\theta^2+b\lambda_\kappa^2(\theta)-1] =$$
$$= (b-d) \ (1-a\theta^2) \ [d\theta^2+b\lambda_\kappa^2(\theta)-1] + bc^2\theta^2\lambda_\kappa^2(\theta) \tag{F.7}$$

$$K_1K_2 = L^2 - 4abd^2 \tag{F.8}$$

$$L \ (b+d) - M = 2bd \ (a+d) \tag{F.9}$$

$$M^2+4bdc^2N_1 = (b-d)^2 \ K_1K_2 \tag{F.10}$$

$$L \ (b-d) + M = 2bN_3 \tag{F.11}$$

$$L \ (b-d) - M = 2d \ [d(b-d) + c^2] \tag{F.12}$$

The length of OP (Fig. 2) is given by the expression

$$(OP)_\kappa = \frac{[4b^2d^2\lambda_\kappa^2(\theta_\kappa)+\theta_\kappa^2\psi_\kappa^2(\theta_\kappa)]^{\frac{1}{2}}}{\phi_\kappa(\theta_\kappa)}$$

(F.13)

APPENDIX G

ISOTROPY AS A SPECIAL CASE

An anisotropic material of the class considered in this study which has elastic parameters satisfying the conditions

$$a=b$$

$$c=a-d \tag{G.1}$$

$$e=d$$

forms the special case of isotropy. Let λ and μ be the Lamé constants. Then, it is not difficult to see that

$$\lambda = \rho(a-2d)$$

$$\mu = \rho d \tag{G.2}$$

Whenever Eqs. (G.1) hold, the expressions of Chapters 2 and 3 yield the solutions to dynamic problems for an isotropic material with constants defined by Eq. (G.2). It is useful to give some of the expressions which were used to develop the anisotropic solutions in their simplified form for isotropy, i.e.

$$K_1 = 4d\,(a-d)$$

$$K_2 = M = N_1 = 0$$

$$N_2 = N_3 = d(a-d)$$

191

$$L = 2ad$$

$$Q\ (\theta) = (a-d)^2$$

$$\lambda_1(\theta) = (a^{-1} - \theta^2)^{\frac{1}{2}}$$

$$\lambda_2(\theta) = \lambda_3(\theta) = (d^{-1} - \theta^2)^{\frac{1}{2}}$$

$$\lambda_1^2(\theta) - \lambda_2^2(\theta) = -\frac{(a-d)}{ad}$$

$$a\theta^2 + d\lambda_1^2(\theta) - 1 = -(a-d)(a^{-1} - \theta^2)$$

$$d\theta^2 + b\lambda_1^2(\theta) - 1 = -(a-d)\theta^2$$

$$a\theta^2 + d\lambda_2^2(\theta) - 1 = (a-d)\theta^2$$

$$d\theta^2 + b\lambda_2^2(\theta) - 1 = (a-d)(d^{-1} - \theta^2)$$

$$[\lambda_1(\theta) - \lambda_2(\theta)]\ R(\theta) = d(a-d)\ (a^{-1} - \theta^2)^{\frac{1}{2}} R_I(\theta)$$

(G.3)

where

$$R_I(\theta) = (d^{-1} - 2\theta^2)^2 + 4\theta^2(a^{-1} - \theta^2)^{\frac{1}{2}} (d^{-1} - \theta^2)^{\frac{1}{2}}$$

is the Rayleigh function for isotropic media.

DISTRIBUTION LIST

for

UNCLASSIFIED TECHNICAL REPORTS

The ONR Structural Mechanics Contract Research Program

<u>This list consists of:</u>

Part 1 - Government Activities
Part 2 - Contractors and Other
             Technical Collaborators

Notes:

    Except as otherwise indicated, forward <u>one</u>
    copy of all Unclassified Technical Reports
    to each of the addressees listed herein.

    Where more than one attention addressee is
    indicated, the individual copies of the
    report should be mailed separately.

Part 1 - Government
Administrative and Liaison Activities

Office of Naval Research
Department of the Navy
Arlington, Virginia 22217
Attn: Code 474 (2)
        Code 471
        Code 200

Director
Office of Naval Research
  Eastern/Central Regional Office
666 Summer Street
Boston, Massachusetts 02210

Director
Office of Naval Research
  Branch Office
536 South Clark Street
Chicago, Illinois 60605

Director
Office of Naval Research
New York Area Office
715 Broadway - 5th Floor
New York, New York 10003

Director
Office of Naval Research
  Western Regional Office
1030 East Green Street
Pasadena, California 91106

Naval Research Laboratory (6)
Code 2627
Washington, D.C. 20375

Defense Technical Information Center (12)
Cameron Station
Alexandria, Virginia 22314

Navy

Undersea Explosion Research Division
Naval Ship Research and Development
  Center
Norfolk Naval Shipyard
Portsmouth, Virginia 23709
Attn: Dr. E. Palmer, Code 177

Navy (Con't.)

Naval Research Laboratory
Washington, D.C. 20375
Attn: Code 8400
             8410
             8430
             8440
             6300
             6390
             6380

David W. Taylor Naval Ship Research
  and Development Center
Annapolis, Maryland 21402
Attn: Code 2740
             28
             281

Naval Weapons Center
China Lake, California 93555
Attn: Code 4062
             4520

Commanding Officer
Naval Civil Engineering Laboratory
Code L31
Port Hueneme, California 93041

Naval Surface Weapons Center
White Oak
Silver Spring, Maryland 20910
Attn: Code R-10
             G-402
             K-82

Technical Director
Naval Ocean Systems Center
San Diego, California 92152

Supervisor of Shipbuilding
U.S. Navy
Newport News, Virginia 23607

Navy Underwater Sound
  Reference Division
Naval Research Laboratory
P.O. Box 8337
Orlando, Florida 32806

Chief of Naval Operations
Department of the Navy
Washington, D.C. 20350
Attn: Code OP-098

Navy (Con't.)

Strategic Systems Project Office
Department of the Navy
Washington, D.C. 20376
Attn: NSP-200

Naval Air Systems Command
Department of the Navy
Washington, D.C. 20361
Attn: Code 5302 (Aerospace and Structures)
             604 (Technical Library)
             320B (Structures)

Naval Air Development Center
Warminster, Pennsylvania 18974
Attn: Aerospace Mechanics
        Code 606

U.S. Naval Academy
Engineering Department
Annapolis, Maryland 21402

Naval Facilities Engineering Command
200 Stovall Street
Alexandria, Virginia 22332
Attn: Code 03 (Research and Development)
             04B
             045
           14114 (Technical Library)

Naval Sea Systems Command
Department of the Navy
Washington, D.C. 20362
Attn: Code 05H
             312
             322
             323
             05R
             32R

Navy (Con't.)

Commander and Director
David W. Taylor Naval Ship
  Research and Development Center
Bethesda, Maryland 20084
Attn: Code 042
             17
             172
             173
             174
             1800
             1844
             012.2
             1900
             1901
             1945
             1960
             1962

Naval Underwater Systems Center
Newport, Rhode Island 02840
Attn: Bruce Sandman, Code 3634

Naval Surface Weapons Center
Dahlgren Laboratory
Dahlgren, Virginia 22448
Attn: Code G04
             G20

Technical Director
Mare Island Naval Shipyard
Vallejo, California 94592

U.S. Naval Postgraduate School
Library
Code 0384
Monterey, California 93940

Webb Institute of Naval Architecture
Attn: Librarian
Crescent Beach Road, Glen Cove
Long Island, New York 11542

Army

Commanding Officer (2)
U.S. Army Research Office
P.O. Box 12211
Research Triangle Park, NC 27709
Attn: Mr. J. J. Murray, CRD-AA-IP

Army (Con't.)

Watervliet Arsenal
MAGGS Research Center
Watervliet, New York 12189
Attn: Director of Research

U.S. Army Materials and Mechanics
  Research Center
Watertown, Massachusetts 02172
Attn: Dr. R. Shea, DRXMR-T

 U.S. Army Missile Research and
   Development Center
Redstone Scientific Information
  Center
Chief, Document Section
Redstone Arsenal, Alabama 35809

Army Research and Development
  Center
Fort Belvoir, Virginia 22060

NASA

National Aeronautics and Space
  Administration
Structures Research Division
Langley Research Center
Langley Station
Hampton, Virginia 23365

National Aeronautics and Space
  Administration
Associate Administrator for Advanced
  Research and Technology
Washington, D.C. 20546

Air Force

Wright-Patterson Air Force Base
Dayton, Ohio 45433
Attn: AFFDL (FB)
            (FBR)
            (FBE)
            (FBS)
      AFML (MBM)

Chief Applied Mechanics Group
U.S. Air Force Institute of Technology
Wright-Patterson Air Force Base
Dayton, Ohio 45433

Air Force (Con't.)

Chief, Civil Engineering Branch
WLRC, Research Division
Air Force Weapons Laboratory
Kirtland Air Force Base
Albuquerque, New Mexico 87117

Air Force Office of Scientific Research
Bolling Air Force Base
Washington, D.C. 20332
Attn: Mechanics Division

Department of the Air Force
Air University Library
Maxwell Air Force Base
Montgomery, Alabama 36112

Other Government Activities

Commandant
Chief, Testing and Development Division
U.S. Coast Guard
1300 E Street, NW.
Washington, D.C. 20226

Technical Director
Marine Corps Development
  and Education Command
Quantico, Virginia 22134

Director Defense Research
 ' and Engineering
Technical Library
Room 3C128
The Pentagon
Washington, D.C. 20301

Dr. M. Gaus
National Science Foundation
Environmental Research Division
Washington, D.C. 20550

Library of Congress
Science and Technology Division
Washington, D.C. 20540

Director
Defense Nuclear Agency
Washington, D.C. 20305
Attn: SPSS

Other Government Activities (Con't)

Mr. Jerome Persh
Staff Specialist for Materials
  and Structures
OUSDR&E, The Pentagon
Room 3D1089
Washington, D.C. 20301

Chief, Airframe and Equipment Branch
FS-120
Office of Flight Standards
Federal Aviation Agency
Washington, D.C. 20553

National Academy of Sciences
National Research Council
Ship Hull Research Committee
2101 Constitution Avenue
Washington, D.C. 20418
Attn: Mr. A. R. Lytle

National Science Foundation
Engineering Mechanics Section
Division of Engineering
Washington, D.C. 20550

Picatinny Arsenal
Plastics Technical Evaluation Center
Attn: Technical Information Section
Dover, New Jersey 07801

Maritime Administration
Office of Maritime Technology
14th and Constitution Avenue, NW.
Washington, D.C. 20230

PART 2 - Contractors and Other Technical
        Collaborators

Universities

Dr. J. Tinsley Oden
University of Texas at Austin
345 Engineering Science Building
Austin, Texas 78712

Professor Julius Miklowitz
California Institute of Technology
Division of Engineering
  and Applied Sciences
Pasadena, California 91109

Universities (Con't)

Dr. Harold Liebowitz, Dean
School of Engineering and
  Applied Science
George Washington University
Washington, D.C. 20052

Professor Eli Sternberg
California Institute of Technology
Division of Engineering and
  Applied Sciences
Pasadena, California 91109

Professor Paul M. Naghdi
University of California
Department of Mechanical Engineering
Berkeley, California 94720

Professor A. J. Durelli
Oakland University
School of Engineering
Rochester, Missouri 48063

Professor F. L. DiMaggio
Columbia University
Department of Civil Engineering
New York, New York 10027

Professor Norman Jones
The University of Liverpool
Department of Mechanical Engineering
P. O. Box 147
Brownlow Hill
Liverpool L69 3BX
England

Professor E. J. Skudrzyk
Pennsylvania State University
Applied Research Laboratory
Department of Physics
State College, Pennsylvania 16801

Professor J. Klosner
Polytechnic Institute of New York
Department of Mechanical and
  Aerospace Engineering
333 Jay Street
Brooklyn, New York 11201

Professor R. A. Schapery
Texas A&M University
Department of Civil Engineering
College Station, Texas 77843

Universities (Con't.)

Professor Walter D. Pilkey
University of Virginia
Research Laboratories for the
  Engineering Sciences and
  Applied Sciences
Charlottesville, Virginia 22901

Professor K. D. Willmert
Clarkson College of Technology
Department of Mechanical Engineering
Potsdam, New York 13676

Dr. Walter E. Haisler
Texas A&M University
Aerospace Engineering Department
College Station, Texas 77843

Dr. Hussein A. Kamel
University of Arizona
Department of Aerospace and
  Mechanical Engineering
Tucson, Arizona 85721

Dr. S. J. Fenves
Carnegie-Mellon University
Department of Civil Engineering
Schenley Park
Pittsburgh, Pennsylvania 15213

Dr. Ronald L. Huston
Department of Engineering Analysis
University of Cincinnati
Cincinnati, Ohio 45221

Professor G. C. M. Sih
Lehigh University
Institute of Fracture and
  Solid Mechanics
Bethlehem, Pennsylvania 18015

Professor Albert S. Kobayashi
University of Washington
Department of Mechanical Engineering
Seattle, Washington 98105

Professor Daniel Frederick
Virginia Polytechnic Institute and
  State University
Department of Engineering Mechanics
Blacksburg, Virginia 24061

Universities (Con't)

Professor A. C. Eringen
Princeton University
Department of Aerospace and
  Mechanical Sciences
Princeton, New Jersey 08540

Professor E. H. Lee
Stanford University
Division of Engineering Mechanics
Stanford, California 94305

Professor Albert I. King
Wayne State University
Biomechanics Research Center
Detroit, Michigan 48202

Dr. V. R. Hodgson
Wayne State University
School of Medicine
Detroit, Michigan 48202

Dean B. A. Boley
Northwestern University
Department of Civil Engineering
Evanston, Illinois 60201

Professor P. G. Hodge, Jr.
University of Minnesota
Department of Aerospace Engineering
  and Mechanics
Minneapolis, Minnesota 55455

Dr. D. C. Drucker
University of Illinois
Dean of Engineering
Urbana, Illinois 61801

Professor N. M. Newmark
University of Illinois
Department of Civil Engineering
Urbana, Illinois 61803

Professor E. Reissner
University of California, San Diego
Department of Applied Mechanics
La Jolla, California 92037

Professor William A. Nash
University of Massachusetts
Department of Mechanics and
  Aerospace Engineering
Amherst, Massachusetts 01002

Universities (Con't)

Professor G. Herrmann
Stanford University
Department of Applied Mechanics
Stanford, California 94305

Professor J. D. Achenbach
Northwest University
Department of Civil Engineering
Evanston, Illinois 60201

Professor S. B. Dong
University of California
Department of Mechanics
Los Angeles, California 90024

Professor Burt Paul
University of Pennsylvania
Towne School of Civil and
  Mechanical Engineering
Philadelphia, Pennsylvania 19104

Professor H. W. Liu
Syracuse University
Department of Chemical Engineering
  and Metallurgy
Syracuse, New York 13210

Professor S. Bodner
Technion R&D Foundation
Haifa, Israel

Professor Werner Goldsmith
University of California
Department of Mechanical Engineering
Berkeley, California 94720

Professor R. S. Rivlin
Lehigh University
Center for the Application
  of Mathematics
Bethlehem, Pennsylvania 18015

Professor F. A. Cozzarelli
State University of New York at
  Buffalo
Division of Interdisciplinary Studies
Karr Parker Engineering Building
Chemistry Road
Buffalo, New York 14214

Universities (Con't)

Professor Joseph L. Rose
Drexel University
Department of Mechanical Engineering
  and Mechanics
Philadelphia, Pennsylvania 19104

Professor B. K. Donaldson
University of Maryland
Aerospace Engineering Department
College Park, Maryland 20742

Professor Joseph A. Clark
Catholic University of America
Department of Mechanical Engineering
Washington, D.C. 20064

Dr. Samuel B. Batdorf
University of California
School of Engineering
  and Applied Science
Los Angeles, California 90024

Professor Isaac Fried
Boston University
Department of Mathematics
Boston, Massachusetts 02215

Professor E. Krempl
Rensselaer Polytechnic Institute
Division of Engineering
Engineering Mechanics
Troy, New York 12181

Dr. Jack R. Vinson
University of Delaware
Department of Mechanical and Aerospace
  Engineering and the Center for
  Composite Materials
Newark, Delaware 19711

Dr. J. Duffy
Brown University
Division of Engineering
Providence, Rhode Island 02912

Dr. J. L. Swedlow
Carnegie-Mellon University
Department of Mechanical Engineering
Pittsburgh, Pennsylvania 15213

Universities (Con't)

Dr. V. K. Varadan
Ohio State University Research Foundation
Department of Engineering Mechanics
Columbus, Ohio 43210

Dr. Z. Hashin
University of Pennsylvania
Department of Metallurgy and
  Materials Science
College of Engineering and
  Applied Science
Philadelphia, Pennsylvania 19104

Dr. Jackson C. S. Yang
University of Maryland
Department of Mechanical Engineering
College Park, Maryland 20742

Professor T. Y. Chang
University of Akron
Department of Civil Engineering
Akron, Ohio 44325

Professor Charles W. Bert
University of Oklahoma
School of Aerospace, Mechanical,
  and Nuclear Engineering
Norman, Oklahoma 73019

Professor Satya N. Atluri
Georgia Institute of Technology
School of Engineering and
  Mechanics
Atlanta, Georgia 30332

Professor Graham F. Carey
University of Texas at Austin
Department of Aerospace Engineering
  and Engineering Mechanics
Austin, Texas 78712

Dr. S. S. Wang
University of Illinois
Department of Theoretical and
  Applied Mechanics
Urbana, Illinois 61801

Professor J. F. Abel
Cornell University
Department of Theoretical
  and Applied Mechanics
Ithaca, New York 14853

Universities (Con't)

Professor V. H. Neubert
Pennsylvania State University
Department of Engineering Science
  and Mechanics
University Park, Pennsylvania 16802

Professor A. W. Leissa
Ohio State University
Department of Engineering Mechanics
Columbus, Ohio 43212

Professor C. A. Brebbia
University of California, Irvine
Department of Civil Engineering
School of Engineering
Irvine, California 92717

Dr. George T. Hahn
Vanderbilt University
Mechanical Engineering and
  Materials Science
Nashville, Tennessee 37235

Dean Richard H. Gallagher
University of Arizona
College of Engineering
Tucson, Arizona 85721

Professor E. F. Rybicki
The University of Tulsa
Department of Mechanical Engineering
Tulsa, Oklahoma 74104

Dr. R. Haftka
Illinois Institute of Technology
Department of Mechanics and Mechanical
  and Aerospace Engineering
Chicago, Illinois 60616

Professor J. G. de Oliveira
Massachusetts Institute of Technology
Department of Ocean Engineering
77 Massachusetts Avenue
Cambridge, Massachusetts 02139

Dr. Bernard W. Shaffer
Polytechnic Institute of New York
Route 110
Farmingdale, New York 11735

Industry and Research Institutes

Dr. Norman Hobbs
Kaman AviDyne
Division of Kaman
  Sciences Corporation
Burlington, Massachusetts 01803

Argonne National Laboratory
Library Services Department
9700 South Cass Avenue
Argonne, Illinois 60440

Dr. M. C. Junger
Cambridge Acoustical Associates
54 Rindge Avenue Extension
Cambridge, Massachusetts 02140

Mr. J. H. Torrance
General Dynamics Corporation
Electric Boat Division
Groton, Connecticut 06340

Dr. J. E. Greenspon
J. G. Engineering Research Associates
3831 Menlo Drive
Baltimore, Maryland 21215

Newport News Shipbuilding and
  Dry Dock Company
Library
Newport News, Virginia 23607

Dr. W. F. Bozich
McDonnell Douglas Corporation
5301 Bolsa Avenue
Huntington Beach, California 92647

Dr. H. N. Abramson
Southwest Research Institute
8500 Culebra Road
San Antonio, Texas 78284

Dr. R. C. DeHart
Southwest Research Institute
8500 Culebra Road
San Antonio, Texas 78284

Dr. M. L. Baron
Weidlinger Associates
110 East 59th Street
New York, New York 10022

Industry and Research Institutes (Con't)

Dr. T. L. Geers
Lockheed Missiles and Space Company
3251 Hanover Street
Palo Alto, California 94304

Mr. William Caywood
Applied Physics Laboratory
Johns Hopkins Road
Laurel, Maryland 20810

Dr. Robert E. Dunham
Pacifica Technology
P.O. Box 148
Del Mar, California 92014

Dr. M. F. Kanninen
Battelle Columbus Laboratories
505 King Avenue
Columbus, Ohio 43201

Dr. A. A. Hochrein
Daedalean Associates, Inc.
Springlake Research Road
15110 Frederick Road
Woodbine, Maryland 21797

Dr. James W. Jones
Swanson Service Corporation
P.O. Box 5415
Huntington Beach, California 92646

Dr. Robert E. Nickell
Applied Science and Technology
3344 North Torrey Pines Court
Suite 220
La Jolla, California 92037

Dr. Kevin Thomas
Westinghouse Electric Corp.
Advanced Reactors Division
P. O. Box 158
Madison, Pennsylvania 15663

Dr. H. D. Hibbitt
Hibbitt & Karlsson, Inc.
132 George M. Cohan Boulevard
Providence, Rhode Island 02903

Dr. R. D. Mindlin
89 Deer Hill Drive
Ridgefield, Connecticut 06877

Industry and Research Institutes (Con't)

Dr. Richard E. Dame
Mega Engineering
11961 Tech Road
Silver Spring, Maryland 20904

Mr. G. M. Stanley
Lockheed Palo Alto Research
  Laboratory
3251 Hanover Street
Palo Alto, California 94304

Mr. R. L. Cloud
Robert L. Cloud Associates, Inc.
2972 Adeline Street
Berkeley, California 94703